U.S. DEPARTMENT OF LABOR MSHA
00031608

MINE GROUNDING SYSTEMS

Evaluation of In-Mine Grounding System and Codification of Ground Bed Construction and Measurement Techniques.

U. S. Bureau of Mines
Minneapolis, Minn.
LIBRARY

Prepared for
United States Department of the Interior
Bureau of Mines

by
College of Engineering
West Virginia University
Morgantown, West Virginia 26506

OFR
78-101

West Virginia University

Annual Report for October 16, 1976 to June 30, 1977
on
Grant No. G0144138.

November 16, 1977

MINE GROUNDING SYSTEMS: EVALUATION OF IN-MINE GROUNDING SYSTEM AND CODIFICATION OF GROUND BED CONSTRUCTION AND MEASUREMENT TECHNIQUES.

Prepared for

UNITED STATES DEPARTMENT OF THE INTERIOR
BUREAU OF MINES

by

WEST VIRGINIA UNIVERSITY
MORGANTOWN, WEST VIRGINIA, 26506

Annual Report for October 16, 1976 to June 30, 1977

on

Grant No. G0144138.

November 16, 1977

DISCLAIMER NOTICE

The views and conclusions contained in this document are those of the authors and should not be interpreted as necessarily representing the official policies or recommendations of the Interior Departments' Bureau of Mines or of the U.S. Government.

REPORT DOCUMENTATION PAGE

1. Report No.	2.	3. Recipient's Accession No.
4. Title and Subtitle Mine Grounding Systems: Evaluation of In-Mine Grounding System and Codification of Ground Bed Construction and Measurement Techniques.		5. Report Date Nov. 16, 1977 6.
7. Author(s) Wils L. Cooley		8. Performing Organization Report No.
9. Performing Organization Name and Address Engineering Experiment Station West Virginia Universtiy Morgantown, WV 26506		10. Project/Task/Work Unit No. 11. Contract or Grant No. G0144138
12. Sponsoring Organization Name and Address Office of the Assistant Director - Mining Bureau of Mines Department of the Interior Washington, D.C. 20241		13. Type of Report Annual Report for October 10, 1976 to June 30, 1977. 14.

15. Supplementary Notes

16. Abstract

Several aspects of mine safety grounding systems and equipment are studied. Electrolytic corrosion of test ground beds has shown a high incidence of stray current damage, while efforts to build a reliable continuous ground bed monitor continue. Laboratory and field investigations of trailing cable splices have yielded strong evidence that splices can contribute to stray current problems in the mines, but a method is suggested for discovering deteriorating splices before they pose a serious hazard. A prototype device has been constructed to evaluate the electrical resistance of rail bonds underground as a source of stray current. Theoretical modeling of ground electrodes has advanced considerably, now covering measurements of large cylindrical electrodes, multiple-rod ground beds, rod electrodes in stratified earth, and measurement of connected beds. A prototype instrument design is given for a potential gradient plotter to quickly evaluate voltage gradients near earth electrodes. Additional ground-check monitor testing is reported.

17. Originator's Key Words	18. Availability Statement
Safety ground bed, stray current, rail-bonds, earth electrodes, earth resistance, cable splices, ground-check monitors.	

19. U. S. Security Classif. of the Report	20. U. S. Security Classif. of This Page	21. No. of Pages	22. Price

FOREWORD

This report was prepared by West Virginia University, Engineering Experiment Station, Morgantown, West Virginia under USBM Grant Number G0144138. The grant was initiated under the Coal Mine Health and Safety Research Program. It was administered under the technical direction of the Pittsburgh Mining and Safety Research Center with Mr. Roger L. King acting as the Technical Project Officer. Mr. A. G. Young was the contract administrator for the Bureau of Mines.

This report is a summary of the work recently completed as a part of this grant during the period October 16, 1976 to June 30, 1977. This report was submitted by the authors on November 16, 1977.

TABLE OF CONTENTS

Page

CHAPTER I. GROUND BED MONITORING 1

1.1. GROUND BED MONITOR DESIGN CHANGES 1

1.2. GROUND BED MONITOR TESTS 4

1.3. GROUND BED CORROSION TESTING 4

1.4. CORROSION TEST RESULTS 8

1.5. REFERENCES 22

CHAPTER II. CABLE SPLICES AND SOME OF THEIR EFFECTS ON THE SAFETY GROUND SYSTEM 23

2.1. INTRODUCTION 23

2.2. RELATIVE HUMIDITY INVESTIGATION 23

2.3. ANALYSES OF DATA 26

2.4. ADDED RESISTANCE TO A CONDUCTOR 40

2.5. TEMPERATURE MEASUREMENTS 42

2.6. CORRELATION DEVELOPMENT 48

2.7. IN-MINE MONITORING 54

2.8. MONITORING RESULTS 56

2.9. REFERENCES 72

CHAPTER III. GROUNDING PRACTICE 73

3.1. COUPLING BETWEEN SYSTEM AND SAFETY GROUND 73

3.2. EXPERIMENTAL EVALUATION OF COUPLING 73

3.2.1 Introduction 73
3.2.2 Resistance Measurements 75
3.2.3 Test Results 78
3.2.4 Conclusions 79
3.2.5 Analysis and Discussion on Test Results . . 79

Table of Contents - Continued

		Page
3.3.	RAIL BOND RESISTANCE MEASUREMENT	82
3.3.1	Circuit Design	82
3.3.2	Rail Bond Data	94
3.3.3	Conclusions	95
3.4.	GROUNDING STANDARDS AND REGULATIONS	96
CHAPTER IV.	MULTIPLE-ROD GROUND BEDS	97
4.1.	THE ROD MODEL	97
4.1.1	Choice of Approximation	101
4.1.2	Potential Induced on Rod by Small Hemisphere	101
4.1.3	Resistance Measurement of a Single Rod	105
4.1.4	Improved Method of Calculating Rod Resistance	107
4.2.	MULTIPLE-ROD CALCULATIONS	110
4.2.1	Mutual Resistance Between Rods	110
4.2.2	Resistance Measurement of Multiple Rods	114
4.2.3	Resistance Measurement of Rods on a Circle	121
4.3.	CONCLUSIONS AND RECOMMENDATIONS FOR FUTURE STUDY	124
4.3.1	Recommendations for Future Work	124
4.4.	REFERENCES	127
CHAPTER V.	MEASUREMENT OF GROUND BED CHARACTERISTICS	128
5.1.	RESISTANCE MEASUREMENT IN FINITE VOLUME	128
5.1.1	Resistance of a Hemisphere	128
5.1.2	Correction for Resistance Measurement in Finite Volume	131
5.1.3	Perpendicular Boundary Condition with Equal Spacings	133
5.1.4	Perpendicular Boundary Condition with Unequal Spacings	140
5.1.5	Parallel Boundary Condition with Equal Spacings	150
5.1.6	Parallel Boundary Condition with Unequal Spacings	153
5.1.7	References	162

Table of Contents - Continued

Page

5.2. FIELD TESTING OF CYLINDRICAL-ELECTRODE THEORY . . . 162

5.2.1 Resistivity Measurements Taken 162
5.2.2 Analysis of Resistivity Measurements 166
5.2.3 Resistance Measurements 166

5.3. POTENTIAL GRADIENT PLOTTER. 168

5.3.1 Introduction 168
5.3.2 Description of Equipment 170
5.3.3 Circuitry 171
5.3.4 Power Supply 171
5.3.5 Constant Current Source 174
5.3.6 Voltage Detection 174
5.3.7 Distance Detection 182
5.3.8 Calibration 187
5.3.9 Laboratory Testing 188
5.3.10 Field Testing. 188
5.3.11 References 191

5.4 SURGE IMPEDANCE OF GROUND RODS 191

5.4.1 Discussion 191
5.4.2 References 194

CHAPTER VI. GROUND CHECK MONITORS 196

6.1. MODULAR MONITOR 196

6.1.1 MESA Acceptance 196
6.1.2 Multiple Circuit Monitor 196

6.2. HIGH VOLTAGE MONITOR TESTING 203

6.2.1 Introduction 203
6.2.2 Evaluation Procedure 204
6.2.3 Connection Diagrams 207
6.2.4 Test Results 210
6.2.5 Preliminary Test Conclusions 214
6.2.6 Comments on Atkinson Circuit Design from Patent 214
6.2.7 CEMSCO Monitor Circuit Analysis 216

6.3 MESA SEMINAR 219

Table of Contents - continued

Page

CHAPTER VII. LIGHTNING DAMAGE TO MONITORS 220

7.1. SURGES COUPLED BY SHIELDING FAILURES 220

7.2. SURGES COUPLED BY BACKFLASH 220

7.3. REVISED ESTIMATED SURGE PROBABILITY 220

7.4. REFERENCE 222

APPENDICES

A. FORTRAN PROGRAM FOR SOLUTION OF α, FOR PERPENDICULAR BOUNDARIES WITH EQUAL SPACINGS 223

B. FORTRAN PROGRAM FOR SOLUTION OF α, FOR PERPENDICULAR BOUNDARIES WITH UNEQUAL SPACINGS. 228

C. FORTRAN PROGRAM FOR SOLUTION OF α, FOR PARALLEL BOUNDARIES WITH EQUAL SPACINGS 233

D. FORTRAN PROGRAM FOR SOLUTION OF α, FOR PARALLEL BOUNDARIES WITH UNEQUAL SPACINGS 238

E. WVU CONTRIBUTION TO GROUND-CHECK MONITOR RESEARCH . 243

EXECUTIVE SUMMARY

Progress during the report period was mixed. The tasks which involve laboratory investigation and theoretical study progressed essentially on schedule, while those involving instrument design and field measurement often fell behind. Obtaining the close cooperation of the mining industry has sometimes been a problem. The design of instrumentation which can operate properly in the mine environment continues to take longer than anticipated.

Chapter 1 covers ground bed monitoring. The design of satisfactory field instrumentation continues to be a problem. The severe winter weather delayed field work considerably. When an installation was finally made it was discovered that several circuit changes were necessary. Additional signal filtering was required. The reliability of the chart-paper transport and electronic divider circuit are low, but improvements are planned. Short-term tests were successful on three different ground beds. Ground-bed corrosion testing has continued to yield interesting results. Significant conclusions are that earth electrodes are most susceptible to corrosion just below the earth's surface and that the commonly used copper, copper-clad, and galvanized electrodes perform poorly compared to some other electrode materials.

Chapter 2 covers stray current from cable splices. Laboratory and field investigation showed that electrical leakage from cables was somewhat dependent on the relative humidity of the air, but strikingly dependent on the number of splices in the cable. In numerous field tests stray ground current was found to correlate with the number and age of splices in a cable. It is believed that this stray current is caused by asymmetries in conductor resistance at the point of the splice, but this remains to be proved conclusively. A number of measurements made at cable repair shops shows considerable variability in splice resistance as the result of imperfect workmanship. In some cases the added resistance of the splice was suspected of causing significant heating of the splice under load. When infrared temperature measurements were made of several spliced cables in the field it was discovered that some splices showed steep temperature gradients under load. The steepest gradients were recorded on a cable which failed only a few hours later. It is concluded that the temperature profile of a splice can clearly indicate its electrical resistance, and may possibly have use in predicting incipient cable failure.

Chapter 3 deals with grounding practice. Data was taken to study transferred potentials between system (sub-station) and safety grounds during a series of staged fault tests at an operating coal mine. This data was compared with theoretical predictions of transferred potentials based on earth resistance and system geometry. Meaningful results were obtained only for the case where the mine ground was isolated from the surface ground bed, which drastically reduced the

complexity of the system being studied. In general, some qualitative statements can be made about transferred potentials for complex systems, but the complexity seems to preclude quantitative analysis. Work on a prototype instrument to measure rail-bond resistance was begun. Input from the mining industry indicates that poor bonds are the source of many electrical problems underground. It is hoped that poor bonds are the source of many electrical problems underground. It is hoped that the validity of this claim can be evaluated with the newly-designed instrument. A report is also included of WVU contributions to proposed amendments of Title 30, Part 77 of the Code of Federal Regulations dealing with grounding.

Chapter 4 reports work done on multiple-rod ground beds. Previous analysis dealt with hemispherical electrodes, which are mathematically easy to analyze but impractical to implement. A valid electrical model of a driven-rod electrode was developed. This was used to study the problem of accurately measuring the resistance of large multiple-rod ground beds. It is shown that previously published resistance measurements (from England) are incorrect for large electrodes such as boreholes and well casings.

Chapter 5 deals with several other aspects of the accurate measurement of ground-bed resistance. It derives theoretically a set of correction factors to be used in making resistance measurements in a finite volume. These are especially useful for model studies and simulations, but they have applicability to field measurements made near a discontinuity such as the edge of a mine bench or cliff. A report of field measurements made at a cooperating mine is included in which the theories reported in Chapters 4 and 5 are shown to agree well with observed data. The theory even pointed out a significant oversight on the part of the mine personnel, in which a well casing was believed to be 300 feet long when it was actually only 25 feet long (as revealed by a review of old records). An instrument is also discussed which is to be used to evaluate the expected severity of potential gradients in the earth about safety-grounded equipment in the event of a system fault or lightning strike. The instrument design has been worked out and some preliminary measurements have been made with a prototype device. Surge impedance of ground beds is considered in an effort to predict the severity of lightning transients. Some information was obtained from the literature and several electrical models were considered. No significant conclusions have yet been drawn.

Chapter 6 deals with ground-check monitors. A report is made of the MESA acceptance testing of the modular monitor. Testing is proceeding slowly. The monitor has not yet failed the testing, but MESA requires more evaluation before accepting the device. A testing program was set up to evaluate commercially available high-voltage ground-check monitors. Two such devices were tested. One works very well and the other moderately well, but both seem to have some serious shortcomings. The details of the testing and the conclusions are

reported. A report is also given of extensive WVU participation in a MESA-sponsored seminar to acquaint the mining industry with ground-check monitors.

Chapter 7 deals with lightning damage to monitors, and corrects an error made in the previous annual report. The likelihood of damage to monitors as the result of lightning strokes to the incoming primary line to the substation was underestimated. Revised figures are given which indicate this as probably the primary source of damaging transients.

CHAPTER I: GROUND BED MONITORING

1.1 GROUND BED MONITOR DESIGN CHANGES

Some significant changes were made in the ground bed monitor this year. The major change was the addition of extra filtering and amplification circuits. These changes were found necessary on the basis of results obtained from field tests.

The monitor was first installed in mid-May. It was found that the signal level was insufficient to operate the divider, because approximately 90% of the current went into the mine and about 10% through the ground bed. From previous measurements it has been determined that the ground bed has a resistance of approximately 25 to 30 ohms. So the mine must have a resistance of approximately 2.5 to 3 ohms. It was also observed that the 60 H_z noise on the ground bed was approximately 10 times as large as the signal.

In order to have sufficient signal levels an extra 11 H_z band-pass filter was added to the monitor. However a 1-pole band-pass filter with an 11 H_z center frequency and adjustable gain of 1 to 100 will still amplify a 60 H_z signal. If the filter gain is 10, the 60 H_z signal is amplified by a gain of 2. Similarly if the gain of the filter is 100 the 60 H_z signal is amplified by 20.

To reduce the problem caused by these large amplifications a twin-T 60 H_z notch filter was designed. Ordinarily a twin-T notch filter requires some adjustments using either variable capacitors or variable resistors. The notch filter used in the ground bed monitor used stable 5% polystyrene capacitors and 1% resistors. Figs. 1.1 and 1.2 illustrate the circuit diagrams of the added portions.

The two circuits are similar, but not identical, with respect to gain configurations. The circuit for the voltage amplifier uses a band pass filter with a gain of 1 followed by a 60 H_z notch filter, and an amplifier with an adjustable gain from 1 to 100. The circuit for the current amplifier uses a band pass filter with a gain of 10 followed by a 60 H_z notch filter, and an amplifier with an adjustable gain from 1 to 10. The reason the two circuits are different is because the current signal is extremely small and requires amplification before the notch filter. It is important to realize that the notch filter is not required to eliminate completely the 60 H_z noise. It is used to prevent saturation of the circuits that follow. The multiplier circuits used as synchronous detectors will also eliminate the problems caused by 60 H_z on the ground

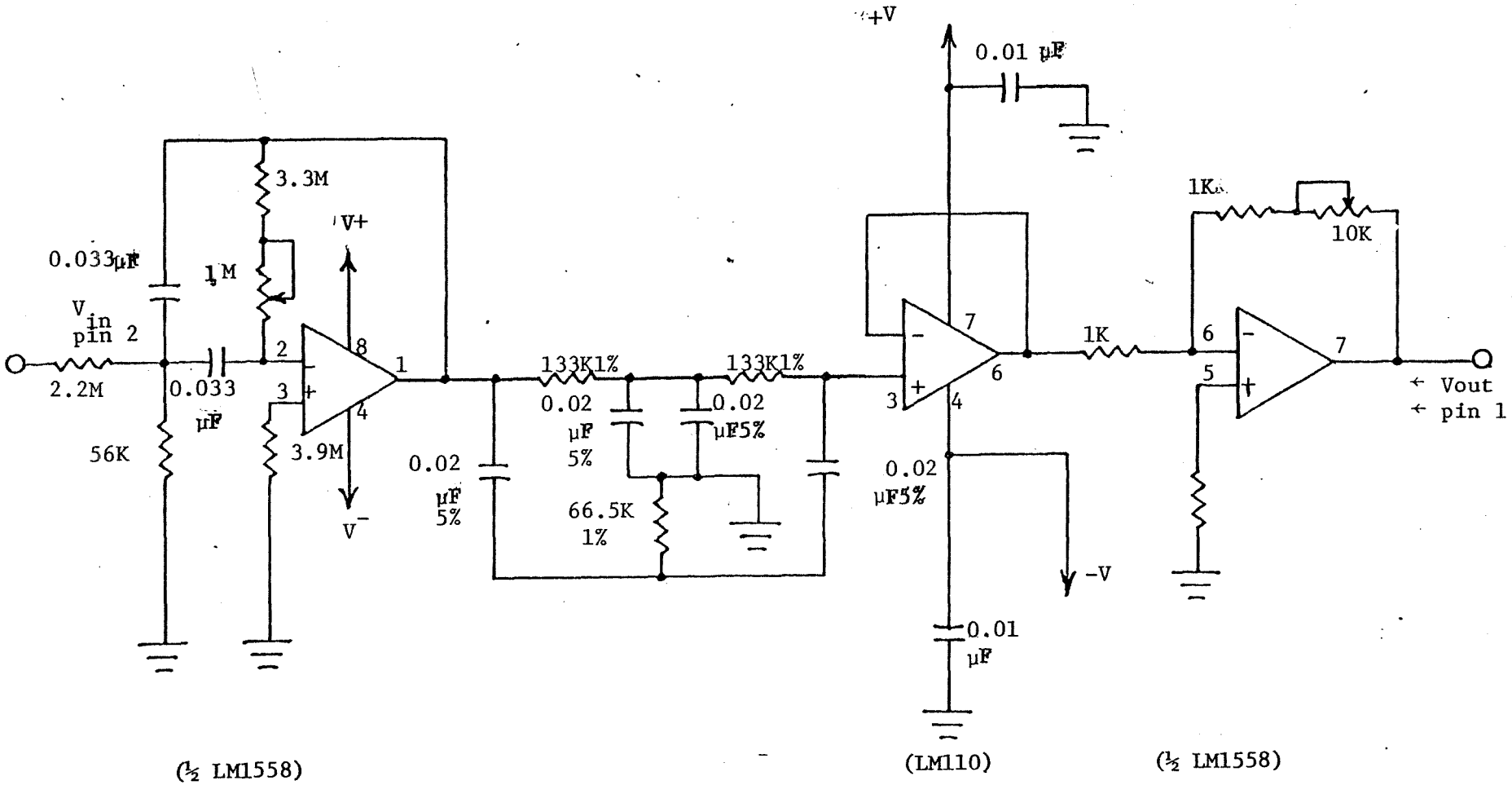


Fig. 1.1: Voltage Amplifier, Bandpass, and Notch Filter on Supplemental Circuit Board #1

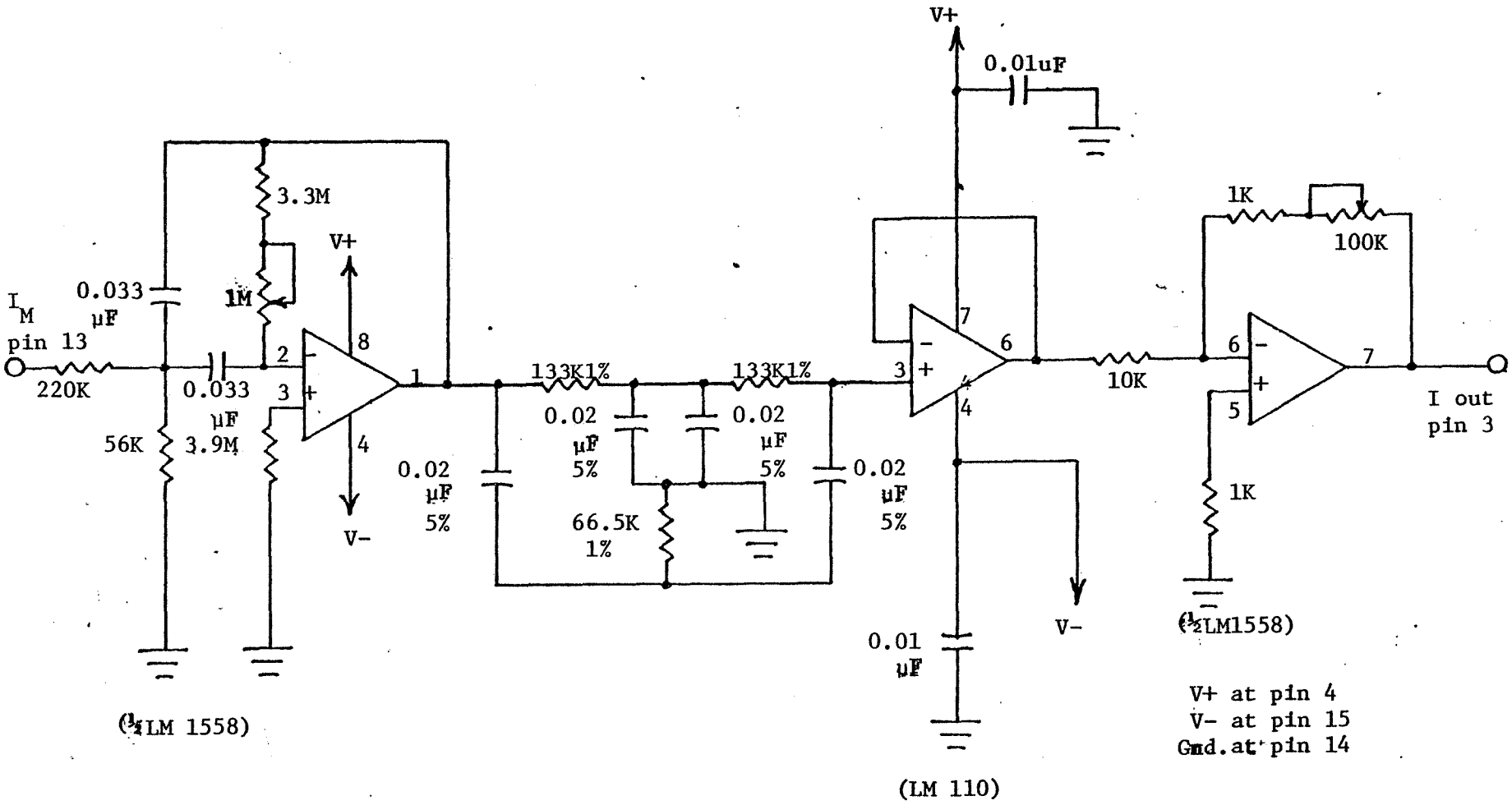


Fig. 1.2: Current Amplifier, Bandpass, and Notch Filter on Supplemental Circuit Board #1.

bed.*

1.2 GROUND BED MONITOR TESTS

The circuitry described in Section 1.1 was incorporated into the ground bed monitor in mid-year. The monitor was reinstalled at the Delmont Mine of Eastern Associated Coal Coampany in May, 1977. Some typical recordings are shown in Fig. 1.3.

There are some interesting points of observation in the recordings. All recordings were made at a chart speed of 1/2 inch/hour with 40 ohms full-scale deflection. Tracing #1 shows a typical night-time tracing from 9:30 P.M. until 9:30 A.M. The resistance apparently varies from 16 ohms to approximately 24 ohms, a situation most likely caused by drift of the instrument. The small oscillations seen in the recording could be due to minor offset errors in the divider circuit. Tracing #2 shows the apparent daytime resistance to be somewhat higher going from 20 ohms to 26 ohms. The oscillations are present in all the recordings. Tracings #3 and #4 show some interesting step-variations and some unexplainable traces. Tracings #5 and #6 were taken during a rain storm. These tracings seem to indicate that the ground bed resistance apparently temporarily increased. It is important to realize however that these tracings were the first to be taken. All the above statements are simple hypotheses, and many more readings need to be taken and studied, before any concrete conclusions can be drawn. It seems that many apparent changes are due to instrumentation problems, an unacceptable situation.

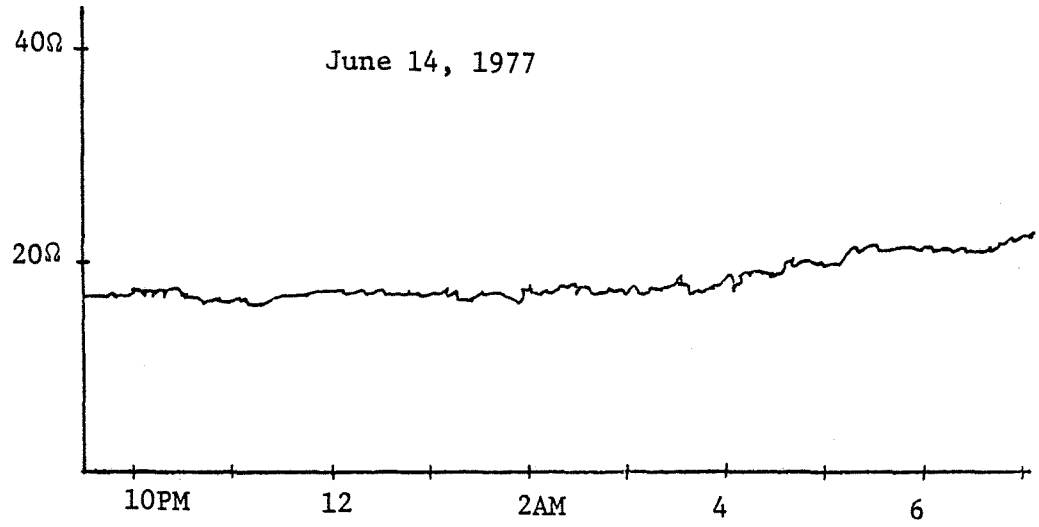
In the month during which the recorder has been installed at Delmont Mine there has been one component failure (an integrated circuit).

1.3 GROUND BED CORROSION TESTING

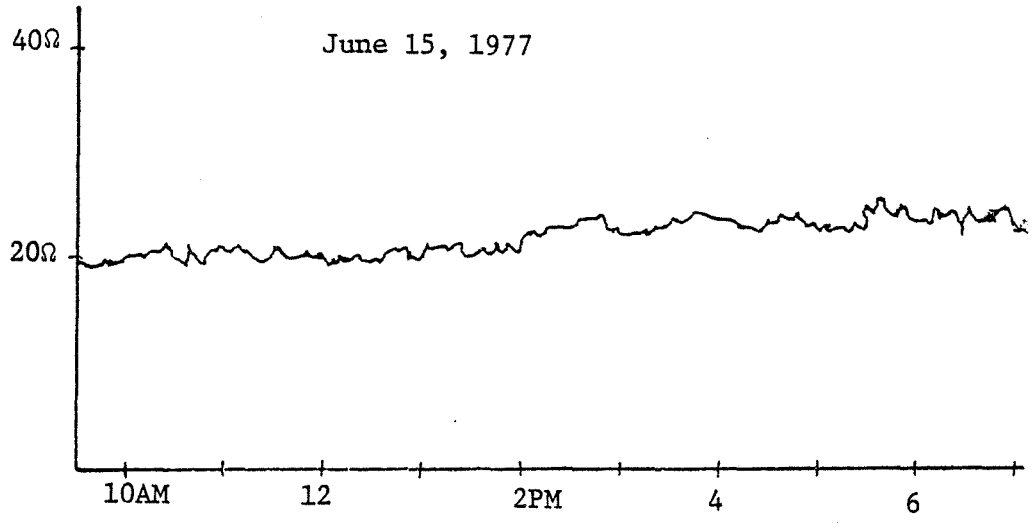
The mine power system's ground beds, both system and safety, are essential to the operation and safety of all mining personnel; that is why it becomes so important to maintain an adequate ground connection. Other areas of this project deal with ways to achieve a low impedance to earth and methods of monitoring this contact. This area of study deals with a third aspect of grounding, electrolytic corrosion due to stray currents. It was shown in the last annual report that corrosion is indeed a problem with grounding systems. Tests in the laboratory proved that extensive corrosion results from moderate dc current levels. The work since the last report has been centered on finding just how much current various ground rods can handle safely and ways to monitor this current with time.

---

* A description of the notch filter can be found in the "I.C. op-amp Cookbook" by Walter C. Jung, pp. 338-339.

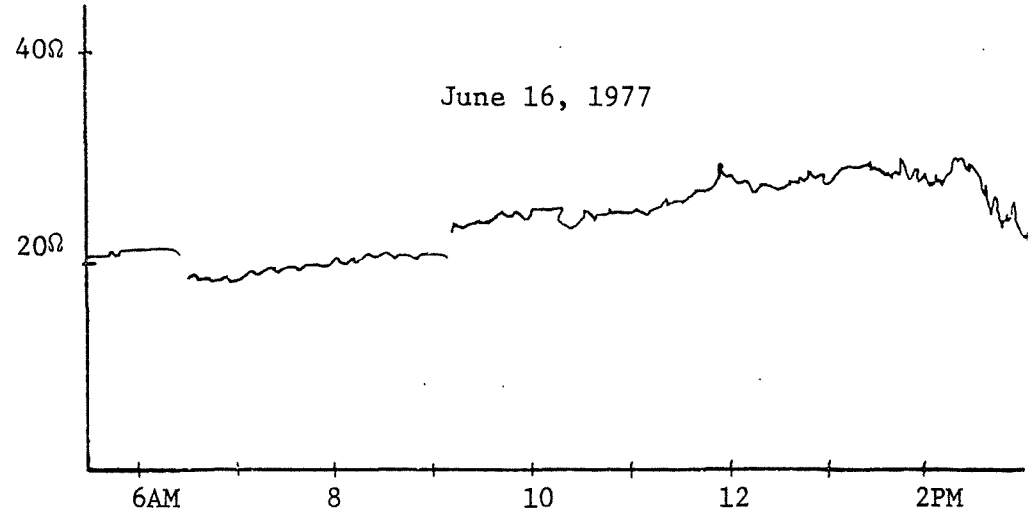


a) Tracing #1: Typical Night-Time Tracing of Ground Bed Resistance

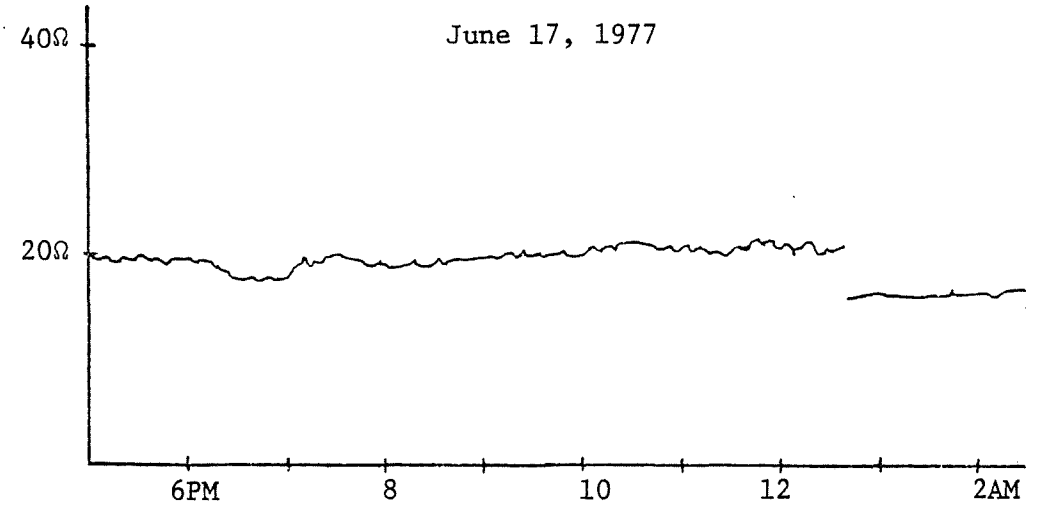


b) Tracing #2: Typical Day-Time Tracing of Ground-Bed Resistance

Fig. 1.3. Tracings from Ground Bed Monitor.

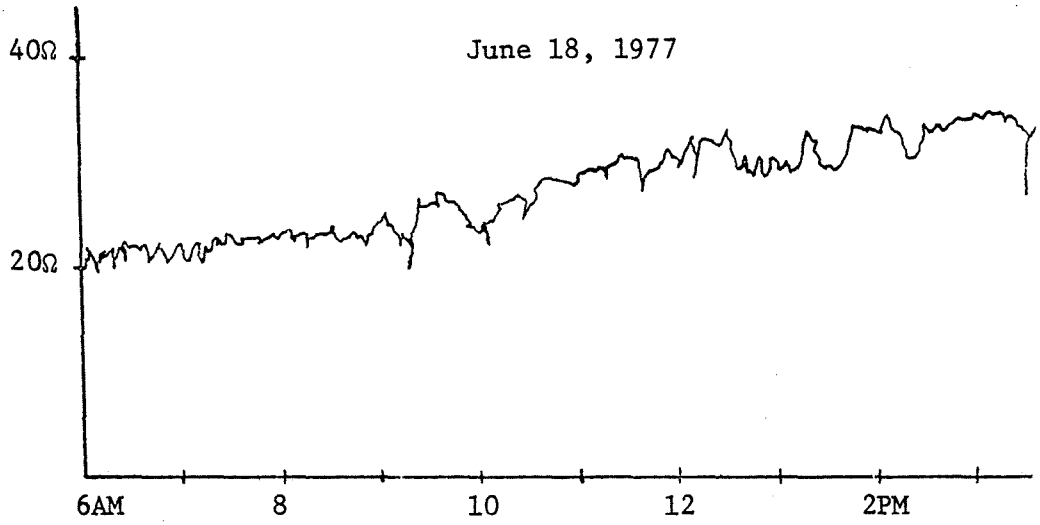


c) Tracing #3: Some Inexplicable Traces Showing Step Variations in Ground Resistance

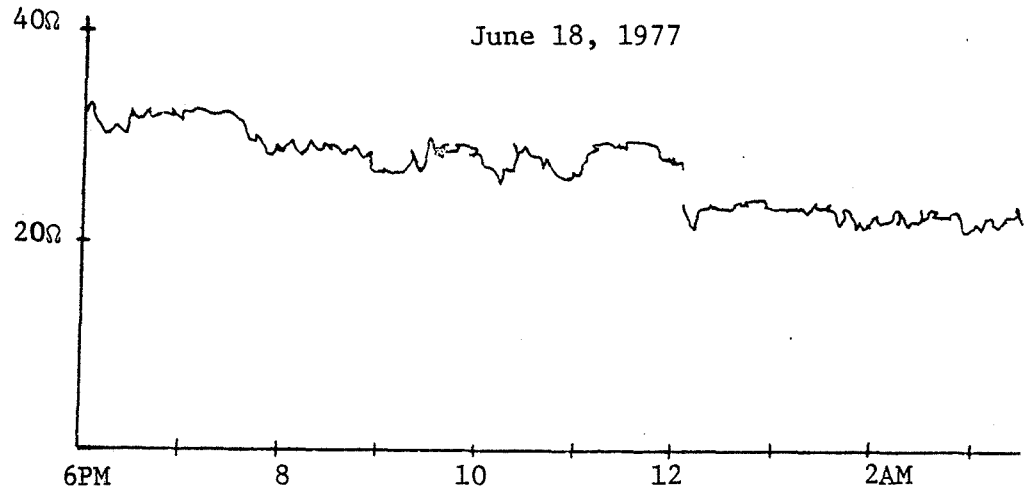


d) Tracing #4: Another Inexplicable Step Change

Fig. 1.3. (continued)



e) Tracing #5: Resistance Tracing Following Early Morning Rain Storm, which Lasted from 6AM to 10AM



f) Tracing #6: Second Portion of Tracing #5.

Fig. 1.3. (continued)

To obtain such information more controlled experiments were started and instrumentation developed. Faraday's law states that if the total amount of current passed through a substance is known one can calculate the theoretical weight loss. Because the experiments are designed to simulate actual mine conditions it was decided to attempt corrosion with modest current flow (0-5A-dc), the approximate magnitude of stray currents.

The problem then becomes one of time and adequate recording. Most electrode studies so far require a minimum of one week's time for significant corrosion. Electronic intergration over extended time periods is a most difficult undertaking, susceptible to drifts and erroneous signals. The most feasible way to integrate current over time, electronically, is by use of a Voltage Controlled Oscillator (VCO). The current is first changed to a voltage using a precision shunt (0-10 A, 50 mV). This voltage is then amplified (200X, 0-10 V) and applied to a VCO (INTECH A 8402); the proportional frequency (0-10K Hz) is counted and recorded. A Random Access Memory (RAM) and a clock to automatically record the current passed every hour were chosen to complete the test apparatus (see Fig 1.4). To date the prototype unit is being tested and the final touches added; when it is fully operational experimental time will be significantly shortened.

Other methods are also being used to monitor current passage with time. Currently a Simpson Multicorder is recording the amplified voltage. With this recorder's slow speed (1"/hour) long range measurements are possible. Following a corrosion period the chart paper is removed and integration done with the use of an HP-97 calculator. The program used comes from the HP-97 Math Pack I Library entitled Numerical Integration. The distance between points and the value at each interval are entered, the calculator computes the integral using the trapezoidal rule.

1.4 CORROSION TEST RESULTS

The experimental approach described in Section 1.3 was implemented on a copperweld standard 5/8" diameter rod and a 5/8" steel reinforcing rod, the results are given in Table 1.1.

Table 1.1

Rod	A-HR	Wt. Loss	Theoretical Corrosion Rate	Actual Corrosion Rate
1' x 5/8" Copper Clad Steel	107.9	143.7gm	*0.7 gm/A-HR	*1.3 gm/A-HR
1' x 5/8" Steel Rebar	110.8	69.8gm	0.7 gm/A-HR	0.6 gm/A-HR

* Neglecting Cu

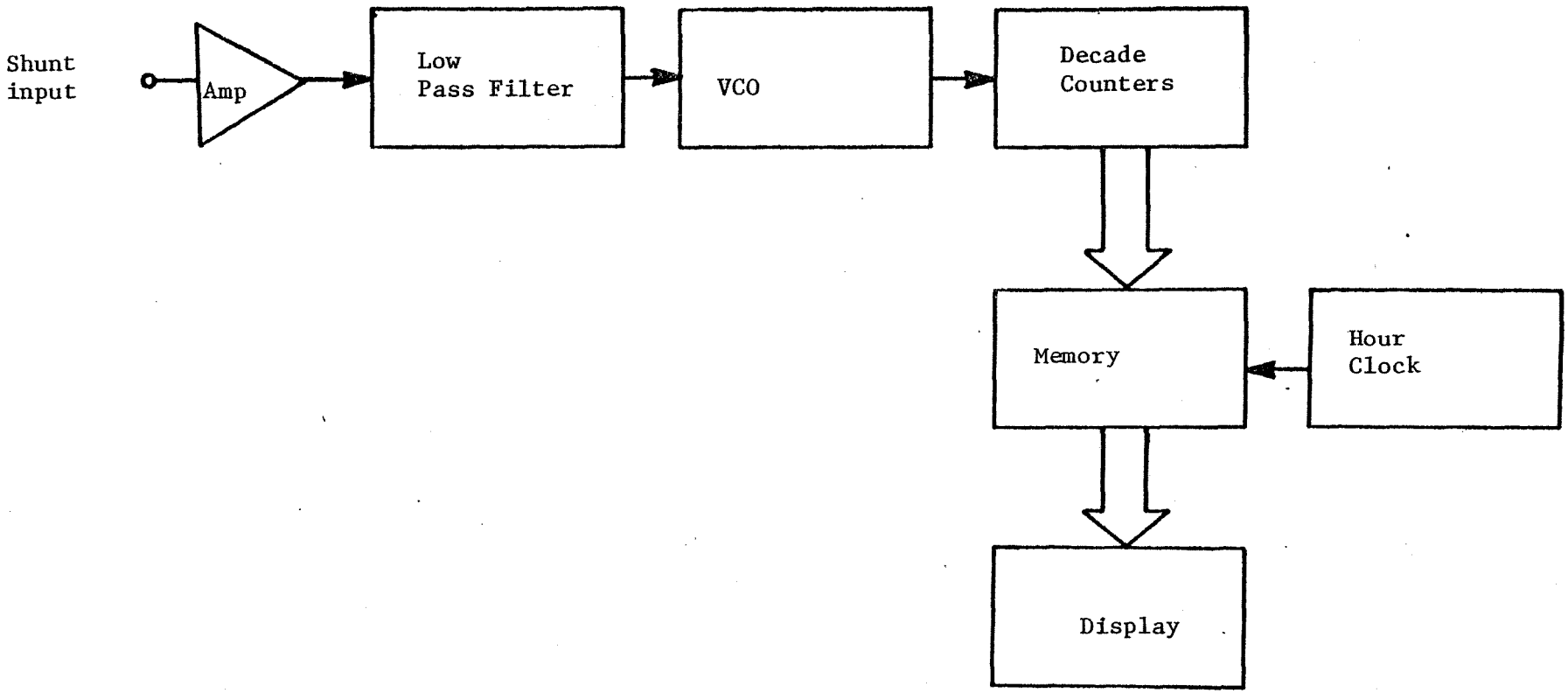


Fig. 1.4. Block Diagram of Electronic Long Term Integrator.

Using Faraday's equation:

$$\text{Wt Lost} = \frac{(\text{Coulombs})\ (\text{Atomic Wt})}{(96{,}500)\ \ (\text{Valence})}$$

one can attempt to calculate the theoretical weight loss. In practice the theoretical weight loss is higher due to the occurrence of side reactions. As one can see the copperweld rod has a greater deviation from theoretical weight loss than steel. This difference can be attributed to the copper plating on the rod. The presence of two metals makes calculations much more difficult. It is hard to say how much current was used in eroding the copper and how much was attributed to steel loss. Steel being lower on the Redox table corrodes before Cu, therefore some weight loss can be attributed to flaking (corrosion of steel from underneath copper). Since the steel rod is mainly composed of iron, the theoretical calculations are much closer to actual weight loss. Because other types of ground rods are of a composite nature e.g. (SiCrFe, Pb-Pt, Pt-Ti) it may be necessary to experimentally plot curves relating current passage to weight loss. The copperweld rod was exposed to current for a much longer time period (6 weeks); this becomes evident when one looks at the before and after pictures page (Fig. 1.6). The copperweld rod actually corroded into two pieces at the soil surface, disconnecting itself from service. This phenomenom of greater corrosion at the soil surface occurred in every rod corroded. At first this was attributed to the cathode being so close to the soil surface, however this was disproven when box #3 was used. Box #3's cathode is located at the mid-soil level (see Figure 1.5). Next, it was thought that the local corrosion was due to improper salting, more salt being concentrated at the surface. This too was disproven when salt was placed beneath the soil surface. A third theory, as yet unproven, is that corrosion products at the surface tend to accumulate near the rod where as these same products under the soil migrate away from the rod. Therefore the electrical connection at the surface is greater, allowing more current flow, thus greater corrosion. By insulating the area of the rod near the soil surface one can test the theory.

H. H. Uhlig in his book Corrosion and Corrosion Control[1] discusses mechanisms of the corrosion process. Corrosion of a metal in a metalic salt e.g. NaCl consists of two primary reactions:

$$M \rightarrow M^{+} + e^{-} \qquad \text{Anode}$$

$$H^{+} \rightarrow 1/2\ H_2 - e^{-} \qquad \text{Cathode}$$

production of a metal ion at the anode and the evolution of hydrogen gas at the cathode. If the voltage is high enough at the anode other reactions may also occur.

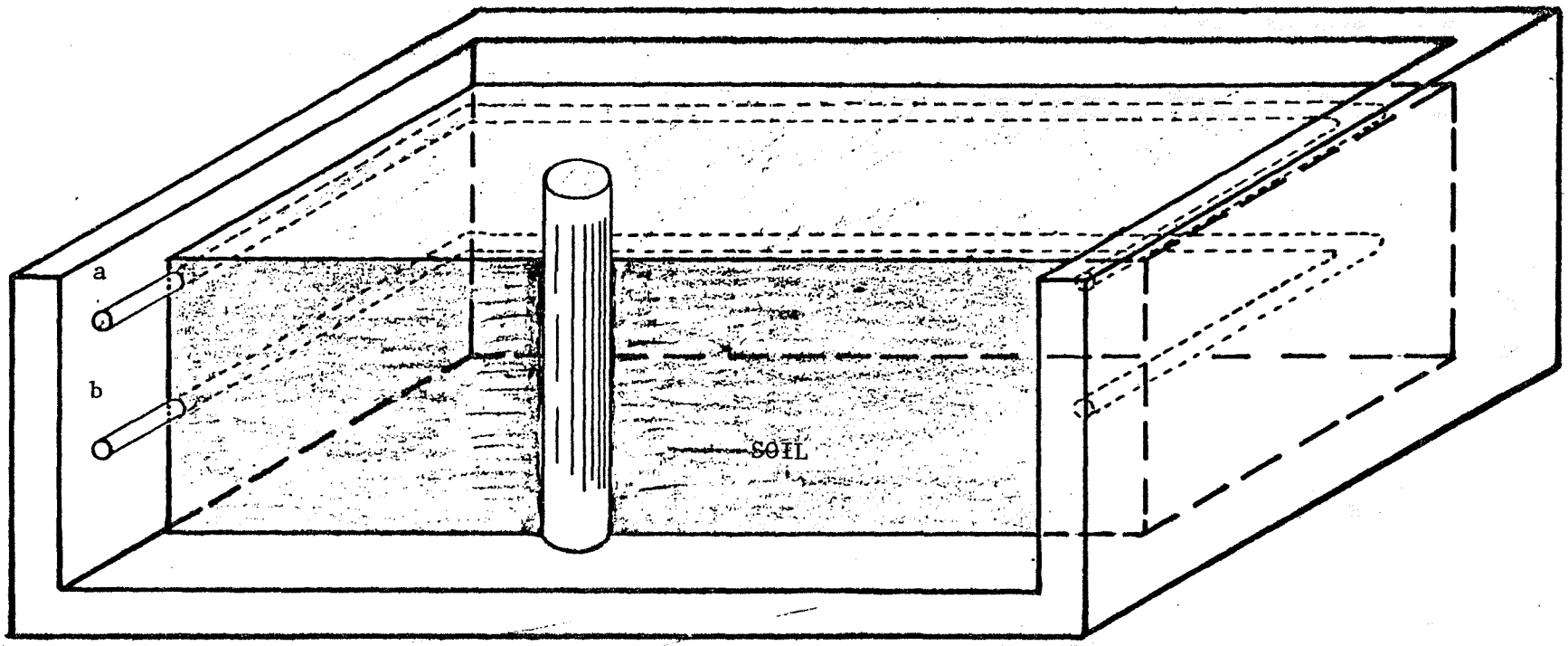


Fig. 1.5 Position of Cathode With Respect to Box Soil.
Box # 1 & 2 (a), Box # 3 (b)



a b

Fig. 1.6: Ground Rods Before and After Corrosion:
(a) Copperweld (b) Steel Rebar
In each case a 1-foot ruler is shown for comparison.

$$2\ OH^- \rightarrow 1/2\ O_2 + H_2O + 2\ e^-$$

$$2\ Cl^- \rightarrow Cl_2 + 2\ e^-$$

$$2\ Br^- \rightarrow Br_2 + 2\ e^-$$

In the case of iron (steel) the two basic reactions still occur:

$$Fe \rightarrow Fe^{++} + 2\ e^- \quad \text{Anode}$$

$$2\ H^+ \rightarrow H_2 - 2\ e^- \quad \text{Cathode}$$

In the presence of oxygen and salt (NaCl) the metallic ion dissolves into solution via two paths:

$$Fe^{++} + 2\ Cl^- \rightarrow FeCl_2$$

$$Fe + H_2O + 1/2\ O_2 \rightarrow Fe(OH)_2$$

The competition between Cl^- and O_2 for Fe^{++} is great and the presence of both greatly enhances the metal loss. The point here is that oxygen and chlorine ion concentrations are greatest near the soil surface, hence it seems reasonable that the largest metal loss will also occur in this area. This may explain why some rods have been known to sever close to the surface even though a substantial amount of rod is left below. Aeration of the rod may be a possible solution, not to stop corrosion but to try and prevent rod breakage.

Another area still under investigation is the effect corroding ground rods have on soil resistivity near the rod. If such an effect is noted it may serve as a way to monitor corrosion. In this new set of experiments more stringent controls were set to insure that any changes in measured resistivity were due solely to the rod corroding and not external factors. Each box was adequately salted and watered to hasten corrosion. A plastic cover was placed on each box to retard resistivity changes due to moisture evaporation. As a second precaution against soil moisture changes a control box was added. Resistivity readings for both boxes are taken with the Bison meter before and after corrosion. Results for the copperweld and steel rod are given in Tables 1.2 through 1.5. Both profile and sounding measurements are taken to cover the entire box; corrections are made for the effect of box boundaries (see Figs. 1.7 through 1.10).

TABLE 1.2
SOUNDING RESISTIVITY PROFILE DATA,
CORROSION EXPERIMENTS

Wenner Electrode Spacing	Copperweld X-Axis		Copperweld Y-Axis		Steel Rebar X-Axis		Steel Rebar Y-Axis	
	BC	AC	BC	AC	BC	AC	BC	AC
2 cm	209.9*	121.0	229.9	154.5	47.0	50.2	45.7	113.2
4 cm	183.8	192.9	206.6	219.2	65.7	96.5	66.3	87.7
6 cm	97.3	203.3	112.9	237.0	84.6	97.1	76.3	87.7
8 cm	92.4	223.0	95.2	213.8	78.4	95.7	82.4	96.9
10 cm	114.5	213.2	148.2	218.4	87.7	104.2	98.0	101.6
15 cm	176.5	184.3	189.9	198.7	107.3	103.4	116.3	110.2
20 cm	209.7	156.7	233.6	209.1	119.3	113.7	117.6	113.6

*All resistivity data in ohm-cm
AC - After Corrosion
BC - Before Corrosion

TABLE 1.3
DISTANCE RESISTIVITY PROFILE DATA,
CORROSION EXPERIMENTS

Distance From Box Center (10 cm Electrode Sp)	Copperweld X-Axis		Copperweld Y-Axis		Steel Rebar X-Axis		Steel Rebar Y-Axis	
	BC	AC	BC	AC	BC	AC	BC	AC
- 40 cm	179.9*	185.5	164.6	241.8	109.2	119.6	114.8	101.5
- 35	184.3	160.0	244.1	235.7	121.3	122.3	100.6	99.4
- 30	245.4	199.6	279,6	228.8	129.7	127.9	116.6	110.9
- 25	308.9	258.0	252.1	208.6	132.8	132.7	129.1	117.8
- 20	271.3	239.4	258.7	251.7	128.1	128.8	110.8	110.5
- 15	243.1	224.1	210.0	242.6	126.9	115.2	124.3	112.3
- 10	215.4	196.4	230.9	235.3	124.5	114.1	98.5	104.8
- 5	189.9	215.3	222.6	228.1	91.4	96.2	108.3	106.6
0	137.0	231.8	114.3	228.3	89.1	100.8	91.9	103.2
5	160.4	210.0	129.8	230.2	87.6	82.0	86.7	96.0
10	239.1	207.4	197.4	164.8	112.3	87.1	100.2	123.6
15	264.9	245.4	223.6	182.8	106.2	102.5	121.0	127.8
20	278.1	214.3	291.8	209.1	101.4	107.0	132.1	139.6
25	288.1	213.9	279.3	224.4	110.9	107.0	127.3	140.4
30	245.3	186.8	353.3	227.8	105.4	99.9	120.1	142.9
35	155.8	156.3	292.6	216.2	94.9	91.9	99.6	102.2
40	157.7	172.3	301.5	227.7	93.7	97.5	82.6	86.7

*All resistivity data in ohm-cm

TABLE 1.4
SOUNDING RESISTIVITY PROFILE DATA,
CONTROL BOX

Wenner Electrode Spacing	Copperweld X-Axis		Copperweld Y-Axis		Steel Rebar X-Axis		Steel Rebar Y-Axis	
	BC	AC	BC	AC	BC	AC	BC	AC
2	83.7*	49.7	71.9	43.3	43.6	101.7	50.4	59.0
4	92.0	75.8	105.8	72.2	112.6	108.8	79.8	78.8
6	107.2	92.4	102.7	70.9	113.9	115.1	96.1	83.5
8	118.7	98.7	101.6	81.0	124.3	118.2	102.2	109.6
10	99.7	102.8	145.0	100.8	124.4	117.4	119.5	111.4
15	131.8	128.9	116.8	115.8	143.4	135.8	147.3	137.2
20	195.4	209.0	190.1	146.6	127.0	123.8	140.4	148.1

*All resistivity data in ohm-cm.

TABLE 1.5
DISTANCE RESISTIVITY PROFILE DATA,
CONTROL BOX

Distance From Box Center (10 cm Electrode Sp)	Copperweld X-Axis		Copperweld Y-Axis		Steel X-Axis		Steel Y-Axis	
	BC	AC	BC	AC	BC	AC	BC	AC
- 40 cm	118.0*	139.5	126.1	128.3	95.3	110.1	144.7	153.1
- 35	133.0	131.5	132.0	126.2	109.7	117.8	161.0	156.3
- 30	149.3	159.5	169.8	145.1	169.7	160.9	160.0	159.2
- 25	164.9	181.8	184.3	157.1	205.9	211.1	174.2	172.7
- 20	170.1	170.6	179.1	143.0	163.2	165.2	192.8	189.4
- 15	173.7	150.8	208.9	152.7	151.4	149.1	152.5	155.0
- 10	106.3	156.3	179.0	117.8	137.2	132.0	145.5	146.3
- 5	107.8	101.1	129.3	110.7	115.8	138.4	141.0	136.3
0	100.7	99.7	103.7	86.0	113.2	116.3	131.9	128.6
5	146.0	99.6	156.4	*853.8	127.9	136.7	145.4	121.7
10	192.3	123.5	196.8	126.9	150.0	140.6	147.6	128.8
15	187.8	133.5	197.6	164.5	175.4	175.1	149.5	135.4
20	142.3	140.2	159.1	172.1	162.1	159.1	168.8	139.7
25	133.0	135.0	138.0	153.3	162.8	162.7	186.8	164.5
30	149.3	154.6	133.7	153.0	124.3	125.5	166.8	155.7
35	132.7	135.9	115.4	125.9	90.3	114.9	165.5	148.5
40	117.5	140.6	99.7	108.1	94.3	100.7	128.7	132.3

*All resistivity data in ohm-cm

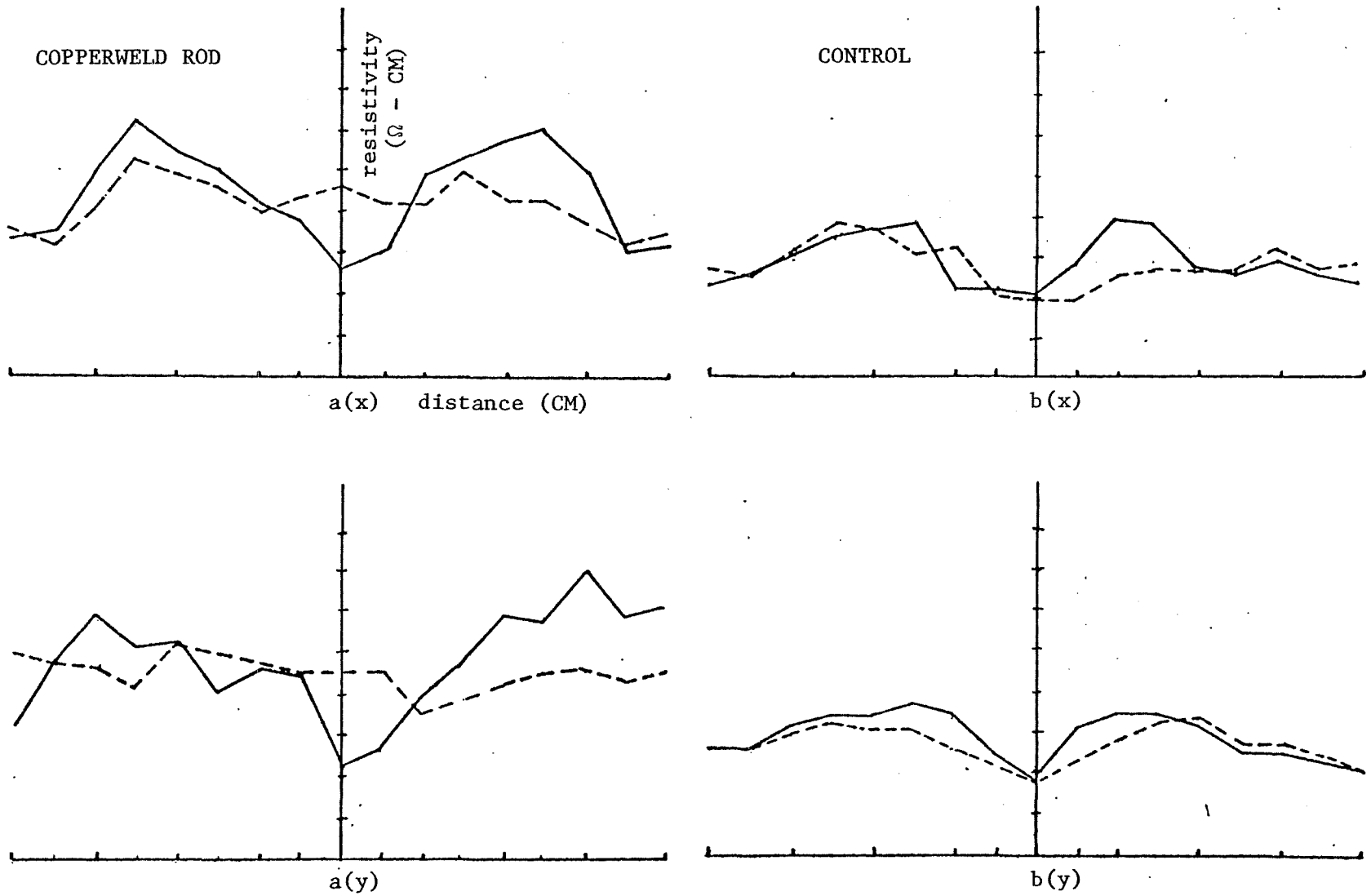


Fig. 1.7 Distance Resistivity Profile for Copperweld Rod (a) & Control (b), Before Corrosion (——), after corrosion (---), for two Wenner electrode arrangements (x, y)

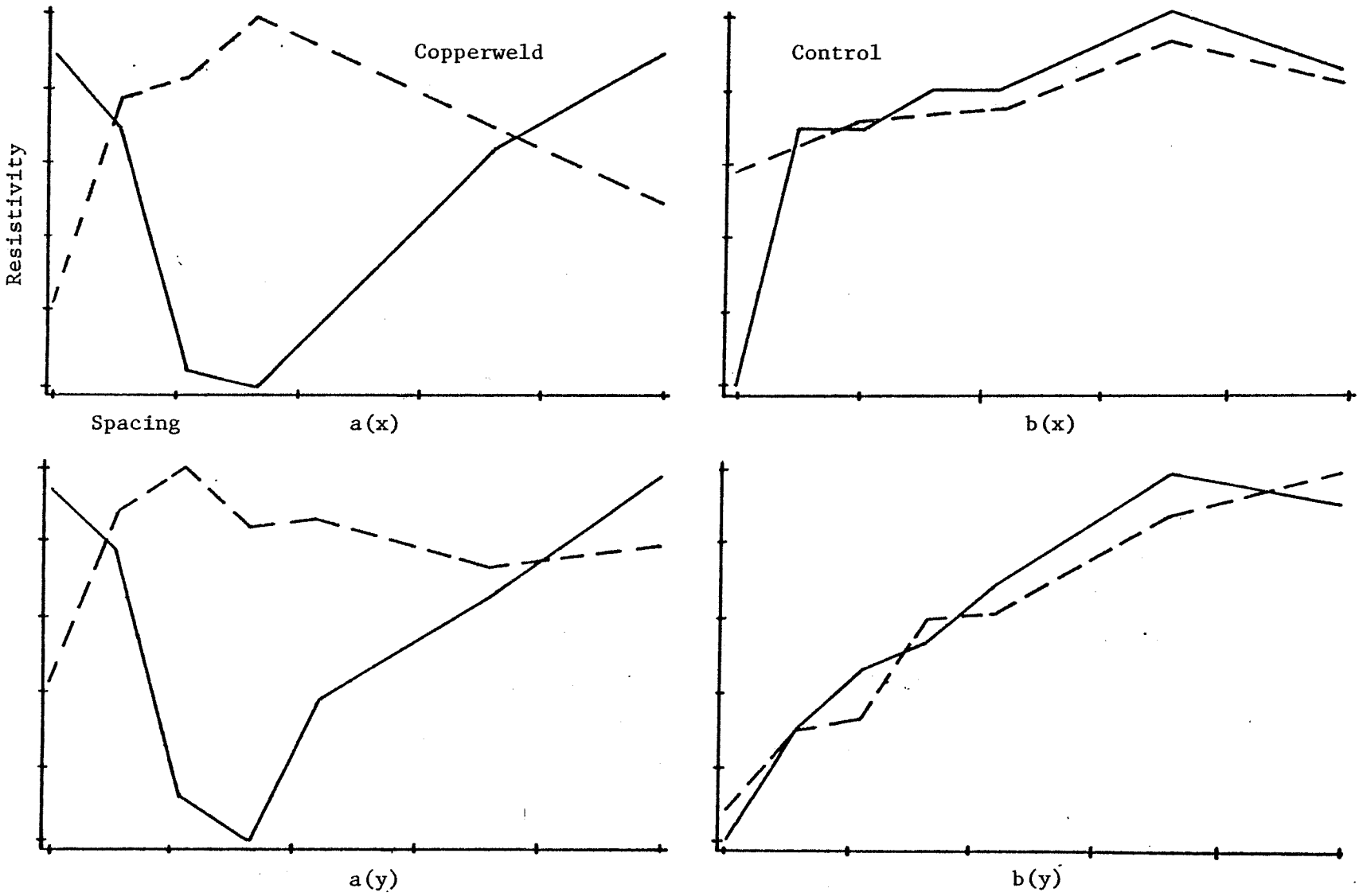


Fig. 1.8 Electrode Spacing (cm) vs. Resistivity (Ω-cm) for Copperweld Corrosion a(x,y) and Control b(x,y), (——) Before Corrosion, (- - -) After Corrosion

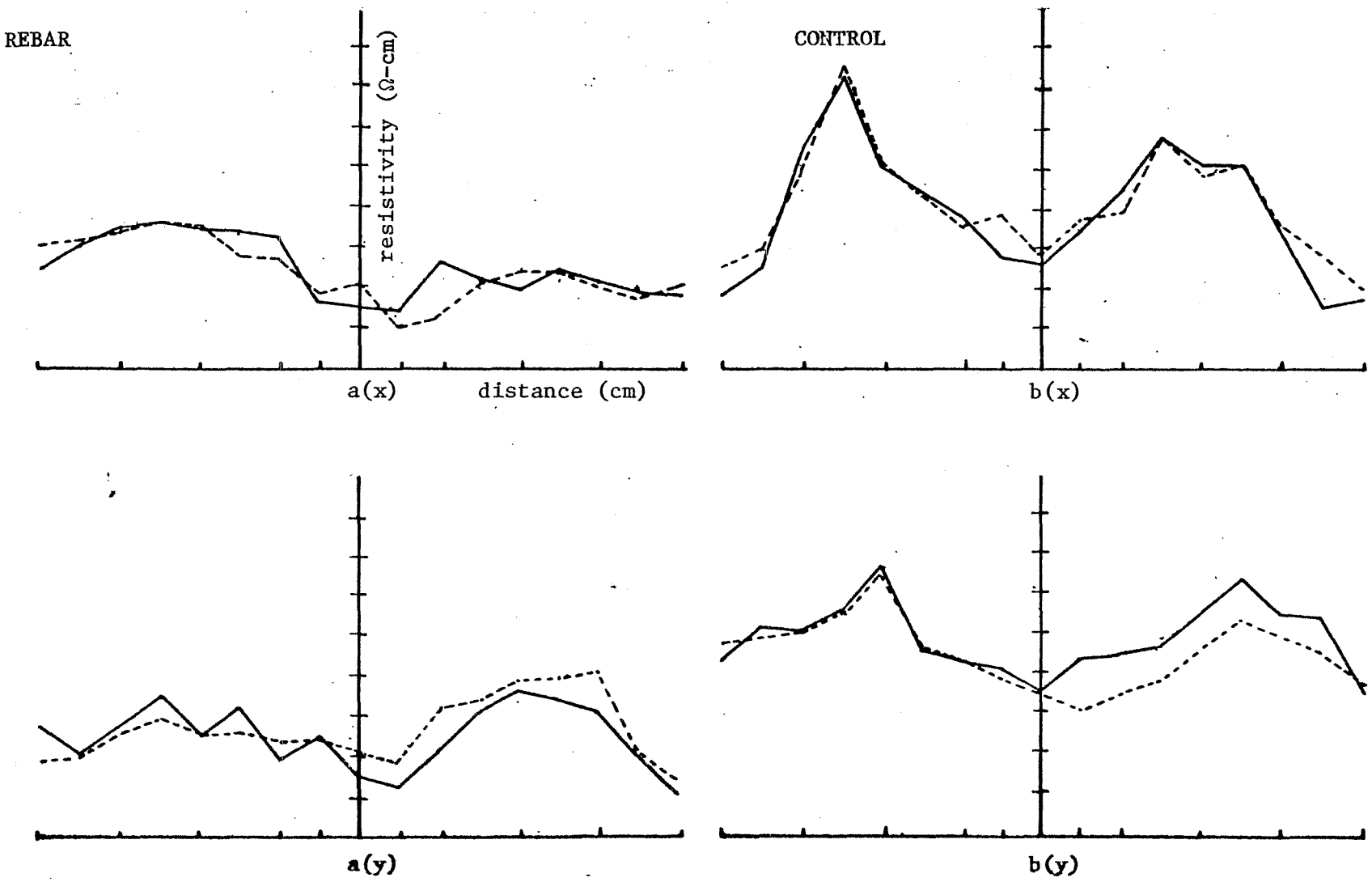


Fig. 1.9 Rebar (a) & Control (b) Resistivity Distance Profile, (——) Before Corrosion, (---) After Corrosion, for Two Wenner Electrode Configurations (x,y)

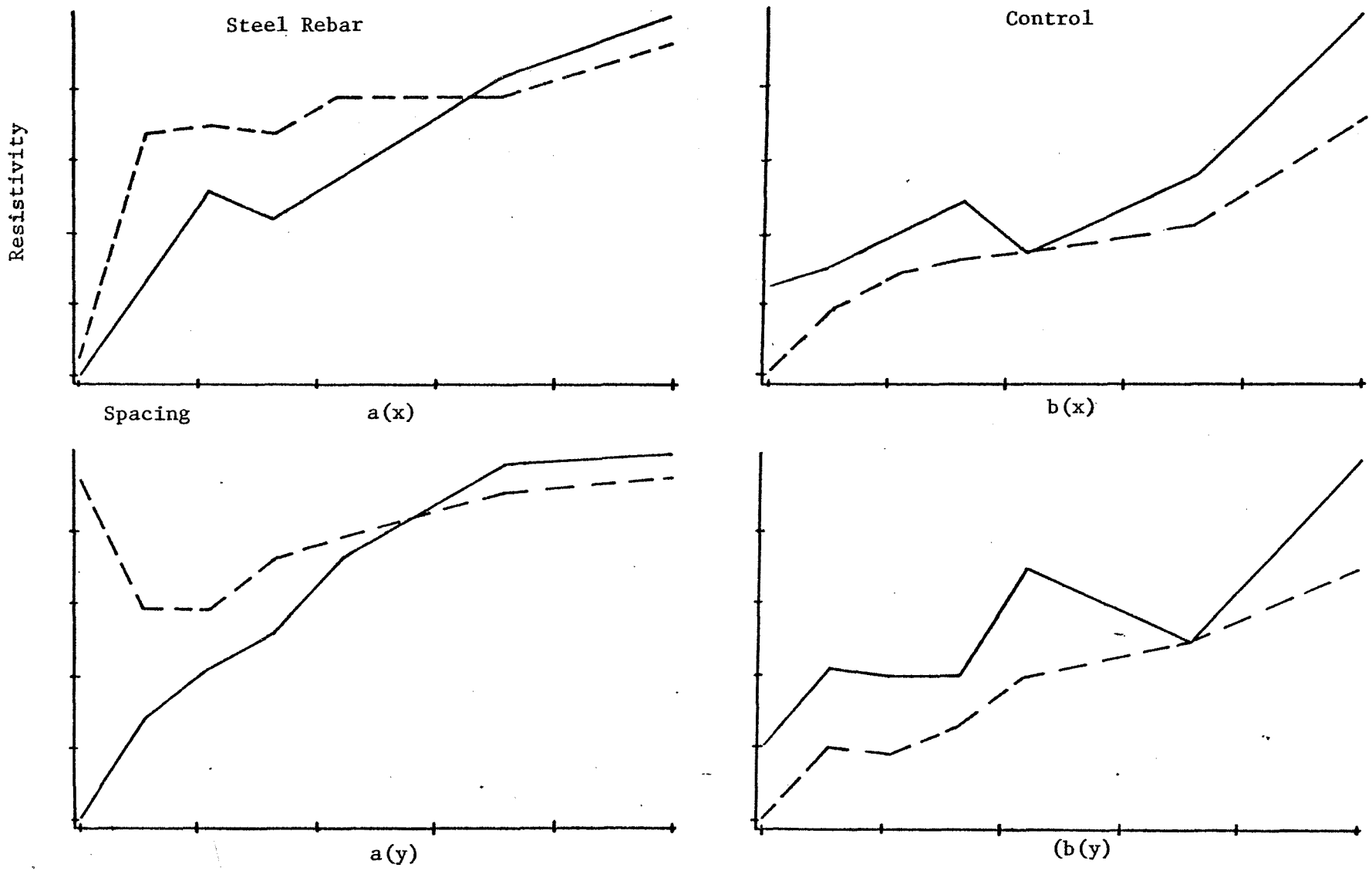


Fig. 1.10 Electrode Spacing (cm) vs. Resistivity (Ω-cm) for Steel Rebar Corrosion a(x,y) and Control b(x,y), (——) Before Corrosion, (---) After Corrosion

Past studies have tried to show a correlation between soil resistivity and corrosion[2,3,4]. The relationship in all cases was not straight forward, there exist far too many variables. It has been shown that if soil resistivity is low the chances of a metal corroding are greatly increased[2]. Rainfall also contributes significantly to corrosion rate; increased rainfall decreases soil resistivity thus increasing corrosion[3]. Using soil resistivity to monitor corrosion is very difficult, as suggested in the references too many variables are present to make hard fast conclusions.

In our experiments an effort was made to keep soil moisture constant. Results from control boxes shows success, in some cases soil resistivity was actually lowered. Resistivity measurements before and after corrosion revealed some known facts but in all cases did not conclusively show corrosion activity. All corrosion boxes exhibited an increase in soil resistivity near the rod due to the migration of water towards the cathode and the drying effect produced by heat generated by the anode[5]. Ideally corrosion should increase the metallic ion concentration around the rod thus decreasing the soil resistivity e.g. the results obtained from the X-axis in Fig. 1.7. Realistically, under tightly controlled conditions, it may be possible to monitor corrosion using soil resistivity measurements; however from our laboratory results even under such conditions variability exists. Use of statistical analysis, suggested by Scott[2], may make it possible to observe trends in resistivity with corrosion.

Although data is slow in coming work progresses and to date some encouraging results have appeared. It has been demonstrated that corrosion is a definite problem in ground beds and if left unchecked can actually sever ground connections. Corrosion while difficult to prevent can be retarded and monitored.

1.5 REFERENCES

1. Uhlig, H. H., "Corrosion and Corrosion Control," John Wiley and Sons, Inc., New York (1971) second edition.

2. Scott, G. N., "The Distribution of Soil Conductivities and Some Consequences," Corr. 14:396 (1958).

3. Costanzo, F. E., "Weather vs. Cathodic Protection of Under-Ground Pipe Lines," 14:363 (1958).

4. Romanoff, M., "Underground Corrosion," Nat. Bureau of Standards Circular 579, Wash. (1957).

5. Uhlig, H. H., "Corrosion Handbook," John Wiley and Sons, Inc. New York, (1948).

CHAPTER II

CABLE SPLICES AND SOME OF THEIR EFFECTS ON THE SAFETY GROUND SYSTEM [4]

2.1 INTRODUCTION

During the past year some extensive research has been administered in the area of cable splices in trailing cables of low voltage coal mining equipment. Conclusions were made concerning the relative humidity of the air and what effects it has on the amount of leakage current into the surrounding soil. Also, a correlation was developed between the power being dissipated from a splice and the added resistance of a conductor due to the connection made within a splice. Finally, some very interesting information was obtained when the ground wires of trailing cables were monitored as splices were added or removed. A detailed discussion is provided on each of these subjects in the following pages.

2.2 RELATIVE HUMIDITY INVESTIGATION

This research was performed inside a laboratory where the primary concern was to maintain as near an underground mine atmosphere as could be maintained without developing or introducing new problems. Portions of portable trailing cables containing cable splices were obtained from a local coal company. Seven-foot segments of cable were prepared containing from one to three cable splices. These splices had been prepared by coal miners upon the working section. By the splices being constructed within the mines, actual coal mine conditions could be better simulated.

The method used to monitor the relative humidity is shown in Fig. 2.1. A Phys-Chemical Research Corporation humidity sensor was used in the portion of the circuit labeled RH^1. The sensor is a non-linear resistive device which decreases in resistance as the relative humidity increases.

Each sensor circuit must be calibrated in order to obtain an accurate relative humidity reading. To achieve the calibration the sensor is replaced by a variable resistor. The range at which one is interested in measuring the relative humidity will determine the value of the variable resistor. For this research the range of 10% to 80% relative humidity was chosen. At each setting of the resistor the voltage (V_{out}) was read and tabulated. A graph was provided with the sensor that showed the resistance value vs. the percent relative humidity. After a significant number of values were obtained a graph displaying the voltage vs. the percent relative humidity was plotted. This graph provided a convenient method to determine what percentage of the relative humidity is being detected by the RH sensor. This plot can be seen in Fig. 2.2. Along with the percent relative humidity measurements, the temperature in degrees centigrade was recorded. From the table it can be seen that the temperature was kept at a relatively constant value as the percent relative humidity fluctuated.

Figure 2.1

Relative Humidity Circuit

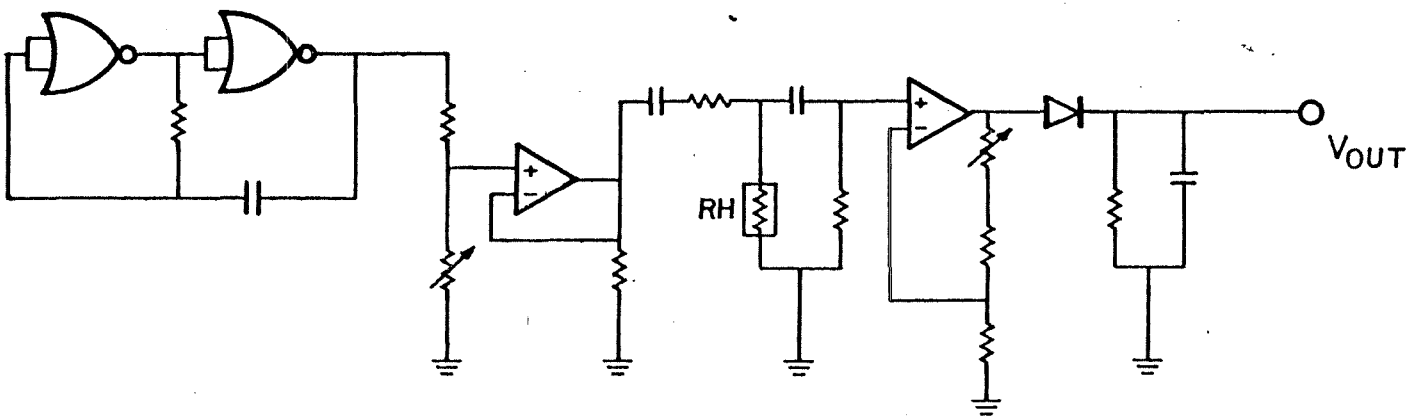
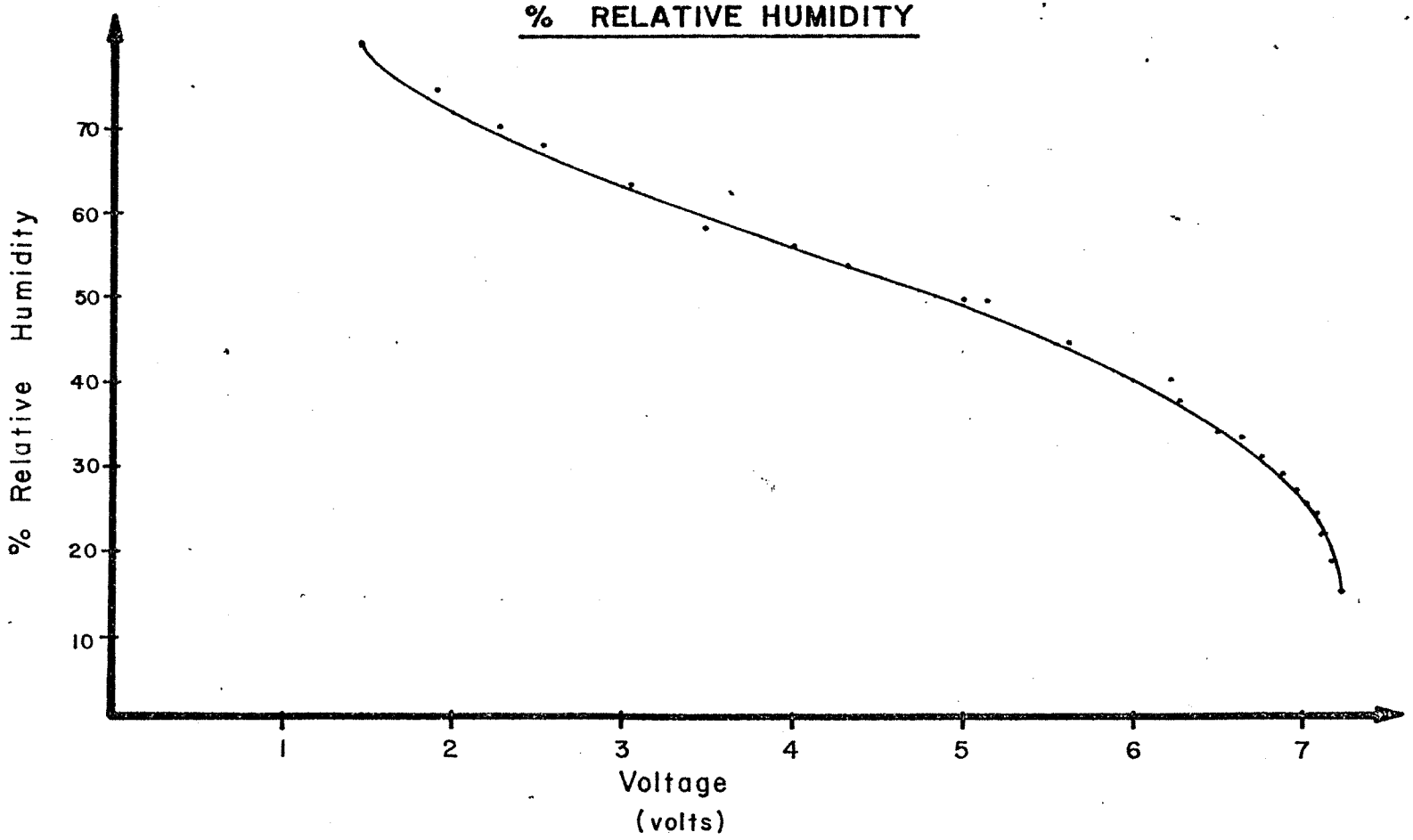


Figure 2.2

VOLTAGE

VS

% RELATIVE HUMIDITY



One gallon of water was added to the soil whenever a ground resistance of 0.91 ohms was measured between the two copper wires embedded within the soil. This was to prevent total desiccation of the soil and to maintain a constant soil resistance. The water was applied by a hand sprinkler.

A cable containing one splice was under test for three months. During this time the percent relative humidity, temperature, and leakage current were recorded daily. To determine the source of the leakage, a segment of cable with no splices was placed upon the soil bed and monitored for one month. The results showed that some leakage did occur, but the magnitude was so very small compared to the magnitude of the current measured when splices were involved that the current was being supplied through the splices. The segment containing no splices was taken from the same piece of cable as the other segments of cable being used to insure that the leakage contributed through the insulation of the cable due to wear remained nearly the same. After this testing, segments of cable with more than one splice were placed upon the soil bed to see if any changes in leakage current could be detected. As can be seen from Tables 2.1 - 2.4, the level of leakage current did increase.

2.3 ANALYSES OF DATA

The data was fed into the computer and analyzed using the Statistical Analysis System (SAS). One interesting outcome was that a quadratic relationship exists between the amount of leakage current and the percent relative humidity.

Fig. 2.3 shows a plot of the leakage current vs. the percent relative humidity where random points represent the data taken from the segment of cable containing no splices. The solid curve was developed by the computer statistical analysis and is represented by:

$$y = 0.16x^2 - 0.04x + 0.007$$

The R^2 value is 0.935 indicating a good approximation. (R^2 is a coefficient indicating the fraction of the experimental data which fits the regression equation that has been generated.) Fig. 2.4 shows the plot of leakage current vs. the percent relative humidity when a segment of trailing cable was used with only one splice. The equation representing the curve shown is:

$$y = -0.66x^2 + 1.40x - 0.235$$

The R^2 value is 0.94, which was not as good an approximation as before, but still good enough to be considered. Fig. 2.5 displays the results of the data taken from a segment of cable containing two splices. The equation was:

TABLE 2.1 LEAKAGE vs RELATIVE HUMIDITY, NO SPLICES

DATE	ϕ_1 (mA)	ϕ_2 (mA)	ϕ_3 (mA)	TEMPERATURE (°C)	RELATIVE HUMIDITY (%)	BED RESISTANCE (Ω)	NO. OF SPLICES
10/9/76	0.030	0.031	0.031	24	55	0.90	0
10/10/76	0.028	0.028	0.028	24	50		0
10/11/76	0.033	0.034	0.033	27	57		0
10/12/76	0.050	0.050	0.050	25	65		0
10/13/76	0.046	0.046	0.046	25	61		0
10/14/76	0.059	0.059	0.059	25	72		0
10/15/76	0.043	0.044	0.043	26	60	0.90	0
10/16/76	0.030	0.030	0.029	24	55		0
10/17/76	0.027	0.027	0.027	25	50		0
10/18/76	0.048	0.047	0.048	25	63		0
10/19/76	0.031	0.031	0.031	25	54		0
10/20/76	0.025	0.025	0.025	23	45		0
10/21/76	0.022	0.023	0.022	24	43	0.89	0
10/22/76	0.028	0.028	0.028	24	49		0
10/23/76	0.018	0.019	0.018	24	40		0
10/24/76	0.022	0.022	0.022	24	43		0
10/25/76	0.015	0.016	0.016	24	38		0

TABLE 2.1 Cont.

DATE	ϕ_1 (mA)	ϕ_2 (mA)	ϕ_3 (mA)	TEMPER-ATURE (°C)	RELATIVE HUMIDITY (%)	BED RE-SISTANCE (Ω)	NO. OF SPLICES
1o/26/76	0.009	0.009	0.009	24	32		0
10/27/76	0.013	0.013	0.013	25	36	0.90	0
10/28/76	0.027	0.027	0.027	25	47		0
10/29/76	0.032	0.030	0.031	26	56		0
10/30/76	0.047	0.047	0.047	25	62		0
10/31/76	0.047	0.047	0.047	25	62		0
11/1/76	0.032	0.032	0.032	25	57		0
11/2/76	0.031	0.031	0.031	25	55	91	0
11/3/76	0.028	0.027	0.029	25	50		0
11/4/76	0.044	0.043	0.044	25	61		0
11/5/76	0.048	0.047	0.048	27	63	0.91	0

TABLE 2.2 LEAKAGE vs RELATIVE HUMIDITY, ONE SPLICE

DATE	ϕ_1 (mA)	ϕ_2 (mA)	ϕ_3 (mA)	TEMPER-ATURE (°C)	RELATIVE HUMIDITY (%)	BED RE-SISTANCE (Ω)	NO. OF SPLICES
07/29/76	.496	.481	.490	23	85	0.90r	1
07/30/76	.528	.528	.533	23	89	0.91r	1
07/31/76	.489	.468	.477	24	83		1
08/1/76	.469	.451	.460	25	82		1
08/2/76	.420	.405	.415	26	67		1
08/3/76	.399	.382	.393	25	62		1
08/4/76	.407	.391	.401	27	66		1
08/5/76	.438	.425	.451	26	80%		1
08/6/76	.420	.424	.433	26	70%	0.89	1
08/7/76	.464	.449	.457	25	81		1
08/8/76	.446	.428	.437	25	72		1
08/9/76	.424	.409	.418	25	68		1
08/10/76	.443	.428	.436	25	71		1
08/11/76	.465	.447	.445	24	79		1
08/12/76	.459	.459	.461	24	82		1
08/13/76	.492	.478	.436	26	84	0.90	1
08/14/76	.483	.471	.480	23	84		1

TABLE 2.2 Cont.

DATE	ϕ_1 (mA)	ϕ_2 (mA)	ϕ_3 (mA)	TEMPER-ATURE (°C)	RELATIVE HUMIDITY (%)	BED RE-SISTANCE (Ω)	NO. OF SPLICES
08/15/76	.440	.430	.453	24	80		1
08/16/76	.444	.436	.444	24	79		1
08/17/76	.420	.407	.415	24	67		1
08/18/76	.415	.405	.413	24	66		1
08/19/76	.395	.378	.389	25	60		1
08/20/76	.402	.384	.392	24	84	0.90	1
08/21/76	.391	.370	.380	24	58		1
08/22/76	.190	.184	.180	22	33		1
08/23/76	.204	.193	.200	22	37		1
08/24/76	.179	.171	170	23	50		1
08/25/76	.216	.200	.205	24	42		1
08/26/76	.301	.296	.291	25	51		1
08/27/76	.325	.316	.316	25	48	0.91	1
08/28/76	.349	.345	.340	25	54		1
08/29/76	.351	.347	.345	26	57		1
08/30/76	.325	.321	.319	24	60		1
08/31/76	.266	.260	.259	24	46		1

TABLE 2.2 Cont.

DATE	ϕ_1 (mA)	ϕ_2 (mA)	ϕ_3 (mA)	TEMPER-ATURE (°C)	RELATIVE HUMIDITY (%)	BED RE-SISTANCE (Ω)	NO. OF SPLICES
09/1/76	.397	.390	.389	24	61		1
09/2/76	.359	.352	.350	24	65		1
09/3/76	.413	.409	.407	23	66	0.89	1
09/7/76	.419	.411	.412	22	67		1
09/8/76	.433	.427	.425	23	70		1
09/9/76	.452	.448	.446	24	76		1
09/10/76	.459	.454	.456	25	80		1
09/11/76	.407	.400	.399	25	65		1
09/12/76	.402	.397	.394	26	64		1
09/13/76	.426	.421	.419	25	68	.90	1
09/14/76	.443	.439	.438	24	72		1
09/15/76	.445	.439	.436	24	71		1
09/16/76	.480	.473	.470	24	83		1
09/17/76	.469	.463	.462	24	81		1
09/18/76	.397	.392	.388	24	61		1
09/19/76	.349	.343	.342	24	55		1
09/20/76	.357	.351	.351	23	57	.90	1

TABLE 2.2 Cont.

DATE	ϕ_1 (mA)	ϕ_2 (mA)	ϕ_3 (mA)	TEMPERATURE (°C)	RELATIVE HUMIDITY (%)	BED RESISTANCE (Ω)	NO. OF SPLICES
09/21/76	.343	.337	.333	24	50		1
09/22/76	.355	.350	.349	24	56		1
09/23/76	.337	.332	.330	24	56		1
09/29/76	.206	.200	.202	25	41		1
09/30/76	.223	.217	.215	25	42		1
10/1/76	.209	.201	.199	27	41		1
10/2/76	.189	.184	.180	26	40	.91	1
10/3/76	.213	.209	.206	24	42		1
10/4/76	.258	.250	.249	22	45		1
10/5/76	.263	.261	.261	24	46		1
10/6/76	.307	.301	.300	25	51		1
10/7/76	.329	.324	.321	25	60		1
10/8/76	.323	.317	.315	25	52	.90	1

TABLE 2.3 LEAKAGE vs RELATIVE HUMIDITY, TWO SPLICES

DATE	ϕ_1 (mA)	ϕ_2 (mA)	ϕ_3 (mA)	TEMPER-ATURE (°C)	RELATIVE HUMIDITY (%)	BED RE-SISTANCE (Ω)	NO. OF SPLICES
11/6/76	.427	.425	.425	25	65	.91	2
11/7/76	.459	.456	.457	25	72		2
11/8/76	.489	.484	.483	24	80		2
11/9/76	.486	.479	.479	24	79		2
11/10/76	.436	.430	.431	24	69		2
11/11/76	.460	.455	.454	24	71		2
11/12/76	.428	.424	.425	23	66	.90	2
11/13/76	.426	.417	.419	23	63		2
11/14/76	.405	.398	.398	23	57		2
11/15/76	.397	.392	.390	23	54		2
11/16/76	.423	.417	.417	23	60		2
11/17/76	.349	.341	.343	24	51		2
11/18/76	.333	.325	.326	25	49	.90	2
11/19/76	.407	.399	.398	25	55		2
11/20/76	.387	.380	.380	25	52		2
11/21/76	.380	.372	.372	25	51		2
11/22/76	.424	.417	.416	24	60		2

TABLE 2.3 Cont.

DATE	ϕ_1 (mA)	ϕ_2 (mA)	ϕ_3 (mA)	TEMPER-ATURE (°C)	RELATIVE HUMIDITY (%)	BED RE-SISTANCE (Ω)	NO. OF SPLICES
11/23/76	.443	.436	.437	24	67		2
11/24/76	.437	.430	.429	25	64	.90	2
11/28/76	.410	.403	.403	25	56		2
11/29/76	.339	.331	.331	25	48		2
11/30/76	.298	.292	.289	25	43		2
12/1/76	.331	.325	.326	24	47		2
12/2/76	.247	.241	.240	25	40		2
12/3/76	.409	.400	.399	24	55	.88	2
12/4/76	.423	.416	.416	24	60		2
12/5/76	.379	.372	.370	24	51		2
12/6/76	.437	.430	.430	24	66	.90	2

TABLE 2.4 LEAKAGE vs RELATIVE HUMIDITY, THREE SPLICES

DATE	ϕ_1 (mA)	ϕ_2 (mA)	ϕ_3 (mA)	TEMPERATURE (°C)	RELATIVE HUMIDITY (%)	BED RESISTANCE (Ω)	NO. OF SPLICES
12/7/76	.483	.495	.482	26	72	.90	3
12/8/76	.506	.516	.507	26	75		3
12/9/76	.521	.529	.521	26	80		3
12/10/76	.490	.499	.490	26	73		3
12/11/76	.457	.462	.454	24	69		3
12/12/76	.434	.441	.435	25	60		3
12/13/76	.441	.450	.441	24	62	.92	3
12/14/76	.427	.438	.427	24	56		3
12/15/76	.366	.377	.368	24	49		3
12/16/76	.419	.424	.417	25	54		3
12/17/76	.415	.423	.415	25	54		3
12/18/76	.439	.446	.438	25	61		3
12/19/76	.450	.455	.449	26	66	.91	3
12/20/76	.427	.437	.429	26	57		3
12/21/76	.408	.416	.408	27	53		3
12/22/76	.359	.368	.359	26	47		3
12/23/76	.300	.317	.301	26	40		3

TABLE 2.4 Cont.

DATE	ϕ_1 (mA)	ϕ_2 (mA)	ϕ_3 (mA)	TEMPER-ATURE (°C)	RELATIVE HUMIDITY (%)	BED RE-SISTANCE (Ω)	NO. OF SPLICES
12/27/76	.382	.389	.382	25	48		3
12/28/76	.409	.415	.407	24	53	.89	3
12/29/76	.431	.440	.432	24	58		3
12/30/76	.450	.462	.450	25	63		3
12/31/76	.436	.444	.435	24	60		3
1/1/77	.453	.464	.453	24	65		3
1/2/77	.479	.493	.480	24	72		3
1/3/77	.456	.466	.457	25	69	.90	3
1/4/77	.452	.460	.452	25	63		3
1/5/77	.455	.466	.457	25	65		3
1/6/77	.461	.470	.462	25	68	.89	3

Figure 2.3

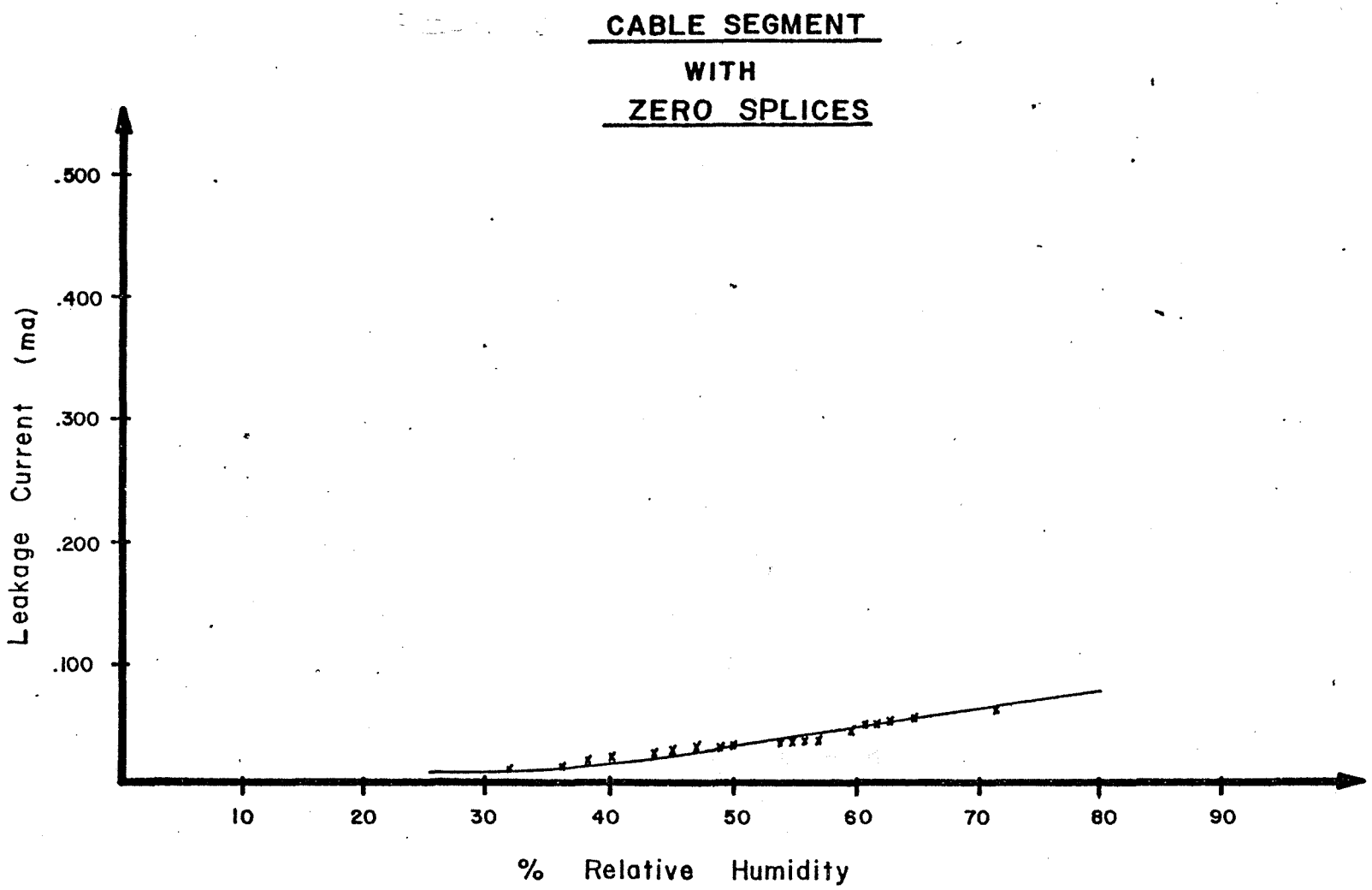

CABLE SEGMENT
WITH
ZERO SPLICES
.500
.400
.300
.200
.100
Leakage Current (ma)
10
20
30
40
50
60
70
80
90
% Relative Humidity

Figure 2.4

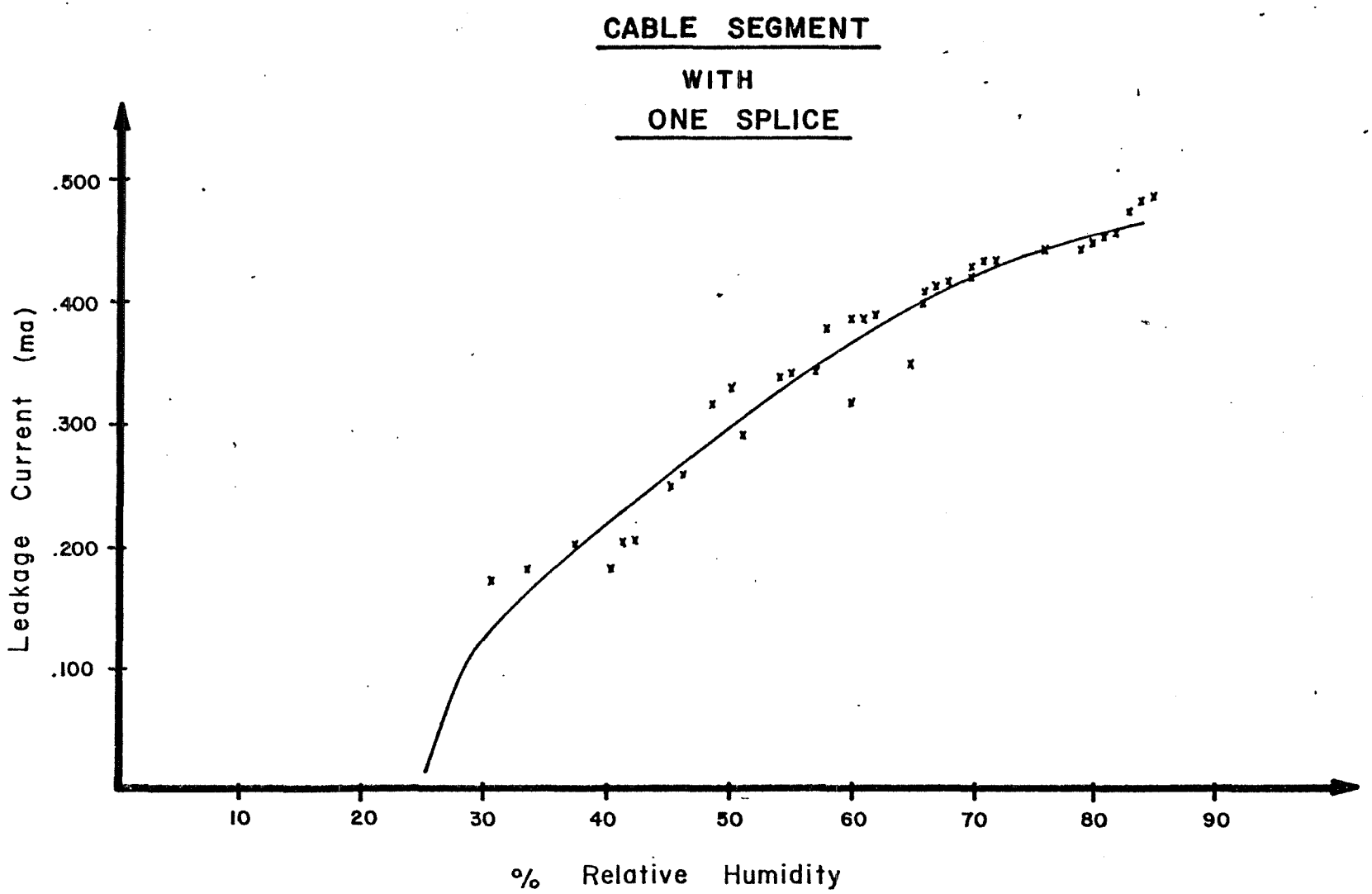
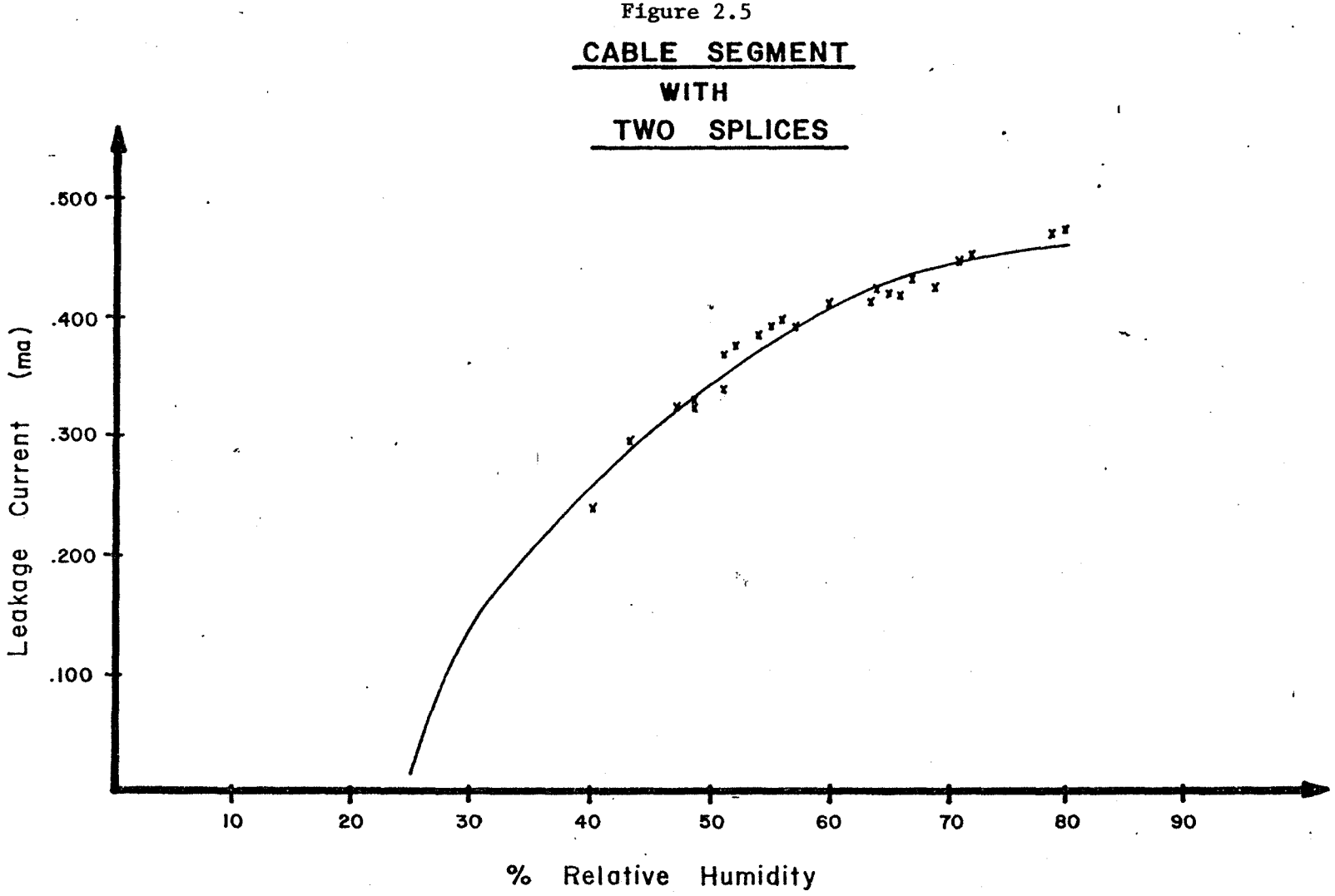

CABLE SEGMENT
WITH
ONE SPLICE
.500
.400
.300
.200
.100
Leakage Current (ma)
10
20
30
40
50
60
70
80
90
% Relative Humidity

Figure 2.5


CABLE SEGMENT
WITH
TWO SPLICES
.500
.400
.300
.200
.100
Leakage Current (ma)
10
20
30
40
50
60
70
80
90
% Relative Humidity

$$y = -1.25x^2 + 2.02x - 0.350$$

and the R^2 value was 0.96. Finally, Fig. 2.6 shows the plot of the data obtained when a segment of trailing cable containing three splices was tested. The equation from which the curve was plotted is:

$$y = -0.61x^2 + 1.21x - 0.069$$

with R^2 having a value of 0.96.

The data used in the statistical analysis was taken from under the heading $\emptyset_3$ of the leakage current located in the tables. Because the other phases maintained basically the same magnitude, as $\emptyset_3$, no statistical analysis was performed upon them.

With the exception of the graph showing the data that was taken from a segment of cable having no splices, one can see from the other three graphs that the curves when plotted followed basically the same pattern. As the number of splices increased new curves were developed indicating that cable splices in portable trailing cables are related to the amount of leakage current that can be detected. This relationship would explain why various magnitudes of leakage could be measured at different intervals of time.

2.4 ADDED RESISTANCE TO A CONDUCTOR

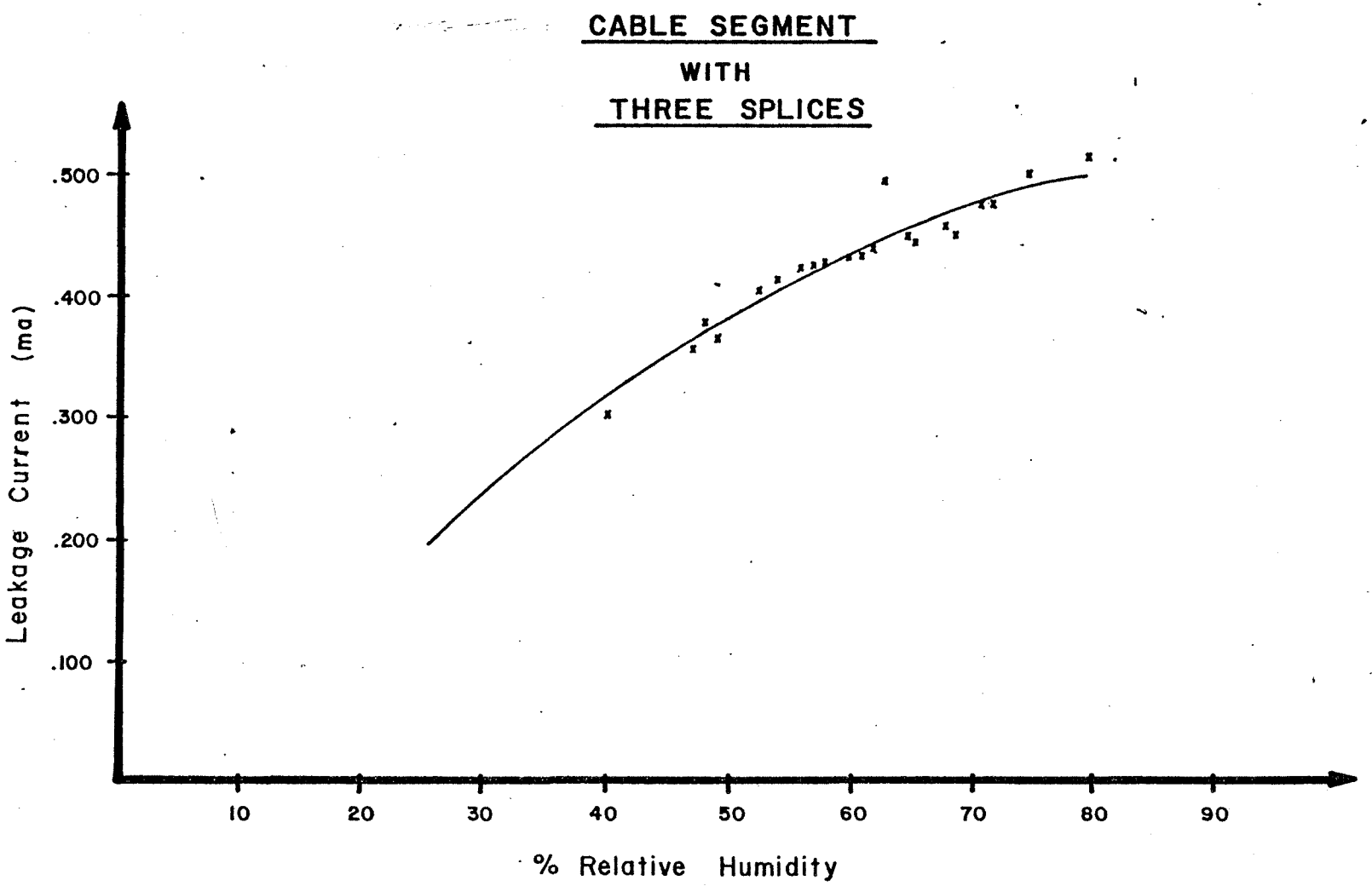
Usually the failure of most cable splices in portable trailing cables of underground coal mining equipment can be linked directly or indirectly to the connector used to join the two ends of a conductor together. Before researchers can improve on the quality of the connections they have to know where they presently stand. An excellent place to begin is to determine, on the average, how much resistance is added to a conductor when a splice is placed within a cable. Because of the in-mine set-up, making direct resistance measurements would be very impractical and inconvenient. So these types of measurements were performed at cable repair shops. At these shops, both ends of the cable are accessible, the length of the cable can be measured, and the number of splices contained within the cable can be readily determined.

The procedure used to conduct the resistance measurements was to arrange a trailing cable so that both ends were accessible, then using a Bison ground resistivity meter and an amplifier, designed expecially for the meter, connect the meter in series with one of the conductors at a time. The size of the conductors ranged from #4/0 - #6 AWG wire, which encompasses about all the sizes of power conductors used in portable trailing cables. The actual resistance measured cannot be read directly from the meter, but has to be calculated in the following manner.

$$\text{Actual Resistance} = (\text{Bison Reading})/(2\pi K)\text{ohms}$$

$$K = \text{Amplification Factor}$$

Figure 2.6


CABLE SEGMENT
WITH
THREE SPLICES
.500
.400
.300
.200
.100
Leakage Current (ma)
10
20
30
40
50
60
70
80
90
% Relative Humidity

These values are listed under the heading "Actual Resistance" in Table 2.5. The values listed under the heading "Calculated Resistance" were obtained from charts provided in a handbook and show what that particular conductor should read if no splices were contained[2]. The rest of the headings should be self-explanatory.

A statistical analysis was performed on the data. Using an HP-25 calculator the mean and standard deviations were calculated for the data. Because of the lack of enough data for each size of conductor these values were not calculated for each individual size. Using the data from the heading "Increase Per Splice" the following information was obtained:

$$\text{Average} \qquad \bar{x} = 0.03516 \text{ ohms}$$

$$\text{Standard Deviation} \qquad S_x = 0.05492 \text{ ohms}$$

Suggesting that if a conductor had as much as 100 amperes traveling along it, then 351 watts of power could be dissipated at the splice.

$$P_D = I^2R$$

$$= (100)^2(0.03516)$$

$$= 351.60 \text{ watts}$$

One must remember that the values for the average includes the whole range and cannot be applied to just one size of conductor, but the value does give a good indication as to the order of magnitude of the resistance that may be added to a conductor through a cable splice.

2.5 TEMPERATURE MEASUREMENTS

The temperature tests were performed on cable splices contained in portable trailing cables where the power conductor size was #1/0 and the cable was connected to a low voltage machine in operation inside the coal mine. A portable infared thermometer (Barnes Engineering Company Model PRT-11) was used to make the temperature measurement. A ruler was placed along the side of the cable and measurements were taken every inch. After several trial measurements a length of 36 inches was found to be sufficient to cover the entire change in temperature experienced across the cable splice. The operating temperature of the cable after several hours of operation by the equipment was found to be around 50°C, which can be expected considering that from 200-400 amperes may be passing along the conductors. The temperature measurements were taken at a place where the air velocity appeared to be minimal. Figures 2.7 through 2.9 show plots of the temperature data taken. The horizontal axis is the change in length and the vertical axis is the change in temperature with zero on the vertical scale representing 50° centigrade.

Fig. 2.7 shows a change in temperature of 17°C over the 36 inch length. The slope of the lines appear to be relatively constant and

TABLE 2.5 RESISTANCE OF CABLE SPLICES

SIZE CONDUCTOR (AWG)	LENGTH (FT)	BISON READING	CALCULATED RESISTANCE (Ω)	ACTUAL RESISTANCE (Ω)	NUMBER OF SPLICES	INCREASE PER SPLICE (Ω)	K FACTOR
6	600	159.6	0.25114	0.25401	3	0.00096	100
6	600	159.0	0.25114	0.25306	3	0.00192	100
6	600	158.7	0.25114	0.25258	3	0.00048	100
4	500	83.19	0.13144	0.13240	6	0.00016	100
4	500	1255.0	0.13144	1.99740	6	0.31099	100
4	500	12.55.0	0.13144	1.99740	6	0.31099	100
1/0	500	49.41	0.05450	0.07864	2	0.01207	100
1/0	500	47.77	0.05450	0.07603	2	0.01207	100
1/0	500	42.68	0.05450	0.06793	2	0.00672	100
6	320	75.62	0.10405	0.02055	2	0.00815	100
6	320	73.31	0.10405	0.11668	2	0.00632	
6	320	71.40	0.10405	0.11364	2	0.00480	100
2	700	103.6	0.11574	0.16488	4	0.01229	100
2	700	106.6	0.11574	0.16966	4	0.01348	100
2	700	109.3	0.11574	0.17396	4	0.01456	100
2	700	101.3	0.11574	0.16122	5	0.00910	100
2	700	101.3	0.11574	0.16122	5	0.00910	100

TABLE 2.5 Cont.

SIZE CONDUCTOR (AWG)	LENGTH (FT)	BISON READING	CALCULATED RESISTANCE (Ω)	ACTUAL RESISTANCE (Ω)	NUMBER OF SPLICES	INCREASE PER SPLICE (Ω)	K FACTOR
1/0	190	6.909	0.02071	0.02199	2	0.01100	50
4	500	66.10	0.13144	0.21040	3	0.07013	50
4	500	66.61	0.13144	.21203	3	0.07068	50
4	500	64.82	0.13144	0.2o633	3	0.06878	50
2	500	28.26	0.08650	0.08995	4	0.02249	50
2	500	34.24	0.08650	0.10899	4	0.02725	50
2	500	29.68	0.08650	0.09447	4	0.02362	50
6	600	93.06	0.25114	0.29622	10	0.02962	50
6	600	100.00	0.25114	0.31831	10	0.03183	50
6	600	91.24	0.25114	0.29043	10	0.02904	50
4	500	64.38	0.08650	0.20493	6	0.03415	50
4	500	65.36	0.08650	0.20805	6	0.03467	50
4	5000	74.22	0.08650	0.23625	6	0.03937	50
4	500	76.16	0.08650	0.24242	6	0.04040	50
4	500	78.49	0.08650	0.24984	10	0.02498	50
4	500	76.70	0.08650	0.24414	10	0.02441	50

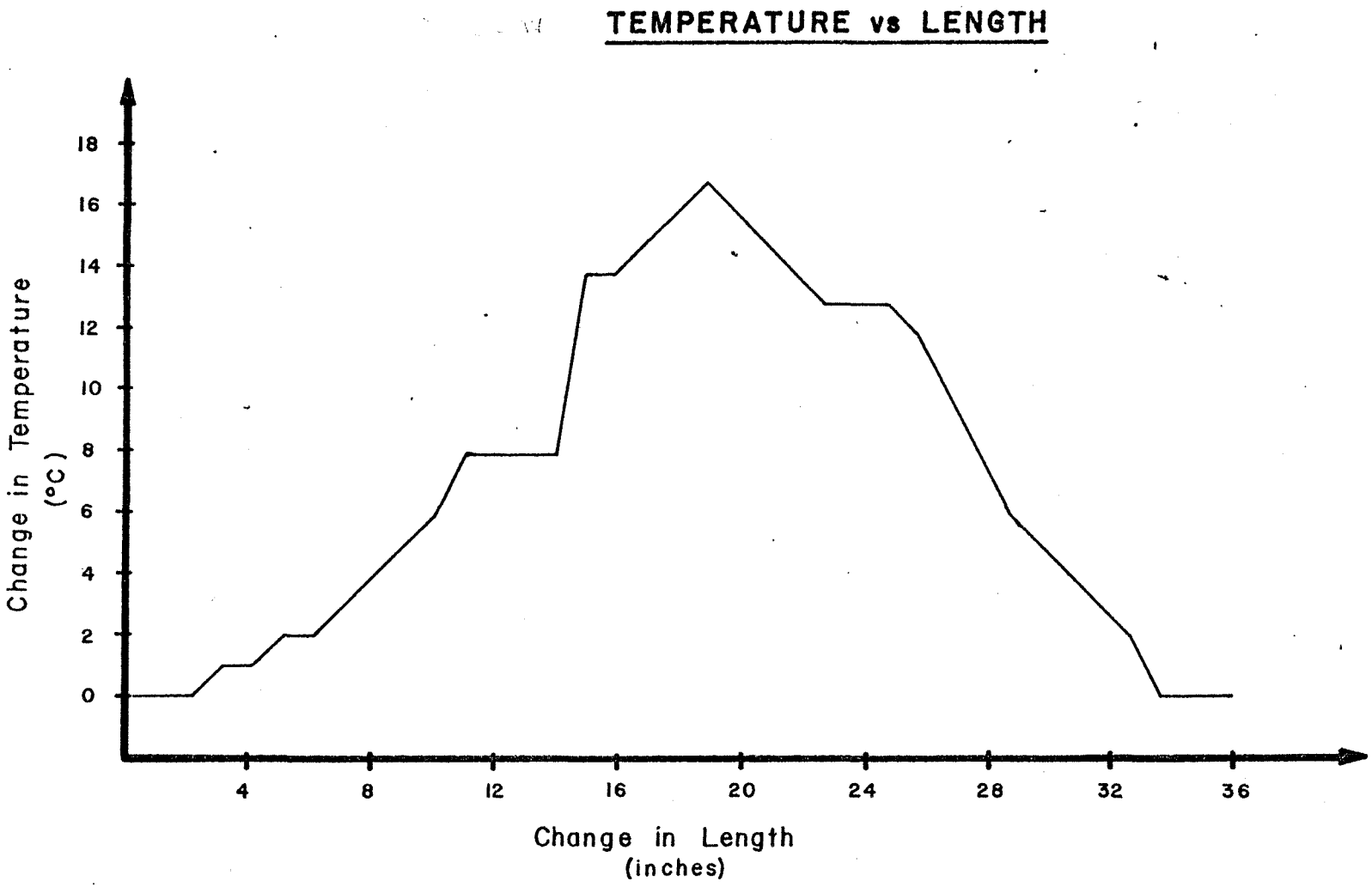
TABLE 2.5 Cont.

SIZE CONDUCTOR (AWG)	LENGTH (FT)	BISON READING	CALCULATED RESISTANCE (Ω)	ACTUAL RESISTANCE (Ω)	NUMBER OF SPLICES	INCREASE PER SPLICE (Ω)	K FACTOR
2	700	101.3	0.11574	0.16122	5	0.00910	100
2	500	60.29	0.08650	0.09595	2	0.00473	100
2	500	59.39	0.08650	0.09452	2	0.00401	100
2	600	101.90	0.10380	0.16218	9	0.00649	100
2	600	102.00	0.10380	0.16234	9	0.00650	100
4/0	800	141.9	0.04320	0.22584	5	0.03653	100
4/0	800	137.8	0.04320	0.21932	5	0.05422	100
4/0	215	2.60	0.01132	0.01730	1	0.00598	23.92
4/0	215	2.60	0.01132	0.01730	1	0.00598	23.92
4/0	215	2.60	0.01132	0.01730	1	0.00598	23.92
6	260	16.65	0.10883	0.11078	4	0.00049	23.92
6	260	16.49	0.10883	0.10972	4	0.00022	23.92
6	260	16.49	0.10803	0.10972	4	0.00022	23.92
#2	125	32.64	0.02163	0.21717	2	0.09777	23.92
#2	125	32.58	0.02163	0.21678	2	0.09758	23.92
4	500	64.66	0.13144	0.20582	3	0.06861	50
4	500	55.94	0.13144	0.17806	3	0.05935	50

TABLE 2.5 Cont.

SIZE CONDUCTOR (AWG)	LENGTH (FT)	BISON READING	CALCULATED RESISTANCE (Ω)	ACTUAL RESISTANCE (Ω)	NUMBER OF SPLICES	INCREASE PER SPLICE (Ω)	K FACTOR
4	500	73.20	0.13144	0.23300	3	0.07767	50
4	500	72.82	0.13144	0.23179	3	0.07726	50
4	500	56.91	0.08650	0.18115	4	0.04529	50
2	800	55.82	0.08650	0.17768	4	0.04442	50
2	500	62.71	0.08650	0.19961	3	0.06654	50
2	500	62.71	0.08650	0.19961	3	0.06654	50
6	500	92.99	0.20928	0.29600	4	0.09867	50
6	500	91.62	0.20928	0.29164	4	0.09721	50
6	500	91.22	0.20928	0.29036	4	0.09679	50
4/0	500	12.18	0.02700	0.03877	6	0.00646	50
4/0	500	12.18	0.02700	0.03877	6	0.00646	50
4/0	500	12.18	0.02700	0.03877	6	0.00646	50
6	650	85.46	0.27206	0.027207	7	0.03886	50
6	650	85.85	0.27206	0.27327	7	0.03904	50
6	650	86.42	.027206	.27508	7	0.03730	50
1/0	190	6.785	0.02071	0.02160	2	0.01080	50
1/0	190	6.478	0.02071	0.02100	2	0.01031	50

Figure 2.7


TEMPERATURE vs LENGTH
Change in Temperature (°C)
0
2
4
6
8
10
12
14
16
18
4
8
12
16
20
24
28
32
36
Change in Length (inches)

approaching 1. With 18 inches representing the middle of the splice, there appears to be one conductor closer to the insulation at that point than any of the others. This would account for the sharp peak and then the decline in temperature. Fig. 2.8 is a good example of a recently made splice with good quality workmanship involved in the construction. The graph shows only a change of 3°C indicating that one of the conductors is a lot closer to the point of insulation being measured than the other conductors. Finally, Fig. 2.9 shows a temperature change that is very high and indicating once again that one conductor was the main cause for the substantial amount of temperature change. Within twenty-one hours after the measurement was made the insulation of the splice burst into flames and completely burned the cable into two pieces. Other splices indicated the same heating problem and after cutting into them the problem was immediately discovered. The connectors used to join the conductors were not crimped sufficiently to secure the strands of the conductor, allowing them free movement. As a result, a high resistance was experienced, causing a lot of heat to be generated.

2.6 CORRELATION DEVELOPMENT

Convection, conduction, and radiation are the three methods by which heat can be dispersed. Because of certain limitations, only convection and radiation were taken under consideration. In order to consider heat lost due to conduction down the wire the temperature of the wire needed to be known, and there was no method available to obtain this information. Free convection was the first factor to be considered.

A horizontal pipe was used to model the conductor and the surrounding gas was air. The following properties were used in the calculations assuming an atmospheric temperature of 60°F.

Viscosity	$N = 0.0455$ lbm ft^{-1} hr^{-1}
Density	$\rho = 0.0719$ 1 bm ft^{-3}
Specific Heat	$\tilde{C}p = 0.236$ BTU lbm^{-1} $^0R^{-1}$
Thermal Conductivity	$K = 0.0152$ BTU hr^{-1} ft^{-1} $^0R^{-1}$
	$\beta = 1/T_f = 1/520$ $^0R^{-1}$
	$g = 4.17 \times 10^8$ ft hr^{-1}

The diameter of the cable was:

$$D = 0.1375 \text{ ft}$$

The equation for heat being dissipated is:[3]

$$Q = hm \pi D \, dT \, d\ell \quad \text{BTU } hr^{-1}$$

Figure 2.8

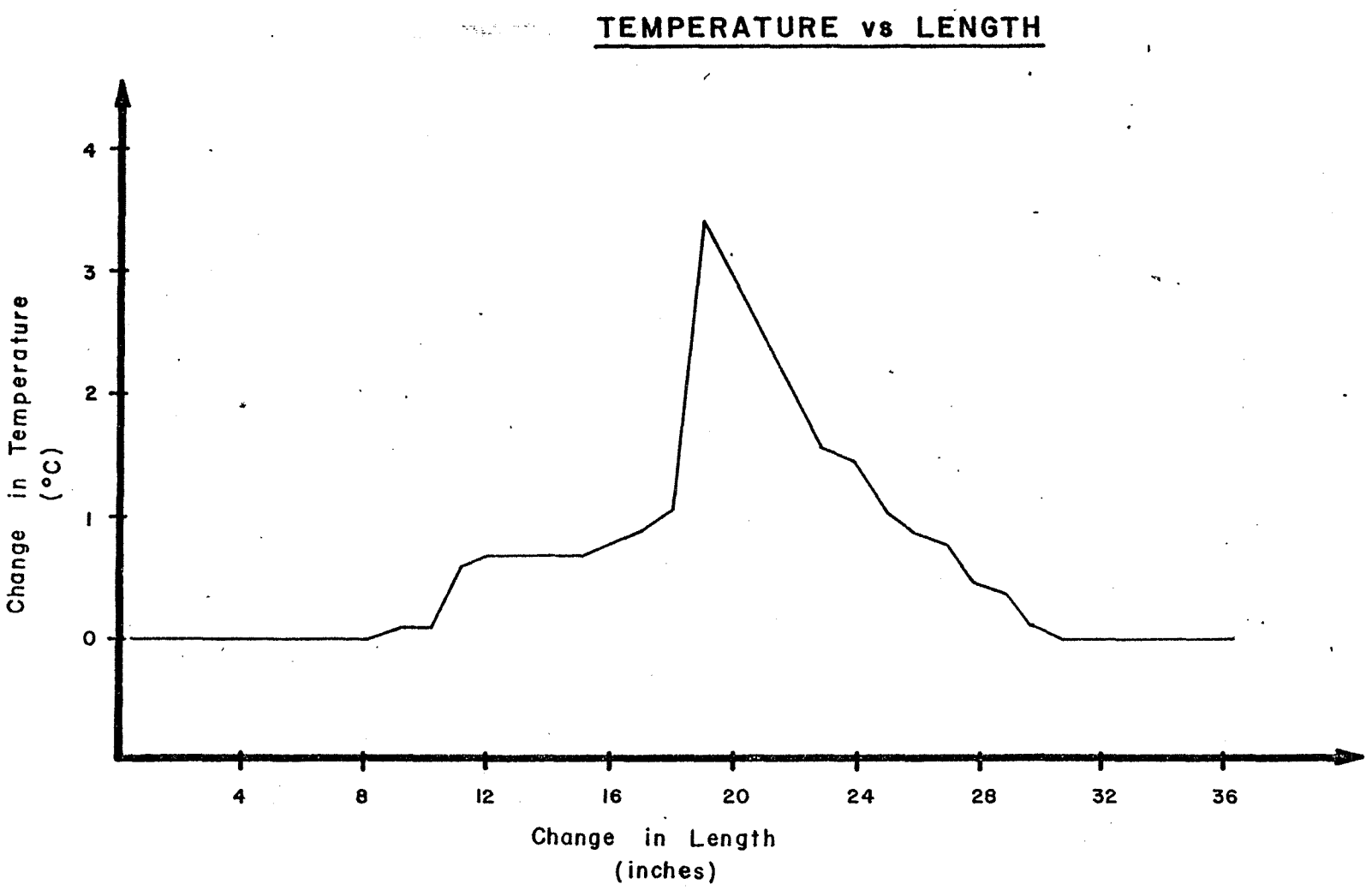
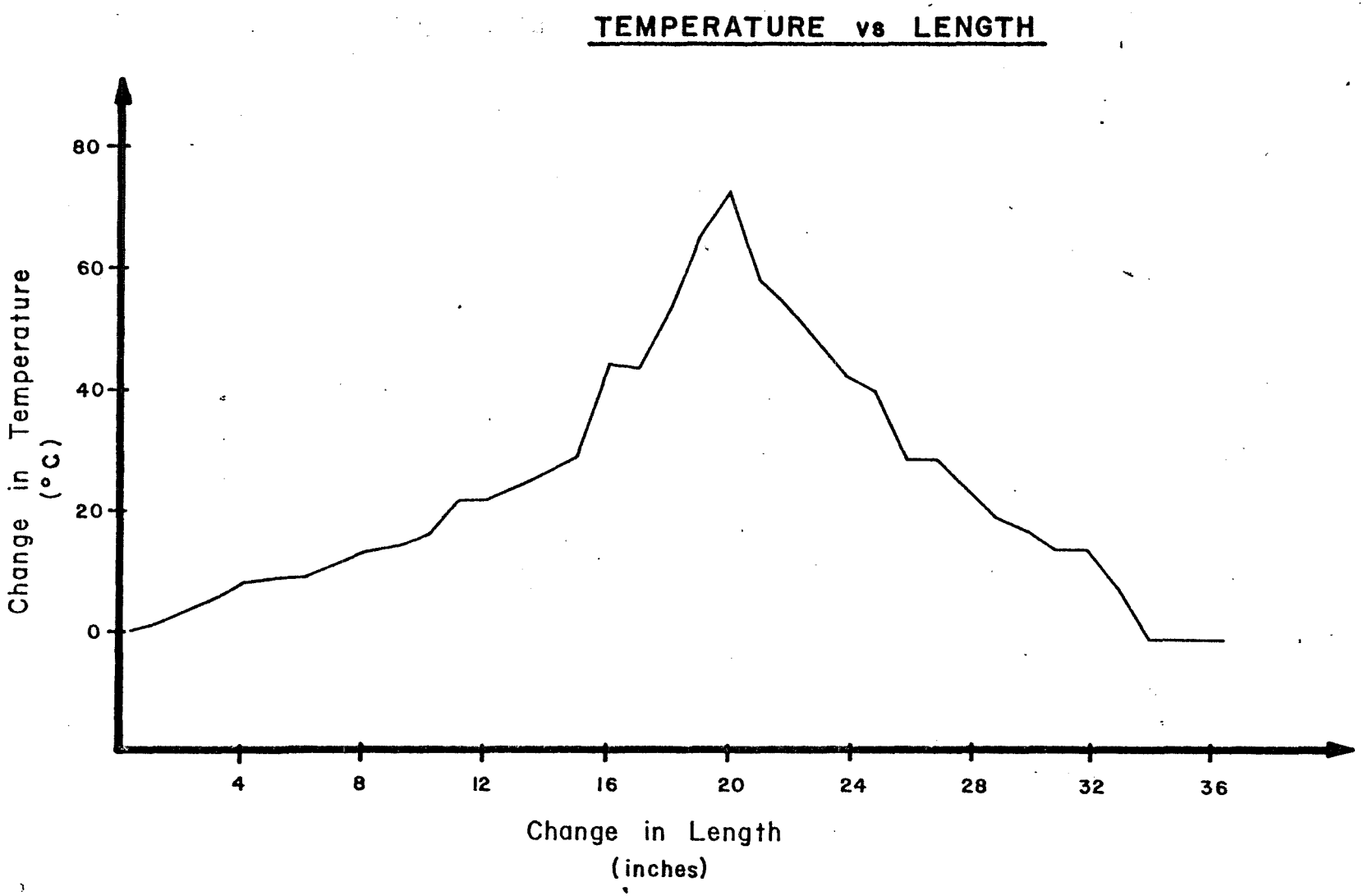

TEMPERATURE vs LENGTH
Change in Temperature (°C)
4
3
2
1
0
4
8
12
16
20
24
28
32
36
Change in Length (inches)

Figure 2.9


TEMPERATURE vs LENGTH
Change in Temperature (°C)
80
60
40
20
0
4
8
12
16
20
24
28
32
36
Change in Length (inches)

where:

Heat-Transfer Coefficient $\quad hm = Num\ K/D$

and:

Nusselt Number $\quad Num = 0.525\ (G_R P_R)^{1/4}$

with:

Grashof-Prandtl Number $\quad G_R P_R = \left(\frac{D^3\ \rho_f^2\ g\ \beta_f\ dT}{N_f^2}\right)\left(\frac{\tilde{C}_p\ N_f}{K_f}\right)$

M = Mean Transfer Coefficient

To simplify matters the following was done:

$$G_R P_R = \left[\frac{(0.1375)^3 (0.0719)^2 (4.17 \times 10^3) \left(\frac{dT}{520}\right)}{(0.0455)}\right] \left(\frac{0.236}{0.0152}\right)$$

$$= 3.67752 \times 10^3\ \Delta T$$

$$Num = 0.525 (3.67752 \times 10^3\ \Delta T)^{1/4}$$

$$= 4.08835\ (\Delta T)^{1/4}$$

$$hm = 4.08835\ (\Delta T)^{1/4} \times 0.0152/0.1375$$

$$= 4.51949\ (\Delta T)^{1/4}$$

$$Q = 4.51949\ (\Delta T)^{1/4} \times \pi \times 0.1375 \times \Delta T \times \Delta \ell \times 0.293$$

$$= 5.72017 \times 10^{-2}\ (\Delta T)^{5/4}\ \Delta \ell \text{ watts}$$

By programming the HP-25 and using the graphs the following information was calculated:

Fig. 2.7 $\quad \Delta \ell = 3$ ft.

$$Q = 719.514 \text{ watts}$$

$$R = (Q/I^2) \times 2/3$$

$$= [(719.514)/(200)^2] \times 2/3$$

$$= 11.9919 \times 10^{-3} \text{ ohms}$$

Fig. 2.8

$$\Delta \ell = 2 \text{ ft.}$$

$$Q = 247.34 \text{ watts}$$

$$R = (Q/I^2) \times 2/3$$

$$= [(247.34/(200)^2] \times 2/3$$

$$= 4.12132 \times 10^{-3} \text{ ohms}$$

Fig. 2.9

$$\Delta \ell = 3 \text{ ft.}$$

$$Q = 1258.15 \text{ watts}$$

$$R = (Q/I^2) \times 2/3$$

$$= [(1258.25)/(200)^2] \times 2/3$$

$$= 20.9709 \times 10^{-3} \text{ ohms}$$

The 2/3 value is used because heat is traveling in two directions and there are three power conductors. The 0.293 value is a conversion factor used to convert BTU hr^{-1} to watts.

The next step is to consider the heat loss due to radiation. With the same model for the conductor being the horizontal pipe under the same conditions, the equation for heat loss is:

$$Q = \sigma A_1 F_{10} (e_1 \Delta T_1^2 - a_1 T_0^4) \text{ BTU } hr^{-1}$$

Because the cable is convex and enclosed by air (0) then F_{10} is unity. Other constants are:

$e_1 = 0.91$ @ 60°F

$a_1 = 0.91$ @ 60°F

$A_1 = 0.01485 \text{ ft}^2$ Cross-sectional Area

$\sigma = 0.1712 \times 10^{-8}$ Stefan-Boltzmann

For convenience of programming on the HP-25 the heat equation for radiation was reduced to the following:

$$Q = (0.1712 \times 10^{-8})(0.01485)[(0.93)\Delta T_1^4 - (0.93)(520)^4]$$

$$= 2.54232 \times 10^{-11}[(0.93)\Delta T_1^4 - (0.93)(7.31162 \times 10^{10})]$$

$$= 2.40249 \times 10^{-11}(\Delta T_1^4 - 7.31162 \times 10^{10}) \times 0.293 \text{ watts}$$

After calculating the ΔT's from the graphs the results are:

Fig. 2.7

$$Q = 6.95724 \text{ watts}$$

$$R = (Q/I^2) \times 2/3$$

$$= [6.95724/(200)^2] \times 2/3$$

$$= 0.115954 \times 10^{-3} \text{ ohms}$$

Fig. 2.8

$$Q = 3.61500 \text{ watts}$$

$$R = (Q/I^2) \times 2/3$$

$$= [3.61500/(200)^2] \times 2/3$$

$$= 0.06025 \times 10^{-3} \text{ ohms}$$

Fig. 2.9

$$Q = 12.4383 \text{ watts}$$

$$R = (Q/I^2) \times 2/3$$

$$= [12.4303/(200)^2] \times 2/3$$

$$= 0.207305 \times 10^{-3} \text{ ohms}$$

The total heat and resistance are:

Fig. 2.7

$$Q_T = 726.471 \text{ watts}$$

$$R_T = 12.1079 \times 10^{-3} \text{ ohms}$$

Fig. 2.8

$$Q_T = 250.955 \text{ watts}$$

$$R_T = 4.18257 \times 10^{-3} \text{ ohms}$$

Fig. 2.9

$$Q_T = 1270.69 \text{ watts}$$

$$R_T = 21.1782 \times 10^{-3} \text{ ohms}$$

What is to be gained from these calculations? As one can see, the range of resistance is from 4.18257 milliohms, which is considered to be a good splice, to 21.1782 milliohms, which is considered to be a bad splice. Looking at Table 2.5 the range of added resistance for a #1/0 conductor is 10.31-12.07 milliohms, which falls well within the calculated range. Naturally the amount of calculated resistance would increase if the heat loss due to conduction was added, but the effect would not be great enough to change any conclusions. Also, the range of the measured resistance would change a little if more data could have been obtained, but once again not enough to affect the results. Judging from some of the data collected on other size conductors the average value for a good splice would probably decrease. Therefore, the conclusion that can be drawn from these results is if a cable splice is made in a portable

trailing cable the resistance can be measured of each conductor, and from the measured values one can determine if the connection in the splice is of good quality. This procedure would be a little inconvenient inside a coal mine, but would be easy to perform in a cable repair shop if there were only one splice. On the other hand, temperature measurements could be taken from splices and by using the given procedure one could determine if a cable splice contained conductors with bad connections. This form of testing would be very useful to mine inspectors as well as maintenance personnel who are interested in maintaining safe and productive working conditions.

2.7 IN-MINE MONITORING

After the random measurements were made of current traveling along the ground wires and analyses were made on the data, which appeared in the last annual report; and were found to be productive, the next step was to develop a method to continuously monitor the ground wires of a trailing cable. Several ideas were considered as to the proper approach that should be used to perform such a test. The procedure finally chosen was to insert a monitoring system within the trailing cable as near the power center as possible. After a considerable amount of thought it was decided to take a segment of trailing cable the size of the largest cable being used by the face equipment and supply a female plug at one end and a male plug at the other end. Fig. 2.10 shows the in-mine test set-up. The monitor box is dust-proof and contains a regulated power supply, a strip-chart recorder (1"/1 hr. is the recording speed), and a splice allowing access to the ground wires of the cable. A current transformer was placed around the ground wires to sense the current for the following reasons:

1. To isolate the recording equipment from direct contact with any extreme transient conditions,

2. To comply with the laws of the U.S. Bureau of Mines, and

3. To filter any direct current from the recordings.

Because of the magnitude of current expected to be detected on the ground wires a current transformer had to be designed. A 80% nickel-iron alloy manufactured to develop the ultimate in high initial permeability and low losses was the type of current transformer used in this circuit. The current transformer's ratio was 200:1 with taps at 200, 150, 75 and 0 and with the following C.T. terminal markings:

4 - 150

5 - 75

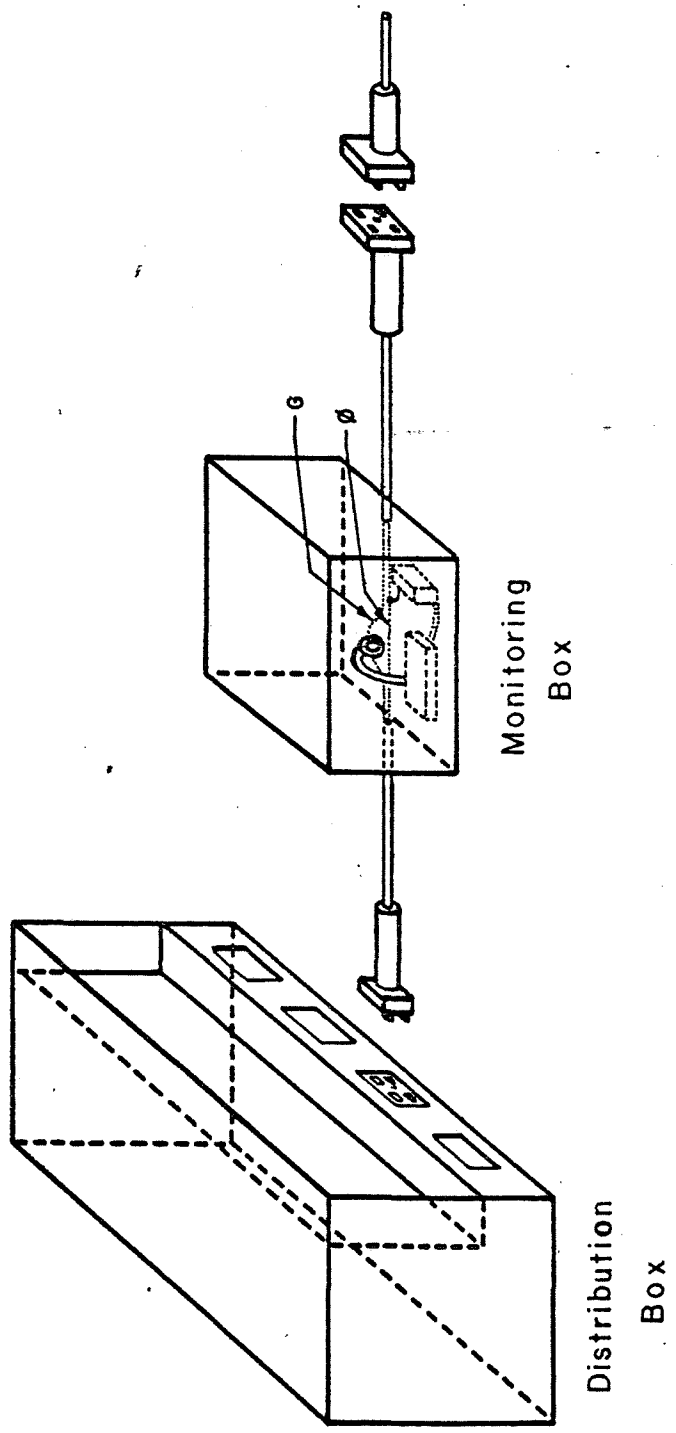
6 - 100

7 - 200

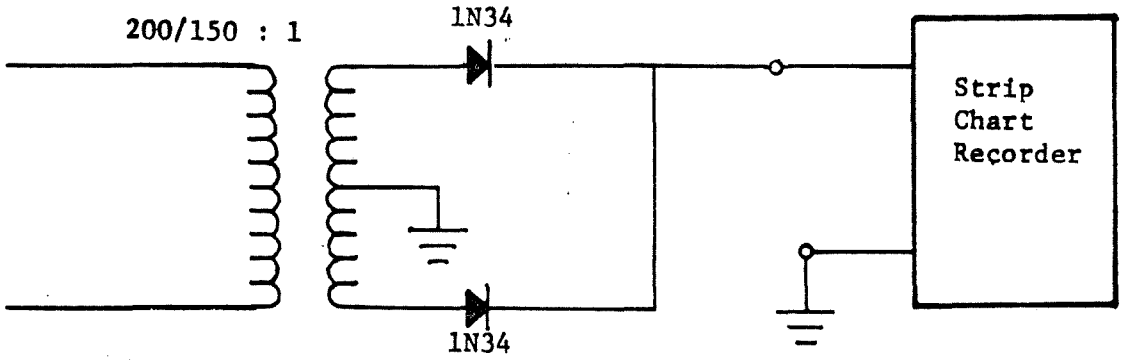
8 - 0

Figure 2.10

In-Mine Test Set-Up



The strip-chart recorder's terminals to which a transducer was to be connected was controlled by direct current; therefore, a rectifier circuit had to be developed. At first a simple four-diode circuit was tried, but the voltage required to overcome the knee of each diode (silicon diodes) became a problem. So the following circuit was developed to drive the strip-chart recorder:



The reason for using the germanium diodes was to reduce the forward voltage drop of the diodes. The voltage and current needed on the secondary to drive the recorder was critical because of the order of magnitude of the current on the primary. A center-tap configuration was used in order to obtain enough voltage to overcome the knee of the diodes and still drive the strip-chart recorder. To obtain a full scale reading on the recorder 0.32 V peak at 807 μA had to be applied to the terminals. By providing taps on the current transformer some flexibility was supplied in the circuit. If the strip-chart recorder reached full scale on the lower set of terminals, then changing two connections would enable the recorder to increase its recording range.

2.8 MONITORING RESULTS

Within days after installing the monitoring equipment some interesting results were being gathered. Because the paper being used in the strip-chart recorder was circular, replotting was necessary. Graphs of sixty minute intervals were plotted.

Cutting machines are the two pieces of equipment to which the following graphs refer. They shall be referred to as Cutting Machine No. 1 and Cutting Machine No. 2. Cutting Machine No. 1 contained a total of 150 HP motors (50 HP pump motor and 100 HP bit motor). With both motors running the phase current is roughly 170 amperes, but may range in the order of 50-500 amperes A.C. depending upon the cutting and running conditions of the machine. Cutting Machine No. 2 contained a total of 100 HP motors (25 HP pump motor and 75 HP bit motor). The normal phase current is roughly 110 amperes, but may range from 25-400 amperes depending upon the conditions as previously stated. Figs. 2.11, 2.12, 2.13, 2.14, 2.20, 2.21 and 2.22 deal with Cutting Machine No. 1 and Figs. 2.15, 2.16, 2.17 2.18 and 2.19 deal with Cutting Machine No. 2.

Figs. 2.11 and 2.12 show conditions recorded before any changes were made to the trailing cable. As can be seen the current level was around 28 milliamperes. One must keep in mind that this is an A.C. level and not a D.C. level. The alternating wave shapes came as somewhat of a surprise. Oddly enough none of the wave shapes had similar patterns. A Fourier analysis was conducted upon the three waveforms to see if any correlation could be detected among the harmonics. The results were:

$$f(t) = \frac{ao}{2} + \sum_{i=1}^{9} Ci \sin\left(\frac{i2\pi t}{T} + \theta i\right)$$

Wave Shape #1

$$f(t) = 36.209 + 9.343 \sin\left(\frac{2\pi t}{17} + 2.588\right)$$

$$+ 6.255 \sin\left(\frac{4\pi t}{17} + 1.268\right) + 5.358 \sin\left(\frac{6\pi t}{17} - 2.659\right)$$

$$+ 3.345 \sin\left(\frac{8\pi t}{17} + 0.286\right) + 2.487 \sin\left(\frac{10\pi t}{17} - 3.046\right)$$

$$+ 1.386 \sin\left(\frac{12\pi t}{17} - 0.211\right) + 0.891 \sin\left(\frac{14\pi t}{17} - 2.637\right)$$

$$+ 1.323 \sin\left(\frac{16\pi t}{17} - 0.114\right) + 0.747 \sin\left(\frac{18\pi t}{17} - 2.848\right)$$

cycles/min

Wave Shape #2

$$f(t)\ 44.518 + 3.902 \sin\left(\frac{2\pi t}{11} + 2.467\right)$$

$$+ 4.280 \sin\left(\frac{4\pi t}{11} - 1.876\right) + 4.542 \sin\left(\frac{6\pi t}{11} - 2.237\right)$$

$$+ 2.325 \sin\left(\frac{8\pi t}{11} - 1.767\right) + 2.050 \sin\left(\frac{10\pi t}{11} - 1.819\right)$$

$$+ 2.035 \sin\left(\frac{12\pi t}{11} - 2.399\right) + 1.703 \sin\left(\frac{14\pi t}{11} - 2.421\right)$$

$$+ 1.028 \sin\left(\frac{16\pi t}{11} - 2.239\right) + 0.958 \sin\left(\frac{18\pi t}{11} - 2.693\right)$$

cycles/min

Figure 2.11

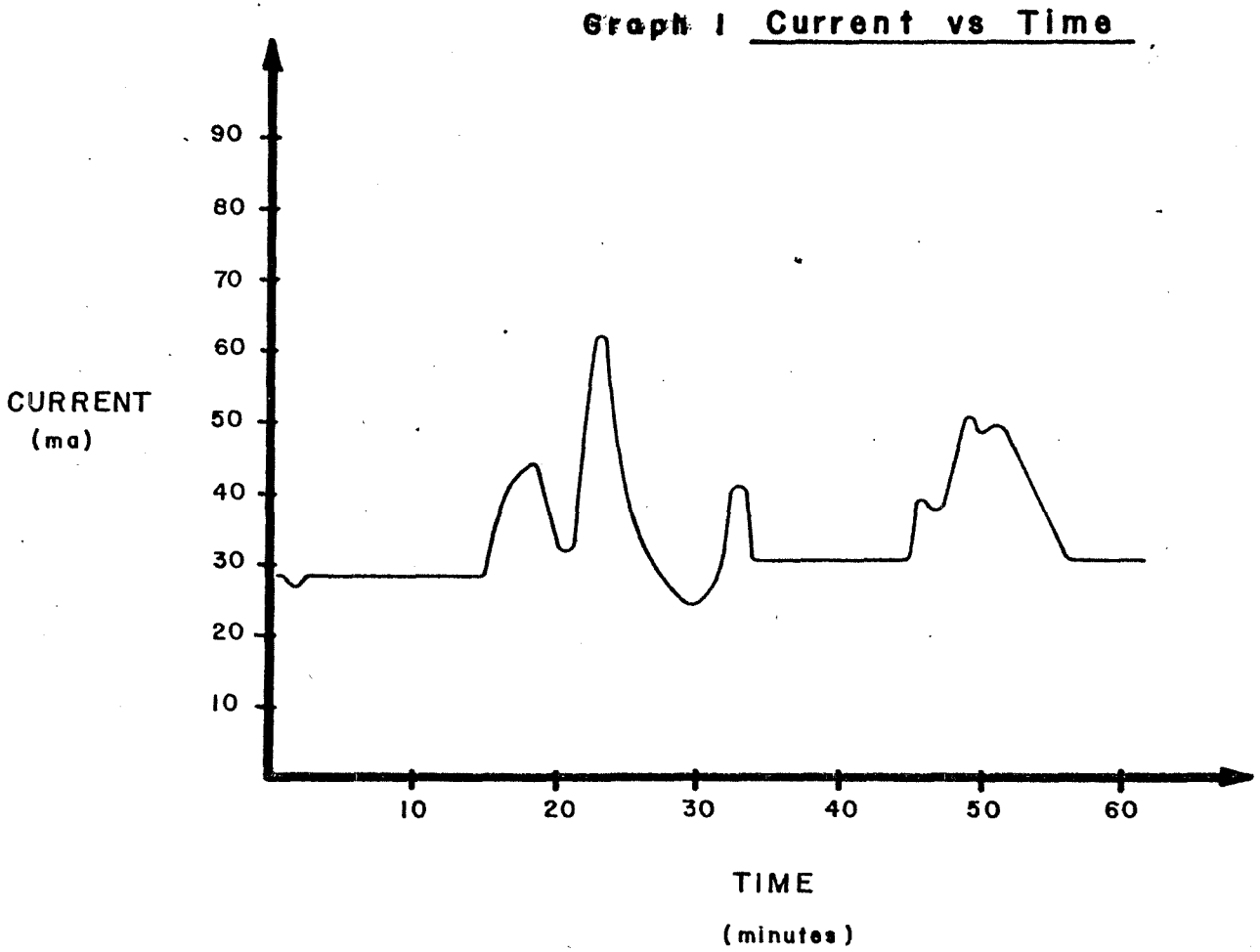
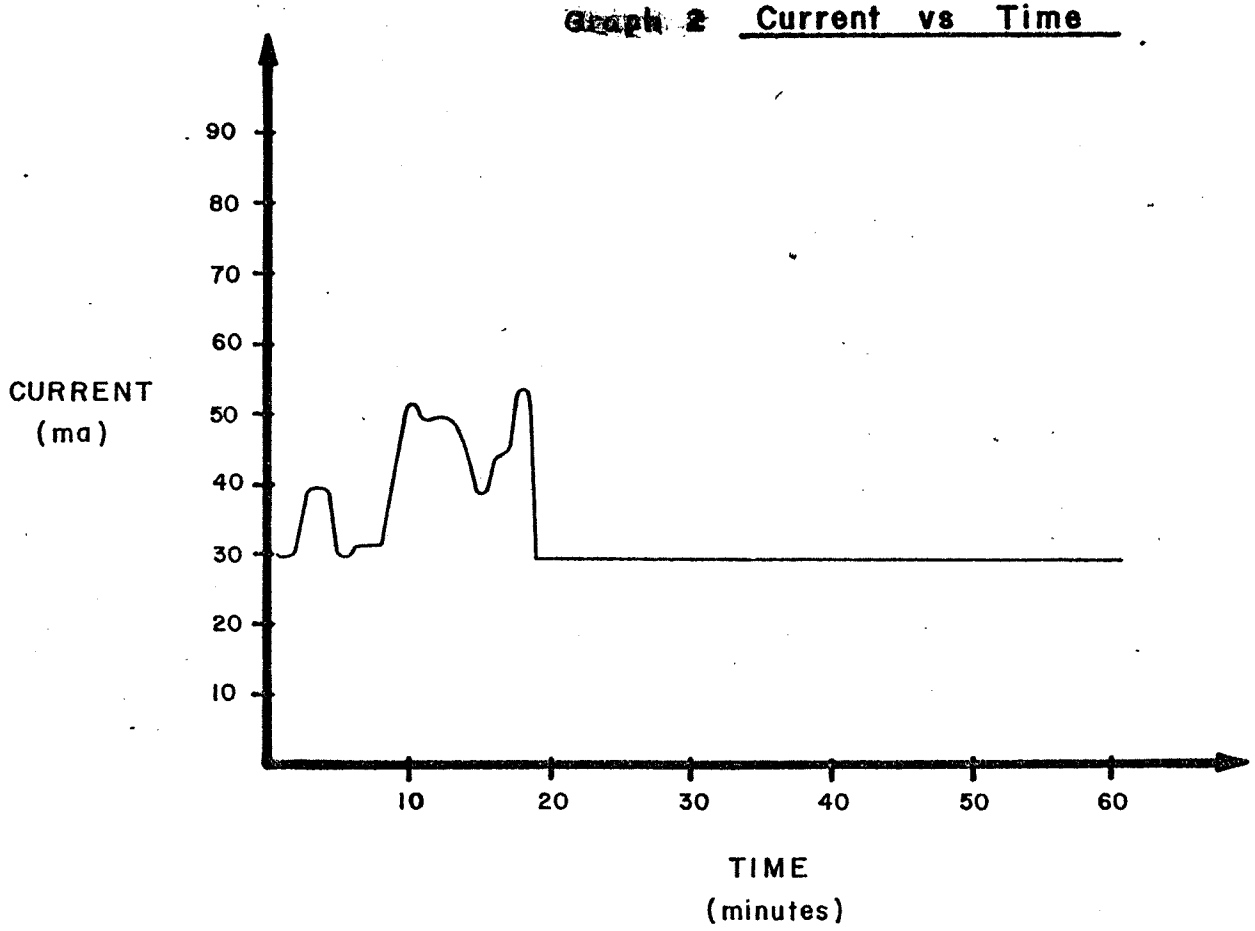

Graph I Current vs Time
CURRENT
(ma)
90
80
70
60
50
40
30
20
10
10
20
30
40
50
60
TIME
(minutes)

Figure 2.12


Graph 2 Current vs Time
CURRENT
(ma)
90
80
70
60
50
40
30
20
10
10
20
30
40
50
60
TIME
(minutes)

Wave Shape #3

$$f(t) = 41.157 + 8.738 \sin\left(\frac{2\pi t}{11} - 3.057\right)$$

$$+ 0.851 \sin\left(\frac{4\pi t}{11} + 1.728\right) + 0.899 \sin\left(\frac{6\pi t}{11} + 2.504\right)$$

$$+ 1.519 \sin\left(\frac{8\pi t}{11} - 2.406\right) + 0.197 \sin\left(\frac{10\pi t}{11} - 2.625\right)$$

$$+ 0.845 \sin\left(\frac{12\pi t}{11} - 2.154\right) + 0.954 \sin\left(\frac{14\pi t}{11} - 0.210\right)$$

$$+ 0.728 \sin\left(\frac{16\pi t}{11} + 2.177\right) + 0.684 \sin\left(\frac{18\pi t}{11} - 1.512\right)$$

Once again the analysis came up null. Assumptions were made as to the source for these waveforms, but the only thing that was determined at first was these waveforms were occurring during the period of time the machine is cutting the coal. To determine this a time study was performed on the machine and the cutting time fell within the range of 7-15 minutes. This agreed with the time period of these waveforms, indicating that as the phase current increased so did the current traveling along the ground wires.

Figures 2.13 and 2.14 show portions of the recordings made after an old splice was removed and replaced with a new one. The old splice was in poor condition both inside and out, and its general appearance was the main factor influencing the decision to replace it.

Surprisingly, a significant change occurred in the data being recorded. When plotted the figures clearly showed that the current level had dropped considerably. Although the current level had been reduced, the magnitude of the peaks remain roughly unchanged, but were beginning to take a more definite shape. Fig. 2.13 clearly demonstrates what happens to the level when the machine is completely deenergized. This is shown during the periods of time the waveforms drop to zero. The change in the level when the splice was replaced was 16.6 milliamperes, which is a substantial drop. An interesting point is that the original splices contained within the portable trailing cables were of the heat-shrinkable type whereas the splices used as replacements were of the cold-bond type.

The next five figures, pertaining to Cutting Machine No. 2, support the information obtained from the first four figures as well as supply some added information. Figs. 2.15 and 2.16 display the stray current conditions of the ground wires of the cable before any changes were made. As can be seen, the irregular wave shapes still appear, but the peak values are not as high and the leakage level appears to be around 20 milliamperes. The reason given for the reduction of the peak values is the phase currents are reduced due to the size motors contained upon the machine. Looking closely at the figures one can see that a shift in levels of 4.15 milliamperes has occurred, indicating that some change did occur within the cable system.

Figure 2.13

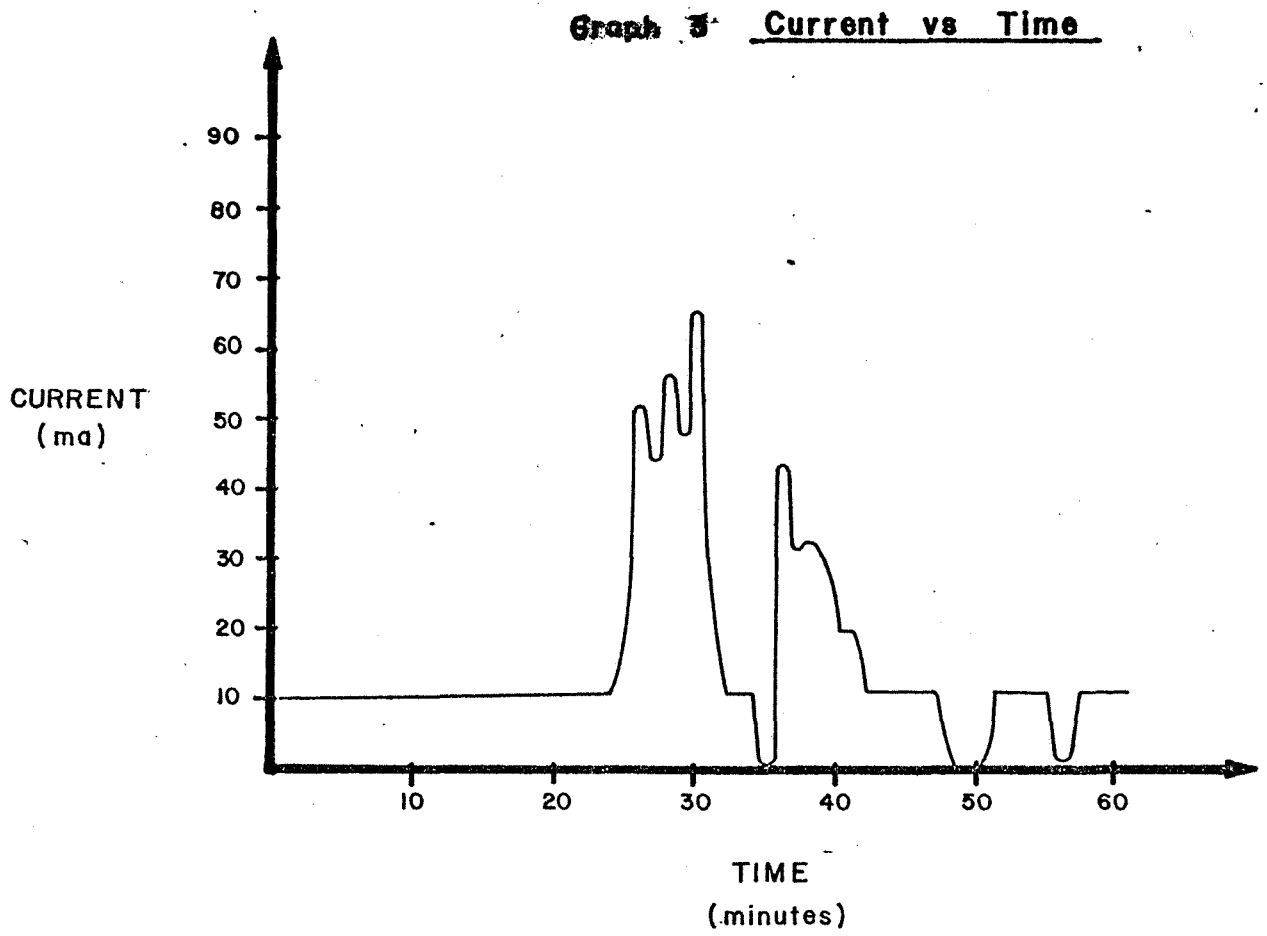

Graph 3 Current vs Time
CURRENT
(ma)
90
80
70
60
50
40
30
20
10
10
20
30
40
50
60
TIME
(minutes)

Figure 2.14

Graph 4 Current vs Time

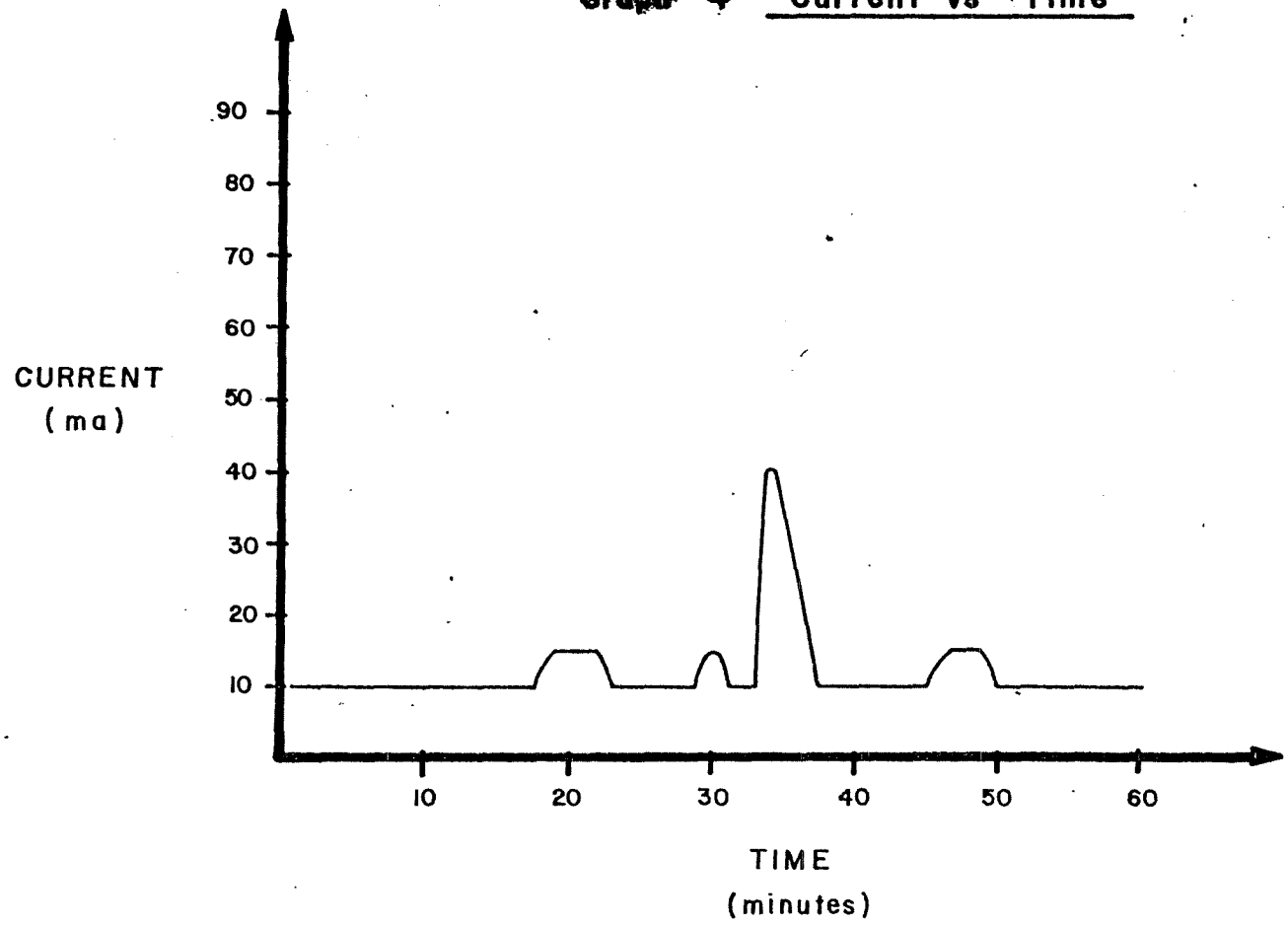


Figure 2.15

Graph 5 Current vs Time

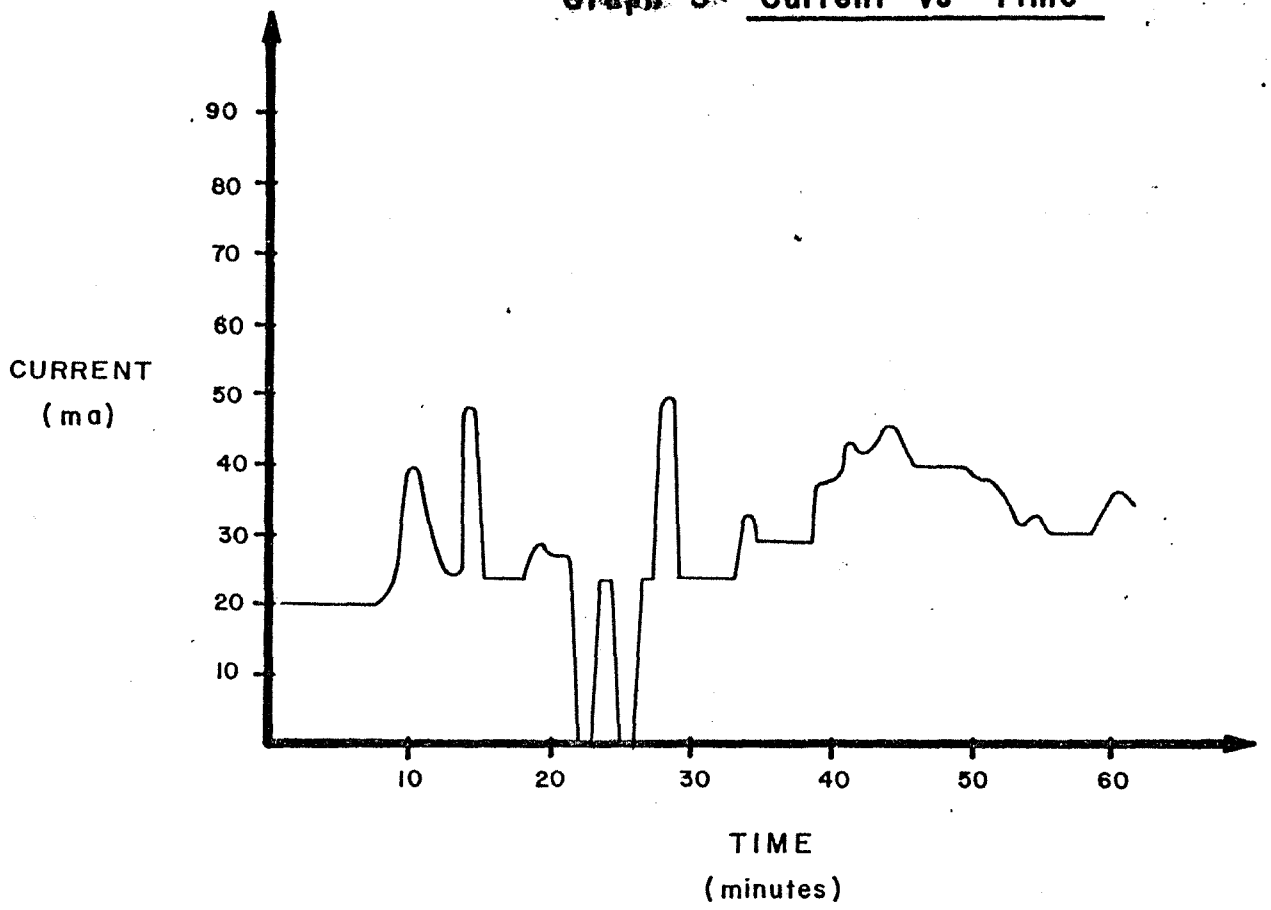


Figure 2.16

Graph 6 Current vs Time

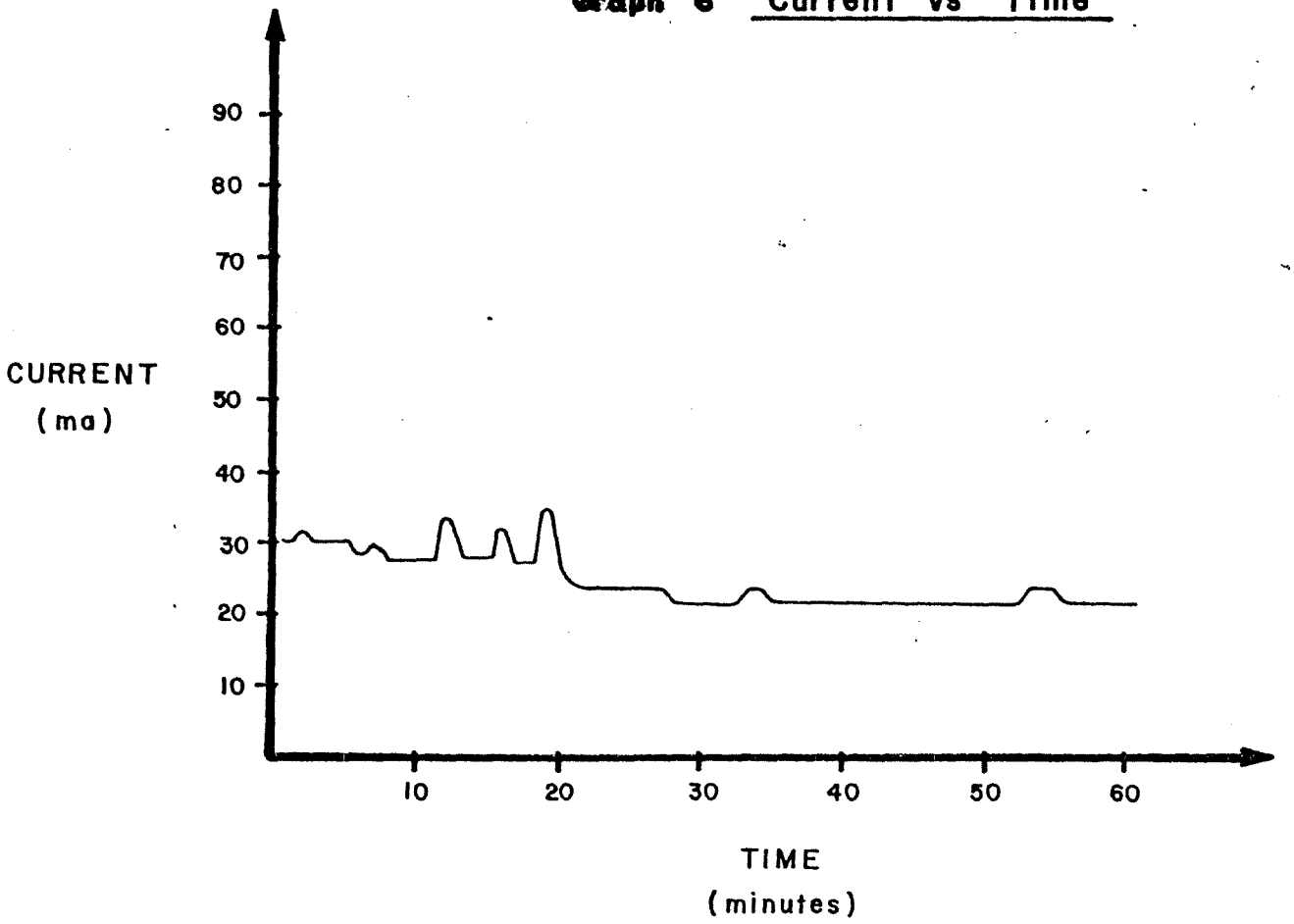


Figure 2.17 shows the conditions on the ground wires after an old splice had been replaced with a new one. The level increased around 3 milliamperes and the irregular wave shape appears to have dampened. The curve went to zero because the machine had been deenergized for some reason. Fig. 2.18 shows the conditions on the ground wires after two other splices were replaced with new ones and an additional splice was put into the cable. After this work was performed the figure shows that the level dropped to around 19 milliamperes even though an extra splice was added. During the time that the machine was cutting into the coal a portion of the roof fell, landing on the cable and damaging one of the cable splices. This accounts for the level of current increasing from 19-27 milliamperes. Finally, Fig. 2.19 shows the conditions of the current on the ground wires after that splice had been repaired and the final old splice had been replaced with a new splice. Interesting factors to note are the level has decreased to 19.10 milliamperes and all the irregular waveforms have been eliminated. This system was monitored for three more weeks and the data remained unchanged.

Sufficient time had elapsed and all the original cable splices had been replaced with new ones. The monitor box was placed back into the trailing cable circuit of Cutting Machine No. 1. The results were identical to those of Cutting Machine No. 2 except for the magnitude. Fig. 2.20 shows the results of the data gathered. The level was 10 milliamperes.

The next step was to wait and see if any changes occurred, what they were, and how much time would elapse before anything did happen. Roughly three weeks passed before any noticeable changes began to occur. As before, the irregular wave shapes were occurring during the time that the machine was performing its functional work. Fig. 2.21 shows a portion of the data gathered. At this time the magnitude of the peaks are not that high, but is expected to increase as the age of the splices increase.

Figure 2.22 shows a unique situation. The data plotted in this figure was obtained during the time the insulation of a cable splice actually became so hot that it burst into flames and completely destroyed the splice. Naturally when the ground fault occurred more current traveled along the ground wires than is shown in the figure, but due to the saturation limits of the strip-chart recorder and the speed at which the data was being recorded the wave shape shown was all that was recorded. Proposals were made at what caused the overheating and finally the ignition. A final conclusion was drawn by inspecting other splices that were heating. After dissecting a couple of these splices the connector used to complete the connection of the wires were found to have been crimped not very tightly. This allowed some of the strands to work free causing damage to the insulation inside of the splice as well as creating a loose connection.

Figure 2.17

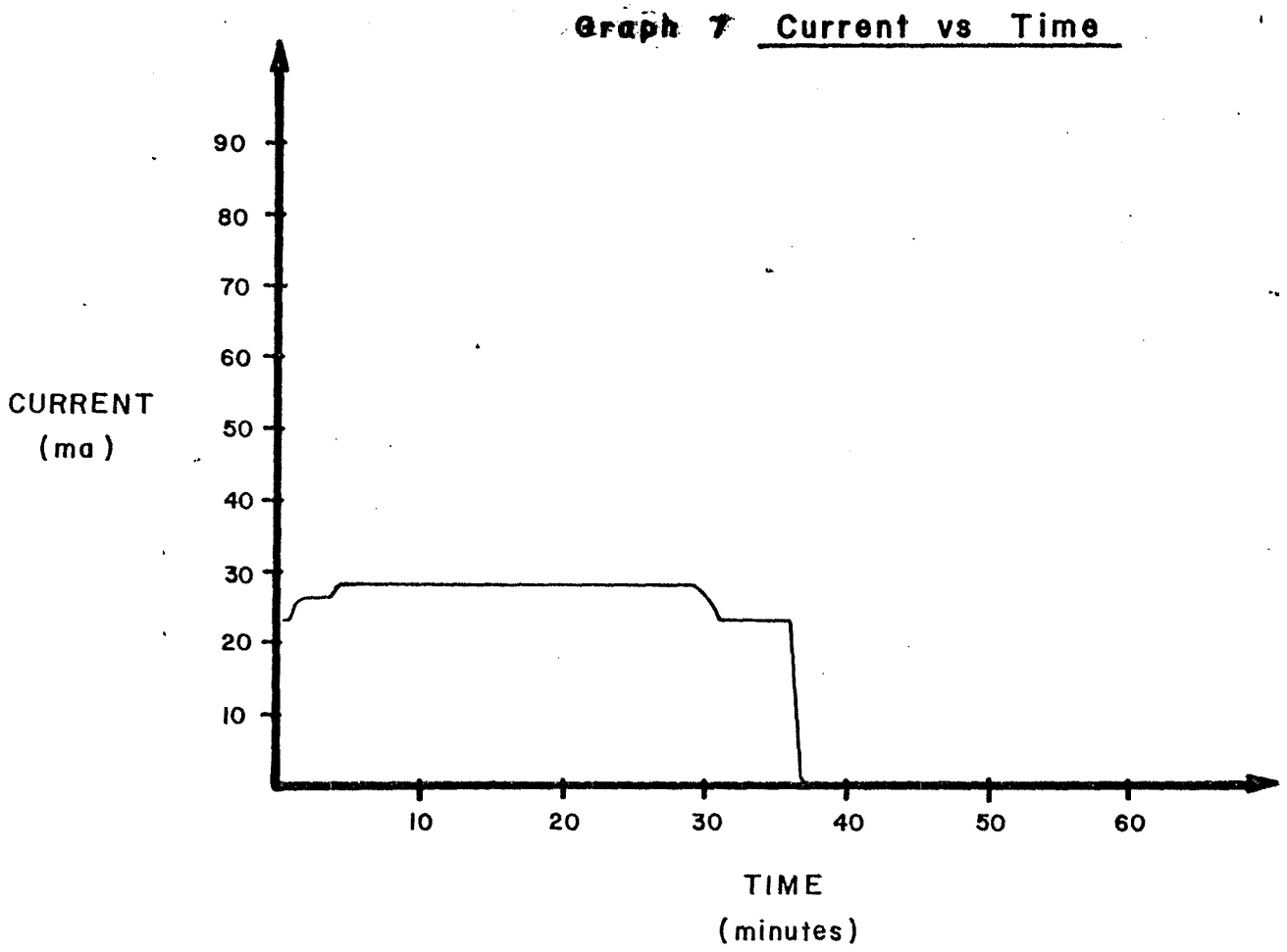

Graph 7 Current vs Time
CURRENT
(ma)
90
80
70
60
50
40
30
20
10
10
20
30
40
50
60
TIME
(minutes)

Figure 2.18

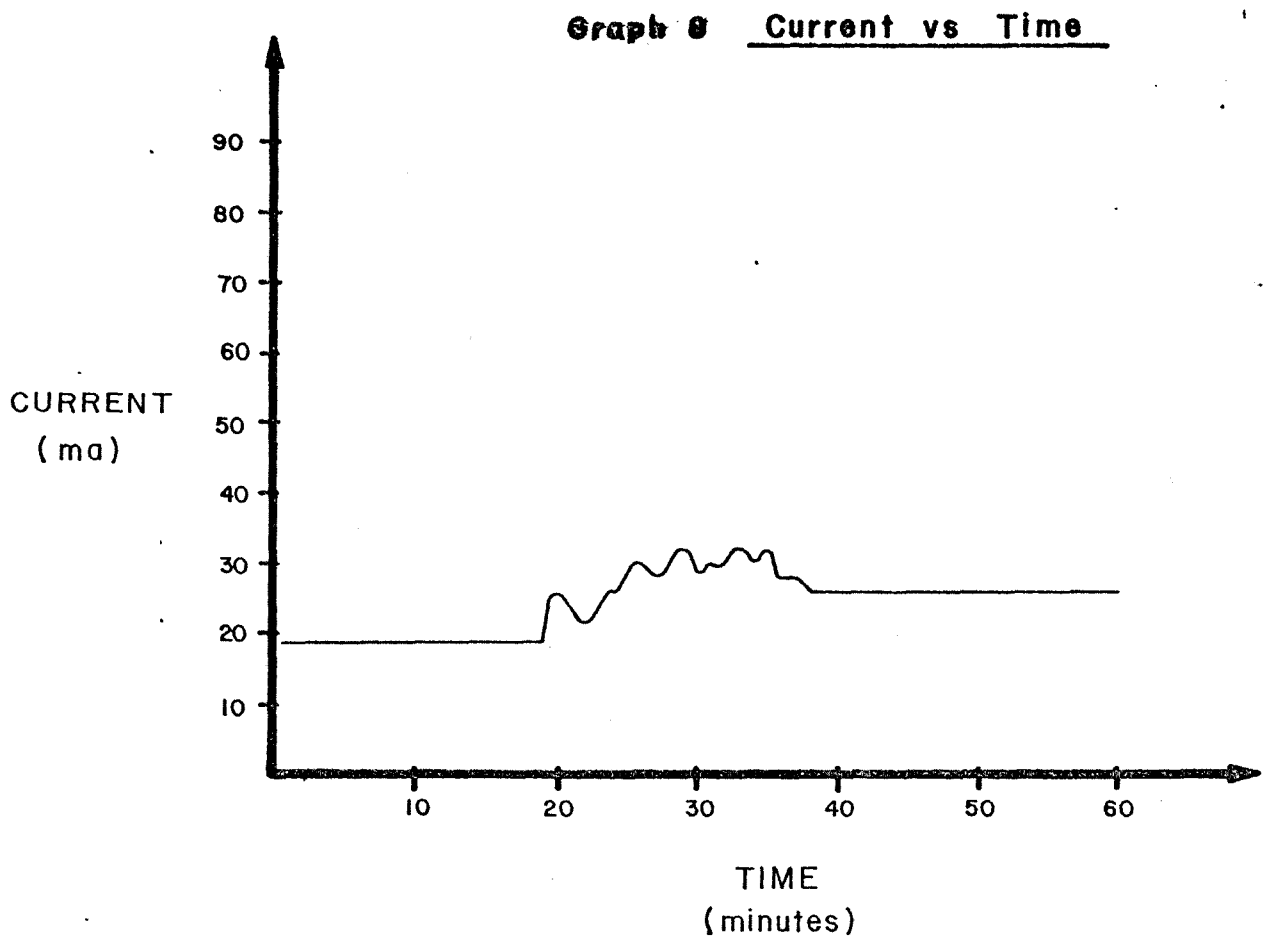

Graph 8 Current vs Time
90
80
70
60
50
40
30
20
10
CURRENT
(ma)
10
20
30
40
50
60
TIME
(minutes)

Figure 2.19

Graph 9 Current vs Time

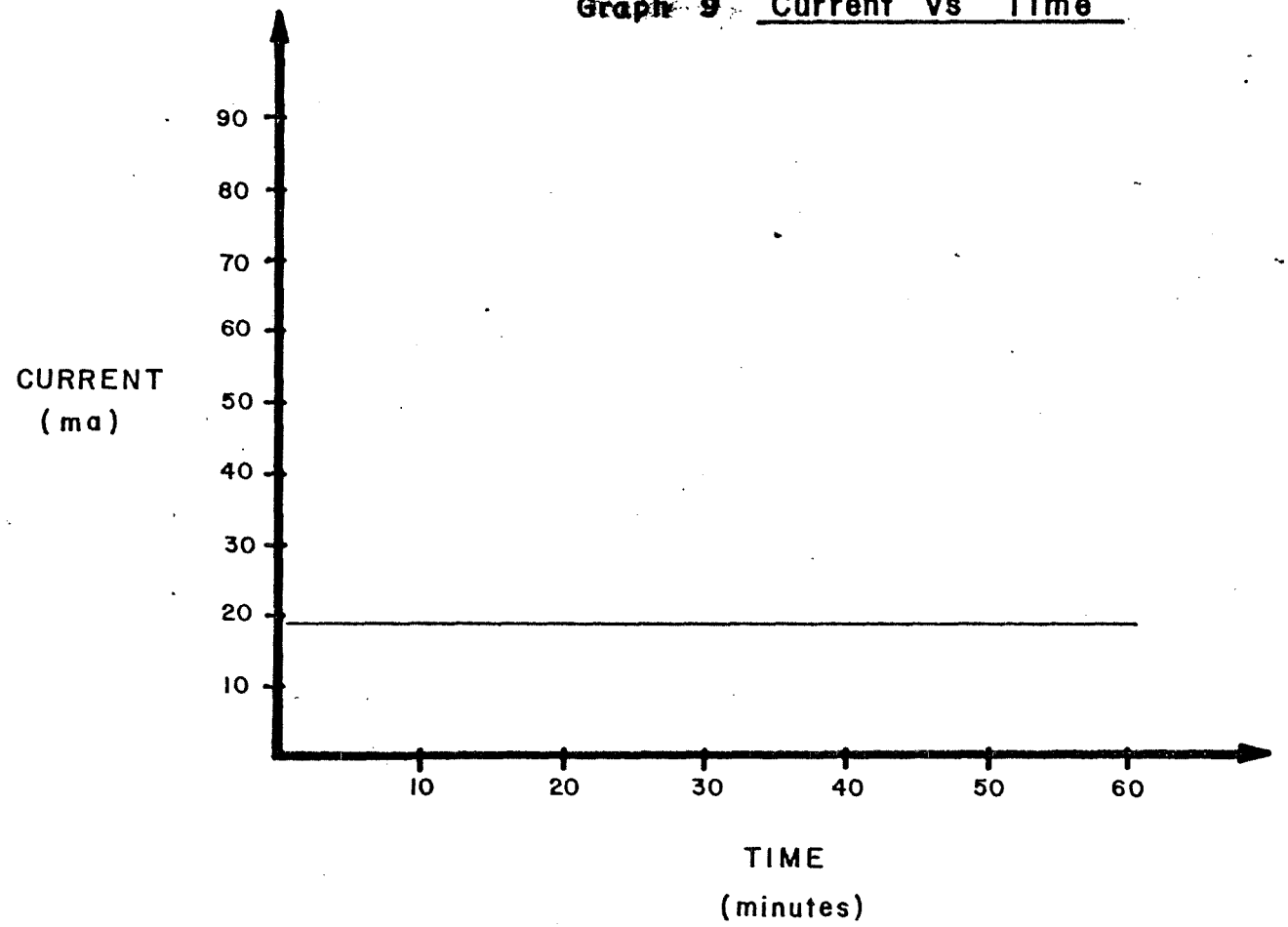


Figure 2.20

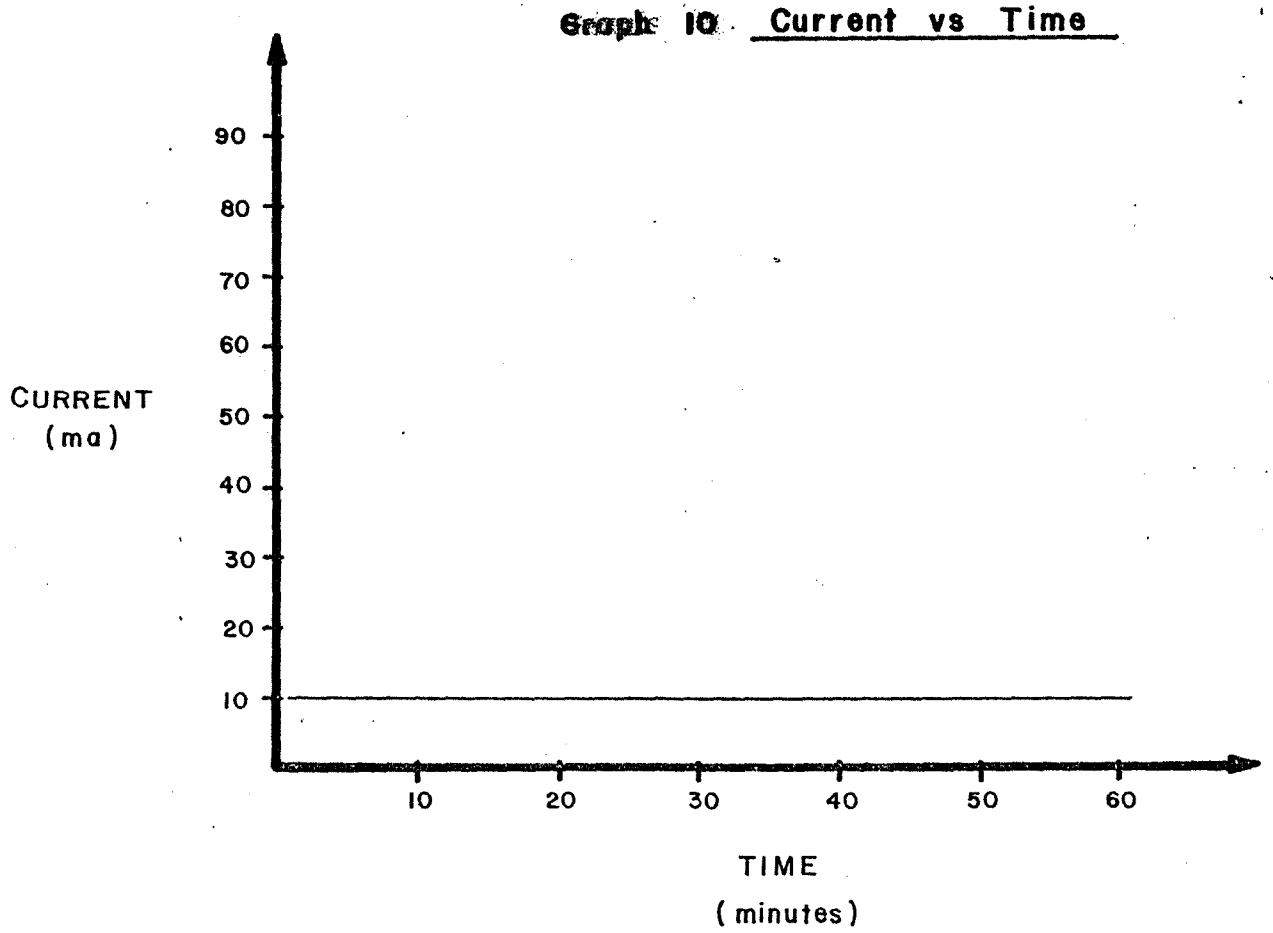

Graph 10 Current vs Time
90
80
70
60
50
40
30
20
10
CURRENT
(ma)
10
20
30
40
50
60
TIME
(minutes)

Figure 2.21

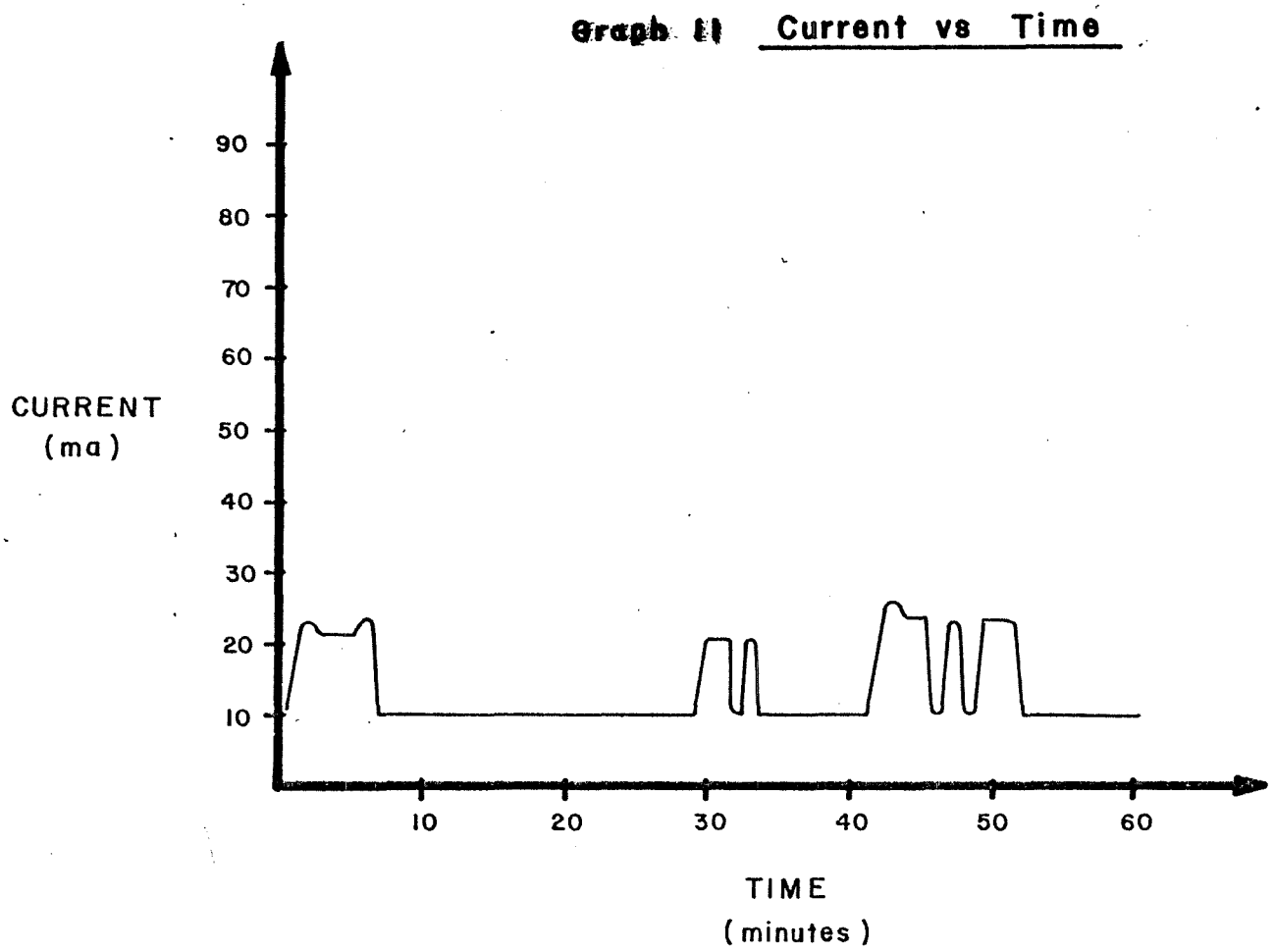
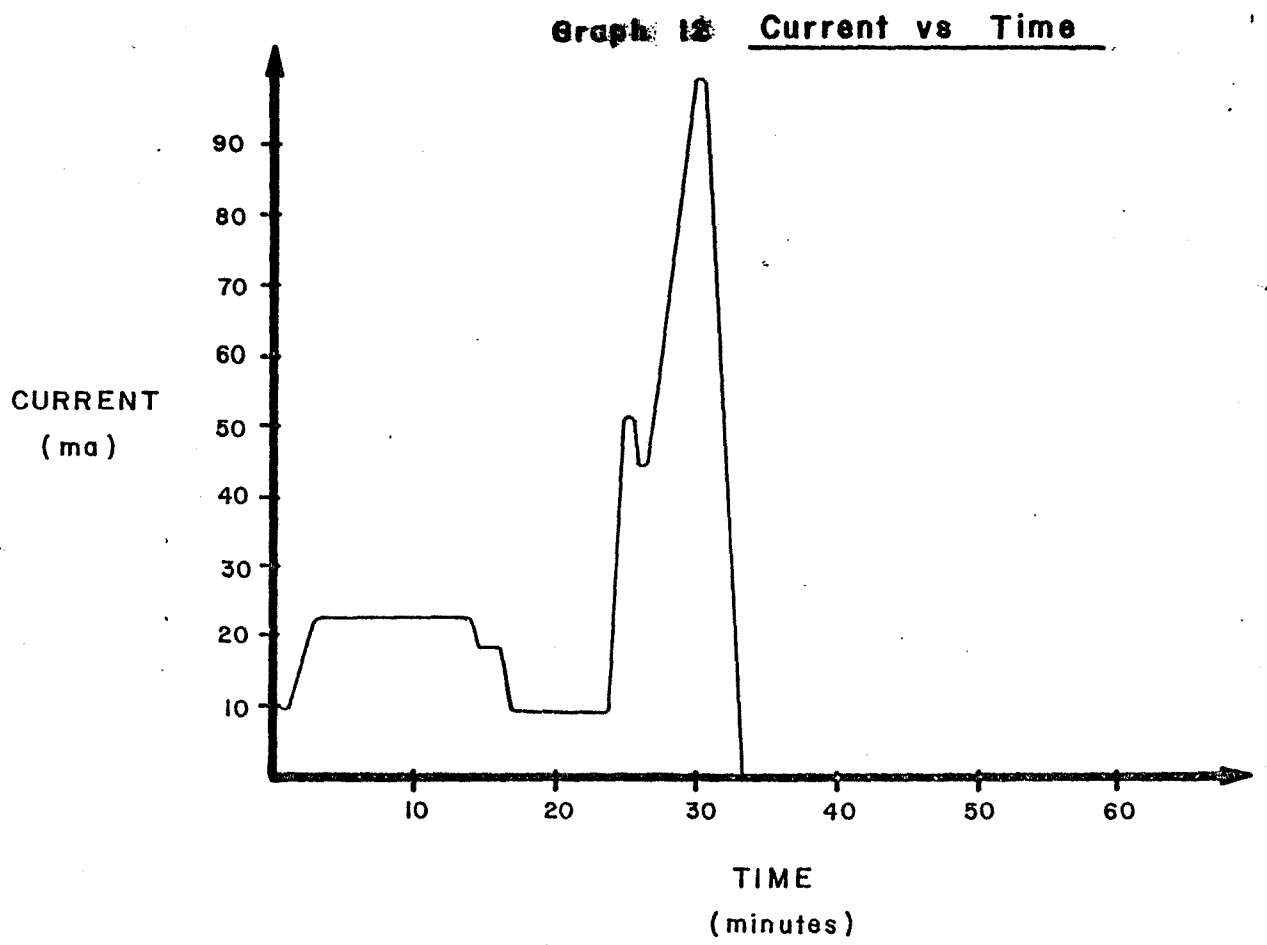

Graph 1 Current vs Time
CURRENT
(ma)
90
80
70
60
50
40
30
20
10
10
20
30
40
50
60
TIME
(minutes)

Figure 2.22


Graph 12 Current vs Time
CURRENT
(ma)
90
80
70
60
50
40
30
20
10
10
20
30
40
50
60
TIME
(minutes)

2.9 REFERENCES

1. Lee, Yin-Han, The Sensor Package of the Mine Safety Monitoring System (Thesis) West Virginia University, 1974.

2. Mining Cable Engineering Handbook, Anaconda, 1976.

3. Bird, Byron R., Stewart Warren E., and Lightfoot, Edwin N., Transport Phenomena, John Wiley & Sons, Inc., New York, 1960.

4. McCoy, William James, Cable Splices and Their Effects on the Safety Ground System (Thesis) West Virginia University, Copyright August, 1977.

CHAPTER III - GROUNDING PRACTICE

3.1 COUPLING BETWEEN SYSTEM AND SAFETY GROUND

Title 30, Parts 75 and 77 of the Code of Federal Regulations specify that resistance - grounded three-phase system have a separately established safety ground bed which is connected to the grounded end of the grounding resistor and to the frames of all portable and mobile equipment receiving circuit power. Separation has been fixed at a minimum spacing from the substation ground mat of 25 feet. Although this physical separation is supposed to effectively isolate the two grounds, there are several indications that it does not in all cases. IEEE Standard 142-1976 recommends 50 feet between grounds, and the separation problem has been discussed in some detail in Chapter II of the previous annual report. No more measurements of that type were carried out. A rare opportunity presented itself, however, when WVU was invited to participate in a series of staged-fault tests to evaluate ground insulation in a working underground mine.

3.2 EXPERIMENTAL EVALUATION OF COUPLING

3.2.1 Introduction

To illustrate the effect of coupling between the system and safety ground beds actual faults were simulated on an existing mine power system. The mine was a large underground operation near Indiana, Pa. This section deals with the description of the tests conducted and a discussion on the test results obtained.

The system layout is given in Fig. 3.1. The main transformer supplying the mine was delta connected on the secondary and thus a zig-zag transformer was used for grounding purposes. All the poles were grounded individually and connected to the over-head static wire. The frame of the surface fan transformer was connected to the static wire.

The following kinds of faults were simulated on the system:

a. Line-to-transformer frame fault: In this fault simulation the frame of the surface fan transformer was shorted to the phase conductor. This could be considered as a low resistance ground fault. Two sets of resistance measurements were made, one with the underground mine system connected and another with the mine system disconnected.

b. Line-to-earth fault: This fault was simulated by connecting the phase conductor to a copper stake driven into the ground. This was equivalent to a high-resistance type fault. In this

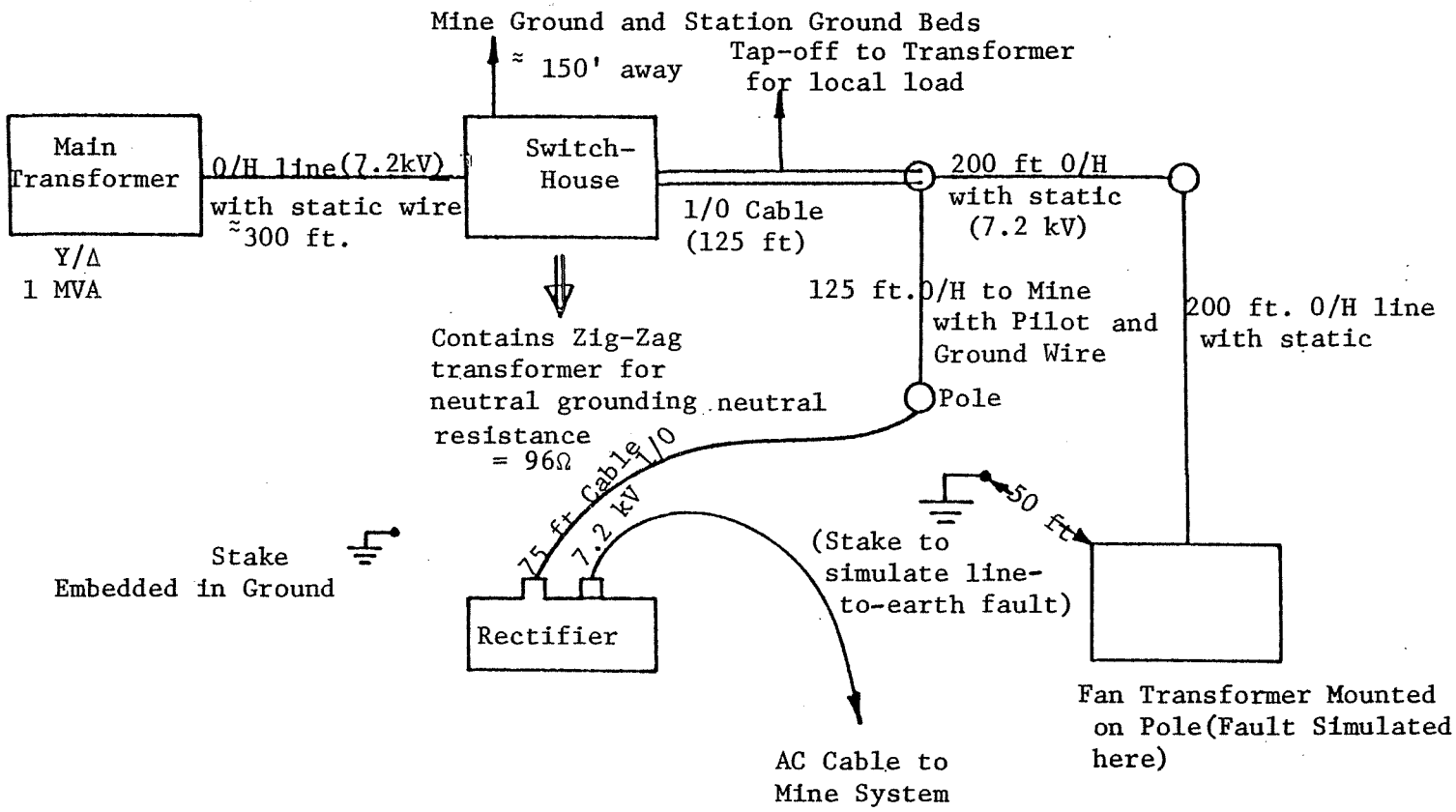


Fig. 3.1. Overall System Layout, Auld's Run Mine

case also two sets of measurements were made, one with the mine system connected and another with the mine system disconnected.

In either case the breaker at the substation was closed on to the fault.

The following test equipment was used to make the various measurements.

1. Simpson Model 260 Multimeter (at rectiffer)

2. Esterline Angus Volt, Amp Recorder (at substation)
   5 amp full scale
   150 volt full scale
   CT: 250/5 with 5 primary turns used

3. Biddle Ground Meggar - null balance type

3.2.2 Resistance Measurements

A series of resistance measurements were made before the actual simulation of the line faults. Since the faults that were to be simulated were line-to-earth fault and line-to-transformer frame fault, the resistances that were of interest were as follows:

a) R_{MG} - Resistance of Mine Ground (Safety Ground)

b) R_{SG} - Resistance of Station Ground (System Ground)

c) R_{MG-SG} - Resistance between Mine Ground and Station Ground

d) R_{MG-EF} - Resistance between Mine Ground and Earth Fault*

e) R_{MG-DG} - Resistance between Mine Ground and Down Ground**

f) R_{MG-MC} - Resistance between Mine Ground and Mine Cable Coupler

g) R_{EF-DG} - Resistance between Earth Fault and Down Ground

h) R_{DG-MC} - Resistance between Down Ground and Mine Cable Coupler

* Earth Fault - A stake driven to earth for simulation of line to earth fault.

** Down Ground - Ground wire running down the pole from the transformer frame to earth.

The Mine Ground and the Station Ground Beds were both made up of X-IT rods. The Station Ground had 5 rods each of 10 feet long

arranged in the manner shown in Fig. 3.2.

The Mine Ground had the same configuration as the Station Ground with 2 of the rods being 8 feet long instead of 10 feet. The 2 ground beds had a physical separation of about 35 feet apart. The pole line where the fault was to occur was about 500 feet from the Mine Coupler and about 700 feet from the two ground beds. The Mine Coupler itself was about 400 feet from the ground beds. The Earth Fault was about 50 feet from the Down Ground.

When measuring the resistance of Mine Ground to Station Ground, three situations were taken into consideration. The first case was with the mine connected; the second case was with the mine disconnected but with the static wire connected; the third case was with the 2 ground beds completely isolated from other connections and from each other. It was noticed that, from the measurements, the mine itself was a very low resistance ground mainly because of its vast area and numerous contacts of equipment to earth.

The values of various resistance are listed in Table 3.1.

TABLE 3.1

Values of Resistances

Resistance	Value	Comments
R_{SG}	5.65Ω	Complete isolation from other connections
R_{MG} *	5.97Ω	Complete isolation (1 out of 4 very close values)
R_{MG-EF}	130Ω	Down ground isolated
R_{MG-DG}	22.5Ω	Station Ground disconnected
R_{MG-MC}	190Ω	Mine disconnected
R_{EF-DG}	124Ω	Down Ground connected to Static wire
R_{DG-MC}	190Ω	Station Ground disconnected, mine disconnected
R_{MG}-SG	3.6Ω	Mine connected
	6.0Ω	Mine disconnected
	9.98Ω	Everything disconnected

* 4 readings were taken for the mine ground and were respectively 6.26Ω, 6.05Ω, 5.97Ω, 5.82Ω.

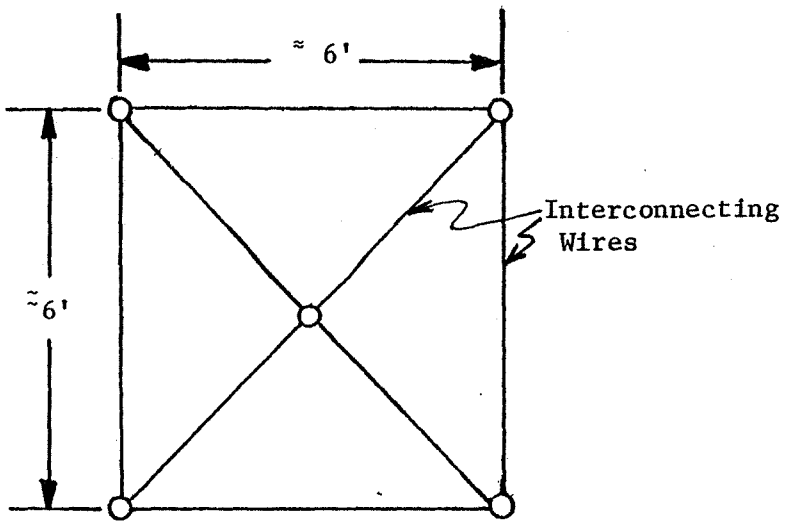


Fig. 3.2. Ground Bed Configuration Using Five X-IT Rods.

3.2.3 Test Results

For each fault simulation the following measurements were made:

1. Voltage between the safety ground and the station ground
2. Fault current
3. Touch voltage between the cable coupler connected to the rectifier and a stake driven into the ground. The cable coupler was connected to the safety ground.

The first two measurements were carried out at the switch-house using the Esterline Anges Volt, Amp Recorder while the third one was made at the rectifier location using a Simpson Voltmeter. Originally it was intended to carry out the measurements of the touch potential using a strip chart recorder. But unfortunately, the recorder failed to function properly, so the Simpson Voltmeter was used instead.

For each fault simulation, two sets of measurements were made, one with the mine system connected and another with the mine system disconnected. The data obtained are listed in Table 3.2.

Table 3.2

Measured Data on Fault Simulation

Types of Faults	Voltage Between Ground Beds	Fault Current	Touch Potential
Phase-to-static line (transformer frame) fault (mine system connected)	48 volts	23.75 amps	29 volts
Phase-to-static line (transformer frame) fault (mine system disconnected)	127 volts	23.25 amps	115 volts
Phase-to-earth fault (mine system connected)	21 volts	16 amps	23 volts
Phase-to-earth fault (mine system disconnected)	75 volts	16 amps	50-75 volts

3.2.4 Conclusions

As seen from the readings, the potential of mine equipment can sometimes rise to about 200V relative to ground, when electrical system faults occur. Mine personnel will have a "touch" potential of this order, when in physical contact with electrical equipment inside the mine. A theoretical-cum-practical study of the hazards associated with "touch" potentials, and evolution of safety measures is therefore of importance and merits attention.

3.2.5 Analysis and Discussion on Test Results

From a preliminary analysis of the results it is obvious that the hazards of touch potentials can be reduced greatly in case all the surface equipment is connected to the safety ground instead of the overhead static wire. In case of any fault on the equipment all of the fault current would flow into the safety ground through the ground wire and the voltage on the equipment frame would be limited to the voltage drop in the ground wire. However, in case of a line-to-earth fault the danger of high touch voltages still exists.

It is very difficult to give a theoretical interpretation to the results because one is in no position to determine the current flows in various sections of the ground through so many connections and interconnections. Analysis is very much simplified, if it is possible to build an electrical analog of any physical system. The modelling of the earth in this connection poses innumerable problems due to its non-homogeneous composition, infinite size and three-dimensional effect.

In this section attempts are made to treat the effect of earth as a lumped resistance. The validity of this model is very questionable to say the least. The purpose here is just to get a feel for the voltage and current distribution in the system. As one is aware, by proper mathematical manipulation any distributed model can be represented as a lumped model with small errors. In the present discussion no such mathematical tools are developed. Most of the resistance values represented are estimations based on the various resistance measurements already alluded to in 6.2.2. The derivation of an improved model is an important study and merits further investigation.

The circuit analog for the system is shown in Fig. 3.3.

The network was solved using IBM's ECAP program available at WVU's computer system. The results of the computer simulation are shown in Table 3.3. The actual measured values are shown in parentheses. A comparison of the results would show that the numbers agreed fairly well with the mine system disconnected. However,

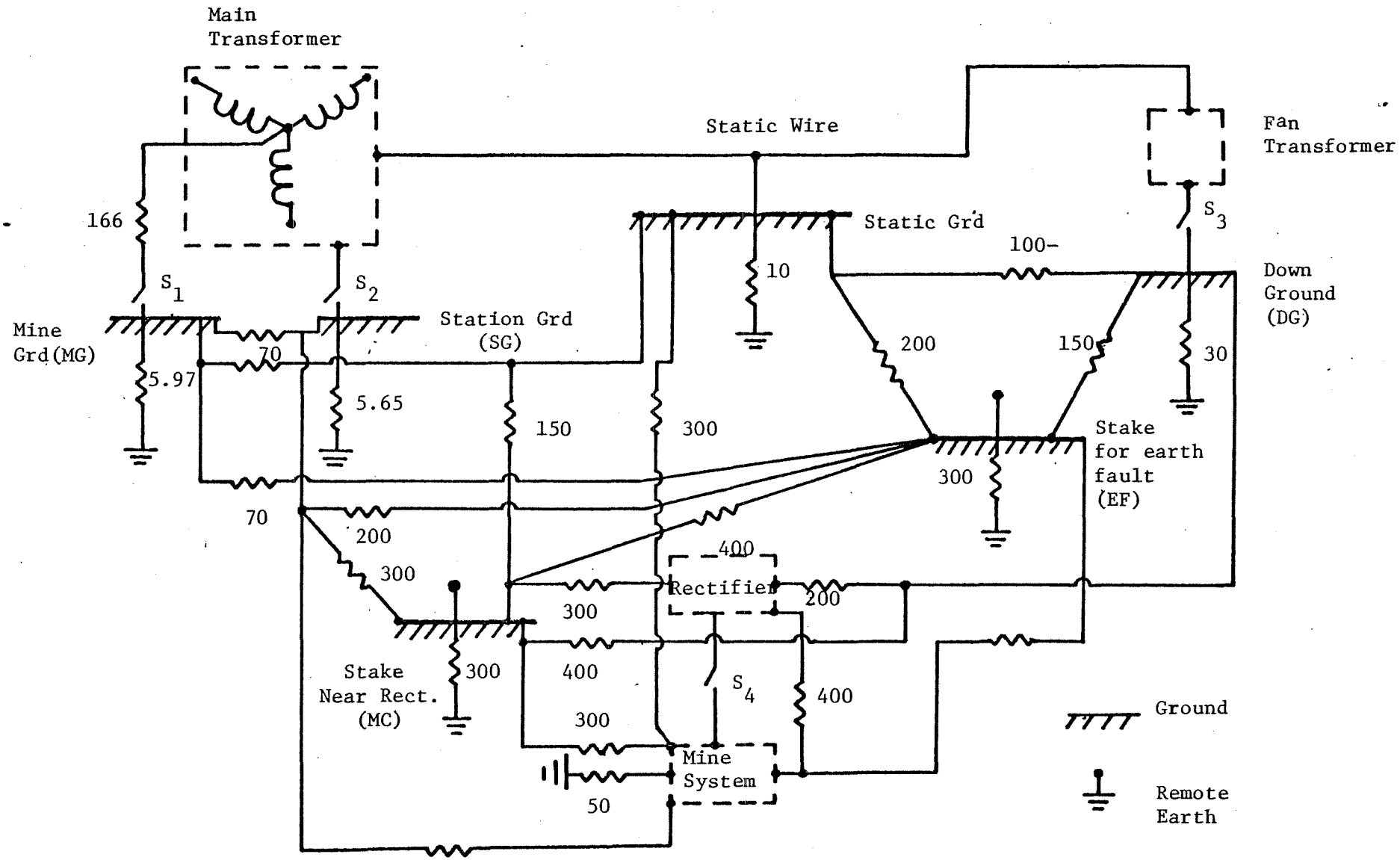


Fig. 3.3 Circuit Analog for the System.

TABLE 3.3

Comparison of Values Obtained by Computer Simulation and Actual Measurements

Fault Description	Fault Current (Amps)	Safety* Ground Voltage (Volts)	Station* Ground Voltage (Volts)	Voltages* of Static Near Rectifier (Volts)	Mine System Voltage (Volts)	Voltage Between Safety & Static Ground (Volts)	Touch Voltage at Rectifier (Volts)
I. Line-to-transformer frame (mine connected)	24.27 (23.75)	-68.52	57.83	13.13	-67.72	126.35(48)	81.65(29)
II. Same as above (mine disconnected)	24.27 (23.25)	-105.0	55.24	16.46	1.34	160.24(127)	121.46(115)
III. Line-to-earth (mine connected)	19.24 (16)	-38.79	24.97	80.75	-38.09	63.76(21)	119.54(23)
IV. Line-to-earth (mine disconnected)	19.08 (16)	-70.94	22.93	83.11	22.20	93.87(75)	153.05(750)

* All voltages with respect to remote earth (measured values in parentheses).

with the mine system connected the numbers differed considerably. Besides the modeling errors, one of the other reasons for the discrepancy could be that the resistance of the mine system to ground could not be determined and the value used in the simulation was based purely on guesswork.

However, all of the above goes to show that building an electrical analog can facilitate the study and give a better insight of the physical system.

Assuming that all the surface equipment was connected to the safety ground, the following fault conditions were studied using the model discussed above.

1. Line-to-fan transformer frame fault
2. Line-to-static wire fault
3. Line-to-earth fault

The results are presented in Table 3.4. A study of the table shows that the touch voltages have been eliminated during line-to-transformer frame fault. But voltages are still present during the other two types of faults.

3.3 RAIL BOND RESISTANCE MEASUREMENT

Previous annual reports have analyzed the leakage of current from haulage track in considerable detail. The analysis showed that leakage current could be quite large, and that it was probably responsible for corrosion problems, some ground-check monitor failures, and possibly some difficulties with protective relay coordination. Among the suggestions given to alleviate these problems was a recommendation that haulage track be inspected for defective rail bonds, since poor bonding significantly increases leakage.

Many defective rail bonds can be detected with a visual inspection, but many bonds passing visual inspection apparently have unacceptably high resistance. Measurement of the resistance of each bond in the mine is possible, but is difficult and time consuming using presently available equipment. An attempt is being made, therefore, to design an instrument that will allow the rapid location of unacceptable rail bonds.

3.3.1 Circuit Design

Since the rail is used as a return path to ground, there may be ac as well as dc current flowing through the rail. The ac current is typically the harmonics and the subharmonics of 60 Hz. Since these current components are constantly changing from the machines being operated in the mine, a constant current of a prime frequency is to be injected into the rail.

TABLE 3.4

Data Obtained by Computer Simulation (All Surface Equipment Connected to Safety Ground)

Fault Type	Fault Current (A)	Safety* Ground Voltage (V)	Station* Ground Voltage (V)	Voltage* of Stake Near Rectifier (V)	Mine* System Voltage (V)	Voltage Between Mine Ground and Safety Ground (V)	Touch Voltage at Rectifier
Line-to-transformer frame (mine connected)	25.04	0	0	0	0	0	0
Line-to-transformer frame (mine disconnected)	25.04	0	0	0	0	0	0
Line-to-static fault (mine connected)	24.25	-68.82	65.67	9.16	-68.02	134.49	77.98
Line-to-static fault (mine disconnected)	24.04	-105.48	63.18	12.45	1.36	168.66	117.93
Line-to-earth fault (mine connected)	19.21	-38.44	19.03	83.68	-37.75	57.47	122.12
Line-to-earth fault (mine disconnected)	19.05	-70.38	17.20	85.93	22.12	87.58	156.31

* All voltages with respect to remote earth.

To properly measure the voltage produced by the injected current, a synchronous detector is required to filter out the harmonics and the subharmonics of 60 Hz. A synchronous detector operates by "synchronously rectifying" the incoming signal. The dc voltage at the output of the detector indicates the presence of only the frequency of interest.

To determine if the copper bond is connected across the joint, some knowledge of the electrical characteristics of the rail, the rail joint, and the copper bond is required. Since the cross bonds create an infinite ladder through which some of the current injected into the rail can flow, its electrical characteristic is also required. As shown later, the resistance to be measured is very small. Therefore, a relatively large current has to be injected into the rail.

The basic alternatives for detecting the condition of the bond connection are the two-probe contact and the four-probe contact methods. With the two-probe contact method, the current is injected into the rail through two probes and the voltage is measured between those two probes. With the four-probe contact method, the current is injected into the outer two probes, and the voltage is measured between the two inner probes.

After considering these two alternatives, it was determined that the four-probe contact could be better adapted to the requirements of the device. The four-probe contact eliminates the effect of the contact resistance on the voltage probes; whereas, the two-probe contact takes into account the contact resistance. Since the contact resistance depends primarily on the pressure between the contact surfaces, this would be changing due to the surface of the rail.

The copper bond is usually about 30 inches in length when straight. When it is welded on the rail, it is usually curved and ranges from 22 to 26 inches between welds. Therefore, the voltage probes should be greater than 26 inches apart. The current probes should be far enough apart to allow the current to penetrate into the rail.

The device is mounted on a cart, shown in Fig. 3.4, so that it can be easily transported along the track. The probes being used are the wheels of the cart. The two inner wheels are about 32 inches apart to allow for some margin of error in locating the bond between the voltage probes. A piece of metal in a V-shape is connected to the frame of each wheel, which rubs against the wheel to make good electrical contact between the wheel and the frame. The pivot joint at the probes are to allow for some irregularities in the height of the rail. The rail is not always level, and to avoid having an open circuit occur, these pivot joints allow the wheels to be independent of each other.

The block diagram in Fig. 3.5 shows the instrumentation chosen for this project. A Wien bridge oscillator of 41 Hertz is used as

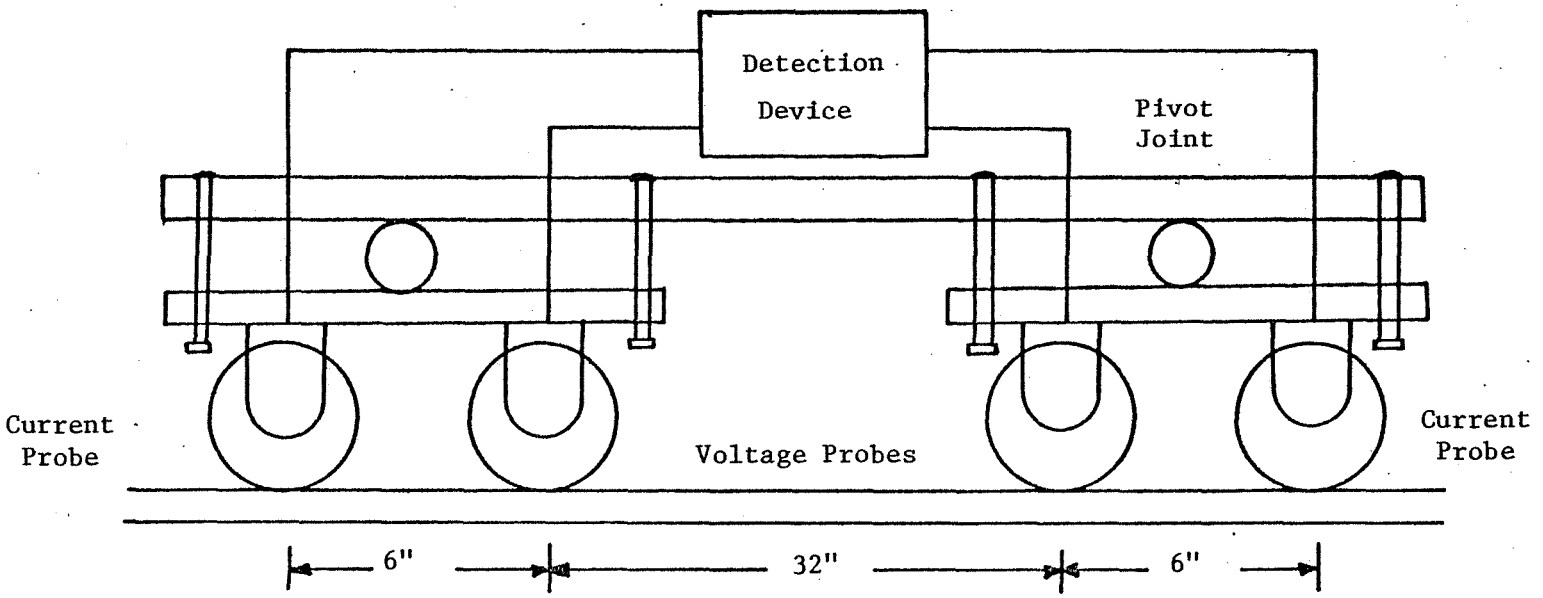


Figure 3.4 Cart Carrying the Broken Bond Detector

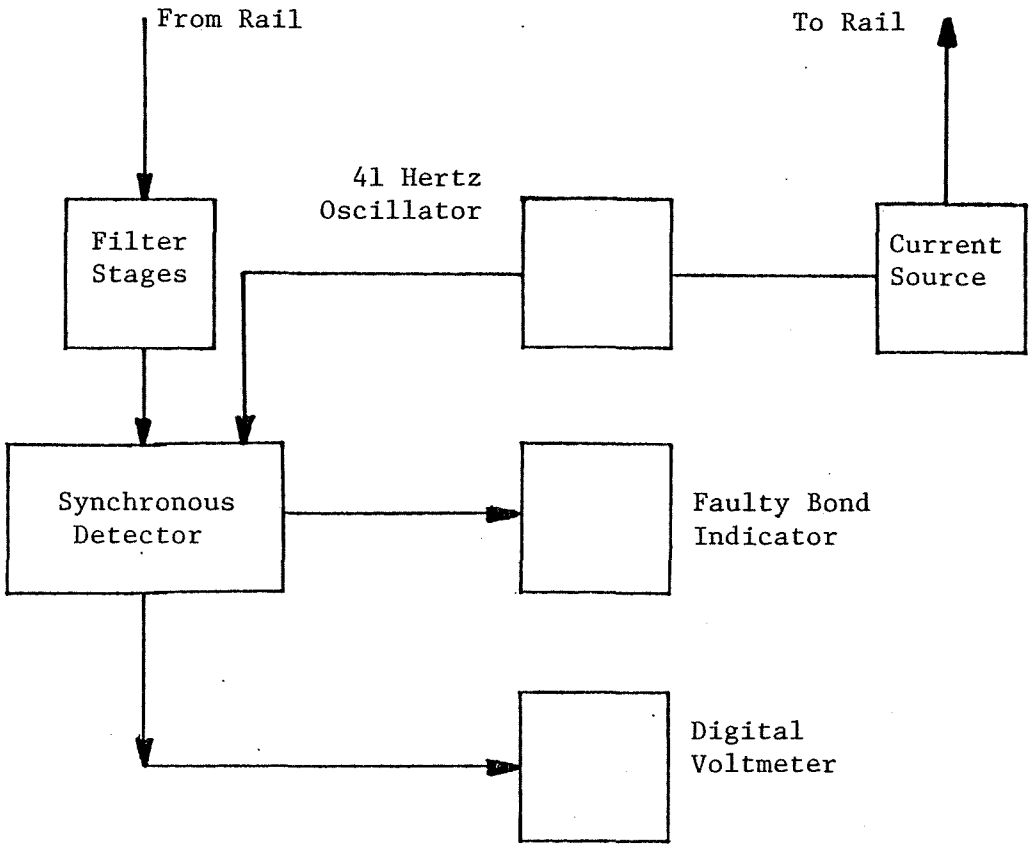


Fig. 3.5 Instrumentation Block Diagram

the frequency source. A 41 Hertz source is used since it is not a harmonic or subharmonic of 60 Hertz, and it is able to pass through a transformer. The original design called for an 11 Hertz oscillator, but it was rejected since it is hard to find a transformer that will pass this frequency at the high current anticipated.

The output of the oscillator goes into two buffer stages to prevent overloading. The output of the first buffer goes to the power driver (NE 540). The power driver (see Fig. 3.6) is used as a constant current source with the capability of driving approximately one ampere. The power driver has a gain of two and delivers a constant current through the 8 ohm load as well as through the transformer into the rail.

The output of the second buffer, going to the synchronous detector (see Fig. 3.7), requires some prior knowledge of the signal to be received. This poses no problem for the bond detector since this information is readily obtainable.

The 41 Hertz signal goes to a phase shifter that provides a phase shift from 0 to 180 degrees. The output of the phase shifter goes to two zero-crossing detectors (LM 311) whose outputs are 180 degrees out of phase, as in Fig. 3.8. The two outputs are used to control an analog switching device (CD 4066). The other inputs to the switching device are from the filter stages between the rails and the switching device.

Whenever the control is positive, the switch has a very low resistance, and the output is equal to the input. Whenever the control is negative, the switch exhibits a very high resistance and the output is grounded. The zero crossing detectors provide the switching rate for the analog switching device.

It is very important to have all the inputs of the 41 Hertz signal into the switching device in phase. This is necessary in order to get a maximum dc output of the synchronous detector that is proportional to the input signal from the rail. If the inputs were not in phase, there would be some ripple in the output and the reading on the voltmeter would be changing constantly. If the signal coming into the analog switching device is something else instead of the test 41 Hertz signal, it will have an overall average of zero and would not be detected by the synchronous detector.

Both outputs of the switching device are amplified, one inverted, and then they are run into a summing amplifier. The result of the summer gives an inverted full wave rectification of the desired signal with the other signals on top of it.

The output of the summer then goes into an inverting low-pass filter with a gain of one. The output of the low-pass filter is proportional only to the test signal from the rail. Any other signals

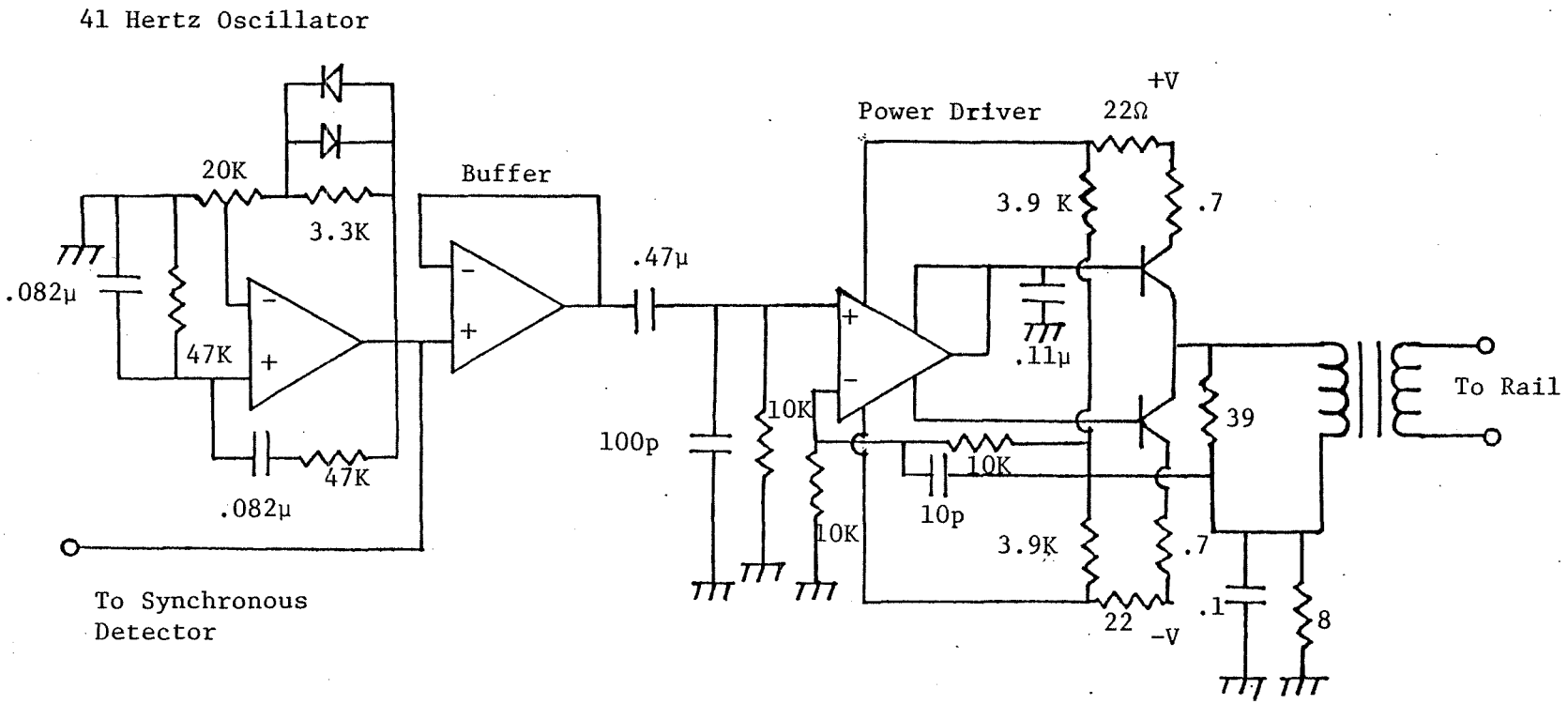


Fig. 3.6 Circuit Diagram of Oscillator, Buffer, and Power Driver

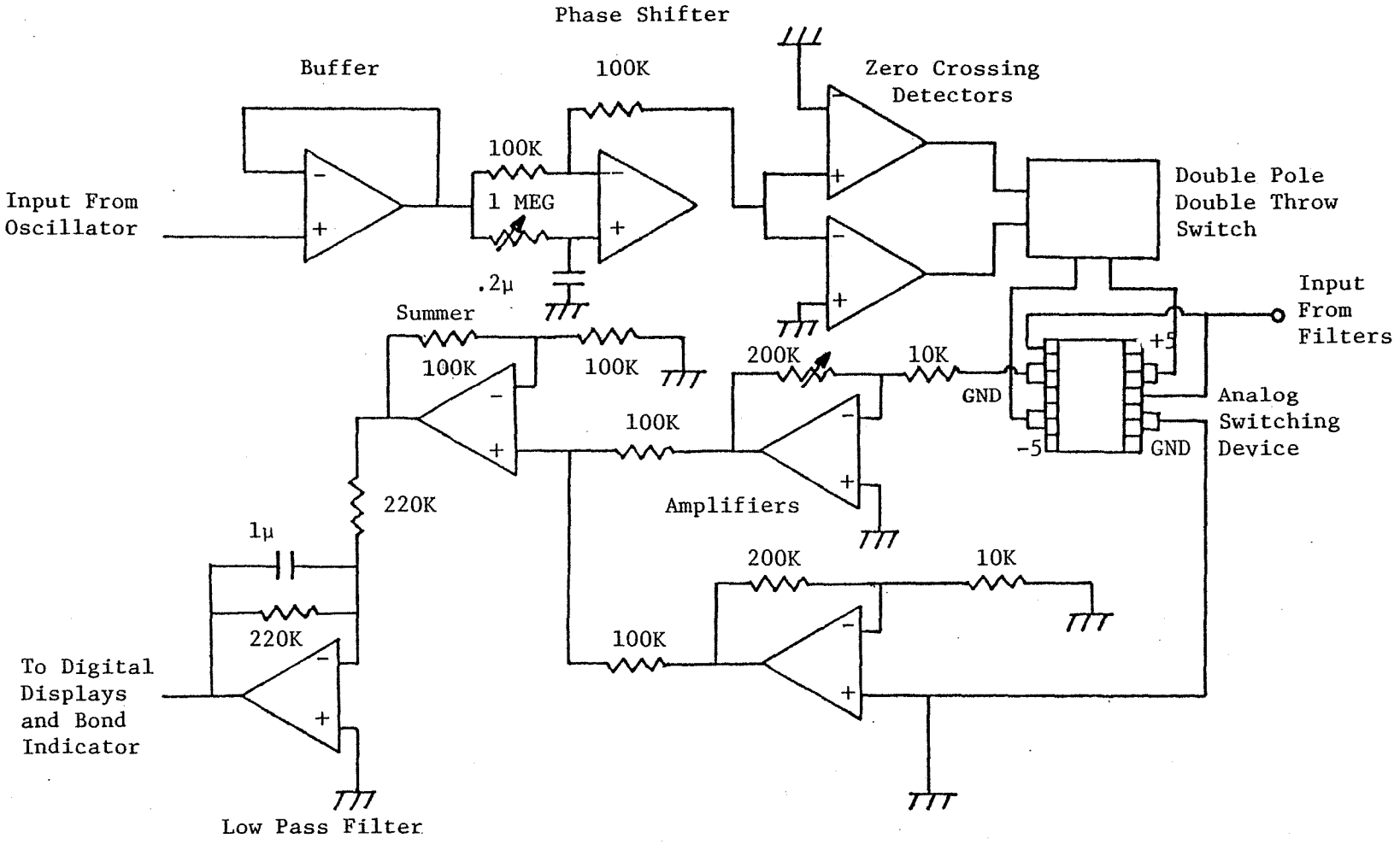


Fig. 3.7 Circuit Diagram of Synchronous Detector

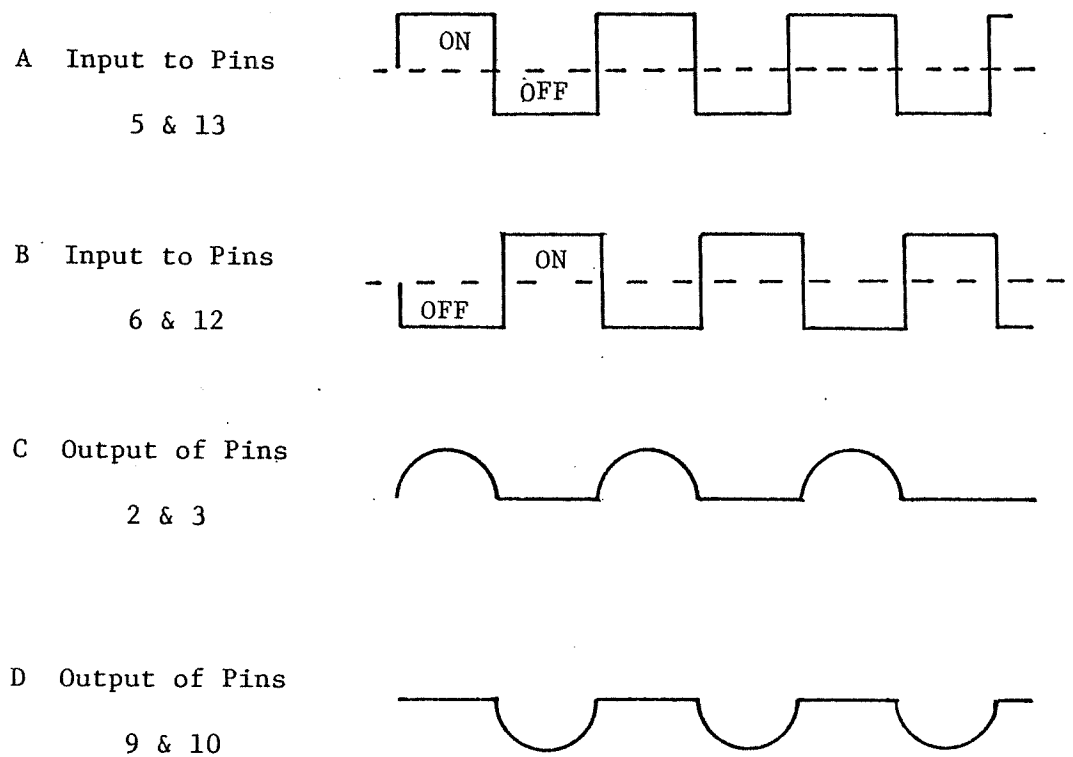


Fig. 3.8 Output Signals from Zero-Crossing Detectors

from the rail will not be detected. The pole of this filter should be at a very low frequency to obtain a dc output. Therefore, the resistance-capacitance time constant was set at 1.25 seconds which yields a pole at 0.8 Hz.

The dc output of the synchronous detector is then run into a 3½ digit digital voltmeter and a comparator (see Fig. 3.9). The reference voltage of the comparator (LM 311) is set at a particular value determined by calculations or tests. The output of the comparator goes into a NAND gate used as an inverter, and then to the gate of a silicon controlled rectifier (SCR). Whenever the voltage of the synchronous detector exceeds the reference voltage, the output of the comparator goes to a low level. The output of the inverter then goes positive, which triggers the SCR. The SCR is turned on and a light emitting diode (LED) flashes. This indicates that the bond resistance is too high. The 2 Hz oscillator is used so that when the voltage is less than the reference voltage, the SCR will automatically shut itself off. This will save the operator from resetting the bad-bond indicator.

The input from the voltage probes goes into a buffer, so that the effect of the contact resistance of the wheel on the rail does not have any effect on the voltage to be measured. The output of the buffer is run into two low-pass filters. At first, only a multiple feedback filter was used to block out the dc voltage, but this gave a gain of 0.8 at 60 Hz. So a 3 dB Chebychev filter with a pole at 70 Hz was added to cut down the 60 Hz gain to 0.3. These two filters give a voltage gain of one for the 41 Hz test signal. The 5- and 12-volt Zener diodes are required to protect the chips from being damaged by excessively large input voltages from the rail (see Fig. 3.10).

By using a summing amplifier to represent the input from the rail, several tests show that the detector gives a dc output that is only dependent upon the test signal. Care has been taken to make sure that both voltage gains are the same so that the other signal does not filter through. The input impedances to the two amplifiers are equal to each other so that the previous stage is not loaded down. The detector has a gain of approximately three times the zero-to-peak input voltage.

The 3½ digit digital voltmeter depends upon the accuracy of the reference voltage, which is either 2 volts or 2 millivolts. The input voltage should not exceed the reference voltage as this will cause an inaccurate reading and may damage the chips.

The unbonded joint indicator has been tested and it is working. The reference voltage has to be calculated in order to take it down in the mine.

The power driver has a constant current drive of about 0.2 amperes through the high side of the transformer. The 39 ohm load in parallel with the transformer is to protect the circuit in case an

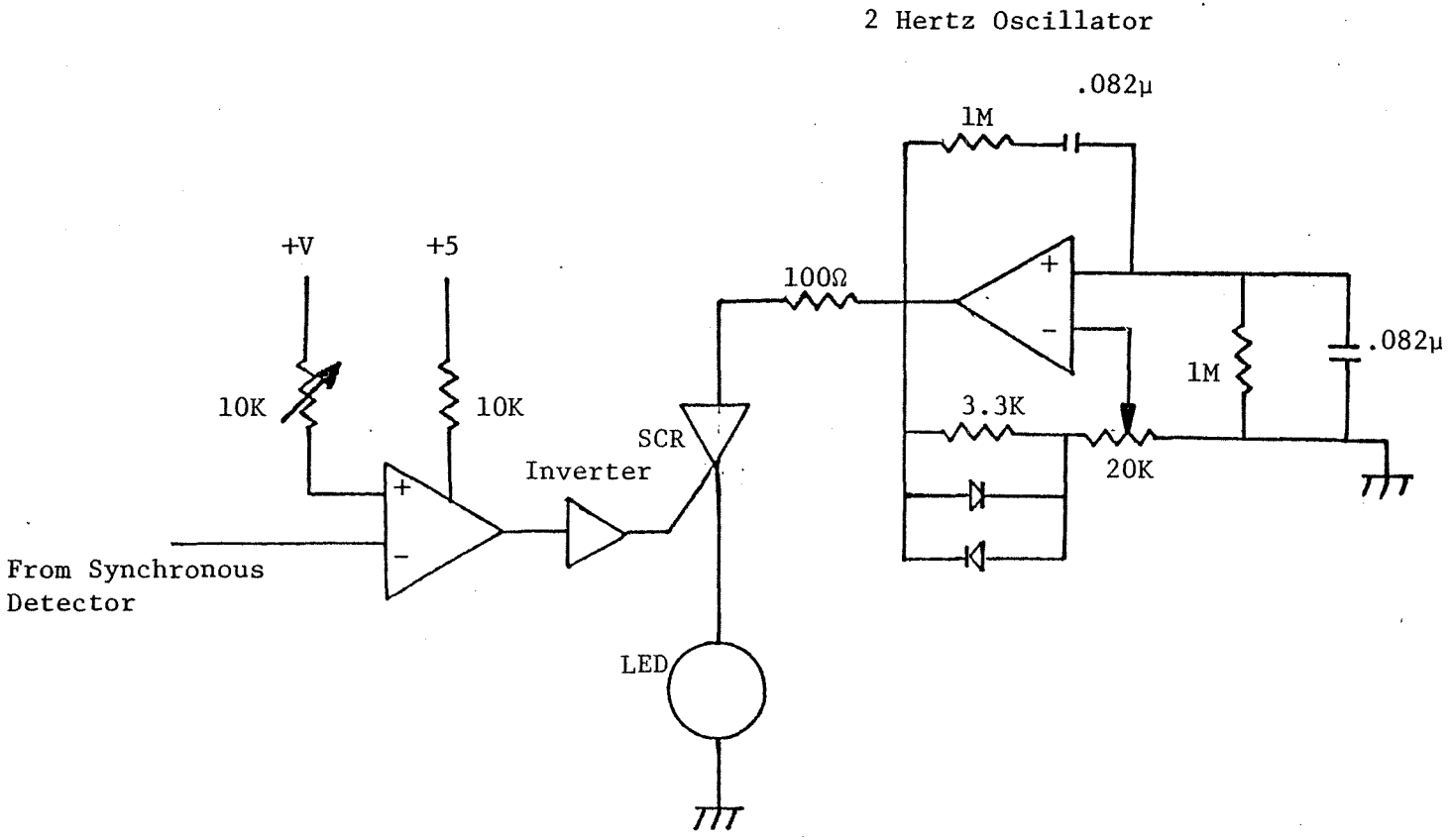


Fig. 3.9 Circuit Diagram of Comparator and Indicator

Multiple Feedback Low Pass Filter

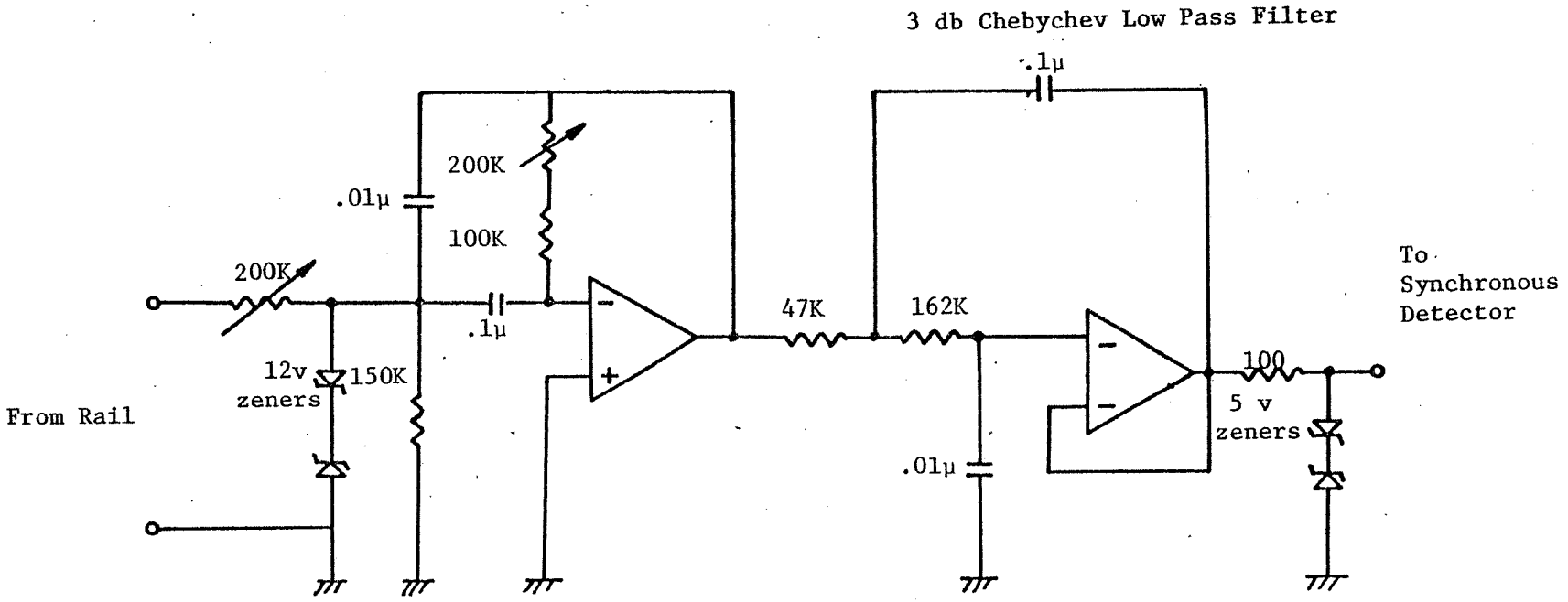


Fig. 3.10 Input Filtering and Protection

open circuit accidentally occurs at the terminals of the transformer. The 0.7 ohm resistors from the supply voltages to the collector of the power transistors are to limit the current if a short circuit accidentally occurs at the output of the transistors. The power driver is also protected by the power limiting resistor of 22 ohms. If the voltage across these resistors exceeds a certain level set by the chip the power driver automatically shuts itself off until that voltage is below the set level.

All of the circuitry is mounted on printed circuit boards. Tests made when all of the circuitry was connected together gave good results. All the inputs to the synchronous detectors are in phase and all stages are well protected.

3.3.2 Rail Bond Data

Although the cart has not yet been taken down into a mine for field tests, a moderate amount of pertinent information has been obtained from literature, theoretical analysis, and simulations.

The electrical characteristics of the rail, the rail joint, and the copper bond are shown in Table 3.5. The table and the following calculations show that the resistance to be detected is very small. There is, however, a relatively big difference between a bonded joint and an unbonded joint. The resistance of the bonded joint is approximately equal to the resistance of the copper bond. The unbonded joint has a resistance approximately equal to 4000 feet of track. The resistance of the rail listed in the table is provided that each rail is cross bonded and bonded across the joints (2).

TABLE 3.5
Electrical Characteristics of Haulage Rail

Weight of Rail Per Yard (lbs)	Resistance Ohms/1000 feet	Resistance of Unbonded Joints (Ohms)
30	0.018	0.072
40	0.0135	0.054
50	0.0108	0.0432
60	0.009	0.036
70	0.0077	0.0308
80	0.0067	0.0268
90	0.006	0.024
100	0.0054	0.0216

The copper bond has a resistance of 0.052 ohms/1000 feet. The resistance of the 30 inch copper bond is:

$$\left(\frac{.052\ \Omega}{1000\ \text{ft}}\right)\ \left(\frac{1\ \text{ft}}{12\ \text{in}}\right)\ (30\ \text{in}) = .13\ \text{m}\Omega\ (\text{milliohms})$$

The resistance of the bond in parallel with the joint is:

$$(.13\ m\Omega)\ 11(.072\ \Omega) = 0.12977\ m\Omega$$

The cross bonds are required by the Federal Government for safety reasons. They cause an infinite ladder network, whose equivalent resistance of the circuit can be determined by a relatively simple computer program.

Several tests were run on the computer to find the equivalent resistance of the infinite ladder. The tests are slightly different in that certain cross bonds and bonds across the joints were considered to be broken. This data is used to roughly calculate the amount of current flowing through the bonded and unbonded rail joint.

Various combinations of broken rail bonds and cross bonds were simulated. The largest change in ladder resistance was found to be about .06%. On the other hand, estimates are that the breaking of a rail bond directly under the instrument will increase the joint resistance by ten times. Although shunted by the ladder network, this should produce a significant change. Therefore, since the exact topology of the ladder has relatively little effect on its resistance, a bad bond will be relatively easy to identify once the instrumentation has been put into operation.

Two pieces of mine rail with a joint have been obtained for simulation of test conditions. Tests so far indicate that there may be a problem of high contact resistance between the wheels and the rail. Initial readings on weathered rail indicate the resistance is about 250 KΩ, an unacceptably high value. It is not known if rail which is in daily use will exhibit such a high contact resistance. If so, it may be necessary to incorporate a rotary wire brush ahead of the wheels to clean the rail.

3.3.3 Conclusions

The device shows promise as a way to eliminate most of the physical labor required to check all the bonds down in the mine, making the return on the money invested well worth the effort.

The device can be improved by obtaining a higher current. This can be done by lowering the current limiting and the power limiting resistors or using a higher turns-ratio transformer to achieve a higher secondary current. This will help to reduce some of the noise problems down in the mine, and is being implemented.

Whenever the unbonded joint indicator flashes, an SCR could also be triggered to spray a blast of paint on the rail. This will make

it easier for the welder to spot the unbonded joint location while the operator of the device continues along the track. It will significantly decrease the number of hours required to check the rail bonds.

Ultimately, the device can be expanded to do both rails at the same time. Then the device will not only detect bonds across the joints on both rails, but it will also be able to detect broken cross bonds.

The device will probably be pulled by a mine locomotive along the track in the future. For now, it has to be set directly above the joint to detect faulty rail bonds. Power from the overhead cable could possibly be used in the future.

3.4 GROUNDING STANDARDS AND REGULATIONS

The principal investigator (Dr. W.L. Cooley) participated actively in efforts to set up or revise industry standards for grounding. Meetings were attended which reviewed proposed amendments to Part 77 of Title 30 of the Code of Federal Regulations. A single meeting was attended at which proposed revisions to Part 55 (dealing with electrical practice in metal and non-metal mines) was discussed. As well as participating as a general member of the IAS Mining Industry Committee of IEEE, the principal investigator also served on a special 6-man work group on Part 77, which consisted of Wils Cooley, John Looney, William Lyon, Edward Smith, Thomas Taylor, and James Elliott, Chairman.

CHAPTER IV: MULTIPLE-ROD GROUND BEDS

4.1 THE ROD MODEL

Although the constituent electrodes of the ground beds in the previous annual reports were treated as small hemispheres, the analyses presented are valid for arrangements of electrodes of arbitrary shapes only as long as one condition is satisfied. This condition is that no (test or constituent) electrode, not even a 'small' hemisphere, be placed closer to any of these arbitrarily-shaped electrodes than a distance corresponding to a few times the largest dimension of these electrodes. This limitation exists because the potential of a closely-placed electrode, due to the arbitrarily-shaped electrode, always has been assumed to be that which would exist due to a nearby hemisphere. Only if the displacement is at least a few electrode (largest) dimensions can this assumption be guaranteed.

Removal of this restriction requires that an analytic expression be found for the potential near a given non-hemispheric electrode. There are two difficulties with such expressions. First, they do not exist, at least in exact form, for most practical electrode shapes. Second, even where approximate formulae can be obtained, they are most often transcendental: this means that the resulting equations which contain these expressions cannot be solved analytically. These difficulties are reflected in the state of the art of ground-bed design and measurement: it contains approximate formulae for some common electrodes (often more than one formula exists for a single electrode) but little about multiple-electrode configuration with small spacings. A major portion of the research done here has consisted of studying one particular non-hemispheric electrode, the driven rod, to evaluate the available analytic expressions for its potential distribution and formulate ways of calculating and measuring the resistance of groups of rods. There are no exact formulations for the resistance of a cylinder buried perpendicular to the ground plane. Two approximations exist, which come from entirely different assumptions.

The first approximation assumes that the rod (cylinder) consists of a series of infinitesimally short cylindrical elements. From each of these elements leaves the same infinitesimal leakage current. If the total current carried by the rod is I, analysis[1] yields

$$V(r,z) = \frac{\rho I}{4\pi \ell} \ln \frac{[(z+\ell)^2 + r^2]^{\frac{1}{2}} + (z+\ell)}{[(z-\ell)^2 + r^2]^{\frac{1}{2}} + (z-\ell)} \qquad (4.1)$$

Here r and z are cylindrical coordinates as shown in Figure 4.1. ℓ is the rod length and ρ the earth resistivity.

Two special cases of this expression are of interest: the potential along the surface of the earth due to the rod, and the potential of the rod itself. This first case is obtained by evaluating the above expression at z = 0:

$$V(r,0) = \frac{\rho I}{4\pi\ell} \ln\left[\frac{(r^2 + \ell^2)^{\frac{1}{2}} + \ell}{(r^2 + \ell^2)^{\frac{1}{2}} - \ell}\right]$$

$$= \frac{\rho I}{2\pi\ell} \ln\left[\sqrt{(\frac{\ell}{r})^2 + 1} + \frac{\ell}{r}\right] \qquad (4.2)$$

The potential of the rod itself is found by evaluating the expression for r = a (a being the rod radius) and averaging it over the rod length:

$$V = \frac{1}{\ell}\int_0^{\ell} V(a,z)\, dz$$

$$= \frac{\rho I}{2\pi\ell}\left\{\ln\left[\frac{2\ell}{a}\left(1 + \sqrt{1 + \frac{a}{2\ell}^2}\right)\right] + \frac{a}{2\ell} - \sqrt{1 + \frac{a}{2\ell}^2}\right\}$$

$$= \frac{\rho I}{2\pi\ell}\left[\ln\left(\frac{4\ell}{a}\right) - 1\right] \quad (\ell >> a)$$

or

$$R_{\infty 1} = \frac{V}{I} = \frac{\rho}{2\pi\ell} \ln\frac{4\ell}{a} - 1 \qquad (4.3)$$

Examination of the above expression for V(r,z) shows that equipotential lines are confocal ellipsoids of revolution centered at (0,0). Any of these ellipsoids can be replaced by a conducting shell without changing the potential distribution. Furthermore, the region inside a conducting shell can be filled with a solid conductor, without changing the potential distribution outside the shell (provided the shell is held at the same potential as before). This suggests an alternate approximation for the cylindrical electrode: an ellipsoid of revolution with a large major axis and small minor axis.

If the major axis is denoted by ℓ^* and the minor axis by 'a' (the cylinder radius), these two quantities are related by

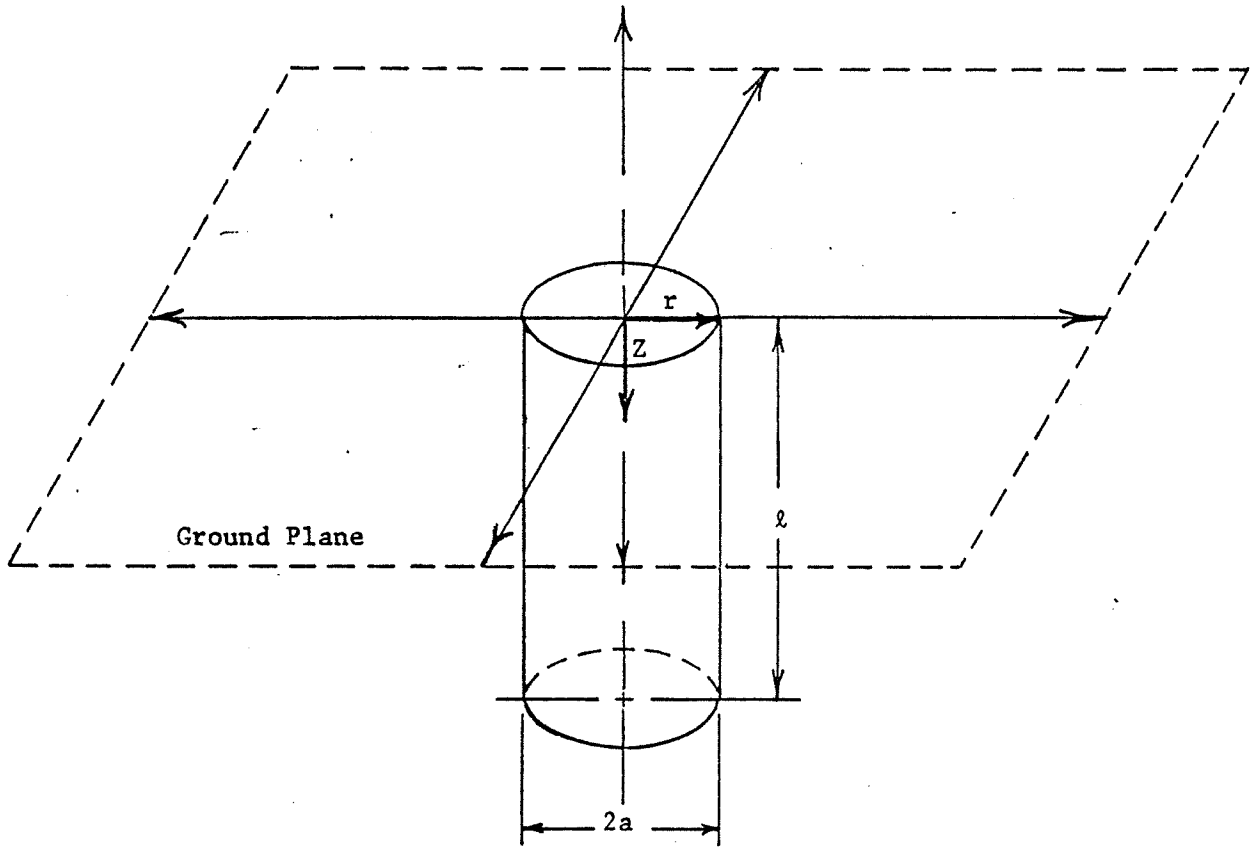


Fig. 4.1. Cylindrical Coordinate System.

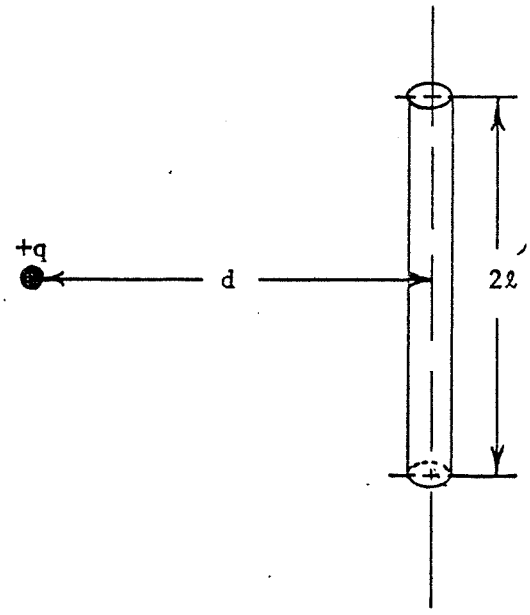


Fig. 4.2. Point Charge and Dielectric Cylinder.

$$\ell^2 = \ell^{*2} - a^2$$

As ℓ^* is of the order of 50 to 100 times 'a' for the rod electrodes of interest here, ℓ^* and ℓ can be used interchangeably with less than 0.02% error. The potential distribution due to an ellipsoidal electrode with minor axis a, major axis ℓ^*, is, to an excellent approximation

$$V(r,z) = \frac{\rho I}{4\pi\ell} \ln \frac{(z+\ell) + \sqrt{(z+\ell)^2 + r^2}}{(z-\ell) + \sqrt{(z-\ell)^2 + r^2}} \qquad (4.4)$$

Evaluation of the rod potential is much simpler for this case, as the rod is an isopotential surface (no averaging is necessary). The rod potential is simply

$$V(a,0) = \frac{\rho I}{4\pi\ell} \ln \frac{\ell + \sqrt{\ell^2 + a^2}}{-\ell + \sqrt{\ell^2 + a^2}} = \frac{\rho I}{2\pi\ell} \ln \frac{2\ell}{a} \quad (\ell >> a)$$

or

$$R_{\infty 2} = \frac{\rho}{2\pi\ell} \ln \frac{2\ell}{a} \qquad (4.5)$$

The two expressions for R_∞ of the rod yield similar numbers for a given rod length and radius. The second equation always yields a higher resistance value, as can be seen by evaluating

$$R_{\infty 2} - R_{\infty 1} = \frac{\rho}{2\pi\ell} \left(\ln \frac{2\ell}{a} - \ln \frac{4\ell}{a} + 1\right)$$

$$= \frac{\rho}{2\pi\ell} \ln \frac{2\ell}{a} \cdot \frac{a}{4\ell} \cdot e = \frac{\rho}{2\pi\ell} \ln \frac{e}{2} \qquad (4.6)$$

which is necessarily positive. The percentage difference between the two,

$$\frac{R_{\infty 2} - R_{\infty 1}}{R_{\infty 2}} = \ln \frac{e}{2} \ln \frac{2\ell^{-1}}{a} \quad (e = 2.718\ldots) \qquad (4.7)$$

lies in the range of 7 to 8 percent for $50 < \frac{\ell}{a} < 100$.

4.1.1 Choice of Approximation

It is difficult to decide, by direct measurement, which of the two expressions for R_∞ is more accurate, as both yield similar values. The first approximation is based on the correct physical shape (especially for a borehole casing) but yields a varying potential (with constant leakage current) along the length of the cylinder. The second (ellipsoidal) approximation is a poorer rendition of a cylindrical electrode (except, perhaps, for a pointed rod), but yields a constant potential surface, with leakage current increasing from a minimum at the surface to a maximum at the rod's end. The electrical properties of the second approximation are much more like that of an actual rod electrode, as it is a nearly isopotential surface; corrosion studies suggest that leakage current is highest near the end of the rod. The more realistic electrical behavior, combined with more conservative resistance predictions, and relative simplicity, make the second approximation a more attractive choice; it is used exclusively in the analysis which follows.

4.1.2 Potential Induced on Rod by Small Hemisphere

The potential induced on a hemisphere, by another hemisphere (which carries a given current) is easily calculated provided the radius of the second hemisphere is small compared to the distance between the two hemispheres' centers. Unfortunately, the corresponding calculation of the potential induced on a cylindrical electrode is not straightforward, particularly if the distance between the center of the hemisphere and the top of the rod is less than the rod length. Exact analysis appears to be quite formidable; the approximate analysis here is valid only if the separation between the hemisphere and rod is several times the rod diameter.

Consider an electric field which, in cylindrical coordinates, is uniform in the r- and θ-direction, but varies with z. (This is a good approximation to the field due to a hemisphere in the vicinity of a far-away rod). If this field exists in isotropic earth of resistivity ρ, there will be current flowing through the earth whose density at any point is proportional to the electric field. Now if a highly conducting (but unconnected) rod is placed in this earth with its axis parallel to the z-axis, currents will flow in the rod such that two conditions are satisfied:

1. The rod must be an isopotential surface.

2. The net current flowing into the rod must be zero.

The first condition arises from the assumption that the rod is highly conductive, the second condition from its being unconnected. The current distribution must be obtained in order to find the potential of the rod due to the applied electric field. To find this current

distribution, it is convenient to solve the analogous electrostatic problem, of a conducting rod immersed in a dielectric medium at some distance from a point charge (see Figure 4.2).

The component of the electric field, due to the point charge in the z-direction at the rod would be

$$E_z = \frac{qz}{4\pi\varepsilon(z^2 + d^2)^{\frac{3}{2}}} \quad (z > 0) \tag{4.8}$$

if the rod were not a conductor. A charge distribution must be found which produces an electric field exactly opposed to this such that the total field is zero. If the z-component (the only component) of this field is denoted by E'_z, Gauss' Law requires that

$$\frac{\partial E'_z}{\partial z} = -\frac{\partial E_z}{\partial z} = \frac{\rho_e}{4\pi\varepsilon_0} \tag{4.9}$$

Here ρ_e is the (unknown) free charge density, and ε the permitivity of the medium. Given the previous assumption of cylindrical symmetry, the previous equation can be written as

$$-\pi a^2 \frac{dE_z}{dz} = \frac{\lambda(z)}{4\pi\varepsilon} \tag{4.10}$$

where $\lambda(z)$ is the line charge density required to nullify the applied field E_z. From above,

$$E_z = \frac{qz}{4\pi\varepsilon(z^2 + d^2)^{\frac{3}{2}}}$$

$$\lambda(z) = q\pi a^2 \frac{2z^2 - d^2}{(z^2 + d^2)^{\frac{5}{2}}} \tag{4.11}$$

In addition to this line charge density, there will be a surface charge on each end of the cylinder:

$$\sigma(\ell) = 4\pi\epsilon E_z(\ell) = \frac{q\ell}{(\ell^2 + d^2)^{\frac{3}{2}}} \quad (\text{at } z = \ell) \tag{4.12}$$

$$\sigma(-\ell) = 4\pi\epsilon E_z(-\ell) = \frac{q\ell}{(\ell^2 + d^2)^{\frac{3}{2}}} \quad (\text{at } z = -\ell) \tag{4.13}$$

The total charge on the cylinder is the sum of the line charge and surface charge:

$$Q_{total} = \int_{-\ell}^{\ell} \lambda(z)dz + \pi a^2[\sigma(\ell) + \sigma(-\ell)] \tag{4.14}$$

$$= (4\pi\epsilon)(\pi a^2)[-E_z(\ell) + E_z(-\ell) + E_z(\ell) - E_z(-\ell)]$$

$$= 0$$

which is as it should be, because the rod (cylinder) is isolated. Now that the charge distribution is known, the potential of the cylinder due to its induced charge can be found. First, the potential at the midpoint of the rod to the line charge:

$$V = \frac{1}{4\pi\epsilon}\int_{z=-\ell}^{z=\ell} \frac{\lambda(z)dz}{(a^2 + z^2)^{\frac{1}{2}}} = \frac{qa^2}{4\epsilon}\int_{-\ell}^{\ell} \frac{(2z^2 - d^2)dz}{(a^2 + z^2)^{\frac{1}{2}}(a^2 + z^2)^{\frac{5}{2}}}$$

$$= \frac{qa^2}{2\epsilon}\int_{0}^{\ell} \frac{(2z^2 - d^2)dz}{(a^2 + z^2)^{\frac{1}{2}}(d^2 + z^2)^{\frac{5}{2}}} \tag{4.15}$$

No analytic solution for this integral has been found, but it can be integrated numerically. The potential at the midpoint of the rod due to the surface charges on the ends of the rod is negligible if $r \ll \ell$, as has been assumed. Therefore the potential of the rod due to all the induced charge on the rod is given by the above integral. The analogous solution for the potential on a rod due to a nearby hemisphere carrying current I, with earth resistivity ρ is obtained by replacing:

1. q by 2I (the electrode is a hemisphere, not a sphere)

2. E by $\frac{1}{\rho}$.

This yields

$$V = \rho I d^2 \int_0^{\ell} \frac{(2z^2 - d^2)dz}{(a^2 + z^2)^{\frac{1}{2}}(z^2 + d^2)^{\frac{5}{2}}}$$

or

$$R'_{hr} = \frac{V}{I} = \rho a^2 \int_0^{\ell} \frac{(2z^2 - d^2)dz}{(a^2 + z^2)^{\frac{1}{2}}(a^2 + d^2)^{\frac{5}{2}}} \qquad (4.16)$$

where R'_{hr} is a mutual resistance between the hemisphere and rod. The total mutual resistance between a hemisphere and rod is sum of this term and another (larger) term which expresses the potential of the rod due to the current flowing in the hemisphere

$$R_{hh} = \frac{\rho}{2\pi d} \qquad (4.17)$$

The subscript 'hh' is used because this term is identical to the mutual resistance between two small hemispheres. The total mutual resistance between a rod and hemisphere is then

$$R_{hr} = R_{hh} + R'_{hr} \qquad (4.18)$$

This can also be written as

$$R_{hr} = R_{hh}(1-E) \qquad (4.19)$$

where E is a "correction factor" defined as

$$E = 2\pi a^2 d \int_0^{\ell} \frac{(d^2 - 2z^2)dz}{(a^2 + z^2)^{\frac{1}{2}}(d^2 + z^2)^{\frac{5}{2}}} \qquad (4.20)$$

In many cases E is quite negligible and R_{hh} and R_{hr} can be used interchangeably. Before evaluating E, however, it is convenient to take advantage of the dimensionlessness of E to reduce the number of independent variables. With the definitions $\alpha = \frac{a}{\ell}$, $\delta = \frac{d}{\ell}$, $\zeta = \frac{z}{\ell}$, E can be written as

$$E = 2\pi\alpha^2\delta \int_0^{\ell} \frac{(\delta^2 - 2\zeta^2)\,d\zeta}{(\alpha^2 + \zeta^2)^{\frac{1}{2}}(\delta^2 + \zeta^2)^{\frac{5}{2}}} \qquad (4.21)$$

As ζ is a dummy variable of integration, E is a function only of α and δ. Figure 4.3 shows a plot of E as a function of δ for various values of α. The plot was obtained by first analytically integrating the expression for E by parts to obtain a smoother integrand. The resulting integral was evaluated by means of a 6-point Gaussian quadrature. The plots were not extended further to the left because the underlying analysis breaks down as δ approaches α. Note that the correction factor is very small if $\delta \gg 0$ for all α, and also if $\alpha \ll 1$ for all δ. The first case corresponds to a large separation between the cylinder and hemisphere, the second case to a very thin rod. For common values of α, say $0.01 < \alpha < 0.03$, E is less than 1% for $\delta > 1$. As a rule of thumb, then, the correction factor can be ignored if the spacing between the rod and hemisphere is more than the rod length.

4.1.3 Resistance Measurement of a Single Rod

The basic resistance measurement procedure for a rod is the same as for a hemisphere. A current I is circulated between the rod and an auxiliary electrode located at a distance r_c from the rod. Voltage V is measured between the rod and a second auxiliary electrode r_p away. For some value(s) of $\frac{r_p}{r_c}$, the ratio $\frac{V}{I}$ yields the true resistance, R_∞, of the rod. As with the hemisphere, a number of schemes suggest themselves.

First, the 0.618 rule: the two auxiliary electrodes are placed on a straight line with the rod center such that

$$r_p = 0.618\, r_c$$

The error resulting from this technique can be calculated as follows. The voltage measured between the rod and the auxiliary hemisphere is

$$V = IR_\infty - \frac{\rho I}{2\pi r_c} - \frac{\rho I}{2\pi\ell} \ln\left[\sqrt{\left(\frac{\ell}{r_p}\right)^2 + 1} + \frac{\ell}{r_p}\right] - \frac{\rho I}{2\pi(r_c - r_p)} \qquad (4.22)$$

The third term in the equation is the potential of the auxiliary electrode due to current flowing in the rod. This was derived at the beginning of the preceding section. R_∞ was also shown to be

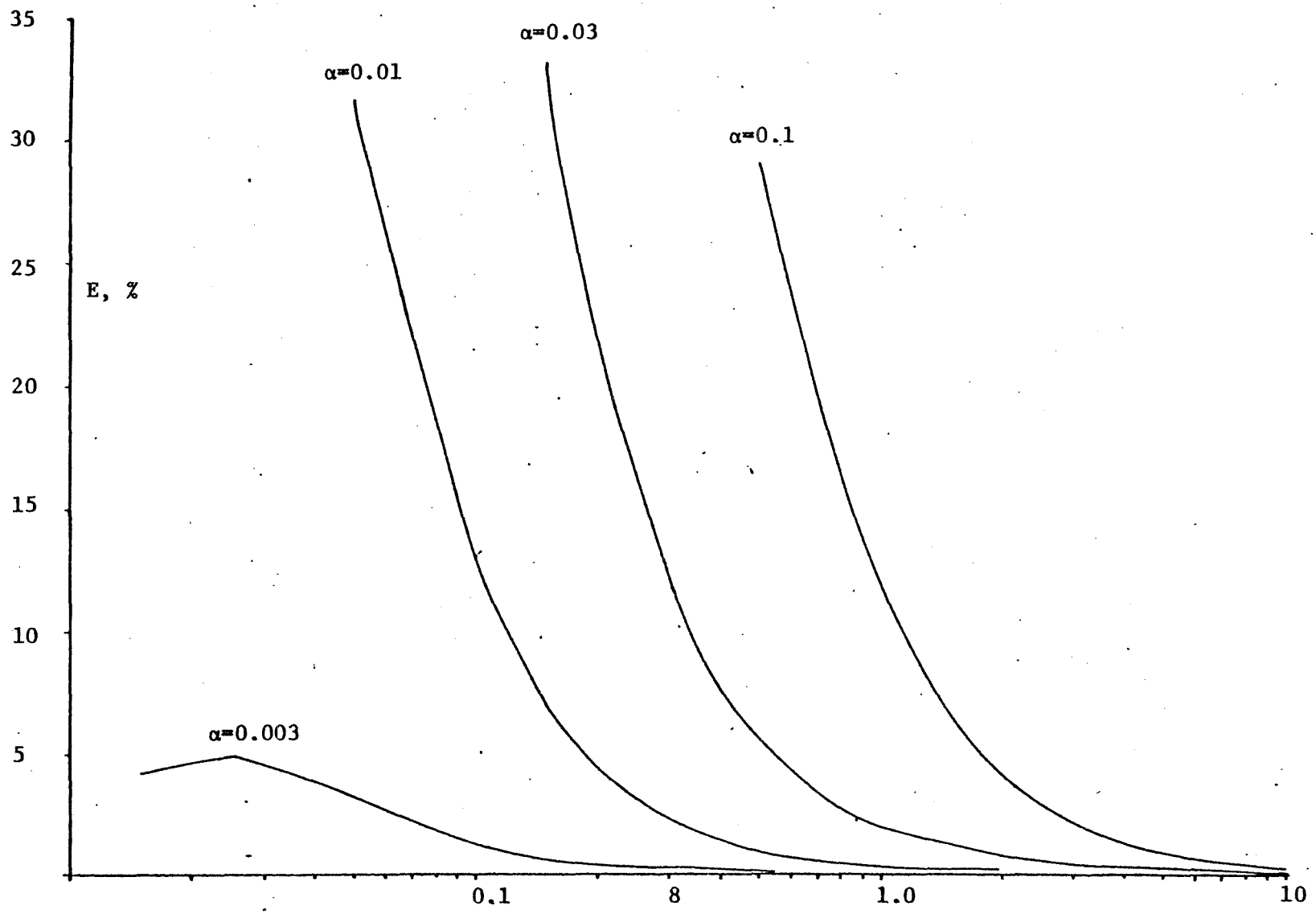


Fig. 4.3. Correction Factor for Hemisphere-Rod Mutual Resistance.

$$R_\infty = \frac{\rho I}{2\pi \ell} \ln \frac{2\ell}{a} \qquad (4.5)$$

Therefore, the percentage error in R_∞ is

$$\frac{\frac{V}{I} - R_\infty}{R_\infty} = \ell \left[\frac{1}{r_c - r_p} - \frac{1}{r_c} - \frac{1}{2\ell} \ln \left(\sqrt{\left(\frac{\ell}{r_p}\right)^2 + 1} + \frac{\ell}{r_p} \right) \right] \left(\ln \frac{2\ell}{a} \right)^{-1}$$

$$= \frac{\ell}{r_c} \left[\frac{1}{1 - \frac{r_p}{r_c}} - 1 - \frac{1}{2\left(\frac{\ell}{r_c}\right)} \ln \left(\sqrt{\left(\frac{\ell}{r_p}\right)^2 + 1} + \frac{\ell}{r_p} \right) \right] \left(\ln \frac{2\ell}{a} \right)^{-1} \qquad (4.23)$$

With the definitions $\lambda = \frac{r_p}{r_c}$, $\alpha = \frac{a}{\ell}$, $\beta = \frac{\ell}{r_c}$,

$$\frac{\frac{V}{I} - R_\infty}{R_\infty} = \beta \left[\frac{1}{1-\gamma} - 1 - \frac{1}{2\beta} \ln \left(\sqrt{\left(\frac{\beta}{\gamma}\right)^2 + 1} + \frac{\beta}{\gamma} \right) \right] \left(\ln \frac{2}{\alpha} \right)^{-1}$$

$$= \left[\frac{\beta\gamma}{1-\gamma} - \frac{1}{2} \ln \left(\sqrt{\left(\frac{\beta}{\gamma}\right)^2 + 1} + \frac{\beta}{\gamma} \right) \right] \left(\ln \frac{2}{\alpha} \right)^{-1} \qquad (4.24)$$

For the typical value of $\alpha = 0.01$, this error is plotted in Figure 4.4 for $\gamma = 0.618$ as a function of β. The ratio $\frac{V}{I}/R_\infty$ is high by 7% for $r_c = \ell$. For larger values of β the error is quite large, reaching +240% for $\beta = 10$. Only for $r_c > 10\ell$ does the method yield errors of less than 1%.

4.1.4 Improved Method of Calculating Rod Resistance

A value of γ can be found for any value of β such that the error is zero. Figure 4.5 shows a plot of the solutions for γ, i.e. $\frac{r_c}{r_p}$. The potential electrode is always located closer than the spacing dictated by the 0.618 rule. Note that although the error curve in Figure 4.4 may change slightly with different cylinder radii, the optimum potential electrode locations dictated by Figure 4.5 are independent of the radius (as long as $r_c \gg a$). As long as $\alpha\beta \ll 1$, the correction factor derived in the previous section does not have to be used.

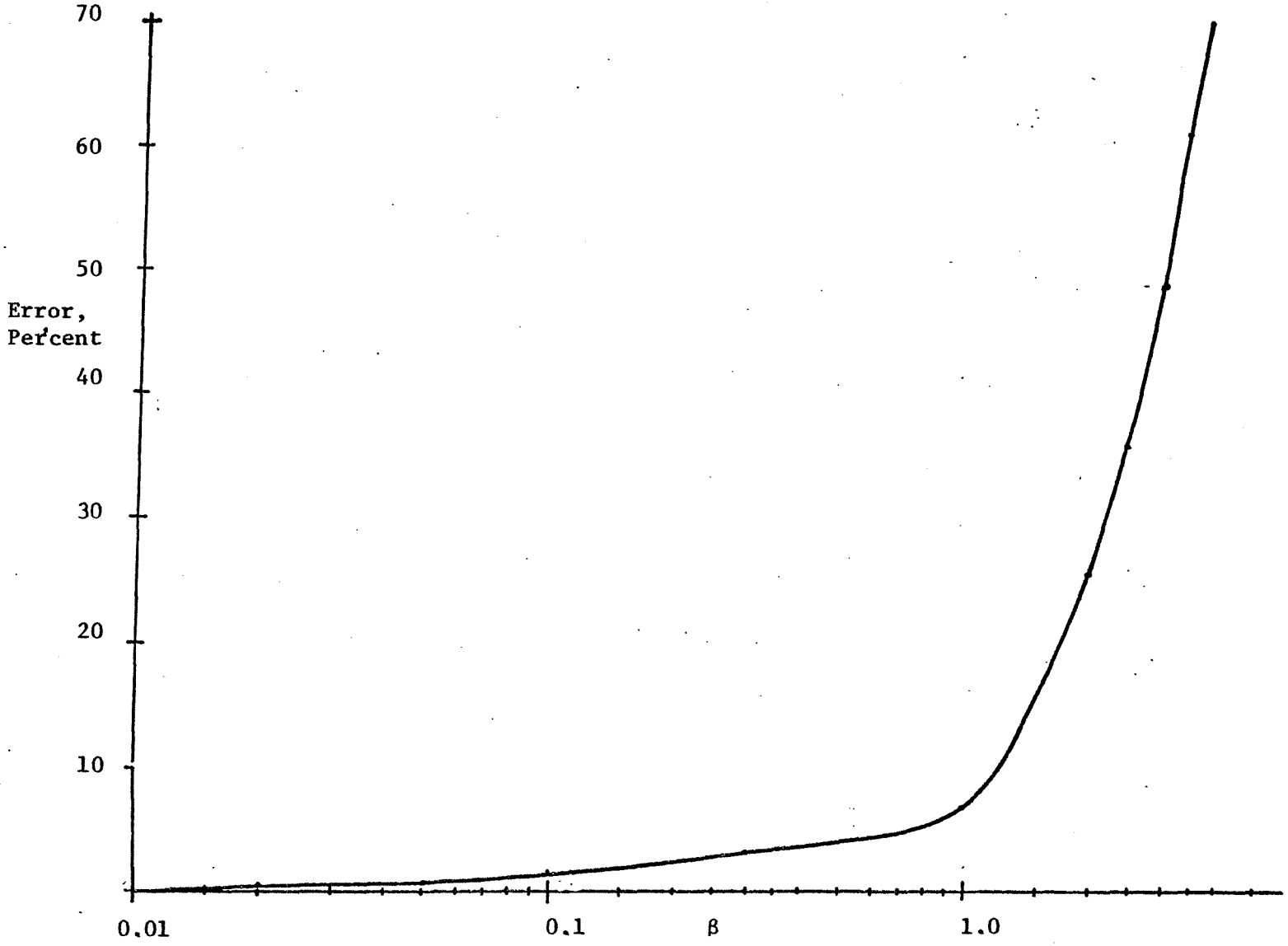


Fig. 4.4. Error in Measurement of Rod Resistance Using 0.618 Rule.

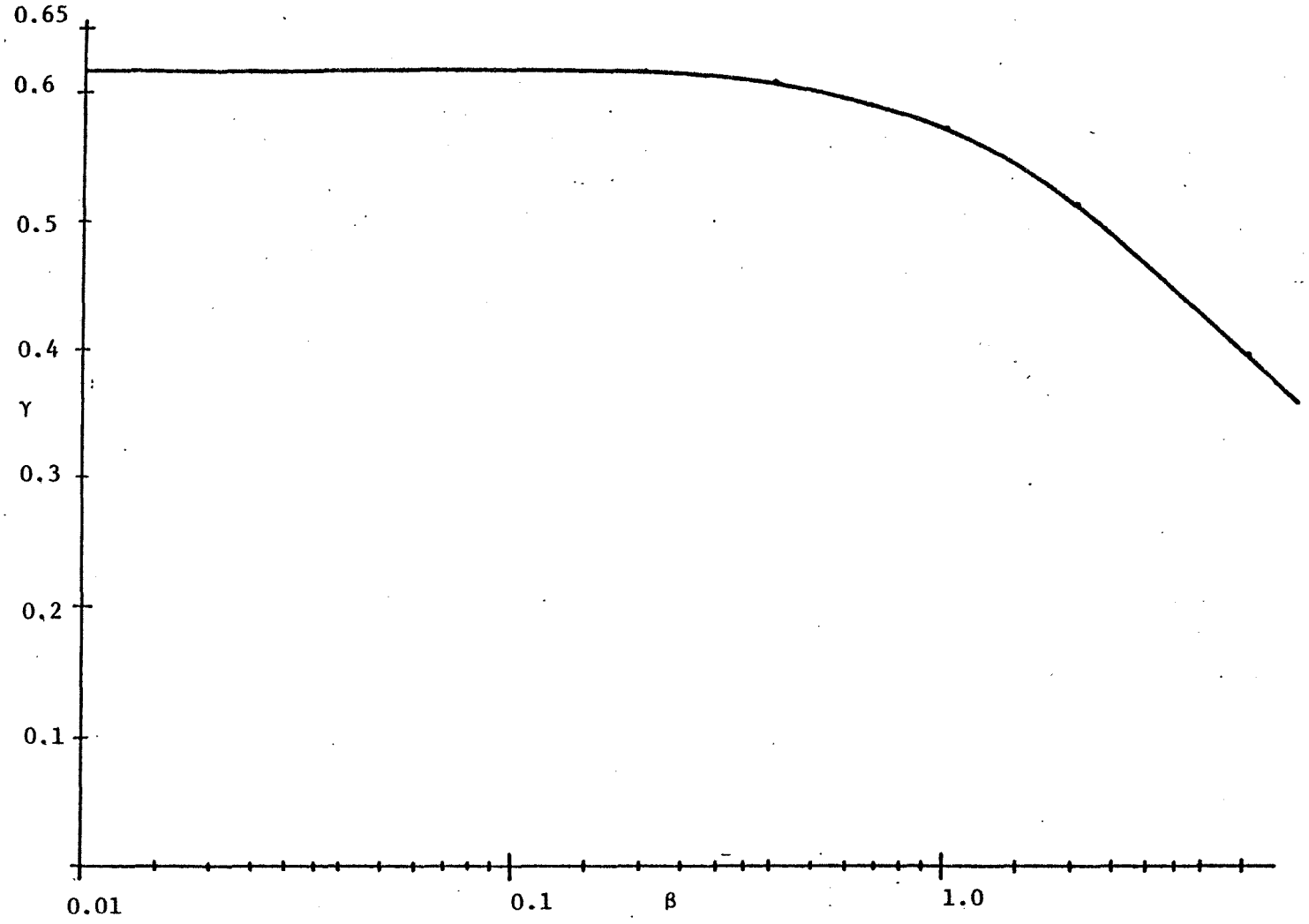


Fig. 4.5. Potential-Electrode Position for Measurement of True Resistance.

4.2 Multiple-Rod Calculations

Once an accurate model has been developed for the rod electrode, it is possible to calculate the resistance of arrays of interconnected ground rods.

4.2.1 Mutual Resistance Between Rods

Multiple-rod ground beds, like multiple-hemisphere beds, do not obey simple parallel-resistor laws. For example, the resistance of two identical rods connected in parallel always exceeds half the resistance of a single rod. This should not be surprising, as the expressions for multiple hemispheres can be used for widely-separated rods. Resistance calculations at short spacings require an expression for the mutual resistance between two rods. For two identical rods driven perpendicular to the ground plane, this mutual resistance can be obtained from the potential expression in Section 4.1.

$$V(r,0) = \frac{\rho I}{2\pi\ell} \ln \left[\sqrt{\left(\frac{\ell}{r}\right)^2 + 1} + \frac{\ell}{r} \right] \qquad (4.2)$$

The potential at the second rod due to the current I carried by the first rod is calculated by evaluating this expression with 'r' equal to the spacing between rods. Dividing by I yields the mutual resistance between rods

$$R_m = \frac{\rho}{2\pi\ell} \ln \left[\sqrt{\left(\frac{\ell}{d}\right)^2 + 1} + \frac{\ell}{d} \right] \qquad (4.25)$$

where d is the separation. The total resistance for two rods is

$$R = 1/2[R_m + R_\infty]$$

$$= \frac{\rho}{4\pi\ell} \left\{ \ln \left[\sqrt{\left(\frac{\ell}{d}\right)^2 + 1} + \frac{\ell}{d} \right] + \ln \frac{2\ell}{a} \right\} \qquad (4.26)$$

$$\text{or} \quad \frac{R}{R_\infty} = 1/2 \left\{ \ln \left[\sqrt{\left(\frac{\ell}{d}\right)^2 + 1} + \frac{\ell}{d} \right] + \ln \frac{2\ell}{a} \right] \left(\ln \frac{2\ell}{a} \right)^{-1} \right\} \qquad (4.27)$$

This last equation is plotted in Figure 4.6 for a typical value of $\ell/a \simeq 75$. Also plotted is the resistance of two paralleled hemispheres,

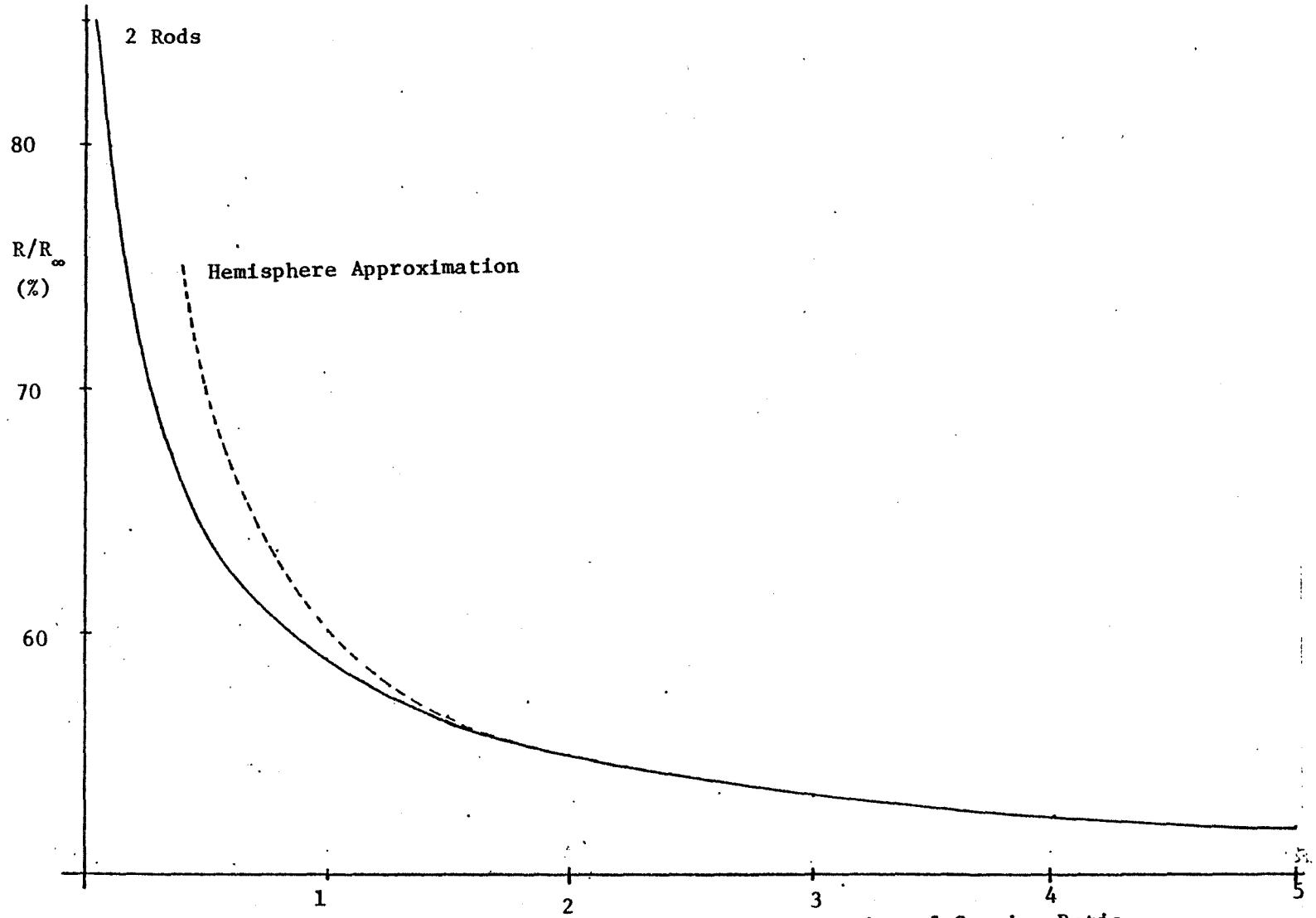


Fig. 4.6. Resistance of Two Parallel Rods as a Function of Spacing Ratio.

each with the same R_∞ as either rod. The hemisphere approximation is seen to be accurate for rods only for $d/\ell > 2$. (actually, the hemisphere formula $R/R_\infty = 1 + s/d$ is only accurate for hemispheres in this region, due to changes in current distributions at close spacings).

As in the case of hemispheres, the relation for the resistance of two parallel rods can be generalized to include n identical rods, placed on a circle of diameter d. If the angular spacing between adjacent rods is $\frac{2\pi}{n}$ radians, the combined resistance is computed as

$$R_{total} = \frac{1}{n}\left[R_\infty + 2\sum_{k=1}^{(n-1)/2} R_m\left(d \sin\frac{k\pi}{n-1}\right)\right] \quad (n \text{ odd}) \qquad (4.28a)$$

$$= \frac{1}{n}\left[R_\infty + 2\sum_{k=1}^{n/2-1} R_m\left(d \sin\frac{k\pi}{n}\right) + R_m(d)\right] \quad (n \text{ even}) \qquad (4.28b)$$

If the rods are not symmetrically placed in a circle, the total ground-bed current is not shared equally among the rods. Again, like the hemispheres, n simultaneous equations must be solved (in general) to determine the total resistance; unfortunately, for the rod case these are n nonlinear equations. Computation of resistance is therefore more difficult than for hemispheres. In addition, the rod has two geometric parameters (length and radius) whereas the hemisphere has only one. The result of this is that there is one more parameter in the solution, meaning that a particular numerical solution is far less general than a numerical solution for hemispheres. Because of the difficulty in obtaining solutions, and their limited applicability, only a few are given here.

The simplest case with non-identical rod currents is that of three rods in a straight line. If the distance between the end rods is d, and the middle rod is placed halfway between these, the potential of either end rod is found as

$$V_e = I_e R_\infty + I_c R_m\left(\frac{d}{2}\right) + I_e R_m(d) \qquad (4.29)$$

The potential of the center rod is

$$V_c = I_c R_\infty + 2I_e R_m\left(\frac{d}{2}\right) \qquad (4.30)$$

The subscripts 'c' and 'e' refer to 'center' and 'end' respectively. With the auxiliary equations

$$V_c = V_e = V \qquad (4.31)$$

$$I_c + 2I_e = I \tag{4.32}$$

The system of equations can be solved, yielding

$$\frac{V}{I} = R_{total} = \frac{R_\infty + 2\gamma\, R_m(\frac{d}{2})}{2\gamma + 1} \tag{4.33}$$

$$\text{where } \gamma = \frac{R_\infty - R_m(\frac{d}{2})}{R_\infty + R_m(d) - 2R_m(d/2)} = \frac{I_e}{I_c} \tag{4.34}$$

$R_m(x)$, the mutual resistance between two rods, is a monotonically decreasing function of x. Therefore, $R_m(d/2)$ is always greater than $R_m(d)$ for $d > 0$, and γ is always greater than one; in other words, the end rods each carry more current than the center rod. In turn, $\gamma > 1$ implies that the resistance of three rods in parallel must always exceed $R_\infty/3$.

This result can be generalized to the case of n rods, n-1 of which are equally spaced on a circle of diameter d, with one rod at the circle center. The potential of any rod on the circle is given by

$$V = I_c R_m(\tfrac{d}{2})(\tfrac{1}{n-1})(I-I_c)[R_\infty + 2\sum_{k=1}^{n/2-1} R_m(d \sin \tfrac{k\pi}{(n-1)})] \quad (n \text{ even}) \tag{4.35a}$$

$$= I_c R_m(\tfrac{d}{2})(\tfrac{1}{n-1})(I-I_c)[R_\infty + 2\sum_{k=1}^{(n-3)/2} R_m(d \sin \tfrac{k\pi}{(n-1)}) + R_m(d)] \quad (n \text{ odd}) \tag{4.35b}$$

The potential of the center rod is

$$V = I_c R_\infty + (I-I_c)R_m(\tfrac{d}{2}). \tag{4.36}$$

With the definition

$$R_{av} \equiv \frac{1}{n-1}\,[R_\infty + \text{appropriate summation}] \tag{4.37}$$

the voltage-to-current ratio can be expressed as

$$\frac{V}{I} = \varepsilon R_\infty + (1-\varepsilon)R_m(\tfrac{d}{2}) \tag{4.38}$$

$$\text{where } \varepsilon = \frac{R_{av} - R_m(d/2)}{R_\infty + R_{av} - 2R_m(d/2)}\,. \tag{4.39}$$

Now the question can be asked, "For a group of n rods placed in a circular plot, what arrangement gives the lowest total resistance?" For small values of n, the minimum is achieved with the purely circular arrangement. As n increases, adjacent rods become closer and closer until the arrangement with one rod at the circle center (and n-1 rods on the periphery) becomes optimum. The question was posed in four hemispheres in the previous annual report; it was shown there that the solution with a hemisphere at the circle center becomes optimum for $n > 10$. Figure 4.7 shows the resistance of each configuration of rods in the following way: Subscript A refers to the configuration of n rods on a circle, and B to the arrangement of n-1 rods on a circle and one in the center. If R_A and R_B are the resistances of each configuration, respectively, the following definitions are made:

$$R'_A = \frac{nR_A}{R_\infty} - 1 \qquad (4.40)$$

$$R'_B = \frac{nR_B}{R_\infty} - 1 \qquad (4.41)$$

The primed quantities represent the fractions by which R_A and R_B exceed the "ideal" resistance value R_∞/n, where R_∞ is the resistance of a single rod. R'_A and R'_B both approach zero for large separations (values of d or δ). This figure shows the relative effects of increasing the size of the circle versus the effect of moving one rod to the center--the second effect is almost insignificant compared with the former. The quotient R'_A/R'_B is plotted in Figure 4.8 to magnify the difference between the two resistances. For $\delta = 10$, $R_B < R_A$ if $n \geq 12$. (That is, the ratio crosses unity for $n = 12$). The same condition is reached for $\delta = 5$ if $n > 13$. For $\delta = 2$, n must be ≥ 21 and $\delta = 1$ requires that $n \geq 45$. The low mutual resistance of rods compared to that of hemispheres results in these high values of n.

4.2.2 Resistance Measurement of Multiple Rods

Resistance measurement of two rods poses the same problems as the measurement of two hemispheres. The current electrode should be located as far as possible from both rods, and the potential electrode located so that the true resistance is measured. As with hemispherical electrodes, the current electrode is (in general) best placed along a line which bisects a second line connecting the two rod centers. There is an infinite number of locations for the potential electrode; for convenience this electrode is placed along the same line as the current electrode.

The potential difference between the rods and the potential electrode is easily found as

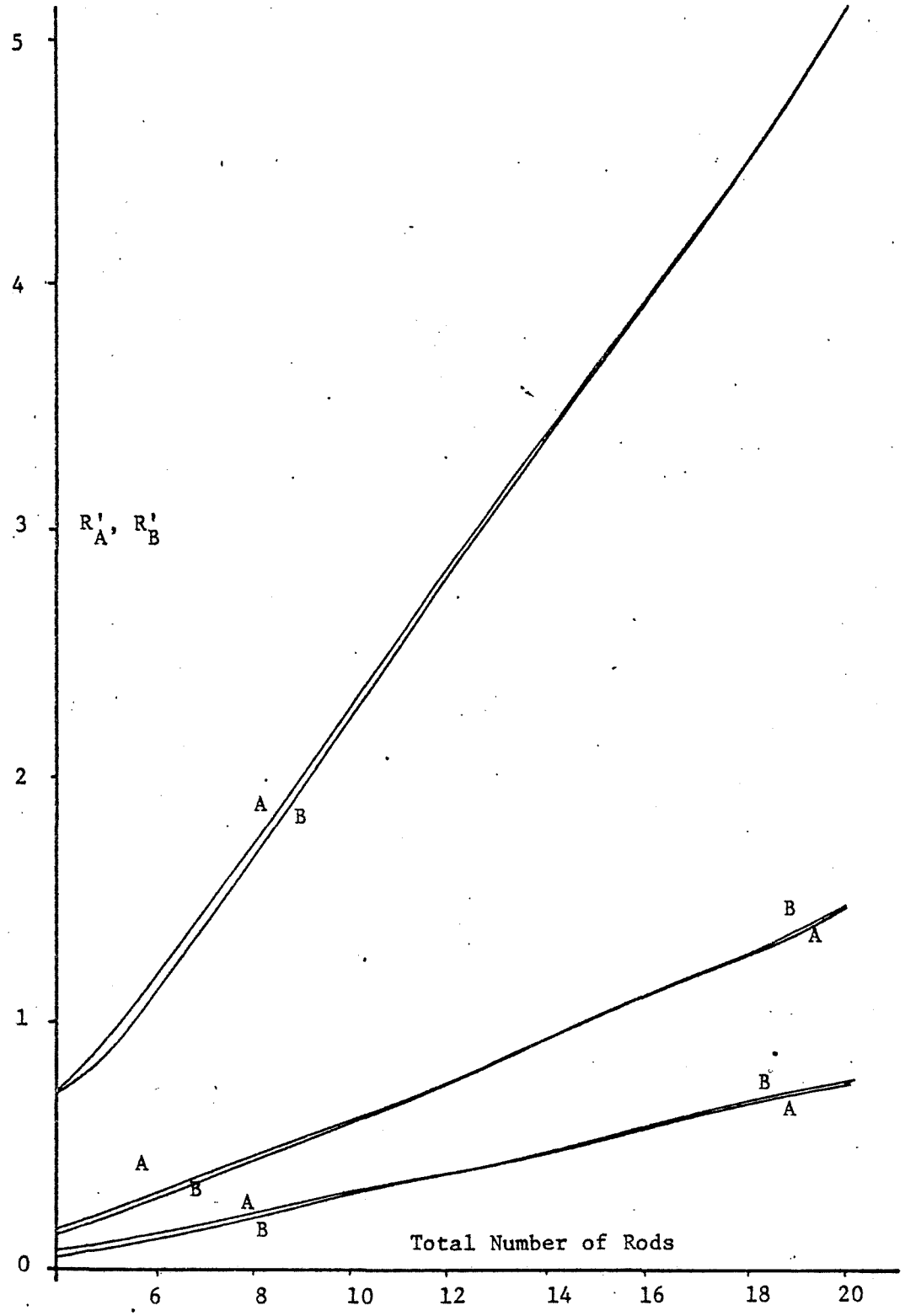


Fig. 4.7. Resistance Plots for Two Configurations of Rods on Circle.

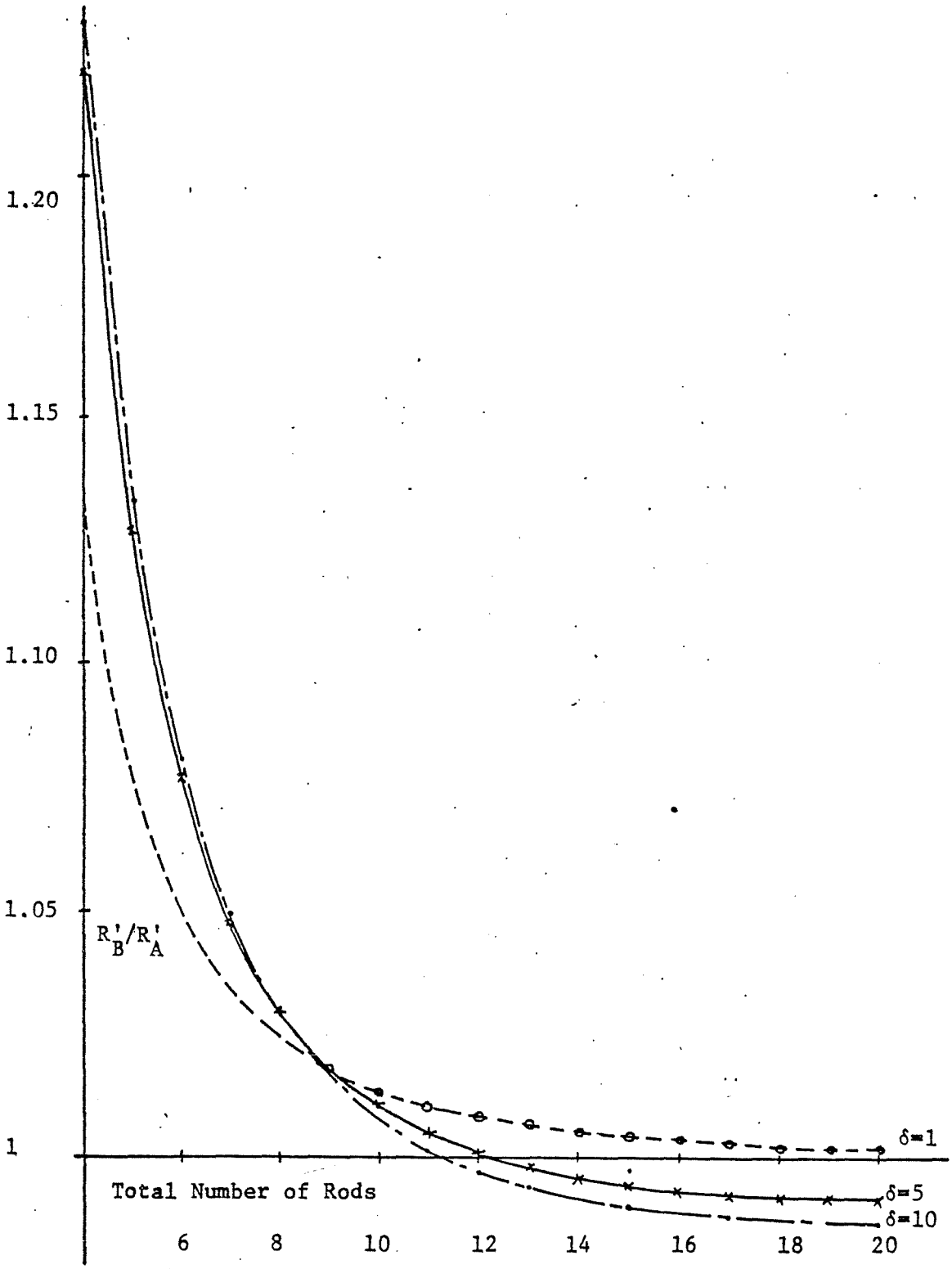


Fig. 4.8. Ratio of Resistances of Circle Configurations of Rods.

$$V = \frac{I}{2}\left[R_m(d)+R_\infty\right] - \frac{\rho I}{2\pi\sqrt{r_c^2+(d/2)^2}} - IR_m\left[\sqrt{\left(\frac{d}{2}\right)^2+r_p^2}+\frac{\rho I}{2\pi(r_c-r_p)}\right] \tag{4.42}$$

where

$$R_m(y) = \frac{\rho}{2\pi\ell}\,\ell n\left[\sqrt{\left(\frac{\ell}{y}\right)^2+1}+\frac{\ell}{y}\right] \tag{4.43}$$

and d, r_p, r_c are shown in Figure 4.9.

The last three terms must sum to zero, requiring

$$\frac{1}{r_c-r_p} = \frac{1}{\ell}\,\ell n\left[\sqrt{\frac{\ell^2}{(d/2)^2+r_p^2}+1}+\frac{\ell}{\sqrt{(d/2)^2+r_p^2}}\right] + \frac{1}{\sqrt{r_c^2+(d/2)^2}} \tag{4.44}$$

Figure 4.10 shows the solutions to this equation as a function of d/ℓ for various values of r_c/ℓ. d/ℓ was chosen as the independent variable rather than r_c/ℓ because it is usually a "given", i.e., value not easily changed, whereas r_c/ℓ is subject to the whims of the person doing the measurement.

The resistance measurement of three rods in a straight line is analyzed similarly. With the definitions in Figure 4.11, the measured potential is

$$V = 2I_e'R_m(d/2+I_c'R_\infty - \frac{\rho I}{2\pi r_c} - I_c'R_m(r_p) - 2I_e'R_m\left[\sqrt{r_p^2+(d/2)^2}+\frac{\rho I}{2\pi(r_c-r_p)}\right] \tag{4.45}$$

I_c' is the center-rod current and I_e' is the current carried by either end rod. These currents are not the same as before (i.e., $I_c' \neq I_c$, $I_e' \neq I_e$) because of the presence of the current electrode. These currents must now satisfy the relations

$$I_c'R_\infty + 2I_e'R_m(d/2) - \frac{\rho I}{2\pi r_c} = I_e\left[R_\infty + R_m(d)1 + I_cR_m(d/2) - \frac{\rho I}{2\pi(\sqrt{r_c^2+(d/2)^2}}\right. \tag{4.46}$$

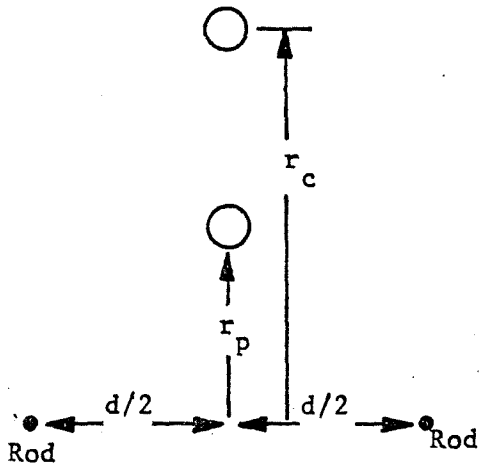


Fig. 4.9. Configuration for Resistance Measurement of Two Rods in Parallel.

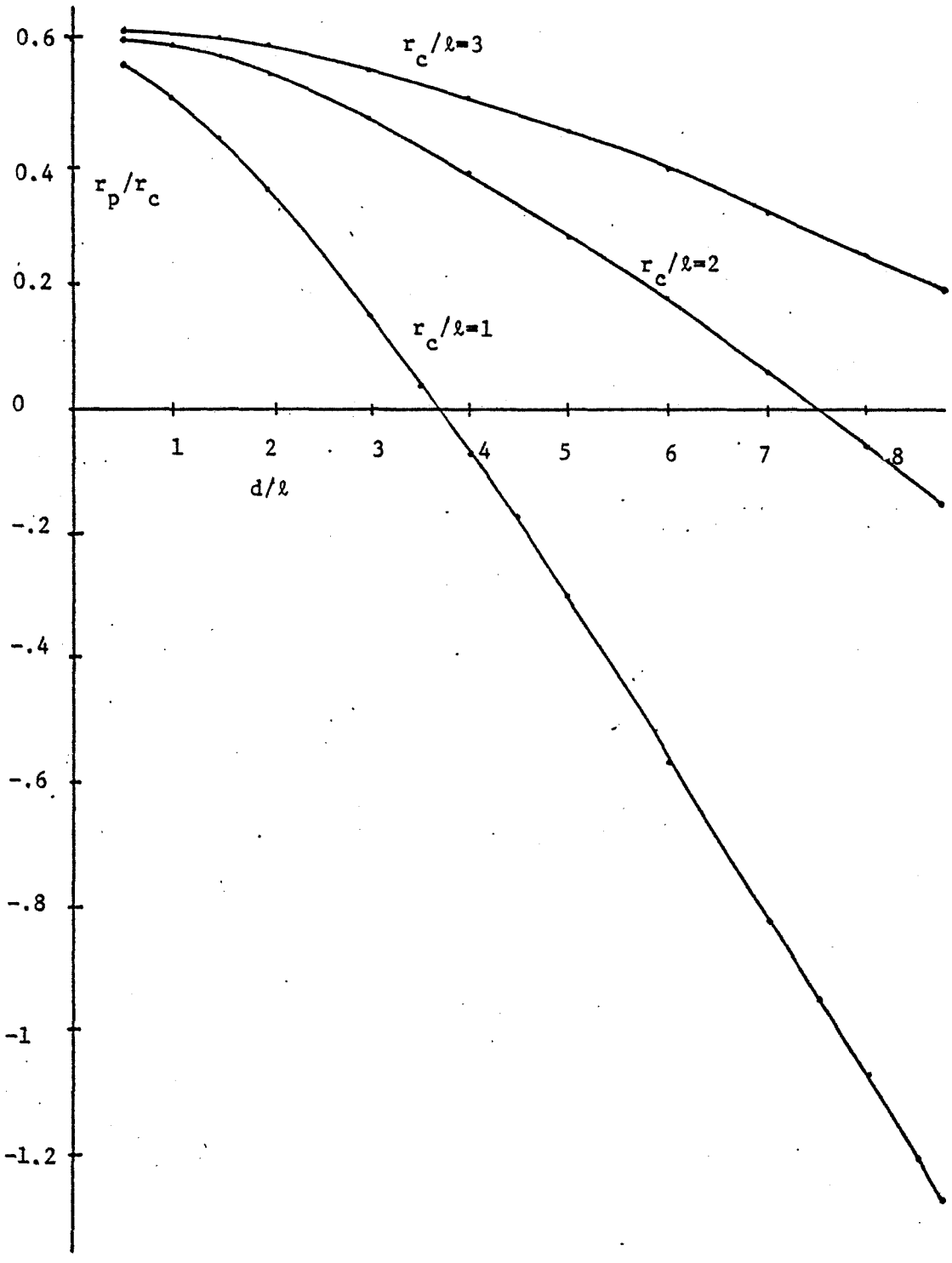


Fig. 4.10. Potential Electrode Position for Resistance Measurement of Two Rods.

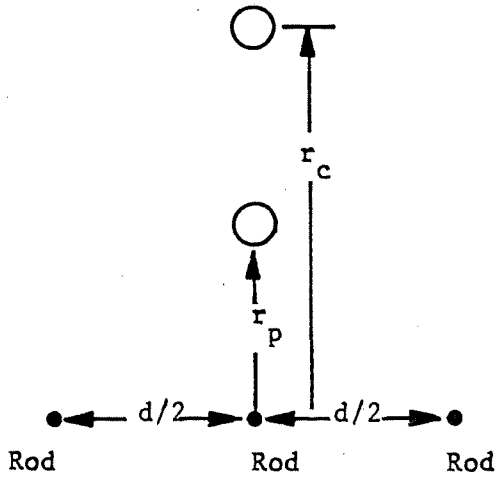


Fig. 4.11. Configuration for Resistance Measurement of Three Rods in Parallel.

and

$$I_c' + 2I_e' = I \tag{4.47}$$

Solving yields

$$\frac{[R_\infty - R_m(d/2) - R_0(r_c) + R_0(\sqrt{r_c^2+(d/2)^2})]}{[R_\infty - 2R_m(d/2) + R_m(d) + 2R_0(r_c) - 2R_0(\sqrt{r_c^2+(d/2)^2}]} \tag{4.48}$$

with the definition

$$R_0(y) = \frac{\rho I}{2\pi y} \tag{4.49}$$

Obviously, I_e' and I_c' are different from I_e and I_c, because $\gamma' \neq \gamma$ (except in the limit as $r_c \to \infty$). The effect of the current electrode is to increase the fraction of current carried by the center electrode. If r_c is small, I_c' can actually exceed I_e'.

Returning now to the problem of measuring the resistance of the three rods, the potential electrode must be located such that

$$(2\gamma'+1)[R_0(r_c) - R_0(r_c - r_p)] + 2\gamma' R_m(\sqrt{r_p^2+(d/2)^2}) + R_m(r_p) = 0 \tag{4.50}$$

The solutions for r_p/r_c are shown in Figure 4.12, as a function of d/ℓ, for various values of r_c/ℓ. When this is compared with Figure 4.10 the effect of the center rod is seen to reduce the range of values of r_p/r_c by an order of magnitude.

4.2.3 Resistance Measurement of Rods on a Circle

The presence of the current electrode alters the current distribution of a ground bed unless this electrode is equidistant from every constituent rod of the bed. Barring this special case, calculation of the correct potential-electrode location requires considerable computation (as can be seen from the last section). The configurations considered are limited to those which yield minimum resistance for a given number of rods and given area: rods easily spaced on a circle. (The configuration of n-1 rods on a circle and one in the center can be tested also if the center rod can be disconnected.) As in the case for hemispheres, the current electrode is placed at the center of the circle, and the potential electrode located along a radial line which passes through a constituent electrode.

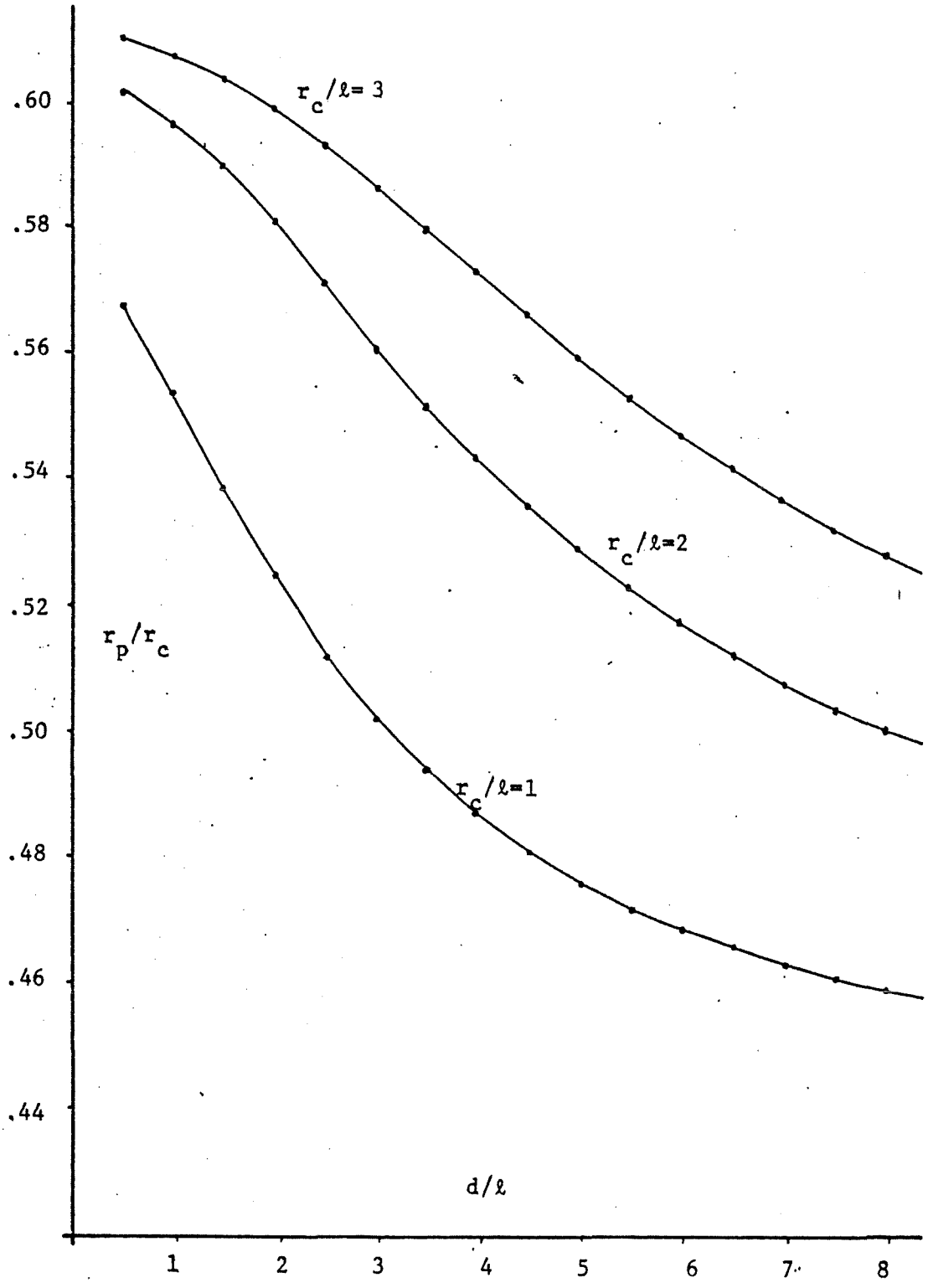


Fig. 4.12. Optimum Potential-Electrode Position for Resistance Measuremen. of Three Rods in a line.

The potential electrode must be located such that the potential (V_3) of the ground bed due to the current electrode equals the sum of the potential (V_1) of the potential electrode due to the ground bed and the potential (V_2) of the potential electrode due to the current electrode. Symbolically,

$$V_3 = V_1 + V_2 \tag{4.51}$$

V_1 can be found from a straightforward geometrical analysis as was done for the hemisphere case. The result is

$$V_1 = I \sum_{k=1}^{K=\frac{n-1}{2}} \frac{1}{n} 2\, R_m(\ell_k) + \frac{1}{n} R_m(d/2 - \alpha d/2) \quad (n \text{ odd}) \tag{4.52a}$$

with

$$\ell_k = d/2\sqrt{\alpha^2 + 2\alpha\cos\frac{(2k-1)\pi}{n} + 1} \quad (n \text{ odd}) \tag{4.53a}$$

or

$$V_1 = I \sum_{k=1}^{\frac{n}{2}-1} 2R_m(\ell_k) + R_m(d/2-\alpha d/2) + R_m(d/2+\alpha d/2) \quad (n \text{ even}) \tag{4.52b}$$

with

$$k = \frac{d}{2}\sqrt{\alpha^2 + 2\alpha\cos\frac{k\pi}{n} + 1} \quad (n \text{ even}) \tag{4.53b}$$

Here r_p is the distance from the circle center to the current electrode, d is the circle diameter, and α is defined as

$$\alpha \equiv \frac{2r_p}{d} \tag{4.54}$$

The remaining potentials are easily calculated, using the same notation

$$V_2 = -\frac{\rho I}{\pi\alpha} \tag{4.55}$$

and

$$V_3 = -\frac{\rho I}{\pi d} \tag{4.56}$$

Values of α which set V_3 equal to the sum of V_1 and V_2 are shown in Figure 4.13. For $n > 7$, the curves are identical to four decimal places. The curves approach the values for hemispheres as $d/\ell \to \infty$.

4.3 CONCLUSIONS AND RECOMMENDATIONS FOR FUTURE STUDY

The research done on this project has been a detailed study of the calculation and measurement of the resistance of driven-rod ground beds. This year's study is a continuation of last year's effort, which consisted of: first, the fall-of-potential method (currently the most popular method for measuring ground-bed resistance) was examined. It was shown that this method is inherently inaccurate, even when used on the (analytically) simplest electrode, the hemisphere. Improvements to the fall-of-potential method, due to Tagg[2], were studied and found not to deal with the major source of errors. Revisions to the method were suggested (in terms of potential-electrode position) which will improve measurement accuracy. Also, an alternate method of measuring ground-bed resistance was developed which is less prone to errors and apparently no more difficult to use.

Second, the design and measurement of multiple-electrode beds was examined, keeping the underlying assumption that the constituent electrodes were, or could be considered as, hemispheres. The design of standard electrode configurations was reviewed. Use of the fall-of-potential method on these configurations was studied, and a tabulation made of the (often large) errors induced by this method. The design of minimum-resistance ground beds was then discussed, some design configurations given, and methods developed for measuring the resistance of these optimum beds.

Based on these developments, the research continued this year with a third focus, the rod electrode itself. It was concluded that the hemisphere is a poor model for representing the electrical behavior of a rod at distances from the rod of the order of its length. This region near the rod is of primary concern in low-resistance ground beds. Low resistance is achieved either by using a small number of very long rods (in which case the resistance measurement must be done "close" to the rod) or a large number of short rods placed near each other (in which case the mutual resistance between closely-spaced rods must be known for resistance calculations). Alternate models for the rod were evaluated and an ellipsoidal model selected as the most accurate. Using this model, the resistance of several standard rod arrangements was approached and results tabulated as a function of the number of rods and the geometric parameters. Methods of measuring the resistance of each of these configurations were developed.

4.3.1 Recommendations for Future Work

The analyses in this paper have been verified, where possible, by comparing their predictions for cases where prior, less rigorous

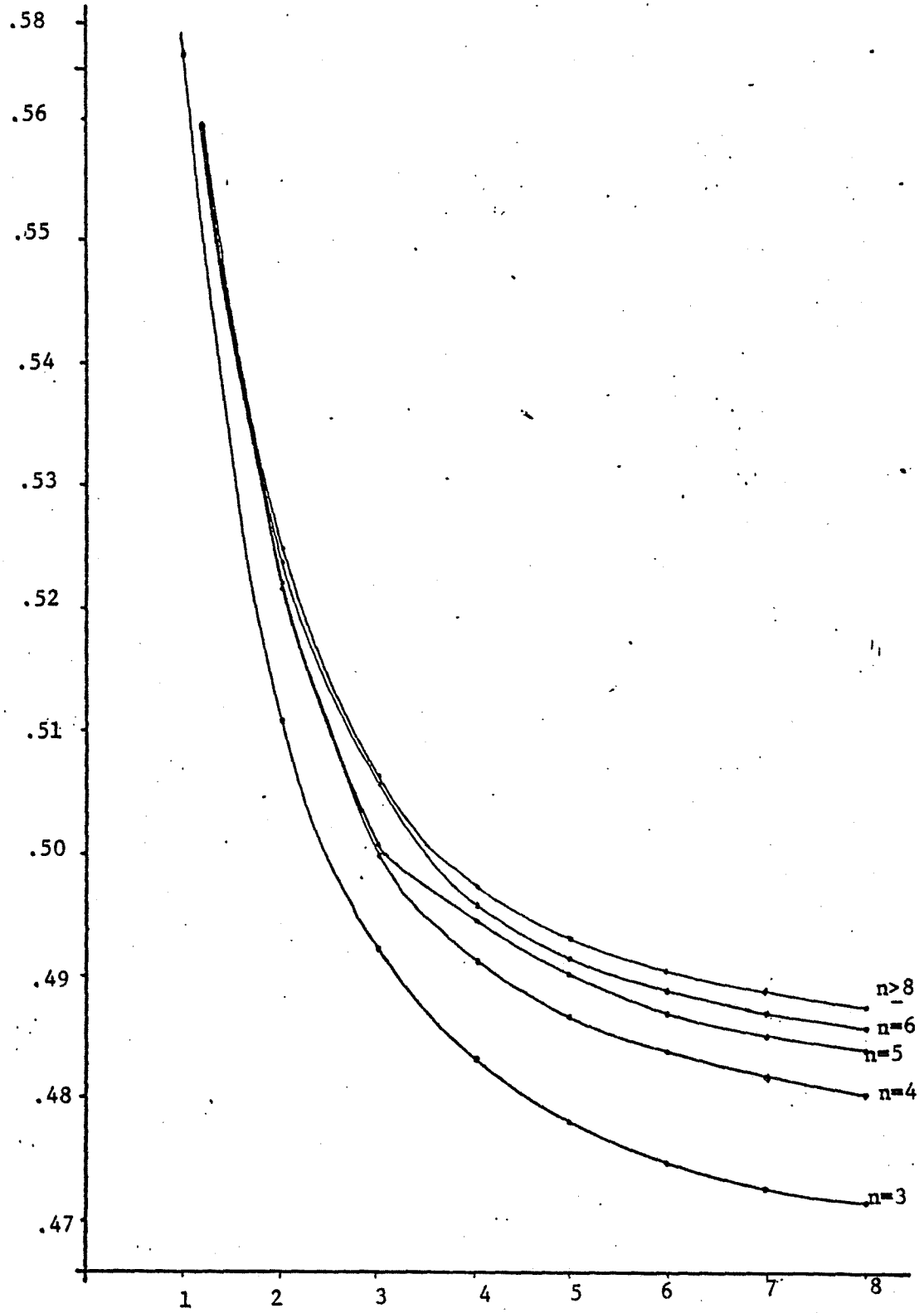


Fig. 4.13. Optimum Potential-Electrode Position for Resistance Measurement of Rods on Circle.

studies are valid. For the most part, the possible test cases are limiting ones, where, for example, the radius of a hemisphere or the length of a rod becomes very small compared to other dimensions of the problem. More verification than this is necessary. As the analyses were done with the explicit assumption of homogeneous (i.e. constant-resistivity) earth, they should first be tested in a homogeneous medium to see if they are, in fact, correct. This will probably have to be done with a physical model. More important, but more difficult, is the full-scale testing and evaluation with actual ground beds in the real world. To do this testing and evaluation, it will be necessary to measure the resistance of one of the ground-bed designs here by some method other than the fall-of-potential method (which has been shown to be inaccurate) or the methods developed here (which are untested). This will probably involve placing electrodes at great distances (kilometers) from the test bed. Once the bed resistance is known, the given measurement procedure herein can also then be evaluated.

Possible extensions of the present work on ground-bed design are endless. The multiple-hemisphere analysis could be refined considerably by developing an approximation for the mutual resistance between two identical hemispheres separated by a distance comparable to their radius. The design of a minimum-resistance ground bed with more than a dozen or so closely placed hemispherical electrodes hinges on the development of such an expression. The optimum configuration for large numbers of rods remains unknown, and yet suitable mutual-resistance expressions are available.

Likewise, much remains undone in ground-bed measurement. All present techniques require making some assumptions about the way earth potentials fall off around the bed under test. Quite often, the assumptions are crude or almost completely baseless. By increasing the number of auxiliary test electrodes in a new technique it should be possible to eliminate, or at least reduce, the need for such assumptions. A trade-off would have to be made between the accuracy and complexity of the measurement.

The work done on both design and measurement techniques could be extended to construction and resistance measurement in non-homogeneous earth. This may require quite elaborate mathematical modelling; certainly the most general cases will require numerical techniques such as finite-element modelling.

One theoretical question arose during the course of research is that of reciprocity of mutual resistances: Is the potential of ground bed number one, due to current 'I' flowing in ground bed number two, always the same as the potential measured in ground bed two when 'I' flows in ground bed one? For ground beds made of single or multiple hemispheres, the answer is 'yes'. For electrodes other than hemispheres, the answer may be'no', but no two electrodes have been

found such that there is a significant difference between the two measurements. Conventional proofs of reciprocity for antennas and for electrical circuits appear to be inapplicable, as they are developed for two-port systems and use a different definition of mutual resistance.

4.4 REFERENCES

1. Ernst Weber, Electromagnetic Theory, p. 113

2. G. F. Tagg, Earth Resistances, Pitman New York, 1954.

CHAPTER V MEASUREMENT OF GROUND BED CHARACTERISTICS

5.1 RESISTANCE MEASUREMENT IN FINITE VOLUME

A desirable characteristic of any scale-model work is the simple extension of the result to full-size electrodes buried in the infinite earth. Such an extension is possible if the three-dimensional model can be assumed to represent an infinite medium, in which it would be possible to locate two points which are essentially infinitely far away from each other. In practice, it can be seen that depending upon the dimensions of the three-dimensional model and the electrode spacings; the discrete side boundaries of the model have some effect on the model measurements. If the model is assumed to be exposed to air, the side boundaries would be non-conducting type.

The effect of non-conducting model side boundaries on the resistivity measurements was investigated in the previous annual report[1]. Correction factors and graphs were developed for the non-conducting boundaries oriented perpendicular and parallel to the line of resistivity measurement electrodes. It can be seen from the graphs that model side boundaries have considerable effect on the resistivity measurements on the model, especially when the boundaries are very close to the electrodes.

After the resistivity measurements are made on the model surface, resistance measurements using the fall-of-potential method could be done to measure the ground bed resistance. Again the non-conducting side boundaries would affect the resistance measurements, since the measurements are made on the model of finite size, as in the case of resistivity measurements. In the following sections the effect of non-conducting model side boundaries on the resistance measurements is analyzed mathematically.

5.1.1 Resistance of a Hemisphere[2]

Fig. 5.1 shows a hemispherical electrode E, an auxiliary current electrode, B and an auxiliary potential electrode A, as in the conventional fall-of-potential method. The distance of the current and potential electrodes from the center of the hemisphere is C and P respectively. Current I is passed through E and B and potential V is measured between E and A.

Now the potential at E due to the current entering at E is $\frac{\rho I}{2\pi r}$ and that due to the current leaving at B is $\frac{-\rho I}{2\pi (C-r)}$, so that the total potential at E is

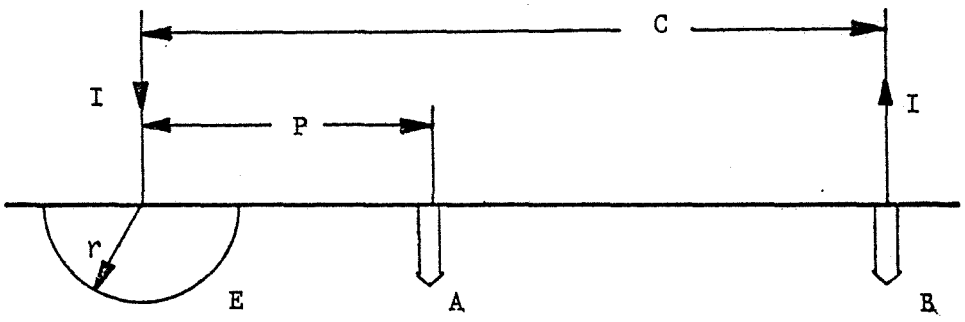


Fig. 5.1 Hemispherical Electrode

$$\frac{\rho I}{2\Pi}\left(\frac{1}{r}-\frac{1}{C-r}\right) \tag{5.1}$$

Similarly the potential at A due to current I entering at E is $\frac{\rho I}{2\Pi P}$ and that due to the current leaving at B is $-\frac{\rho I}{2\Pi(C-P)}$, so that the total potential at A is

$$\frac{\rho I}{2\Pi}\left(\frac{1}{P}-\frac{1}{C-P}\right) \tag{5.2}$$

Hence from the equations (5.1) and (5.2) the potential difference V is given by

$$V=\frac{\rho I}{2\Pi}\left(\frac{1}{r}-\frac{1}{C-r}-\frac{1}{P}+\frac{1}{C-P}\right) \tag{5.3}$$

In most of the practical cases r (radius of the equivalent hemisphere) can be neglected as compared to C. Therefore equation (5.3) can be rewritten as

$$V=\frac{\rho I}{2\Pi r}\left(1-\frac{1}{c}-\frac{1}{p}+\frac{1}{c-p}\right) \tag{5.4}$$

where $c=\frac{C}{r}$ and $p=\frac{P}{r}$.

The true resistance (R_∞) of a hemispherical electrode is $\frac{\rho}{2\Pi r}$ and the measured resistance (R) is $\frac{V}{I}$. Therefore,

$$\frac{R}{R_\infty}=1-\frac{1}{c}-\frac{1}{p}+\frac{1}{c-p} \tag{5.5}$$

By examining equation (5.5), for a given value of C, there exists a ρ for which the value $\frac{R}{R_\infty}=1$ and this value should be such that

$$-\frac{1}{c}-\frac{1}{p}+\frac{1}{c-p}=0$$

or $$p^2+cp-c^2=0 \tag{5.6}$$

By solving the quadratic equation (5.6)

$$p = \frac{-c \pm \sqrt{5\ c^2}}{2}$$

or $$p = c\ (\frac{\sqrt{5}-1}{2}) = 0.618c$$

or $$p = 0.618c \text{ and } P = 0.618C \qquad (5.7)$$

Equation (5.7) is normally called as the 61.8 percent rule and gives the location of the potential electrode at which the true resistance can be measured, given the current electrode spacing.

The following two assumptions are made in the preceding analysis:

1. Earth is assumed to be homogeneous.
2. Conducting medium is infinite.

If α is defined as the ratio of P and C, then according to the equation (5.7) under normal conditions $\alpha = 0.618$. Naturally, when the conduction medium is finite α will have a different value depending upon the type of the discrete boundaries and their locations.

5.1.2 Correction for Resistance Measurement in Finite Volume

Fig. 5.2 depicts the plan view of the model when the fall-of-potential electrodes are oriented along the length of the model. Two types of boundaries exist. One pair of boundaries is perpendicular to the line of electrodes and the other is parallel. The following four types of boundary conditions exist:

1. Perpendicular boundaries with equal spacings, i.e., $L_1 = L_2 = L$
2. Perpendicular boundaries with unequal spacings, i.e., $L_1 \neq L_2$
3. Parallel boundaries with equal spacings, i.e., $L_3 = L_4 = L$
4. Parallel boundaries with unequal spacings, i.e., $L_3 \neq L_4$

These four boundary conditions are treated separately in the following sections. Convention used is:

R = Measured Resistance = $\frac{V}{I}$

R_∞ = True Resistance

r = Radius of equivalent hemisphere

C = Distance of auxiliary current electrode from the center of the hemisphere

P = Distance of auxiliary potential electrode from the center of the hemisphere

$c = \frac{C}{r}$

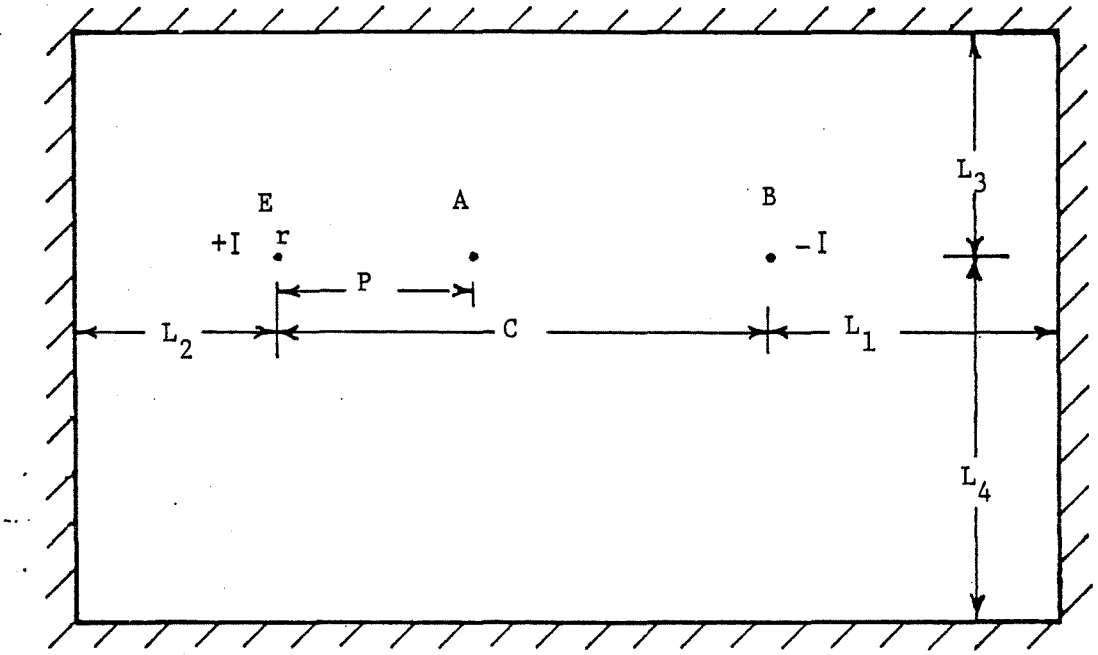


Fig. 5.2 Plan View of the Model, Showing Perpendicular and Parallel Boundaries.

$p = \frac{P}{r}$

L_1, L_2 = Distance of the perpendicular boundaries from the electrodes

L_3, L_4 = Distance of the parallel boundaries from the electrodes

$\ell = \frac{L}{r}$

$\alpha = \frac{P}{C}$

$x = \frac{\ell_1}{c}$

for perpendicular boundaries

$y = \frac{\ell_2}{c}$

$x = \frac{\ell_3}{c}$

for parallel boundaries

$y = \frac{\ell_4}{c}$

ρ = Resistivity of the medium

A = Length of the model

B = Width of the model

5.1.3 Perpendicular Boundary Condition with Equal Spacings

The model is shown in Fig. 5.3. A pair of non-conducting boundaries is perpendicular to the line of the fall-of-potential electrodes. Electrode 1 carries +I current and electrode 3 carries -I. Potential difference is measured between the electrodes 1 and 2, i.e., potential difference $V_f = V_{f1} - V_{f2}$. Electrode 1 is the grounding electrode whose resistance is being measured. When considering perpendicular boundaries, it is assumed that the parallel boundaries are absent and the material is semi-infinite in that direction.

Again by the use of optics analogy[1], multiple image sources are drawn as shown in Fig. 5.3 and the effect of all these infinite image sources is considered on the measured potential V_f. The floating potential V at a distance r from an electrode carrying a current I in a material of resistivity ρ is given by

$$V = \frac{\rho I}{2\pi r} \qquad (5.8)$$

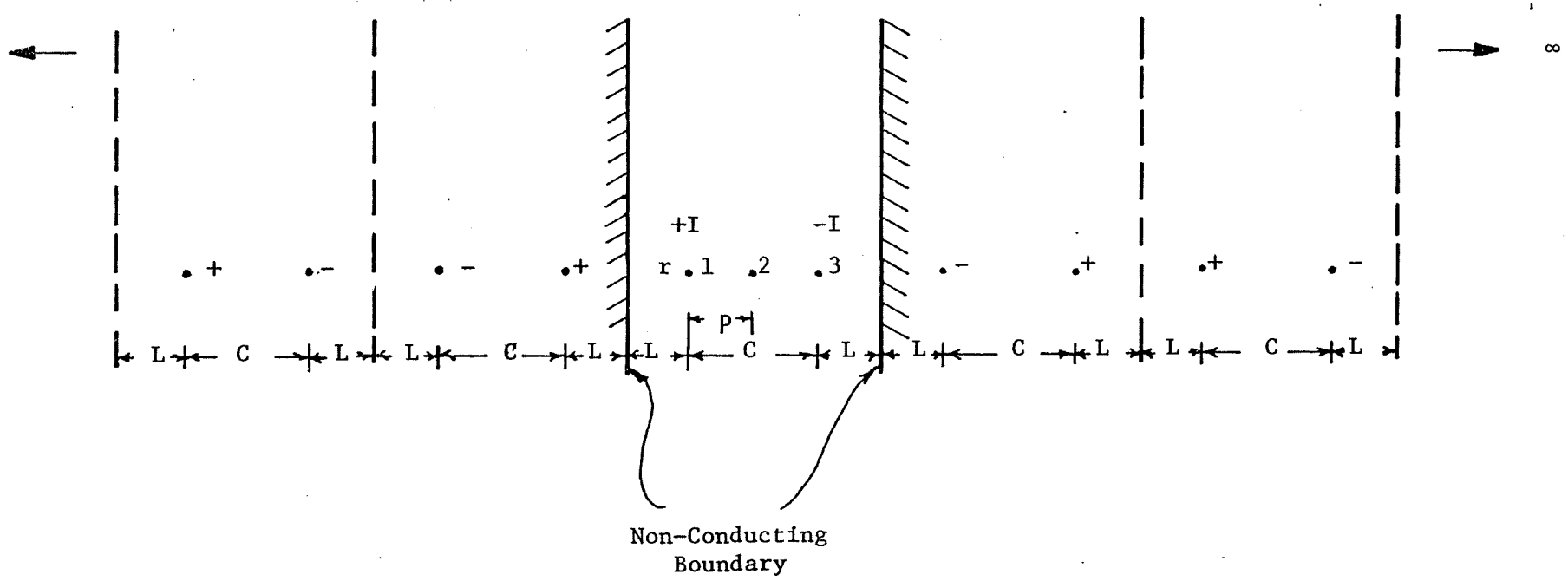


Fig. 5.3 Fall-of-Potential Electrodes Perpendicular to Non-Conducting Boundary. (Equal Spacings)

$L_1 = L_2 = L$

Thus the floating potential V_{f_1} and V_{f_2} can be written:

$$V_{f_1} = \frac{\rho I}{2\pi}\left[-\frac{1}{C-r} - \frac{1}{C+2L} + \frac{1}{2C+2L} + \frac{1}{2C+4L} - \frac{1}{3C+4L} - \frac{1}{3C+6L}\right.$$

$$+ \frac{1}{4C+6L} + \frac{1}{4C+8L} - \cdots$$

$$+ \frac{1}{r} + \frac{1}{2L} - \frac{1}{C+2L} - \frac{1}{C+4L} + \frac{1}{2C+4L} + \frac{1}{2C+6L} - \frac{1}{3C+6L}$$

$$\left. - \frac{1}{3C+8L} + \frac{1}{4C+8L} + \ldots\right] \qquad (5.9)$$

$$V_{f_2} = \frac{\rho I}{2\pi}\left[-\frac{1}{C-P} - \frac{1}{C-P+2L} + \frac{1}{2C-P+2L} + \frac{1}{2C-P+4L} - \frac{1}{3C-P+4L} - \frac{1}{3C-P+6L}\right.$$

$$+ \frac{1}{4C-P+6L} + \frac{1}{4C-P+8L} - \cdots$$

$$+ \frac{1}{P} + \frac{1}{P+2L} - \frac{1}{C+P+2L} - \frac{1}{C+P+4L} + \frac{1}{2C+P+4L} + \frac{1}{2C+P+6L}$$

$$\left. - \frac{1}{3C+P+6L} - \frac{1}{3C+P+8L} + \ldots\right] \qquad (5.10)$$

$$V_f = V_{f_1} - V_{f_2} \qquad (5.11)$$

In equation (5.9) in the term $-\frac{1}{C-r}$, for all practical purposes r can be neglected as compared to C. Hence by removing $\frac{1}{r}$ outside the bracket and substituting $\frac{C}{r} = c$, $\frac{P}{r} = p$ and $\frac{L}{r} = \ell$, equation (5.11) can be written as follows:

$$V_f = \frac{\rho I}{2\pi r}\left[1 - \frac{1}{c} - \frac{1}{p} + \frac{1}{c-p} - \frac{2}{c+2\ell} + \frac{2}{2c+4\ell} - \frac{2}{3c+6\ell} + \frac{2}{4c+8\ell} - \cdots\right.$$

$$+ \frac{1}{2c+2\ell} - \frac{1}{3c+4\ell} + \frac{1}{4c+6\ell} - \cdots$$

$$+ \frac{1}{2\ell} - \frac{1}{c+4\ell} + \frac{1}{2c+6\ell} - \frac{1}{3c+8\ell} + \cdots$$

$$+ \frac{1}{c-p+2\ell} - \frac{1}{2c-p+2\ell} - \frac{1}{2c-p+4\ell} + \frac{1}{3c-p+4\ell} + \frac{1}{3c-p+6\ell}$$

$$- \frac{1}{4c-p+6\ell} - \frac{1}{4c-p+8\ell} - \cdots$$

$$- \frac{1}{p+2\ell} + \frac{1}{c+p+2\ell} + \frac{1}{c+p+4\ell} - \frac{1}{2c+p+4\ell} - \frac{1}{2c+p+6\ell} + \frac{1}{3c+p+6\ell}$$

$$\left. + \frac{1}{3c+p+8\ell} - \ldots\right] \qquad (5.12)$$

The infinite series of equation (5.12) can be broken down into a sum of subseries. Each subseries is finally represented as Σnth term.

Subseries 1:

$$-\frac{2}{c+2\ell}+\frac{2}{2c+4\ell}-\frac{2}{3c+6\ell}+\frac{2}{4c+8\ell}-\cdots$$

$$\text{subseries 1} = \sum_{n=1}^{\infty}\frac{2(-1)^n}{n(c+2\ell)} \tag{5.13}$$

Subseries 2:

$$-\frac{1}{c}+\frac{1}{2c+2\ell}-\frac{1}{3c+4\ell}+\frac{1}{4c+6\ell}-\frac{1}{5c+8\ell}+\cdots$$

This could be represented as

$$\text{subseries 2} = \sum_{n=1}^{\infty}\frac{(-1)^n}{n(c+2\ell)-2\ell} \tag{5.14}$$

Subseries 3:

$$+\frac{1}{2\ell}-\frac{1}{c+4\ell}+\frac{1}{2c+6\ell}-\frac{1}{3c+8\ell}+\cdots$$

$$\text{subseries 3} = \sum_{n=1}^{\infty}\frac{(-1)^{n+1}}{n(c+2\ell)-c} \tag{5.15}$$

Subseries 4:

$$+\frac{1}{c-p}-\frac{1}{2c-p+2\ell}+\frac{1}{3c-p+4\ell}-\frac{1}{4c-p+6\ell}+\cdots$$

$$\text{subseries 4} = \sum_{n=1}^{\infty}\frac{(-1)^{n+1}}{n(c+2\ell)-p-2\ell} \tag{5.16}$$

Subseries 5:

$$+\frac{1}{c-p+2\ell}-\frac{1}{2c-p+4\ell}+\frac{1}{3c-p+6\ell}-\frac{1}{4c-p+8\ell}+\cdots$$

$$\text{subseries 5} = \sum_{n=1}^{\infty}\frac{(-1)^{n+1}}{n(c+2\ell)-p} \tag{5.17}$$

Subseries 6:

$$-\frac{1}{p}-\frac{1}{c+p+2\ell}-\frac{1}{2c+p+4\ell}+\frac{1}{3c+p+6\ell}-\cdots$$

$$\text{subseries 6} = \sum_{n=1}^{\infty}\frac{(-1)^{n}}{n(c+2\ell)-c+p-2\ell}$$

Subseries 7:

$$-\frac{1}{p+2\ell}+\frac{1}{c+p+4\ell}-\frac{1}{2c+p+6\ell}+\frac{1}{3c+p+8\ell}-\cdots$$

$$\text{subseries 7} = \sum_{n=1}^{\infty}\frac{(-1)^n}{n(c+2\ell)-c+p} \qquad (5.19)$$

Hence by adding the subseries 1 to 7, the expression for the potential V_f becomes

$$V_f = \frac{\rho I}{2\pi r}\left[1+(-1)^n\sum_{n=1}^{\infty}\frac{2}{n(c+2\ell)}+\frac{1}{n(c+2\ell)-2\ell}-\frac{1}{n(c+2\ell)-c}\right.$$

$$\left.-\frac{1}{n(c+2\ell)-p-2\ell}-\frac{1}{n(c+2\ell)-p}+\frac{1}{n(c+2\ell)-c+p-2\ell}+\frac{1}{n(c+2\ell)-c+p}\right] \qquad (5.20)$$

Now $\frac{\rho}{2\pi r} = R_\infty$ and $\frac{V_f}{I} = R$, the measured resistance. Therefore,

$$\frac{R}{R_\infty} = [1 + \Sigma \text{ sum}] \qquad (5.21)$$

where sum represents the infinite series in the bracket in equation (5.20). Now considering the infinite terms in the sum, for the given values of c and ℓ, there exists a value of p which makes Σ sum = 0 and hence $R = R_\infty$. This argument is the same as described in Section 5.2.1. Therefore the problem reduces to solving for p, given c and ℓ, in the question Σ sum = 0. By removing $\frac{1}{c}$ outside and substituting $\frac{p}{c} = \alpha$ and $\frac{\ell}{c} = x$, the equation Σ sum = 0 can be rewritten as follows:

$$(-1)^n\cdot\frac{1}{c}\left[\sum_{n=1}^{\infty}\frac{2}{n(1+2x)}+\frac{1}{n(1+2x)-2x}-\frac{1}{n(1+2x)-1}-\frac{1}{n(1+2x)-\alpha-2x}\right.$$

$$\left.-\frac{1}{n(1+2x)-\alpha}+\frac{1}{n(1+2x)-1+\alpha-2x}+\frac{1}{n(1+2x)-1+\alpha}\right] = 0 \qquad (5.22)$$

The following method is adopted to calculate α which will satisfy equation (5.22) given c and x. First the convergence of the infinite series was improved by using Euler's Transformation[3]. The Euler's Transformation is most efficient when the alternating series converges very slowly. A computer program was written to calculate the sum using Euler's Transformation and for different values of the variable n. A suitable value of n was decided upon (n = 65) which would yield results within the practical accuracy limits and was used in the subsequent analysis. Then equation (5.22) was solved for α, using digital computations. The program is listed in Appendix A.

Table 5.1 lists the values of coefficient α and x and Fig. 5.4 shows a graph of $\alpha = \frac{p}{c}$ (α is also equal to $\frac{p}{c}$) against $x = \frac{\ell}{c}$ (x is also equal to $\frac{L}{C}$).

TABLE 5.1
Measurement Correction Factor

C	$x = \frac{L}{C}$	$\alpha = \frac{P}{C}$
100	.025	.0808
100	.05	.1596
100	.1	.2975
100	.2	.4588
100	.3	.5277
100	.4	.5611
100	.5	.5794
100	.6	.5905
100	.7	.5976
100	.8	.6024
100	.9	.6058
100	1.0	.6083
100	1.5	.6141
100	2.0	.6161
100	2.5	.6169
100	3.0	.6173
100	3.5	.6176
100	4.0	.6177
100	4.5	.6178
100	5.0	.6179

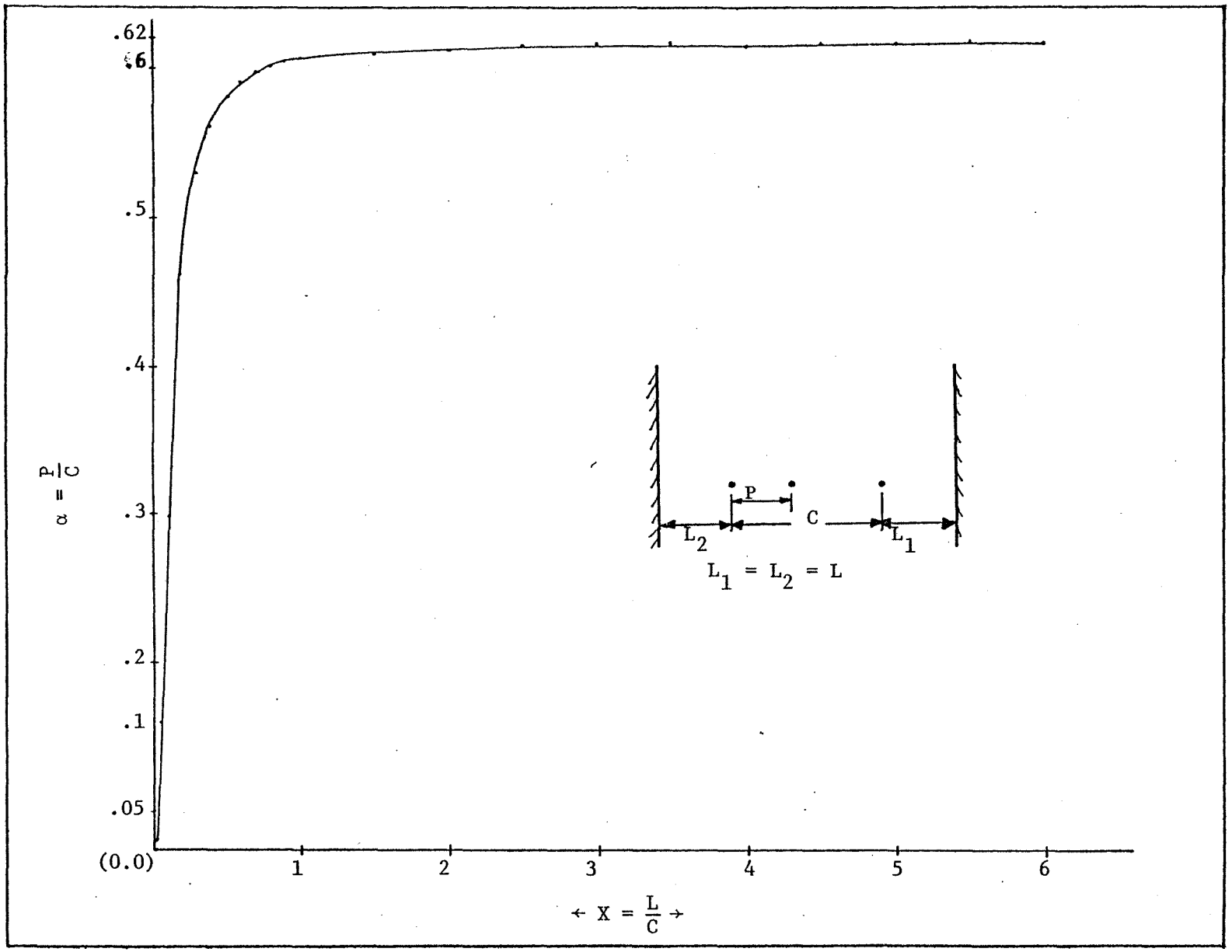


Fig. 5.4 Plot of $\alpha = \frac{P}{C}$ Against $X = \frac{L}{C}$ for Perpendicular Boundaries With Equal Spacings

5.1.4 Perpendicular Boundary Condition with Unequal Spacings

The model is shown in Fig. 5.5. The only difference in the model of Section 5.1.3 and the present one is that the current electrodes 1 and 3 are spaced unequally from the non-conducting boundaries. This case is more complicated than the previous one owing to the introduction of two variables x and y, where x and y are defined in Section 5.1.2.

The floating potentials V_{f_1} and V_{f_2} are as follows:

$$V_{f_1} = \frac{\rho I}{2\pi}\left[-\frac{1}{C-r} - \frac{1}{C+2L_1} + \frac{1}{2C+2L_1} + \frac{1}{2C+2L_1+2L_2} - \frac{1}{3C+2L_1+2L_2}\right.$$

$$- \frac{1}{3C+4L_1+2L_2} + \frac{1}{4C+4L_1+2L_2} - \frac{1}{4C+4L_1+4L_2} - \frac{1}{5C+4L_1+4L_2} - \frac{1}{5C+6L_1+4L_2}$$

$$+ \frac{1}{6C+6L_1+4L_2} + \frac{1}{6C+6L_1+6L_2} - \ldots$$

$$+ \frac{1}{r} + \frac{1}{2L_2} + \frac{1}{C+2L_2} - \frac{1}{C+2L_1+2L_2} - \frac{1}{2C+2L_1+2L_2} + \frac{1}{2C+2L_1+4L_2}$$

$$- \frac{1}{3C+2L_1+4L_2} - \frac{1}{3C+4L_1+4L_2} + \frac{1}{4C+4L_1+4L_2} + \frac{1}{4C+4L_1+6L_2} - \frac{1}{5C+4L_1+6L_2}$$

$$\left. - \frac{1}{5C+6L_1+6L_2} + \frac{1}{6C+6L_1+6L_2} + \ldots\right] \qquad (5.23)$$

$$V_{f_2} = \frac{\rho I}{2\pi}\left[-\frac{1}{C-P} - \frac{1}{C-P+2L_1} + \frac{1}{2C-P+2L_1} + \frac{1}{2C-P+2L_1+2L_2} - \frac{1}{3C-P+2L_1+2L_2}\right.$$

$$- \frac{1}{3C-P+4L_1+2L_2} + \frac{1}{4C-P+4L_1+2L_2} + \frac{1}{4C-P+4L_1+4L_2} - \frac{1}{5C-P+4L_1+4L_2}$$

$$- \frac{1}{5C-P+6L_1+4L_2} + \frac{1}{6C-P+6L_1+4L_2} + \ldots$$

$$+ \frac{1}{P} + \frac{1}{P+2L_2} - \frac{1}{C+P+2L_2} - \frac{1}{C+P+2L_1+2L_2} + \frac{1}{2C+P+2L_1+2L_2} + \frac{1}{2C+P+2L_1+4L_2}$$

$$- \frac{1}{3C+P+2L_1+4L_2} - \frac{1}{3C+P+4L_1+4L_2} + \frac{1}{4C+P+4L_1+4L_2}$$

$$\left. + \frac{1}{4C+P+4L_1+6L_2} - \frac{1}{5C+P+4L_1+6L_2} - \ldots\right] \qquad (5.24)$$

and

$$V_f = V_{f_1} - V_{f_2} \qquad (5.25)$$

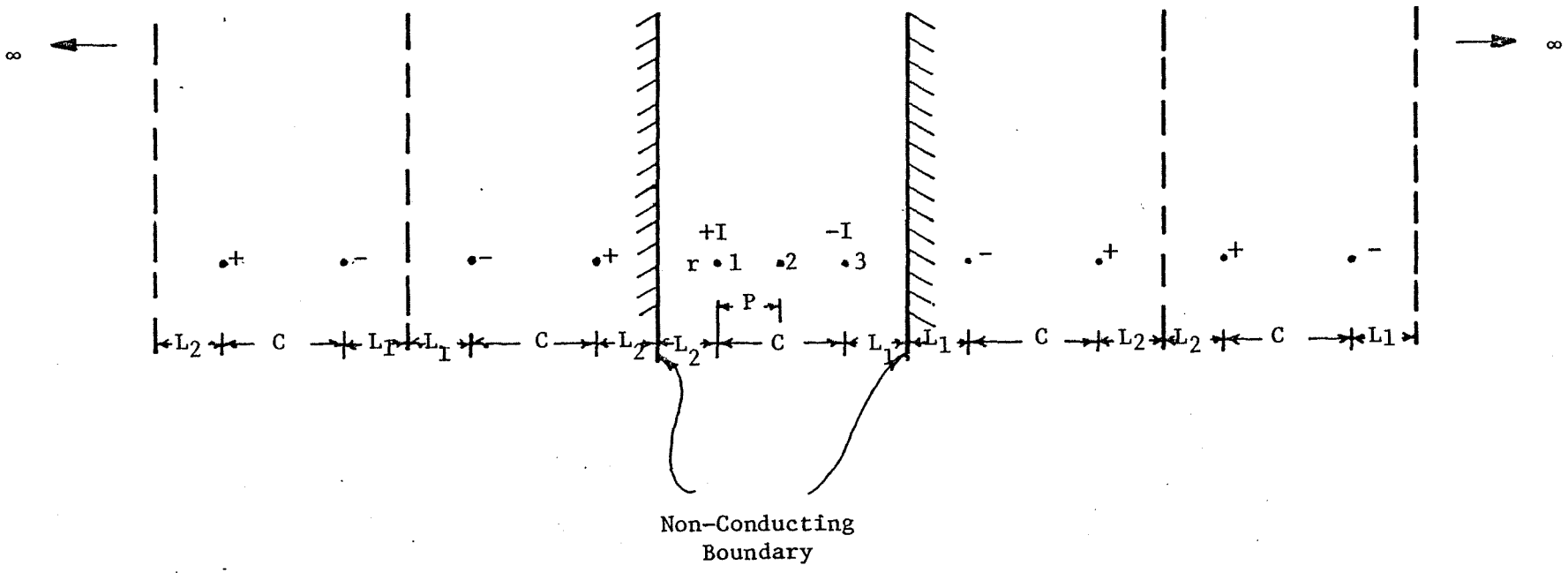


Fig. 5.5 Fall-of-Potential Electrodes Perpendicular to Non-Conducting Boundary. (Unequal spacings) $L_1 \neq L_2$

Again the equation (5.23) in the term $-\frac{1}{C-r}$, r can be neglected as compared to C. Now by removing $\frac{1}{r}$ outside the bracket and substituting $\frac{C}{r} = c$, $\frac{P}{r} = p$, $\frac{L_1}{r} = \ell_1$, and $\frac{L_2}{r} = \ell_2$, equation (5.26) is obtained from equation (5.25).

$$V_f = \frac{\rho I}{2\pi r}\left[1 - \frac{1}{c} - \frac{1}{p} + \frac{1}{c-p} + \frac{2}{2c+2\ell_1+2\ell_2} + \frac{2}{4c+4\ell_1+4\ell_2} + \frac{2}{6c+6\ell_1+6\ell_2} + \cdots\right.$$

$$- \frac{1}{c+2\ell_1} + \frac{1}{2c+2\ell_1} - \frac{1}{3c+2\ell_1+2\ell_2} - \frac{1}{3c+4\ell_1+2\ell_2} + \frac{1}{4c+4\ell_1+2\ell_2} - \frac{1}{5c+4\ell_1+4\ell_2}$$

$$- \frac{1}{5c+6\ell_1+4\ell_2} + \frac{1}{6c+6\ell_1+4\ell_2} + \cdots$$

$$+ \frac{1}{2\ell_2} - \frac{1}{c+2\ell_2} - \frac{1}{c+2\ell_1+2\ell_2} + \frac{1}{2c+2\ell_1+4\ell_2} - \frac{1}{3c+2\ell_1+4\ell_2} - \frac{1}{3c+4\ell_1+4\ell_2}$$

$$+ \frac{1}{4c+4\ell_1+6\ell_2} - \frac{1}{5c+4\ell_1+6\ell_2} - \frac{1}{5c+6\ell_1+6\ell_2} + \cdots$$

$$+ \frac{1}{c-p+2\ell_1} - \frac{1}{2c-p+2\ell_1} - \frac{1}{2c-p+2\ell_1+2\ell_2} + \frac{1}{3c-p+2\ell_1+2\ell_2} + \frac{1}{3c-p+4\ell_1+2\ell_2}$$

$$- \frac{1}{4c-p+4\ell_1+2\ell_2} - \frac{1}{4c-p+4\ell_1+4\ell_2} + \frac{1}{5c-p+4\ell_1+4\ell_2} + \frac{1}{5c-p+6\ell_1+4\ell_2}$$

$$- \frac{1}{6c-p+6\ell_1+4\ell_2} - \cdots$$

$$- \frac{1}{p+2\ell_2} + \frac{1}{c+p+2\ell_2} + \frac{1}{c+p+2\ell_1+2\ell_2} - \frac{1}{2c+p+2\ell_1+2\ell_2} - \frac{1}{2c+p+2\ell_1+4\ell_2}$$

$$+ \frac{1}{3c+p+2\ell_1+4\ell_2} + \frac{1}{3c+p+4\ell_1+4\ell_2} - \frac{1}{4c+p+4\ell_1+4\ell_2} - \frac{1}{4c+p+4\ell_1+6\ell_2}$$

$$\left. + \frac{1}{5c+p+4\ell_1+6\ell_2} + \cdots\right] \qquad (5.26)$$

As seen in the following analysis, this infinite series can be represented as a sum of subseries which in turn are represented as Σnth term.

Subseries 1:

$$+ \frac{2}{2c+2\ell_1+2\ell_2} + \frac{2}{4c+4\ell_1+4\ell_2} + \frac{2}{6c+6\ell_1+6\ell_2} + \cdots$$

This can be represented as follows

$$\text{Subseries 1} = \sum_{n=1}^{\infty} \frac{2}{n(c+\ell_1+\ell_2)} \qquad (5.27)$$

Subseries 2:

$$-\frac{1}{c}-\frac{1}{3c+2\ell_1+2\ell_2}-\frac{1}{5c+4\ell_1+4\ell_2}-\cdots$$

$$\text{Subseries 2} = \sum_{n=1}^{\infty}\frac{-1}{(2n-1)c+2(n-1)(\ell_1+\ell_2)} \tag{5.28}$$

Subseries 3:

$$-\frac{1}{c+2\ell_1}-\frac{1}{3c+4\ell_1+2\ell_2}-\frac{1}{5c+6\ell_1+4\ell_2}-\cdots$$

$$\text{Subseries 3} = \sum_{n=1}^{\infty}\frac{-1}{(2n-1)c+2n\ell_1+2(n-1)\ell_2} \tag{5.29}$$

Subseries 4:

$$+\frac{1}{2c+2\ell_1}+\frac{1}{4c+4\ell_1+2\ell_2}+\frac{1}{6c+6\ell_1+4\ell_2}$$

$$\text{Subseries 4} = \sum_{n=1}^{\infty}\frac{1}{2nc+2n\ell_1+2(n-1)\ell_2} \tag{5.30}$$

Subseries 5:

$$+\frac{1}{2\ell_2}+\frac{1}{2c+2\ell_1+4\ell_2}+\frac{1}{4c+4\ell_1+6\ell_2}+\cdots$$

$$\text{Subseries 5} = \sum_{n=1}^{\infty}\frac{1}{2(n-1)c+2(n-1)\ell_1+2n\ell_2} \tag{5.31}$$

Subseries 6:

$$-\frac{1}{c+2\ell_2}-\frac{1}{3c+2\ell_1+4\ell_2}-\frac{1}{5c+4\ell_1+6\ell_2}-\cdots$$

$$\text{Subseries 6} = \sum_{n=1}^{\infty}\frac{-1}{(2n-1)c+2(n-1)\ell_1+2n\ell_2} \tag{5.32}$$

Subseries 7:

$$-\frac{1}{c+2\ell_1+2\ell_2}-\frac{1}{3c+4\ell_1+4\ell_2}-\frac{1}{5c+6\ell_1+6\ell_2}-\cdots$$

$$\text{Subseries 7} = \sum_{n=1}^{\infty}\frac{-1}{(2n-1)c+2n\ell_1+2n\ell_2} \tag{5.33}$$

Subseries 8:

$$+\frac{1}{c-p}+\frac{1}{3c-p+2\ell_1+2\ell_2}+\frac{1}{5c-p+4\ell_1+4\ell_2}+\cdots$$

$$\text{Subseries 8} = \sum_{n=1}^{\infty} \frac{1}{(2n-1)c-p+2(n-1)(\ell_1+\ell_2)} \tag{5.34}$$

Subseries 9:

$$+\frac{1}{c-p+2\ell_1}+\frac{1}{3c-p+4\ell_1+2\ell_2}+\frac{1}{5c-p+6\ell_1+4\ell_2}+\cdots$$

$$\text{Subseries 9} = \sum_{n=1}^{\infty} \frac{1}{(2n-1)c-p+2n\ell_1+2(n-1)\ell_2} \tag{5.35}$$

Subseries 10:

$$-\frac{1}{2c-p+2\ell_1}-\frac{1}{4c-p+4\ell_1+2\ell_2}-\frac{1}{6c-p+6\ell_1+4\ell_2}-\cdots$$

$$\text{Subseries 10} = \sum_{n=1}^{\infty} \frac{-1}{2nc-p+2n\ell_1+2(n-1)\ell_2} \tag{5.36}$$

Subseries 11:

$$-\frac{1}{2c-p+2\ell_1+2\ell_2}-\frac{1}{4c-p+4\ell_1+4\ell_2}-\frac{1}{6c-p+6\ell_1+6\ell_2}-\cdots$$

$$\text{Subseries 11} = \sum_{n=1}^{\infty} \frac{-1}{2nc-p+2n\ell_1+2n\ell_2} \tag{5.37}$$

Subseries 12:

$$-\frac{1}{p}-\frac{1}{2c+p+2\ell_1+2\ell_2}-\frac{1}{4c+p+4\ell_1+4\ell_2}-\cdots$$

$$\text{Subseries 12} = \sum_{n=1}^{\infty} \frac{-1}{2(n-1)c+p+2(n-1)(\ell_1+\ell_2)} \tag{5.38}$$

Subseries 13:

$$-\frac{1}{p+2\ell_2}-\frac{1}{2c+p+2\ell_1+4\ell_2}-\frac{1}{4c+p+4\ell_1+6\ell_2}-\cdots$$

$$\text{Subseries 13} = \sum_{n=1}^{\infty} \frac{-1}{2(n-1)c+p+2(n-1)\ell_1+2n\ell_2} \tag{5.39}$$

Subseries 14:

$$+\frac{1}{c+p+2\ell_2}+\frac{1}{3c+p+2\ell_1+4\ell_2}+\frac{1}{5c+p+4\ell_1+6\ell_2}+\cdots$$

$$\text{Subseries 14} = \sum_{n=1}^{\infty}\frac{1}{(2n-1)c+p+2(n-1)\ell_1+2n\ell_2} \tag{5.40}$$

Subseries 15:

$$+\frac{1}{c+p+2\ell_1+2\ell_2}+\frac{1}{3c+p+4\ell_1+4\ell_2}+\frac{1}{5c+p+6\ell_1+6\ell_2}+\cdots$$

$$\text{Subseries 15} = \sum_{n=1}^{\infty}\frac{1}{(2n-1)c+p+2n\ell_1+2n\ell_2} \tag{5.41}$$

Now considering all these subseries, equation (5.42) is formed as follows:

$$\begin{aligned}V_f = \frac{\rho I}{2\pi r}\Bigg[1 &+ \sum_{n=1}^{\infty}\frac{1}{nc+n\ell_1+n\ell_2}-\frac{1}{(2n-1)c+2(n-1)\ell_1+2(n-1)\ell_2}\\
&-\frac{1}{(2n-1)c+2n\ell_1+2(n-1)\ell_2}+\frac{1}{2nc+2n\ell_1+2(n-1)\ell_2}\\
&+\frac{1}{2(n-1)c+2(n-1)\ell_1+2n\ell_2}-\frac{1}{(2n-1)c+2(n-1)\ell_1+2n\ell_2}\\
&-\frac{1}{(2n-1)c+2n\ell_1+2n\ell_2}+\frac{1}{(2n-1)c-p+2(n-1)\ell_1+2(n-1)\ell_2}\\
&+\frac{1}{(2n-1)c-p+2n\ell_1+2(n-1)\ell_2}-\frac{1}{2nc-p+2n\ell_1+2(n-1)\ell_2}\\
&-\frac{1}{2nc-p+2n\ell_1+2n\ell_2}-\frac{1}{2(n-1)c+p+2(n-1)\ell_1+2(n-1)\ell_2}\\
&-\frac{1}{2(n-1)c+p+2(n-1)\ell_1+2n\ell_2}+\frac{1}{(2n-1)c+p+2(n-1)\ell_1+2n\ell_2}\\
&+\frac{1}{(2n-1)c+p+2n\ell_1+2n\ell_2}\Bigg]\end{aligned} \tag{5.42}$$

Removing $\frac{1}{c}$ outside the sum and substituting $R_\infty = \frac{\rho}{2\pi r}$, $R = \frac{V_f}{I}$, $\frac{\ell 1}{c} = x$, $\frac{\ell 2}{c} = y$ and $\frac{p}{c} = \alpha$, equation (5.42) can be rewritten as follows:

$$\frac{R}{R_\infty} = 1 + \frac{1}{c}\left[\sum_{n=1}^{\infty} \frac{1}{n(1+x+y)} - \frac{1}{2n(1+x+y)-2(x+y)-1} - \frac{1}{2n(1+x+y)-2y-1}\right.$$

$$+ \frac{1}{2n(1+x+y)-2y} + \frac{1}{2n(1+x+y)-2x-2} - \frac{1}{2n(1+x+y)-2x-1} - \frac{1}{2n(1+x+y)-1}$$

$$+ \frac{1}{2n(1+x+y)-2(x+y)-\alpha-1} + \frac{1}{2n(1+x+y)-2y-\alpha-1} - \frac{1}{2n(1+x+y)-2y-\alpha}$$

$$- \frac{1}{2n(1+x+y)-\alpha} - \frac{1}{2n(1+x+y)-2(x+y)+\alpha-2} - \frac{1}{2n(1+x+y)-2x+\alpha-2}$$

$$\left. + \frac{1}{2n(1+x+y)-2x+\alpha-1} + \frac{1}{2n(1+x+y)+\alpha-1}\right] \qquad (5.43)$$

or

$$\frac{R}{R_\infty} = [1 + \Sigma \text{ sum}] \qquad (5.44)$$

By similar argument as in Section 5.1.3, the equation Σ sum = 0 is solved for α, given the values of ℓ_1, ℓ_2 and c. The computer program is listed in Appendix B.

Referring back to the Fig. 5.5, a relationship between x and y can be easily derived as follows:

$$L_1 + L_2 + C = A$$

where A is the length of the model. Dividing by C throughout,

$$\frac{L_1}{C} + \frac{L_2}{C} + 1 = \frac{A}{C}$$

Now $\frac{L_1}{C} = \frac{\ell_1}{C}$ =xx and $\frac{L_2}{C} = \frac{\ell_2}{C} = y$

Therefore

$$x + y + 1 = \frac{A}{C}$$

or

$$y = \frac{A}{C} - x - 1 \qquad (5.45)$$

In the equation (5.45), if A, C and L_1 are known, then y can be computed and the effect of perpendicular boundaries can be found out for that particular x and y. Table 5.2 lists the values of x, y and α. Fig. 5.6 displays a graph of α against

$$x = \frac{\ell_1}{c} \left(= \frac{L_1}{C}\right)$$

TABLE 5.2
MEASUREMENT CORRECTION FACTOR

A	C	$x = \frac{L_1}{C}$	$y = \frac{L_2}{C}$	$\alpha = \frac{P}{C}$
150	10	.1	13.9	.5540
		.2	13.8	.5769
		.3	13.7	.5903
		.4	13.6	.5985
		.5	13.5	.6037
		.6	13.4	.6072
		.7	13.3	.6096
		.8	13.2	.6114
		.9	13.1	.6127
		1.0	13.0	.6136
		1.1	12.9	.6144
		2.1	11.9	.6171
		3.1	10.9	.6176
		4.1	9.9	.6178
		5.1	8.9	.6178
		6.1	7.9	.6179
		7.1	6.9	.6179
		8.1	5.4	.6178
		9.1	4.9	.6178
		10.1	3.9	.6117
		11.1	2.9	.6175
		12.1	1.9	.6165

TABLE 5.2 (continued)

A	C	$x = \frac{L_1}{C}$	$y = \frac{L_2}{C}$	$\alpha = \frac{P}{C}$
150	10	12.1	1.9	.6165
↓	↓	13.1	.9	.6097
		13.2	.8	.6073
		13.3	.7	.6038
		13.4	.6	.5984
		13.5	.5	.5897
		13.6	.4	.5747
		13.7	.3	.5452
		13.8	.2	.4776
		13.9	.1	.3043

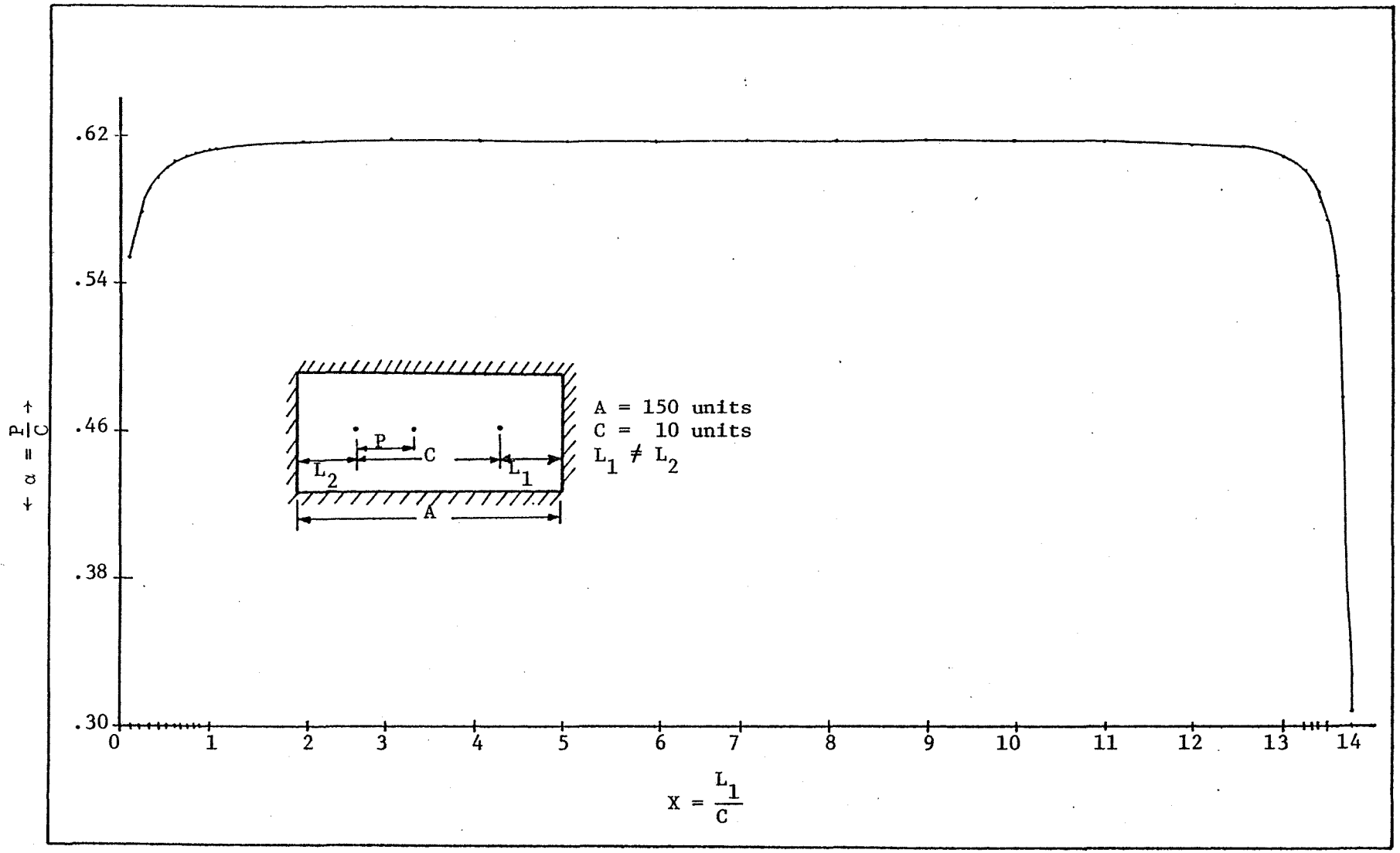


Fig. 5.6 Plot of $\alpha = \frac{P}{C}$ Against $X = \frac{L_1}{C}$ for Perpendicular Boundaries with Unequal Spacings

5.1.5 Parallel Boundary Condition with Equal Spacings

The model for this type of boundary condition is shown in Fig. 5.7. The non-conducting boundaries are parallel to the orientation of the fall-of-potential electrodes. The floating potentials V_{f_1} and V_{f_2} are as follows:

$$V_{f_1} = \frac{\rho I}{2\pi}\left[\frac{1}{r} + \frac{1}{C-r} + \frac{1}{2L} + \frac{1}{4L} + \frac{1}{6L} + \frac{1}{8L} + \ldots\right.$$

$$- \frac{1}{\sqrt{C^2+(2L)^2}} - \frac{1}{\sqrt{C^2+(4L)^2}} - \frac{1}{\sqrt{C^2+(6L)^2}} - \frac{1}{\sqrt{C^2+(8L)^2}} - \ldots$$

$$+ \frac{1}{2L} + \frac{1}{4L} + \frac{1}{6L} + \frac{1}{8L} + \ldots$$

$$\left. - \frac{1}{\sqrt{C^2+(2L)^2}} - \frac{1}{\sqrt{C^2+(4L)^2}} - \frac{1}{\sqrt{C^2+(6L)^2}} - \frac{1}{\sqrt{C^2+(8L)^2}} - \ldots\right] \quad (5.46)$$

$$V_{f_2} = \frac{\rho I}{2\pi}\left[\frac{1}{P} - \frac{1}{C-P} + \frac{1}{\sqrt{P^2+(2L)^2}} + \frac{1}{\sqrt{P^2+(4L)^2}} + \frac{1}{\sqrt{P^2+(6L)^2}} + \frac{1}{\sqrt{P^2+(8L)^2}} + \ldots\right.$$

$$+ \frac{1}{\sqrt{P^2+(2L)^2}} + \frac{1}{\sqrt{P^2+(4L)^2}} + \frac{1}{\sqrt{P^2+(6L)^2}} + \frac{1}{\sqrt{P^2+(8L)^2}} + \ldots$$

$$- \frac{1}{\sqrt{(C-P)^2+(2L)^2}} - \frac{1}{\sqrt{(C-P)^2+(4L)^2}} - \frac{1}{\sqrt{(C-P)^2+(6L)^2}} - \frac{1}{\sqrt{(C-P)^2+(8L)^2}} - \ldots$$

$$- \frac{1}{\sqrt{(C-P)^2+(2L)^2}} - \frac{1}{\sqrt{(C-P)^2+(4L)^2}} - \frac{1}{\sqrt{(C-P)^2+(6L)^2}} -$$

$$\left. - \frac{1}{\sqrt{(C-P)^2+(8L)^2}} - \ldots\right] \quad (5.47)$$

$$V_f = V_{f_1} - V_{f_2} \quad (5.48)$$

In the equation (5.46) in the term $-\frac{1}{C-r}$, r can be neglected as compared to C. Now by removing $\frac{1}{r}$ outside the bracket and substituting $\frac{C}{r} = c$, $\frac{P}{r} = p$ and $\frac{L}{r} = \ell$, equation (5.49) is obtained.

$$V_f = \frac{\rho I}{2\pi r}\left\{1 - \frac{1}{c} - \frac{1}{p} + \frac{1}{c-p} + \frac{1}{\ell} + \frac{1}{2\ell} + \frac{1}{3\ell} + \frac{1}{4\ell} + \ldots\right.$$

$$- 2\left[\frac{1}{\sqrt{c^2+(2\ell)^2}} + \frac{1}{\sqrt{c^2+(4\ell)^2}} + \frac{1}{\sqrt{c^2+(6\ell)^2}} + \frac{1}{\sqrt{c^2+(8\ell)^2}} + \ldots\right]$$

$$- 2\left[\frac{1}{\sqrt{p^2+(2\ell)^2}} + \frac{1}{\sqrt{p^2+(4\ell)^2}} + \frac{1}{\sqrt{p^2+(6\ell)^2}} + \frac{1}{\sqrt{p^2+(8\ell)^2}} + \ldots\right]$$

$$+ 2\left[\frac{1}{\sqrt{(c-p)^2+(2\ell)^2}} + \frac{1}{\sqrt{(c-p)^2+(4\ell)^2}} + \frac{1}{\sqrt{(c-p)^2+(6\ell)^2}} + \right.$$

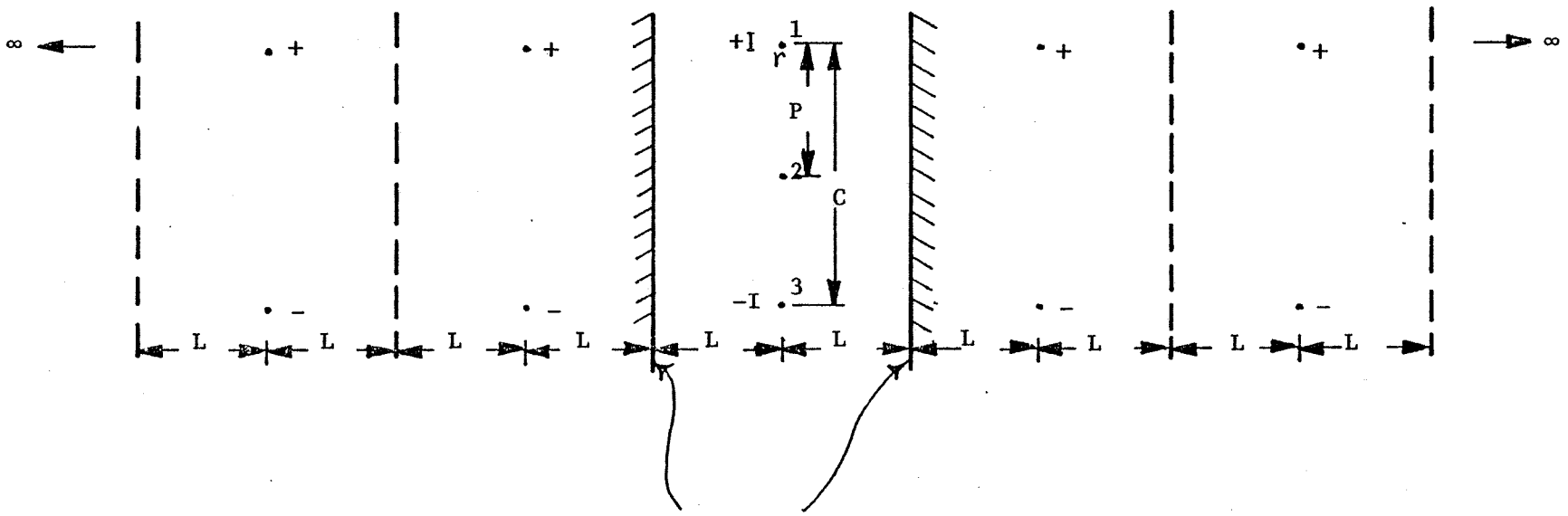


Fig. 5.7 Fall-of-Potential Electrodes Parallel to Non-Conducting Boundary (Equal Spacing) $L_3 = L_4 = L$

$$+\frac{1}{\sqrt{(c-p)^2+(8\ell)^2}}+\ldots]\} \tag{5.49}$$

The infinite series in the equation (5.49) can be grouped into subseries as shown below:

Subseries 1:

$$\frac{1}{\ell}+\frac{1}{2\ell}+\frac{1}{3\ell}+\frac{1}{4\ell}+\ldots$$

$$\text{Subseries 1} = \sum_{n=1}^{\infty}\frac{1}{n\ell} \tag{5.50}$$

Subseries 2:

$$-2\left(\frac{1}{c}+\frac{1}{\sqrt{c^2+(2\ell)^2}}+\frac{1}{\sqrt{c^2+(4\ell)^2}}+\frac{1}{\sqrt{c^2+(6\ell)^2}}+\ldots\right)$$

$$\text{Subseries 2} = -2\sum_{n=1}^{\infty}\frac{1}{\sqrt{c^2+[2(n-1)\ell]^2}} \tag{5.51}$$

Subseries 3:

$$-2\left(\frac{1}{p}+\frac{1}{\sqrt{p^2+(2\ell)^2}}+\frac{1}{\sqrt{p^2+(4\ell)^2}}+\frac{1}{\sqrt{p^2+(6\ell)^2}}+\ldots\right)$$

$$\text{Subseries 3} = -2\sum_{n=1}^{\infty}\frac{1}{\sqrt{p^2+[2(n-1)\ell]^2}} \tag{5.52}$$

Subseries 4:

$$+2\left(\frac{1}{c-p}+\frac{1}{\sqrt{(c-p)^2+(2\ell)^2}}+\frac{1}{\sqrt{(c-p)^2+(4\ell)^2}}+\frac{1}{\sqrt{(c-p)^2+(6\ell)^2}}+\ldots\right)$$

$$\text{Subseries 4} = +2\sum_{n=1}^{\infty}\frac{1}{\sqrt{(c-p)^2+[2(n-1)\ell]^2}} \tag{5.53}$$

Hence by adding all these subseries V_f becomes

$$V_f = \frac{\rho I}{2\pi r}\left\{1+\frac{1}{c}+\frac{1}{p}-\frac{1}{c-p}+\sum_{n=1}^{\infty}\frac{1}{n\ell}-\frac{2}{\sqrt{c^2+[2(n-1)\ell]^2}}\right.$$

$$\left.-\frac{2}{\sqrt{p^2+[2(n-1)\ell]^2}}+\frac{2}{\sqrt{(c-p)^2+[2(n-1)\ell]^2}}\right\} \tag{5.54}$$

Now by removing $\frac{1}{c}$ outside all the sum terms and substituting $R_\infty = \frac{\rho}{2\pi r}$, $R = \frac{rf}{I}$, $\frac{p}{c} = \alpha$ and $\frac{\ell}{c} = x$, equation (5.55) is formed as follows:

$$\frac{R}{R_\infty} = 1 + \frac{1}{C}\left\{1 + \frac{1}{\alpha} - \frac{1}{1-\alpha} + \sum_{n=1}^{\infty} \frac{1}{nx} - \frac{2}{\sqrt{1+[2(n-1)x]^2}} - \frac{2}{\sqrt{\alpha^2+[2(n-1)x]^2}}\right.$$

$$\left. + \frac{2}{\sqrt{(1-\alpha)^2+[2(n-1)x]^2}}\right\} = 0 \qquad (5.55)$$

or

$$\frac{R}{R_\infty} = [1 + \text{sum}]$$

The equation sum = 0 is solved for α, given the values of c and $x = \frac{\ell}{c}$ $(= \frac{L}{C})$ by using the method outlined in Section 5.1.3. The computer program is listed in Appendix C. Table 5.3 lists the values of x and corresponding values of α. Fig. 5.8 shows a graph of $\alpha = \frac{P}{C}$ against $x = \frac{\ell}{c}(= \frac{L}{C})$.

5.1.6 Parallel Boundary Condition with Unequal Spacings

The model for this case is shown in Fig. 5.9. Again, the only difference between this model and that of Section 5.1.5 is that the electrodes are placed at unequal distances from the non-conducting boundaries. The floating potentials V_{f_1} and V_{f_2} are found in the same way as done previously.

$$V_{f_1} = \frac{\rho I}{2\pi}\left[\frac{1}{r} - \frac{1}{C-r} + \frac{1}{2L_3} + \frac{1}{2L_3+2L_4} + \frac{1}{4L_3+2L_4} + \frac{1}{4L_3+4L_4} + \frac{1}{6L_3+4L_4}\right.$$

$$+ \frac{1}{6L_3+6L_4} + \frac{1}{8L_3+6L_4} + \ldots$$

$$+ \frac{1}{2L_4} + \frac{1}{2L_3+2L_4} + \frac{1}{2L_3+4L_4} + \frac{1}{4L_3+4L_4} + \frac{1}{4L_3+6L_4}$$

$$+ \frac{1}{6L_3+6L_4} + \frac{1}{6L_3+8L_4} + \ldots$$

$$- \frac{1}{\sqrt{C^2+(2L_3)^2}} - \frac{1}{\sqrt{C^2+(2L_3+2L_4)^2}} - \frac{1}{\sqrt{C^2+(4L_3+2L_4)^2}} - \frac{1}{\sqrt{C^2+(4L_3+4L_4)^2}}$$

$$- \frac{1}{\sqrt{C^2+(6L_3+4L_4)^2}} - \frac{1}{\sqrt{C^2+(6L_3+6L_4)^2}} - \ldots$$

$$- \frac{1}{\sqrt{C^2+(2L_4)^2}} - \frac{1}{\sqrt{C^2+(2L_3+2L_4)^2}} - \frac{1}{\sqrt{C^2+(2L_3+4L_4)^2}} - \frac{1}{\sqrt{C^2+(4L_3+4L_4)^2}}$$

$$\left. - \frac{1}{\sqrt{C^2+(4L_3+6L_4)^2}} - \frac{1}{\sqrt{C^2+(6L_3+6L_4)^2}} - \ldots\right] \qquad (5.56)$$

TABLE 5.3
MEASUREMENT CORRECTION FACTOR

$x = L/C$	$\alpha = P/C$
.1	.1796
.2	.3055
.3	.3992
.4	.4690
.5	.5177
.6	.5494
.7	.5697
.8	.5828
.9	.5916
1.0	.5976
1.1	.6019
1.6	.6114
2.1	.6144
2.6	.6157
3.1	.6163
3.6	.6167
4.1	.6170
4.6	.6171
5.1	.6172
5.6	.6173
6.1	.6174
6.6	.6175

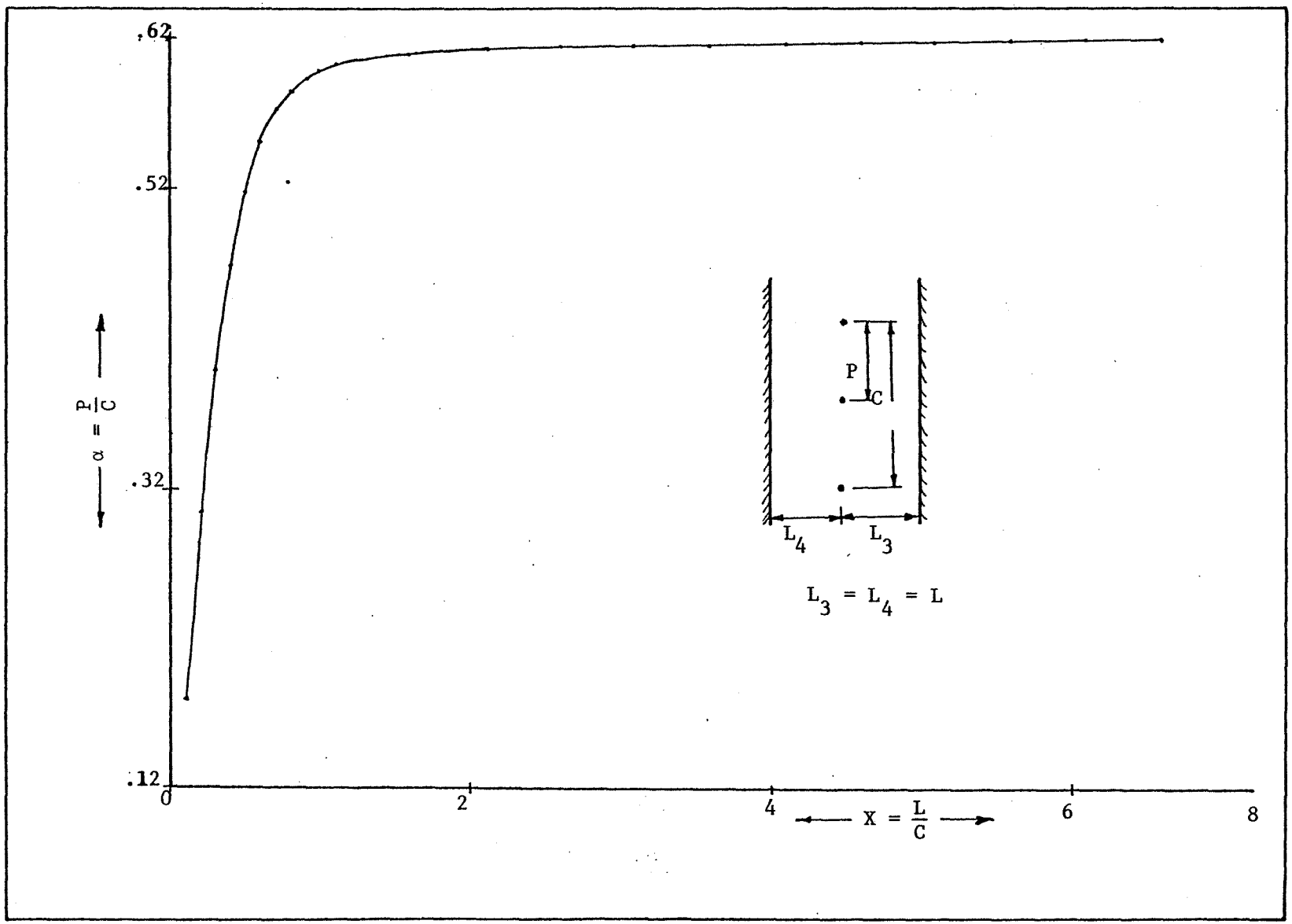


Fig. 5.8 Plot of $\alpha = \frac{P}{C}$ Against $X = \frac{L}{C}$ for Parallel Boundaries with Equal Spacings

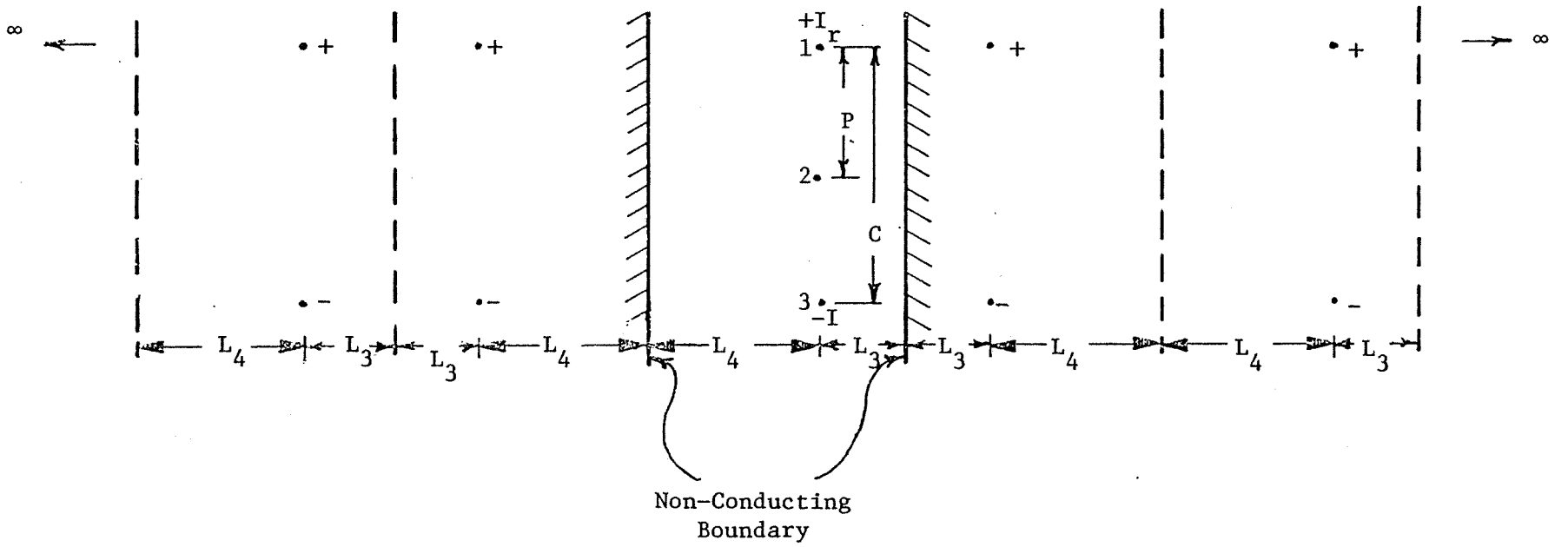


Fig. 5.9 Fall-of-Potential Electrodes Parallel to Non-Conducting Boundary. (Unequal spacing) $L_3 \neq L_4$

$$V_{f_2} = \frac{\rho I}{2\pi}\left[\frac{1}{P} - \frac{1}{C-P} + \frac{1}{\sqrt{P^2+(2L_3)^2}} + \frac{1}{\sqrt{P^2+(2L_3+2L_4)^2}} + \frac{1}{\sqrt{P^2+(4L_3+2L_4)^2}}\right.$$

$$+ \frac{1}{\sqrt{P^2+(4L_3+4L_4)^2}} + \frac{1}{\sqrt{P^2+(6L_3+4L_4)^2}} + \frac{1}{\sqrt{P^2+(6L_3+6L_4)^2}} + \ldots$$

$$+ \frac{1}{\sqrt{P^2+(2L_4)^2}} + \frac{1}{\sqrt{P^2+(2L_3+2L_4)^2}} + \frac{1}{\sqrt{P^2+(2L_3+4L_4)^2}} + \frac{1}{\sqrt{P^2+(4L_3+4L_4)^2}}$$

$$+ \frac{1}{\sqrt{P^2+(4L_3+6L_4)^2}} + \frac{1}{\sqrt{P^2+(6L_3+6L_4)^2}} + \ldots$$

$$- \frac{1}{\sqrt{(C-P)^2+(2L_3)^2}} - \frac{1}{\sqrt{(C-P)^2+(2L_3+2L_4)^2}} - \frac{1}{\sqrt{(C-P)^2+(4L_3+2L_4)^2}}$$

$$- \frac{1}{\sqrt{(C-P)^2+(4L_3+4L_4)^2}} - \frac{1}{\sqrt{(C-P)^2+(6L_3+4L_4)^2}} - \ldots$$

$$- \frac{1}{\sqrt{(C-P)^2+(2L_4)^2}} - \frac{1}{\sqrt{(C-P)^2+(2L_3+2L_4)^2}} - \frac{1}{\sqrt{(C-P)^2+(2L_3+4L_4)^2}}$$

$$\left. - \frac{1}{\sqrt{(C-P)^2+(4L_3+4L_4)^2}} - \frac{1}{\sqrt{(C-P)^2+(4L_3+6L_4)^2}} - \ldots\right] \qquad (5.57)$$

In the equation (5.56) in the term $-\frac{1}{C-r}$, r can be neglected as compared to C for all practical purposes.

Now $V_f = V_{f_1} - V_{f_2}$ (5.58)

Hence by removing $\frac{1}{r}$ outside the bracket and substituting $\frac{C}{r} = c$, $\frac{P}{r} = p$, $\frac{L3}{r} = \ell_3$ and $\frac{L4}{r} = \ell_4$ equation (5.58) is transformed into equation (5.59)

$$V_f = \frac{\rho I}{2\pi r}\left[\frac{1}{r} - \frac{1}{c} + \frac{1}{2\ell_3} + \frac{1}{2\ell_3+2\ell_4} + \frac{1}{4\ell_3+2\ell_4} + \frac{1}{4\ell_3+4\ell_4} + \frac{1}{6\ell_3+4\ell_4}\right.$$

$$+ \frac{1}{6\ell_3+6\ell_4} + \frac{1}{8\ell_3+6\ell_4} + \ldots$$

$$+ \frac{1}{2\ell_4} + \frac{1}{2\ell_3+2\ell_4} + \frac{1}{2\ell_3+4\ell_4} + \frac{1}{4\ell_3+4\ell_4} + \frac{1}{4\ell_3+6\ell_4}$$

$$+ \frac{1}{6\ell_3+6L_4} + \frac{1}{6L_3+6L_4} + \ldots$$

$$- \frac{1}{\sqrt{c^2+(2\ell_3)^2}} - \frac{1}{\sqrt{c^2+(2\ell_3+2\ell_4)^2}} - \frac{1}{\sqrt{c^2+(4\ell_3+2\ell_4)^2}} - \frac{1}{\sqrt{c^2+(4\ell_3+4\ell_4)^2}}$$

$$\left. - \frac{1}{\sqrt{c^2+(6\ell_3+4\ell_4)^2}} - \frac{1}{\sqrt{c^2+(6\ell_3+6\ell_4)^2}} - \ldots\right.$$

$$- \frac{1}{\sqrt{c^2+(2\ell_4)^2}} - \frac{1}{\sqrt{c^2+(2\ell_3+2\ell_4)^2}} - \frac{1}{\sqrt{c^2+(2\ell_3+4\ell_4)^2}} - \frac{1}{\sqrt{c^2+(4\ell_3+4\ell_4)^2}}$$

$$- \frac{1}{\sqrt{c^2+(4\ell_3+6\ell_4)^2}} - \frac{1}{\sqrt{c^2+(6\ell_3+6\ell_4)^2}} - \cdots$$

$$- \frac{1}{p} + \frac{1}{c-p} - \frac{1}{\sqrt{p^2+(2\ell_3)^2}} - \frac{1}{\sqrt{p^2+(2\ell_3+2\ell_4)^2}} - \frac{1}{\sqrt{p^2+(4\ell_3+2\ell_4)^2}}$$

$$- \frac{1}{\sqrt{p^2+(4\ell_3+4\ell_4)^2}} - \frac{1}{\sqrt{p^2+(6\ell_3+4\ell_4)^2}} - \frac{1}{\sqrt{p^2+(6\ell_3+6\ell_4)^2}} - \cdots$$

$$- \frac{1}{\sqrt{p^2+(2\ell_4)^2}} - \frac{1}{\sqrt{p^2+(2\ell_3+2\ell_4)^2}} - \frac{1}{\sqrt{p^2+(2\ell_3+2\ell_4)^2}} - \frac{1}{\sqrt{p^2+(4\ell_3+4\ell_4)^2}}$$

$$- \frac{1}{\sqrt{p^2+(4\ell_3+6\ell_4)^2}} - \frac{1}{\sqrt{p^2+(6\ell 3+6\ell_4)^2}} - \cdots$$

$$+ \frac{1}{\sqrt{(c-p)^2+(2\ell_3)^2}} + \frac{1}{\sqrt{(c-p)^2+(2\ell_3+2\ell_4)^2}} + \frac{1}{\sqrt{(c-p)^2+(4\ell_3+2\ell_4)^2}}$$

$$+ \frac{1}{\sqrt{(c-p)^2+(4\ell_3+4\ell_4)^2}} + \frac{1}{\sqrt{(c-p)^2+(6\ell_3+4\ell_4)^2}} + \cdots$$

$$+ \frac{1}{\sqrt{(c-p)^2+(2\ell_4)^2}} - \frac{1}{\sqrt{(c-p)^2+(2\ell_3+2\ell_4)^2}} - \frac{1}{\sqrt{(c-p)^2+(2\ell_3+4\ell_4)^2}}$$

$$- \frac{1}{\sqrt{(c-p)^2+(4\ell_3+4\ell_4)^2}} - \frac{1}{\sqrt{(c-p)^2+(4\ell_3+6\ell_4)^2}} - \cdots] \qquad (5.59)$$

The infinite series of equation (5.59) can be represented as a sum of subseries as follows.

Subseries 1:

$$\frac{1}{2\ell_3} + \frac{1}{4\ell_3+2\ell_4} + \frac{1}{6\ell_3+4\ell_4} + \frac{1}{8\ell_3+6\ell_4} + \cdots$$

$$\text{Subseries 1} = \sum_{n=1}^{\infty} \frac{1}{2n\ell_3+2(n-1)\ell_4} \qquad (5.60)$$

Subseries 2:

$$\frac{1}{2\ell_4} + \frac{1}{2\ell_3+4\ell_4} + \frac{1}{4\ell_3+6\ell_4} + \frac{1}{6\ell_3+8\ell_4} + \cdots$$

$$\text{Subseries 2} = \sum_{n=1}^{\infty} \frac{1}{2(n-1)\ell_3+2n\ell_4} \qquad (5.61)$$

Subseries 3:

$$\frac{2}{2\ell_3+2\ell_4} + \frac{2}{4\ell_3+4\ell_4} + \frac{2}{6\ell_3+6\ell_4} + \cdots$$

$$\text{Subseries 3} = \sum_{n=1}^{\infty} \frac{2}{2n\ell_3+2n\ell_4} \tag{5.62}$$

Subseries 4:

$$\frac{1}{\sqrt{c^2+(2\ell_3)^2}} - \frac{1}{\sqrt{c^2+(4\ell_3+2\ell_4)^2}} - \frac{1}{\sqrt{c^2+(6\ell_3+4\ell_4)^2}} - \cdots$$

$$\text{Subseries 4} = \sum_{n=1}^{\infty} \frac{-1}{\sqrt{c^2+[2n\ell_3+2(n-1)\ell_4]^2}} \tag{5.63}$$

Subseries 5:

$$-\frac{1}{\sqrt{c^2+(2\ell_4)^2}} - \frac{1}{\sqrt{c^2+(2\ell_3+4\ell_4)^2}} - \frac{1}{\sqrt{c^2+(4\ell_3+6\ell_4)^2}} - \cdots$$

$$\text{Subseries 5} = \sum_{n=1}^{\infty} \frac{-1}{\sqrt{c^2+[2(n-1)\ell_3+2n\ell_4]^2}} \tag{5.64}$$

Subseries 6:

$$-\frac{2}{\sqrt{c^2+(2\ell_3+2\ell_4)^2}} - \frac{2}{\sqrt{c^2+(4\ell_3+4\ell_4)^2}} - \frac{2}{\sqrt{c^2+(6\ell_3+6\ell_4)^2}} - \cdots$$

$$\text{Subseries 6} = \sum_{n=1}^{\infty} \frac{-2}{\sqrt{c^2+[2n\ell_1+2n\ell_2]^2}} \tag{5.65}$$

Subseries 7:

$$-\frac{1}{\sqrt{p^2+(2\ell_3)^2}} - \frac{1}{\sqrt{p^2+(4\ell_3+2\ell_4)^2}} - \frac{1}{\sqrt{p^2+(6\ell_3+4\ell_4)^2}} - \cdots$$

$$\text{Subseries 7} = \sum_{n=1}^{\infty} \frac{-1}{\sqrt{p^2+[2n\ell_3+2(n-1)\ell_4]^2}} \tag{5.66}$$

Subseries 8:

$$-\frac{1}{\sqrt{p^2+(2\ell_4)^2}} - \frac{1}{\sqrt{p^2+(2\ell_3+4\ell_4)^2}} - \frac{1}{\sqrt{p^2+(4\ell_3+6\ell_4)^2}} - \cdots$$

$$\text{Subseries 8} = \sum_{n=1}^{\infty} \frac{-1}{\sqrt{p^2+[2(n-1)\ell_3+2n\ell_4]^2}} \tag{5.67}$$

Subseries 9:

$$-\frac{2}{\sqrt{p^2+(2\ell_3+2\ell_4)^2}}-\frac{2}{\sqrt{p^2+(4\ell_3+4\ell_4)^2}}-\frac{2}{\sqrt{p^2+(6\ell_3+6\ell_4)^2}}-\cdots$$

$$\text{Subseries 9} = \sum_{n=1}^{\infty}\frac{-2}{\sqrt{p^2+[2n\ell_3+2n\ell_4]^2}} \qquad (5.68)$$

Subseries 10:

$$+\frac{1}{\sqrt{(c-p)^2+(2\ell_3)^2}}+\frac{1}{\sqrt{(c-p)^2+(4\ell_3+2\ell_4)^2}}+\frac{1}{\sqrt{(c-p)^2+(6\ell_3+4\ell_4)^2}}+\cdots$$

$$\text{Subseries 10} = \sum_{n=1}^{\infty}\frac{1}{\sqrt{(c-p)^2+[2n\ell_3+2(n-1)\ell_4]^2}} \qquad (5.69)$$

Subseries 11:

$$\frac{1}{\sqrt{(c-p)^2+(2\ell_4)^2}}+\frac{1}{\sqrt{(c-p)^2+(2\ell_3+4\ell_4)^2}}+\frac{1}{\sqrt{(c-p)^2+(4\ell_3+6\ell_4)^2}}+\cdots$$

$$\text{Subseries 11} = \sum_{n=1}^{\infty}\frac{1}{\sqrt{(c-p)^2+[2(n-1)\ell_1+2n\ell_2]^2}} \qquad (5.70)$$

Subseries 12:

$$\frac{2}{\sqrt{(c-p)^2+(2\ell_3+2\ell_4)^2}}+\frac{2}{\sqrt{(c-p)^2+(4\ell_3+4\ell_4)^2}}+\frac{2}{\sqrt{(c-p)^2+(6\ell_3+6\ell_4)^2}}+\cdots$$

$$\text{Subseries 12} = \sum_{n=1}^{\infty}\frac{2}{\sqrt{(c-p)^2+[2n\ell_3+2n\ell_4]^2}} \qquad (5.71)$$

Now combining all these subseries, the expression for V_f is as follows:

$$V_f = \frac{\rho I}{2\pi r}\left\{1-\frac{1}{c}-\frac{1}{p}+\frac{1}{c-p}+\sum_{n=1}^{\infty}\frac{1}{2n\ell_3+2(n-1)\ell_4}\right.$$

$$+\frac{1}{2(n-1)\ell_3+2n\ell_4}+\frac{1}{2n\ell_3+2n\ell_4}$$

$$-\frac{1}{\sqrt{c^2+[2n\ell_3+2(n-1)\ell_4]^2}}-\frac{1}{\sqrt{c^2+[2(n-1)\ell_3+2n\ell_4]^2}}$$

$$\left.-\frac{2}{\sqrt{c^2+[2n\ell_3+2n\ell_4]^2}}-\frac{1}{\sqrt{p^2+[2n\ell_3+2(n-1)\ell_4]^2}}\right.$$

$$- \frac{1}{\sqrt{p^2+[2(n-1)\ell_3+2n\ell_4]^2}} - \frac{2}{\sqrt{p^2+[2n\ell_3+2n\ell_4]^2}}$$

$$+ \frac{1}{\sqrt{(c-p)^2+[2n\ell_3+2(n-1)\ell_4]^2}} + \frac{1}{\sqrt{(c-p)^2+[2(n-1)\ell_3+2n\ell_4]^2}}$$

$$+ \frac{2}{\sqrt{(c-p)^2+[2n\ell_3+2n\ell_4]^2}}\} \qquad (5.72)$$

Removing $\frac{1}{c}$ outside the sum terms and substituting

$$R_\infty = \frac{\rho}{2\pi r},\ R = \frac{V_f}{I},\ \frac{\ell_3}{c} = x,\ \frac{\ell_4}{c} = y \text{ and } \frac{p}{c} = \alpha$$

$$\frac{R}{R_\infty} = 1 + \frac{1}{c}\left(-1 - \frac{1}{\alpha} + \frac{1}{1-\alpha}\right) + \frac{1}{c}\left[\sum_{n=1}^{\infty} \frac{1}{2nx+2(n-1)y}\right.$$

$$+ \frac{1}{2(n-1)x+2ny} + \frac{2}{2nx+2ny} - \frac{1}{\sqrt{1+[2nx+2(n-1)y]^2}}$$

$$- \frac{1}{\sqrt{1+[2(n-1)x+2ny]^2}} - \frac{1}{\sqrt{1+[2nx+2ny]^2}}$$

$$- \frac{2}{\sqrt{\alpha^2+[2nx+2ny]^2}} + \frac{1}{\sqrt{(1-\alpha)^2+[2nx+2(n-1)y]^2}}$$

$$+ \frac{1}{\sqrt{(1-\alpha)^2+[2(n-1)x+2ny]^2}} + \frac{2}{\sqrt{(1-\alpha)^2+[2nx+2ny]^2}}$$

$$\left. - \frac{1}{\sqrt{\alpha^2+[2nx+2(n-1)y]^2}} - \frac{1}{\sqrt{\alpha^2+[2(n-1)x+2ny]^2}}\right] \qquad (5.73)$$

or

$$\frac{R}{R_\infty} = [1 + \text{sum}] \qquad (5.74)$$

The equation sum = 0 is solved for α, for given values of c, L_3 and L_4, by using the method outlined in Section 5.1.3. A simple relationship can be derived between the two variables x and y.

$$L_3 + L_4 = B$$

where B = width of the model

$$\frac{L_3}{C} + \frac{L_4}{C} = \frac{B}{C}$$

also

$$x = \frac{\ell_3}{c} = \frac{L_3}{C} \text{ and } y = \frac{\ell_4}{c} = \frac{L_4}{C}$$

Therefore $x + y = \frac{B}{C}$

or

$$y = \frac{B}{C} - x \qquad (5.75)$$

The computer program to solve for α is listed in Appendix D. According to equation (5.75), for the given dimensions of the model, x and y can be computed and then used to evaluate α. Table 5.4 lists the values of x, y and α. Fig. 5.10 shows a graph of $\alpha = \frac{P}{C}$ against $x = \frac{\ell_3}{c} (= \frac{L_3}{C})$.

5.1.7 References

1. "Mine Grounding Systems: Evaluation of Ground Beds and Ground Bed Monitors and Evaluation of Modular Ground Wire Monitor," Project Report, Department of Electrical Engineering, West Virginia University, 1975-76.

2. Tagg, G. F., "Earth Resistances" (book), Yemens, 1964.

3. Squire, William, "Integration for Engineers and Scientists," (book), American Elsewer, New York, 1970.

5.2 FIELD TESTING OF CYLINDRICAL-ELECTRODE THEORY

A visit to an underground mine in north-central Pennsylvania provided a test of the theory developed for rods and borehold casings. Mine personnel had had some difficulty in establishing a low-resistance safety ground bed; the purpose of the visit was to determine the source of the problem and recommend solution(s).

5.2.1. Resistivity Measurements Taken

Resistivity measurements taken at the site of the existing safety ground bed, using a Wenner array with 8-foot spacings, indicated a resistivity of approximately 3300 Ω-ft. This extraordinarily high value prompted the undertaking of a resistivity profile, the results of which are shown in Table 5.5.

The measurement at 120-ft spacing produced a very dubious reading on the Bison meter, and no reading could be obtained at the 243-ft. spacing. Both points were discarded in the subsequent analysis.

TABLE 5.4
MEASUREMENT CORRECTION FACTOR

B	C	$x = L_3/C$	$y = L_4/C$	$\alpha = P/C$
100	10	.1	9.9	.3137
		.2	9.8	.4519
		.3	9.7	.5188
		.4	9.6	.5571
		.5	9.5	.5793
		.6	9.4	.5923
		.7	9.3	.6003
		.8	9.2	.6054
		.9	9.1	6087
		1.0	9.0	.6110
		1.1	8.9	.6126
		2.1	7.9	.6171
		3.1	6.9	.6177
		4.1	5.9	.6179
		5.1	4.9	.6179
		6.1	3.9	.6178
		7.1	2.9	.6177
		8.1	1.9	.6169
		9.0	1.0	.6110
		9.1	.9	.6087
		9.2	.8	.6054

TABLE 5.4 (continued)

B B	C	$x = L_3/C$	$y = L_4/C$	$\alpha = P/C$
100	10	9.3	.7	.6003
↓	↓	9.4	.6	.5923
		9.5	.5	.5793
		9.6	.4	.5571
		9.7	.3	.5188
		9.8	.2	.4519
		9.9	.1	.3137

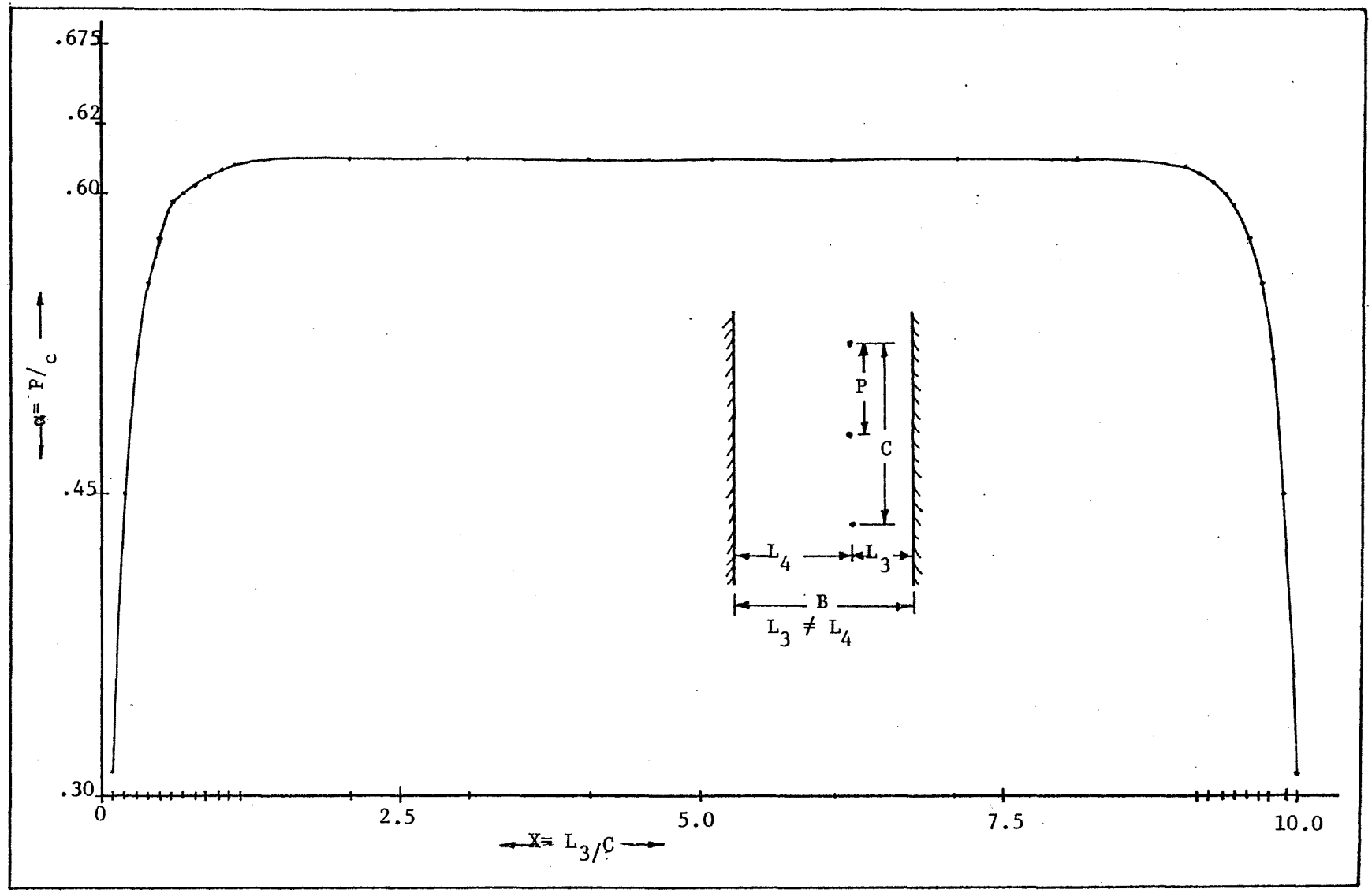


Fig. 5.10 Plot of $\alpha = P/C$ Against $X = L_3/C$ for Parallel Boundaries with Unequal Spacings

Table 5.5: Resistivity Profile Using Wenner Array

Interelectrode Spacing (ft.)	Resistivity (Ω + ft.)
1	928
3	2175
9	4100
27	3694
81	1742
120	9?
243	No reading

5.2.2: Analysis of Resistivity Measurements

Standard curves developed by Orellana and Mooney, were used to convert the "apparent resistivity" measurements of Table 5.5 to a corresponding stratified-earth approximation. Best fit was obtained by a three-layer approximation, shown in Table 5.6.

Table 5.6: Earth Composition

Resistivity of Layer (Ω - ft.)	Depth of Layer (from surface)
700	0~1
7000	1-13
1750	Below 13

5.2.3: Resistance Measurements

While still at the mine site, preliminary calculations had shown that the difficulty in obtaining a low-resistance ground was due to high earth resistivity. Anticipating the need for a large electrode, the resistance was measured of each of two borehole casings near the safety ground bed. The borehole casings were 8" and 12" in diameter, approximately 5 feet apart, and understood to be 300 feet in length. The fall-of-potential curves done for these casings did not reflect the 300 ft. length. Figure 5.11 shows the curve for the 8" casing. Neither the high indicated resistance (60.8Ω) or the rapid fall-off of potential near the borehole casing indicates a long structure.

Two hypotheses were then offered: either the high-restivity layer of earth, or a high-resistance joint in the casing, near the top, prevented current from extending very far down the length of the casing. Table 5.7 lists the calculated and measured resistances of both casings, and shows that the actual effective length must be much less than 300 feet.

Table 5.7 Borehole Resistances, Measured and Calculated

	8" Diameter	12" Diameter
Measured Resistance, Ω	47.0	60.8
Calculated Resistance, Ω, for 300' length	5.56	5.85
Calculated Resistance, Ω, for 25' length	40.9	37.0

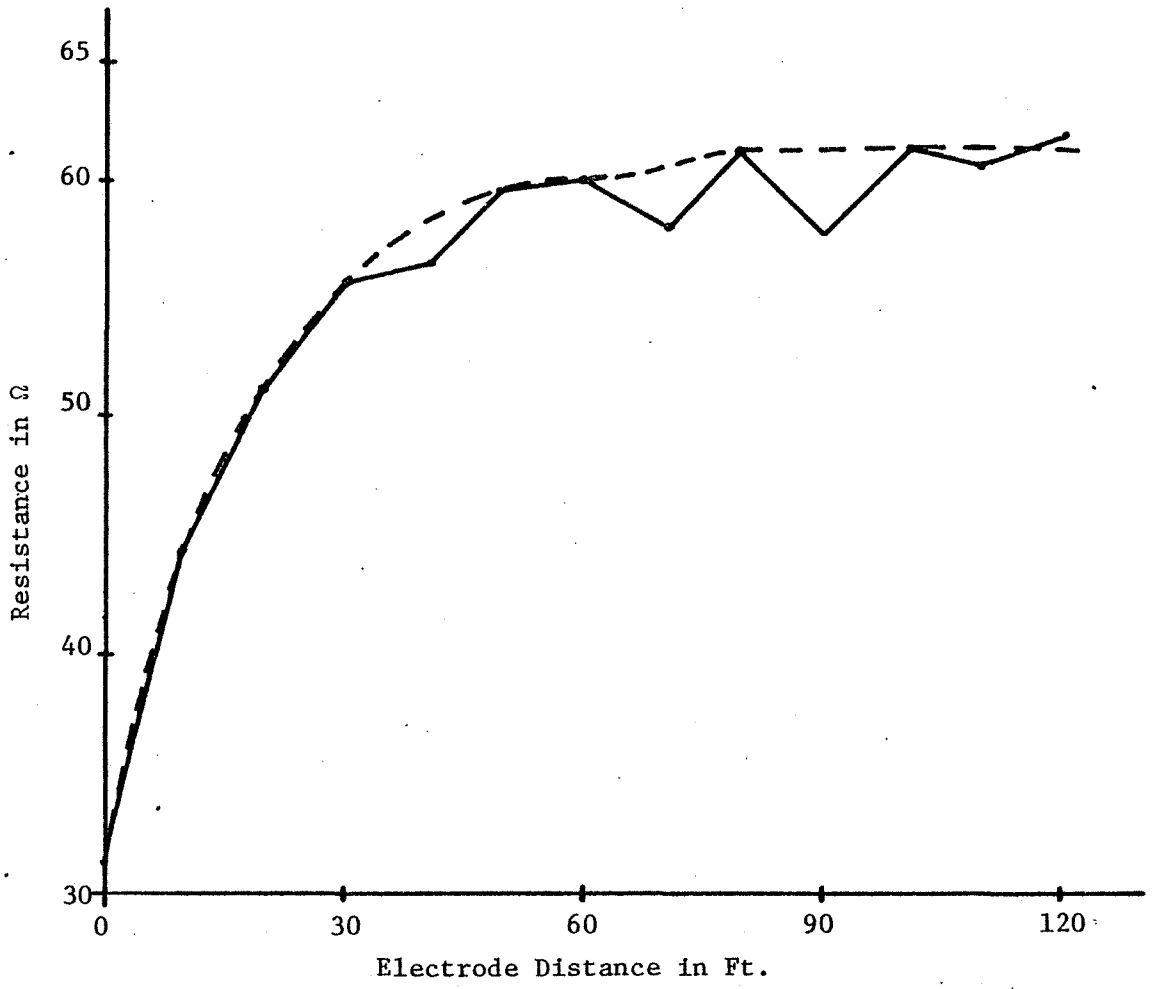


Fig. 5.11. Fall-of-Potential Curve on 8" Diameter Borehole Casing

Two weeks after the tests were done, it was learned that the casings extend only 25 feet, not 300 ft. There still is some uncertainty as to why the smaller casing yielded the lower resistance; some underground pipes near the casing may be the answer. As the principal reason for the tests was to find a low-resistance electrode, and neither borehole casing met this criterion, no more measurements were made. (Another casing which was 300 feet long subsequently was used by mine personnel to reduce the safety-bed resistance to an acceptable level.)

5.3 POTENTIAL GRADIENT PLOTTER

One of the important considerations in the design of a substation or the installation of electrical equipment in coal mines, is the hazard associated with lightning strokes and electrical system faults. Both are liable to generate huge amounts of current. A low resistance ground bed will provide the path to ground for these currents. However potential gradients are generated around electrical equipment due to these currents. Steep gradients could result in large touch-and step-potentials, which may be lethal. ("Touch" potential is the difference of potential between the legs and hands of an operator when he is in touch with the equipment. "Step" potential is the difference of potential between the two legs of an operator when he steps towards or away from a piece of equipment). Even a low resistance ground bed can cause lethal touch-and step-potentials. A good procedure is therefore necessary to minimize the hazard associated with these potentials.

Measurement of these potentials constitutes the first step in this procedure. The following sections gives details on instrumentation developed, to measure surface potential gradients between two electrodes by injecting a low current between the two. The resulting curve can be used to extrapolate results for a large value of current assuming a linear relationship, and also that the earth resistivity will remain unaffected. Mapping of equipotential contours gets greatly simplified. The data obtained can be used as basic information in the procedure used to minimize these potentials.

Periodic measurement of these potentials could convey valuable information on the effectiveness of the procedure for minimizing touch-and step-potentials. The designer could then retrace his steps and improve upon the design. This will be one of the contributions towards the ultimate goal of making mines "electrically" safe.

5.3.1 Introduction

The potential gradient plotter is an instrument designed to obtain a continuous x-y plot of potential vs distance by taking measurements around electrodes buried in the earth. The principle of operation of the plotter is illustrated in Fig. 5.12.

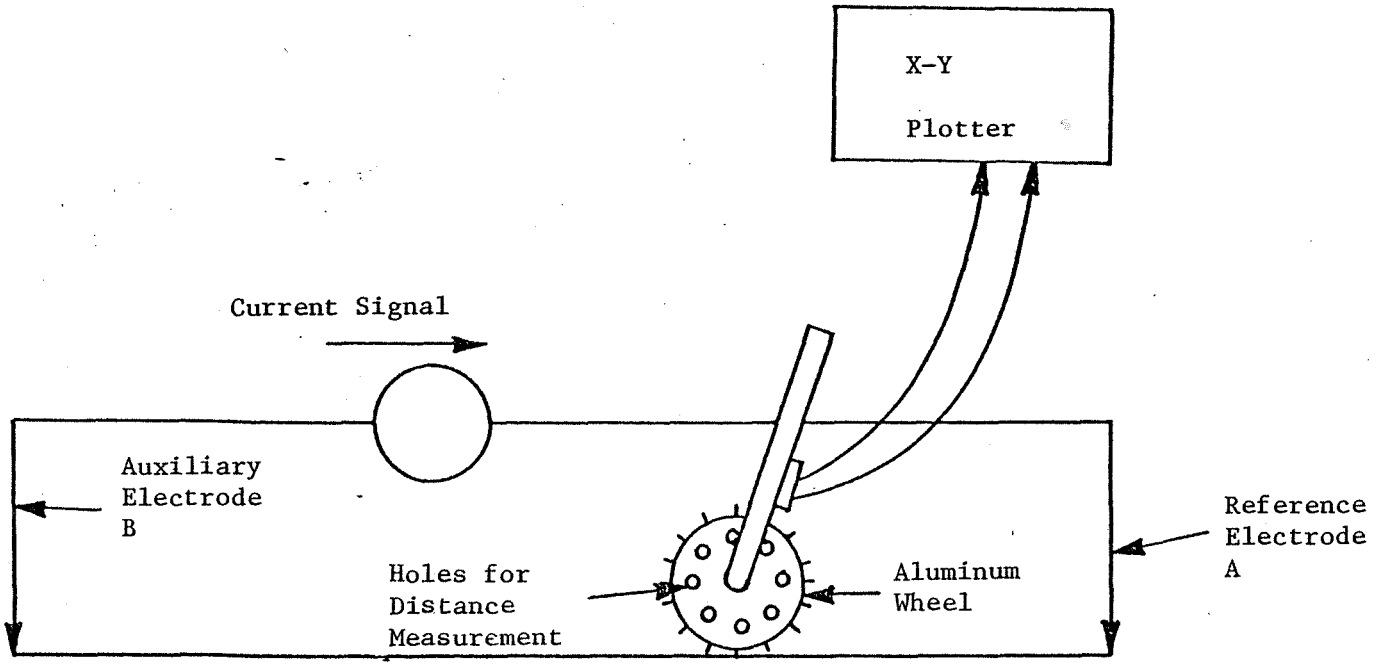


Fig. 5.12 Gradient Plotter.

A current signal is injected between two electrodes embedded in the earth. One of the electrodes, the reference electrode A is the electrode of interest around which it is desired to obtain voltage gradients. The auxiliary electrode B completes the closed path for the current loop. The detecting unit is an aluminum wheel which has good contact with the ground. The voltage signal is transmitted through the aluminum wheel, (which is a good conductor) to circuitry housed in the detecting unit. This circuit generates a signal proportional to the detected signal, and is fed to the Y input of an X-Y recorder. As the wheel moves, it transmits voltage signals at different points from the electrode.

Signals proportional to distance are also generated, so that a plot of voltage vs. distance is obtained in the X-Y plotter. Distance signals are generated by means of a light sensitive diode. A bright light source and the photo diode are mounted on opposite sides of the wheel facing each other and centered with the holes (see Fig. 5.12). As the wheel moves, light cuts through the hole and impinges on the photo-diode, to generate an impulse. The space between two holes is the smallest unit of distance, namely one-tenth of a foot. The impulse is shaped and fed to a counter and then to a D/A converter to generate an analog signal proportional to distance. This signal is fed to the recorder X input. So, as the wheel moves, a continuous plot of voltage vs. distance is obtained.

5.3.2 Description of Equipment

The equipment consists of an aluminum wheel 3 feet in circumference. It has 30 equally spaced holes drilled radially 4 inches from the center. These holes are meant for generating light impulses, and the impulse generated between adjacent holes corresponds to one-tenth of a foot. Steel nails are driven along the wheel rim, projecting 1/8" from the rim to insure good ground contact. The wheel is linked to a well-insulated handle through a fork, and provides for smooth motion as it is pushed along. A spring loaded electrical contact, touches the wheel surface and an electrical lead is taken to the detecting unit. To insure better wheel contact, a circular copper strip is screwed on to the wheel surface and the contact grazes the surface of the copper strip.

The light sensitive diode and the light source are mounted on opposite sides of the wheel facing each other. The source and diode are each mounted inside a teflon piece. The teflon pieces are housed in aluminum tubes and spring loaded so that the teflon pieces constantly touch the wheel surface. This cuts off extraneous light from impinging on the diode but will not hamper the wheel movement, since teflon is self lubricating.

The electronic circuitry is housed in an aluminum chassis 10" x 6" x 8", which is mounted on the wheel handle. Two 12V Gel Cells

are mounted adjacent to the chassis and provide the power supply to the complete circuit.

The circuit control buttons, switches, and potentiometers are housed in a small box, and mounted on the handle within easy reach of the operator. An ammeter indicating the magnitude of current injected into the ground is also mounted on the chassis. All electrical connections are plug-in type which facilitates easy hook-up in the field as well as in the laboratory for simulation tests and calibrations. Holes are drilled on the chassis for access to the various fine adjustment potentiometers mounted on the printed circuit boards. Test points from the boards are brought out and terminated on the chassis to observe the different voltages and currents for field calibration. The unit, which weighs 20 pounds, is shown in Fig. 5.13.

The complete unit is thus designed to be compact and rugged and can be conveniently handled. A 4 conductor twisted pair shielded cable, 250 feet long, provides the interconnection between the wheel unit and the X-Y plotter. Figure 5.14 shows the unit ready to use.

5.3.3 Circuitry

The circuitry can be classified broadly in 4 sections:

1) Power supply: To generate ± 12V and ± 5V regulated voltages to the whole system.

2) Constant current source: To provide a constant square wave 11 Hz current signal for injecting into the ground. The current source can be adjusted between any value from 0 to 100 mA, by means of a control potentiometer.

3) Voltage detecting unit: This circuit receives voltage signals picked up by the aluminum wheel, and filters out only signals corresponding to the voltages developed by injecting the 11 Hz current signal into the ground. A synchronous detector is used to achieve this and its operation is described later.

4) Distance detecting unit: This circuit generates an analog signal corresponding to the distance from the reference electrode. It also generates signals to a 7 segment display, which displays the distance upon operation of a control button. The circuit facilitates measurement and display of distance by counting 'UP' while going away from the electrode and 'DOWN' in the reverse direction. Reset and Display check features are also incorporated. A detailed description of the circuitry is given below:

5.3.4 Power Supply

Two 12 Volt Gel Cells connected in series generate the ± 12V

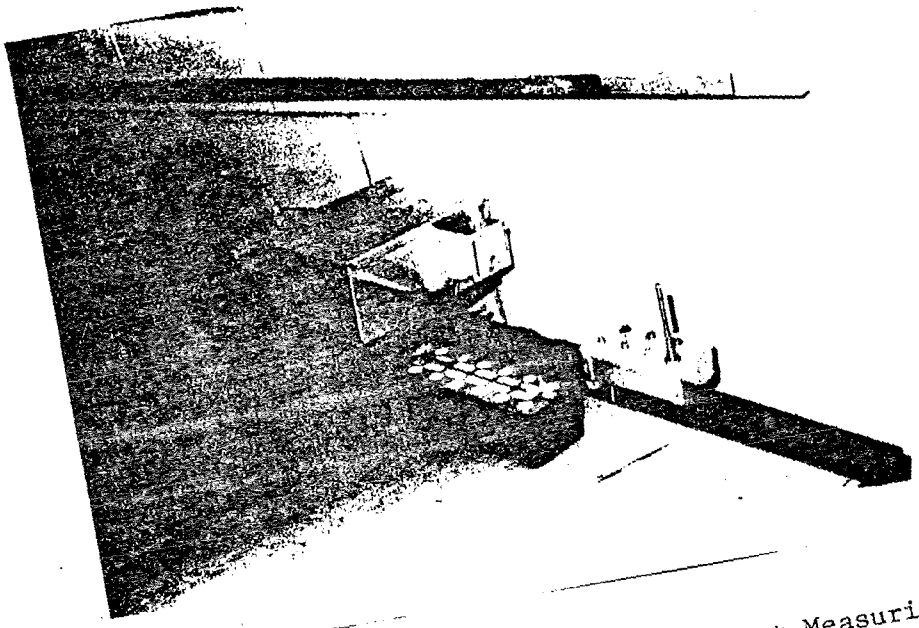


Fig. 5.13. Photo of the Potential Gradient Measuring Unit and Electronics

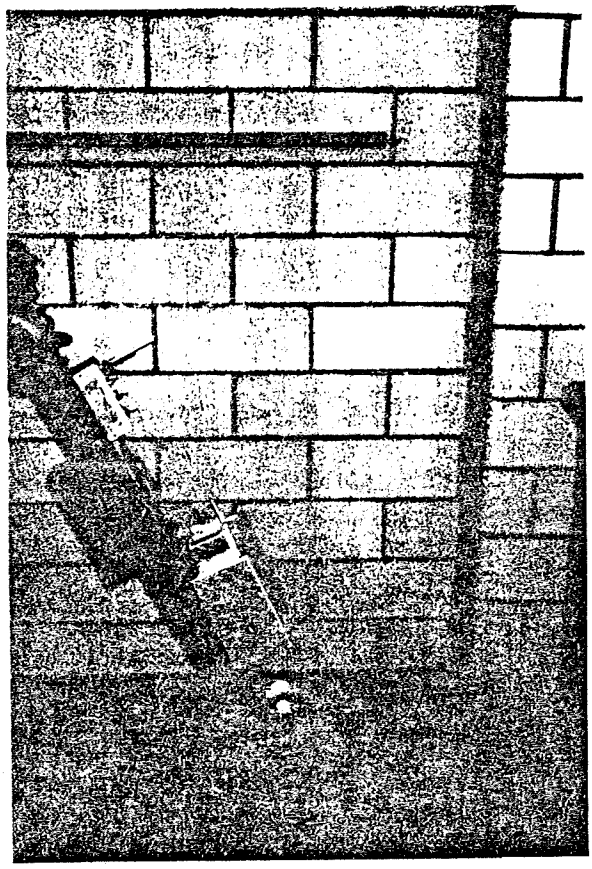


Fig. 5.14. The Potential Gradient Measurement Unit, Held in Operating Position.

supply with center neutral. The ± 12V supply is fed to a 7546 positive voltage regulator and a 7805 negative voltage regulator to generate a regulated ± 5V supply. Filtering capacitors are used at the input and output of the regulators to reduce noise. A control switch for switching the power supply is also provided. Figure 5.15 shows the power supply circuit diagram.

5.3.5 Constant Current Source

Figure 5.16 shows the constant current source block diagram, while Figure 5.17 and 5.18 are the circuit diagram and I. C. Connection respectively. An 11 Hz voltage signal is generated by a 555 oscillator circuit. This signal is fed through potentiometer P1 to a Voltage Controlled Current Source circuit. The voltage signal is fed to the inverting input of a 741 Operational Amplifier whose output is connected to the bases of a complimentary PNP - NPN transistor pair. The transistor emitters are tied together. The emitter output is connected to the reference electrode. The auxiliary electrode is connected to a 10-ohm resistor whose other end is grounded. The voltage across the 10-ohm resistor is fed back through a 1 KΩ resistor to the inverting input of the 741 amplifier. Feedback insures a constant current output into the earth resistance.

A precision rectifier circuit is used for measurement of current. The rectified output is fed to an ammeter of range 0 - 100 μA dc. By selection of appropriate values of resistance the ammeter can be calibrated so that when the pointer deflects by one division it corresponds to 1 mA peak-to-peak.

5.3.6 Voltage Detection

Figure 5.19 shows the block schematic for the voltage detection unit, while Figures 5.20 and 5.21 are the circuit diagram and I. C. interconnection diagram respectively. The input signal to the detection unit consists of the 11 Hz signal and also stray voltages. A synchronous detector circuit is used to detect and filter only voltages corresponding to the 11 Hz current signal. Figure 5.19 explains how this is accomplished.

The current-reference signal is fed through a buffer and phase-shifting circuit into a zero crossing detector. The phase-shifter brings the reference signal and detected signal in phase. The zero-crossing detector generates two square wave signals which are 180° out of phase with each other. These signals are fed into an Analog Switching Device.

The detected signal is fed to the inverting input of a difference amplifier. The current reference signal is fed to the non-inverting input. It should be remembered that the reference electrode is connected at this point. The difference amplifier will therefore generate a signal proportional to the difference of these two signals.

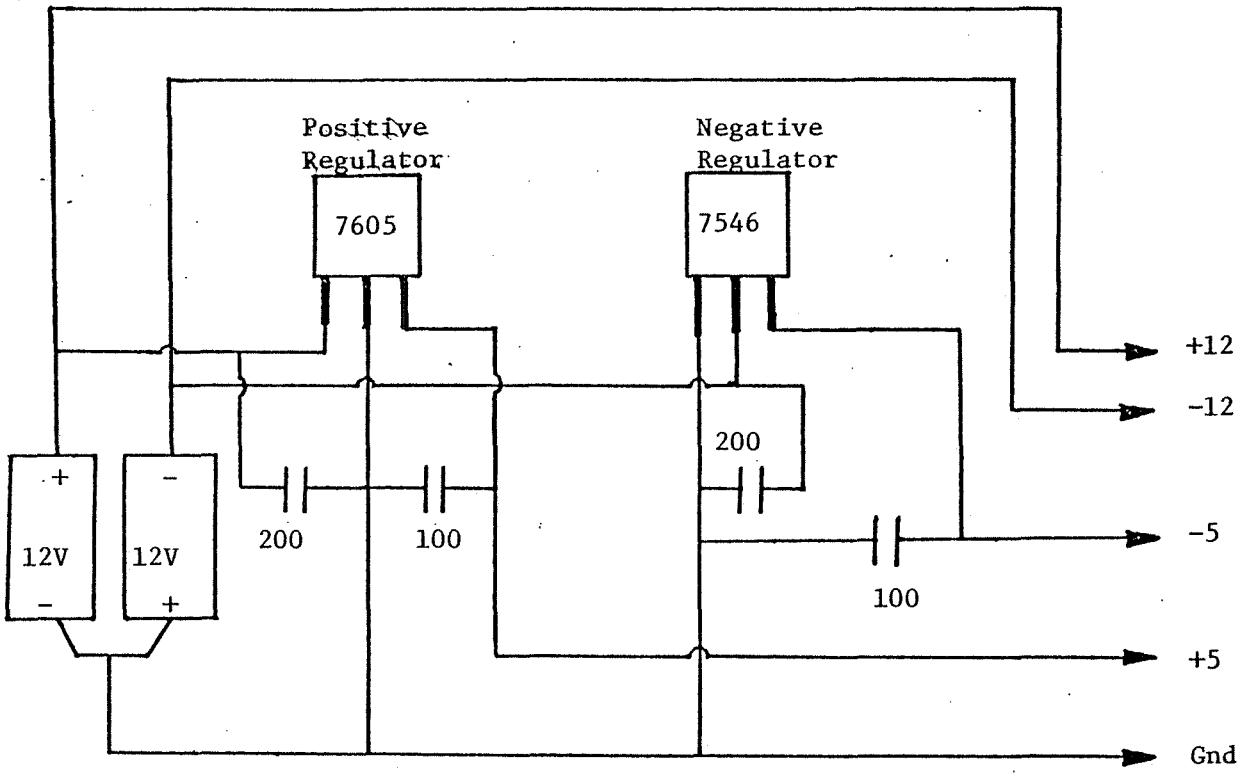


Fig. 5.15. Power Supply Circuit Diagram.

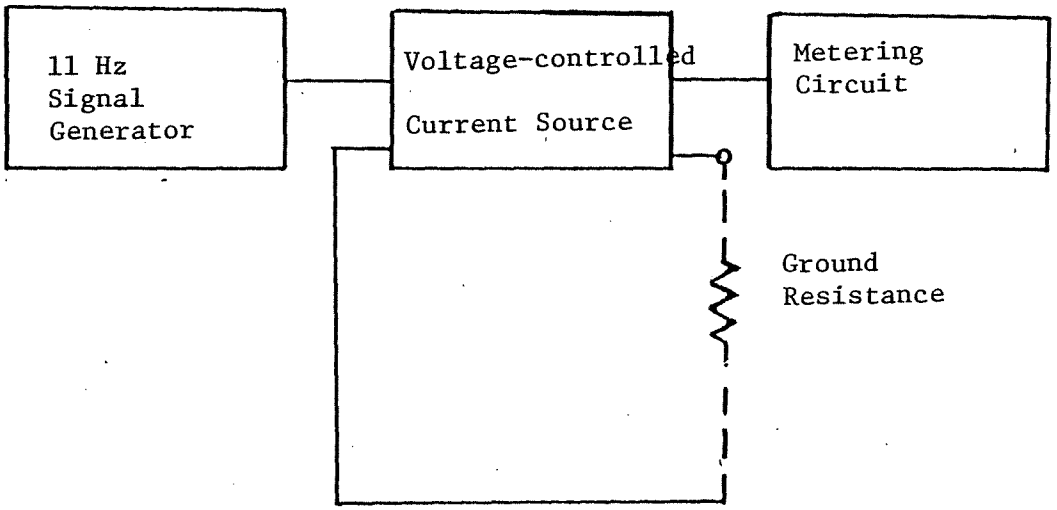


Fig. 5.16. Constant Current Source Block Diagram.

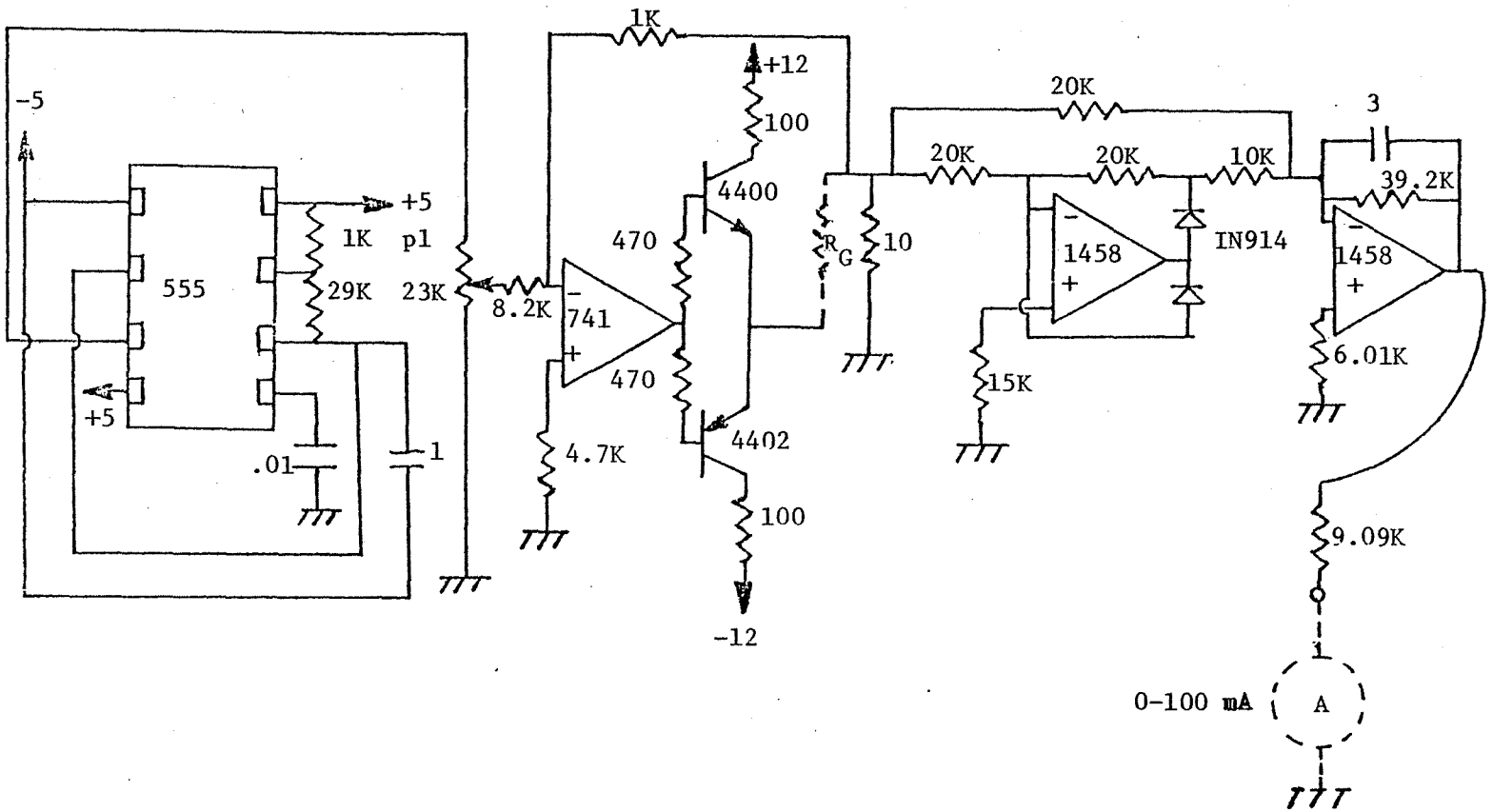


Fig. 5.17. Constant Current Source Circuit Diagram

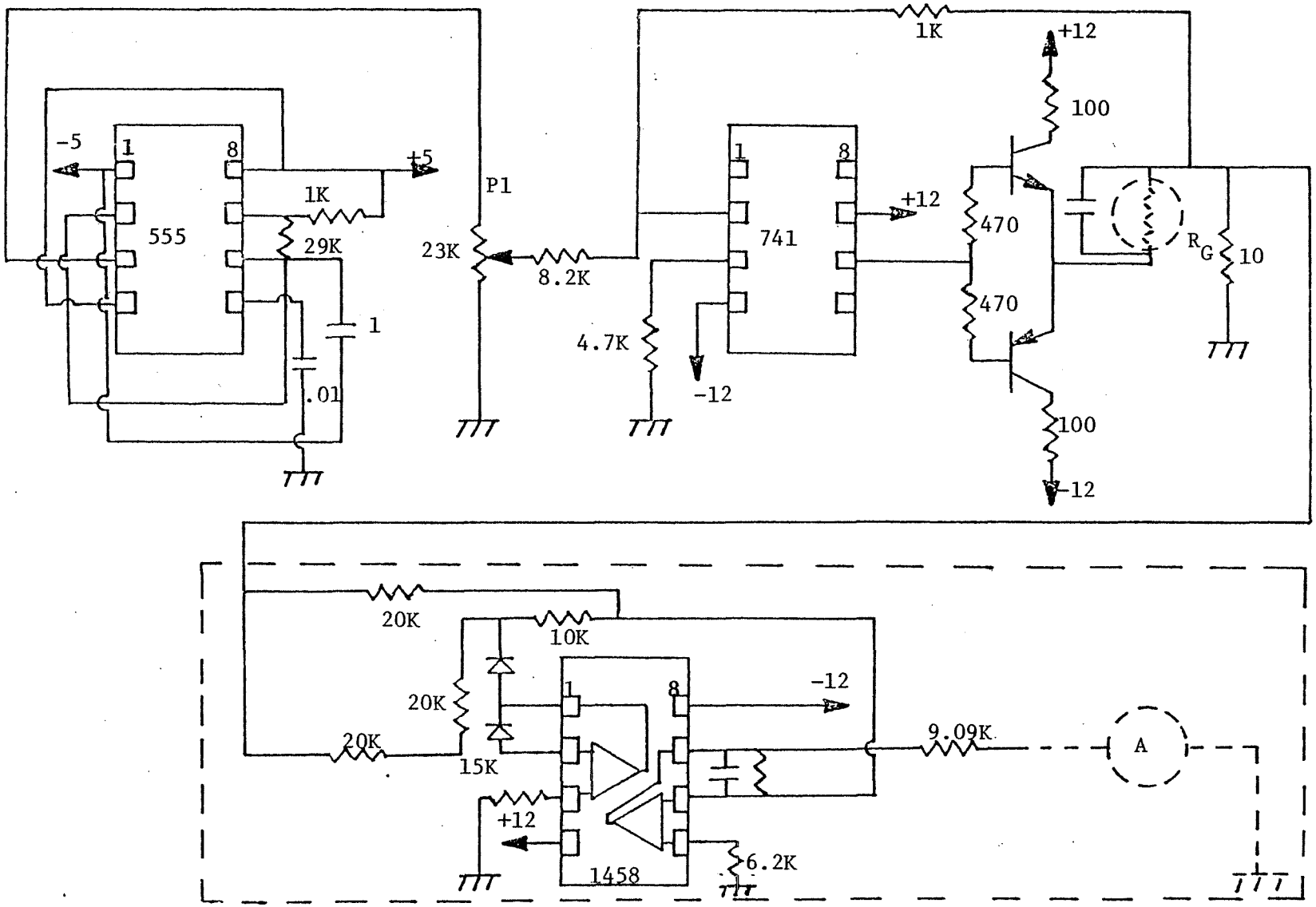


Fig. 5.18. Constant Current Source and Metering Circuit: I. C. Interconnections

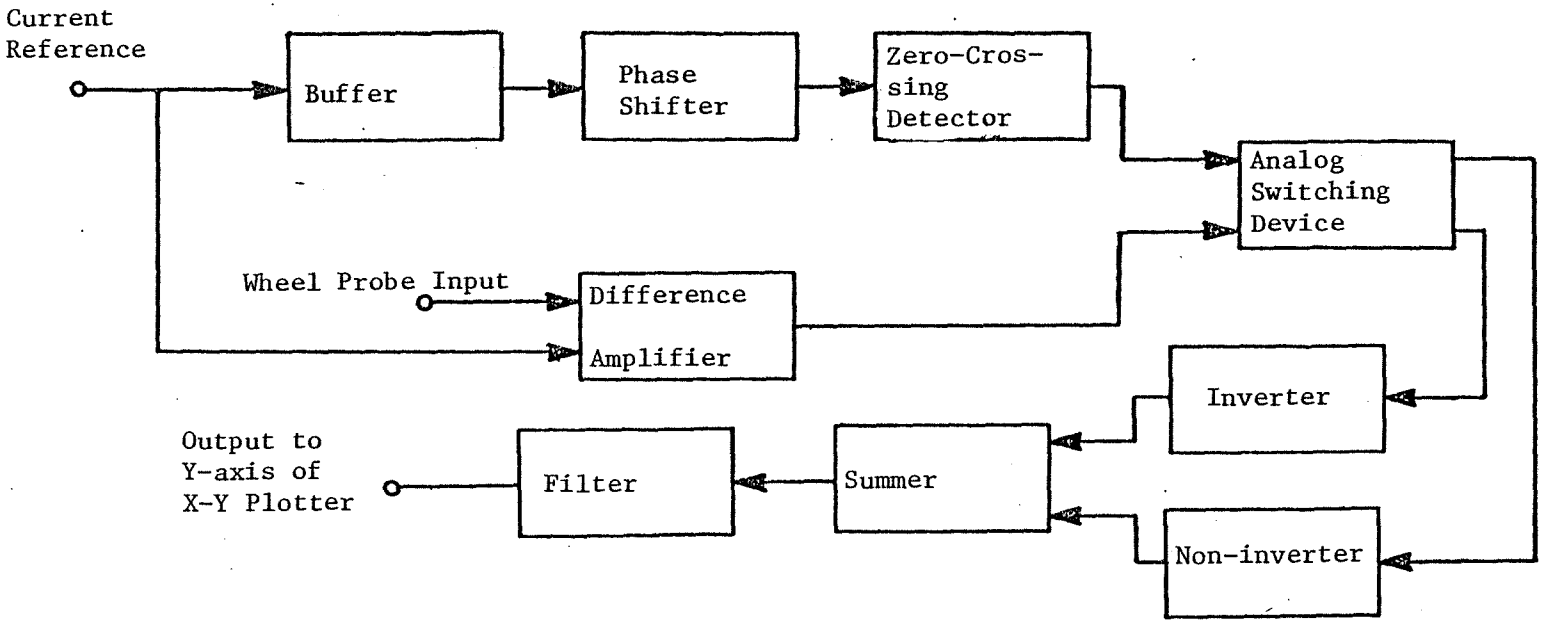


Fig. 5.19. Block Diagram for Synchronous Detector.

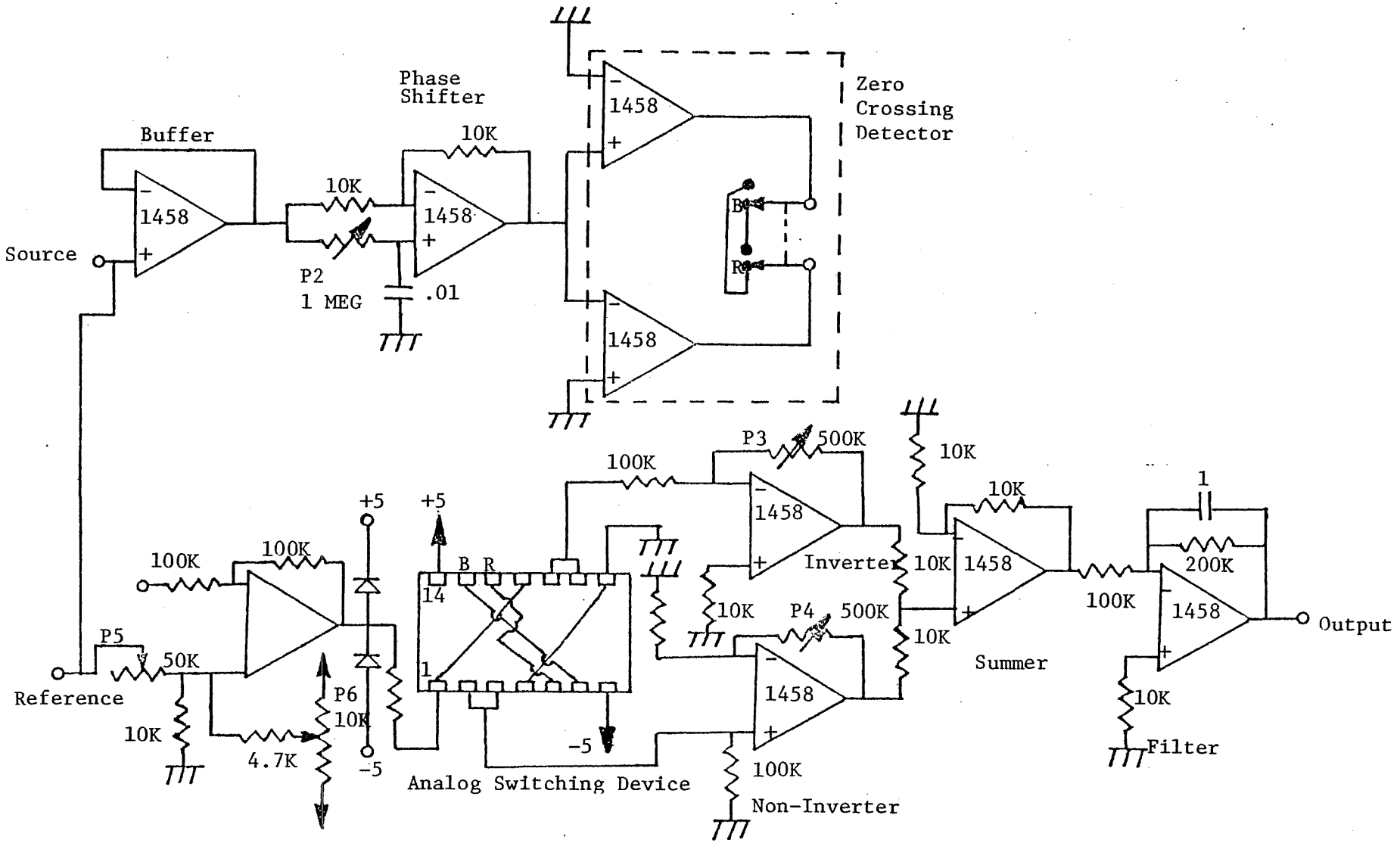


Fig. 5.20. Synchronous Detector Circuit

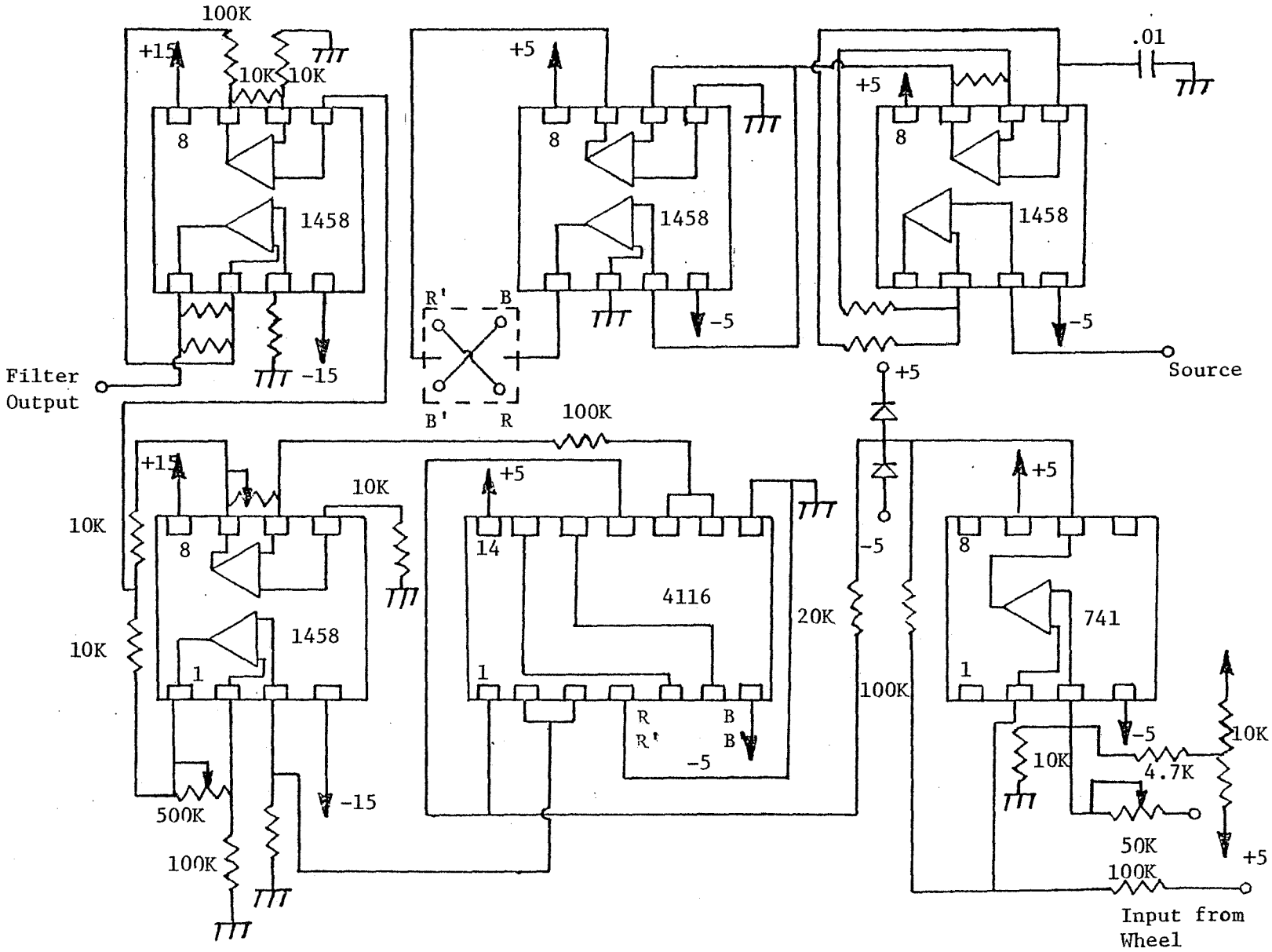


Fig. 5.21. Synchronous Detector: I. C. Connections

So in effect the difference of potential between the reference electrode and the wheel is measured. This signal is also fed to the analog switching device.

The two signals from the zero crossing detector provide the switching rates for the analog switch. When the switching signals are in their positive cycle the output port is shorted to the input port allowing the detected signal to pass through. In the negative cycle the output is shorted to ground. The detected signal is chopped at a frequency of 11 Hz and the analog switch outputs consist of two signals, the positive half and the negative half. These two signals are fed to an inverter and non-inverter, so that one-half signal gets inverted before being summed with the other half signal, in the next stage. The two signals after being summed are fed to a low pass filter, whose output is a dc signal corresponding to 11 Hz. This is fed to the Y input of the recorder. Fig. 5.22 shows the waveforms at the output of the zero crossing detector and analog switching device.

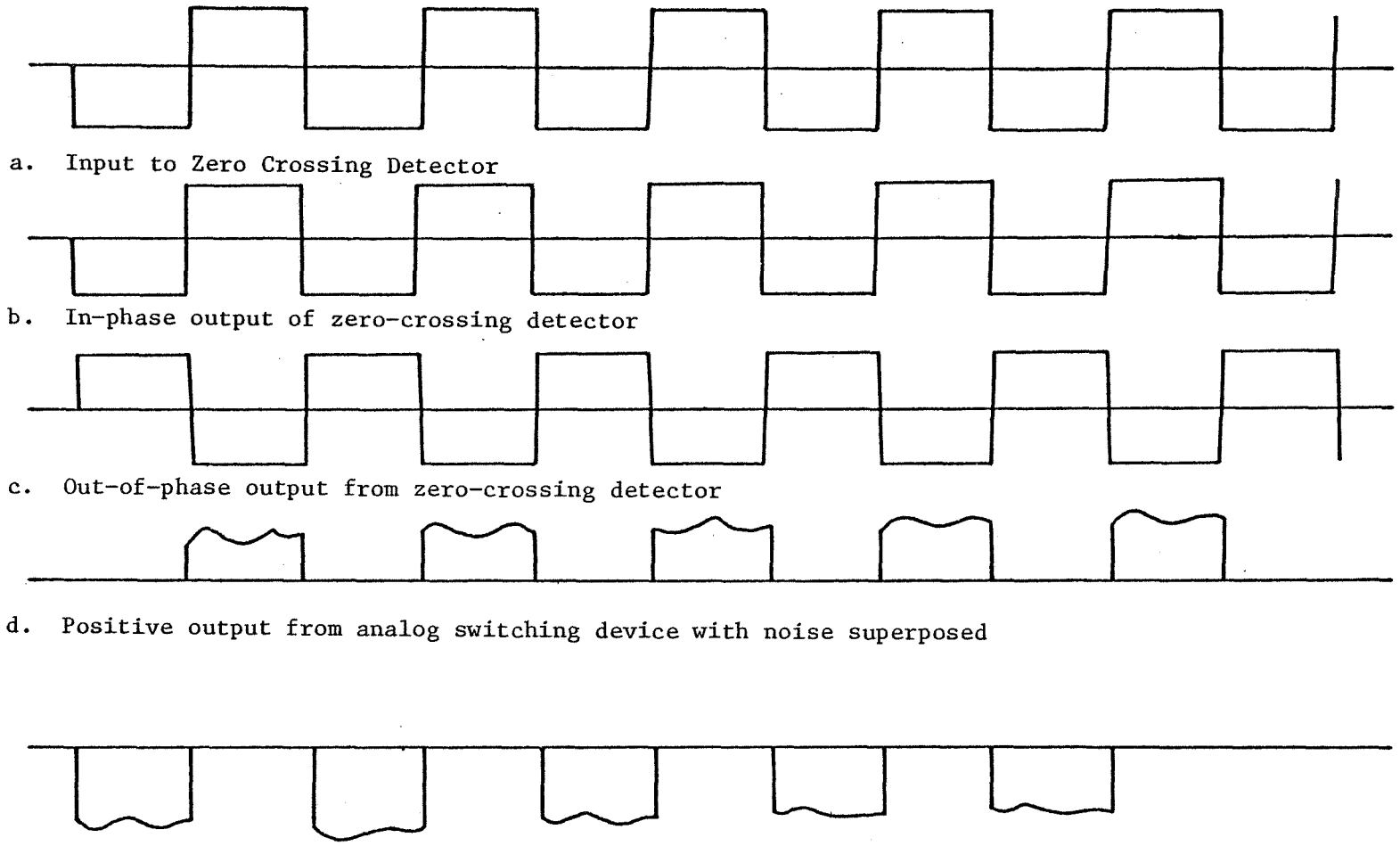
5.3.7 Distance Detection

Fig. 5.23 shows how the distance detection scheme is accomplished. The basic detecting unit is a photo diode which generates a current impulse when a bright source of light impinges upon it. The photo diode and light source are mounted on either side of the wheel inside teflon pieces. The teflon pieces are mounted inside aluminum tubes and spring loaded as explained earlier so that the teflon pieces are flush with the wheel surface, thus cutting off extraneous light. Thirty holes are drilled on the wheel 4 inches from the center with 12 degrees angle between holes so that each hole corresponds to one-tenth of a foot. When light cuts through the hole and impinges on the photo diode a current impulse is generated. So, as the wheel is pushed along a stream of pulses is generated. The pulses are fed into a buffer circuit which converts the current pulses to voltage pulses. These pulses are fed into a Schmidt trigger circuit for wave shaping. The Schmidt trigger output is then fed to an UP-DOWN binary counter chain as well as to an UP-DOWN binary coded decimal (BCD) counter chain. The former generates a 12 bit binary output which is fed through a buffer circuit into a 10 bit D/A Converter. The 10 most significant bits of the binary counter output are fed to the D/A Converter. The converter output is fed to the Recorder X input.

The BCD counter outputs are connected to the inputs of BCD-to-7-segment decoders. The decoder outputs are connected to 7-segment displays for a visual indication of distance.

Fig. 5.24 shows the I.C. connection Schematic for generating the analog output for the X-Y recorder, with the functions of the various I.C. chips clearly designated. Depressing the "CLEAR" button will reset the entire circuit of both the binary and the BCD counters to zero.

Fig. 5.25 shows the I.C. connection Schematic for the BCD counting



a. Input to Zero Crossing Detector

b. In-phase output of zero-crossing detector

c. Out-of-phase output from zero-crossing detector

d. Positive output from analog switching device with noise superposed

e. Negative output from analog switching device with superposed noise.

Fig. 5.22. Synchronous Detector: Typical Waveforms.

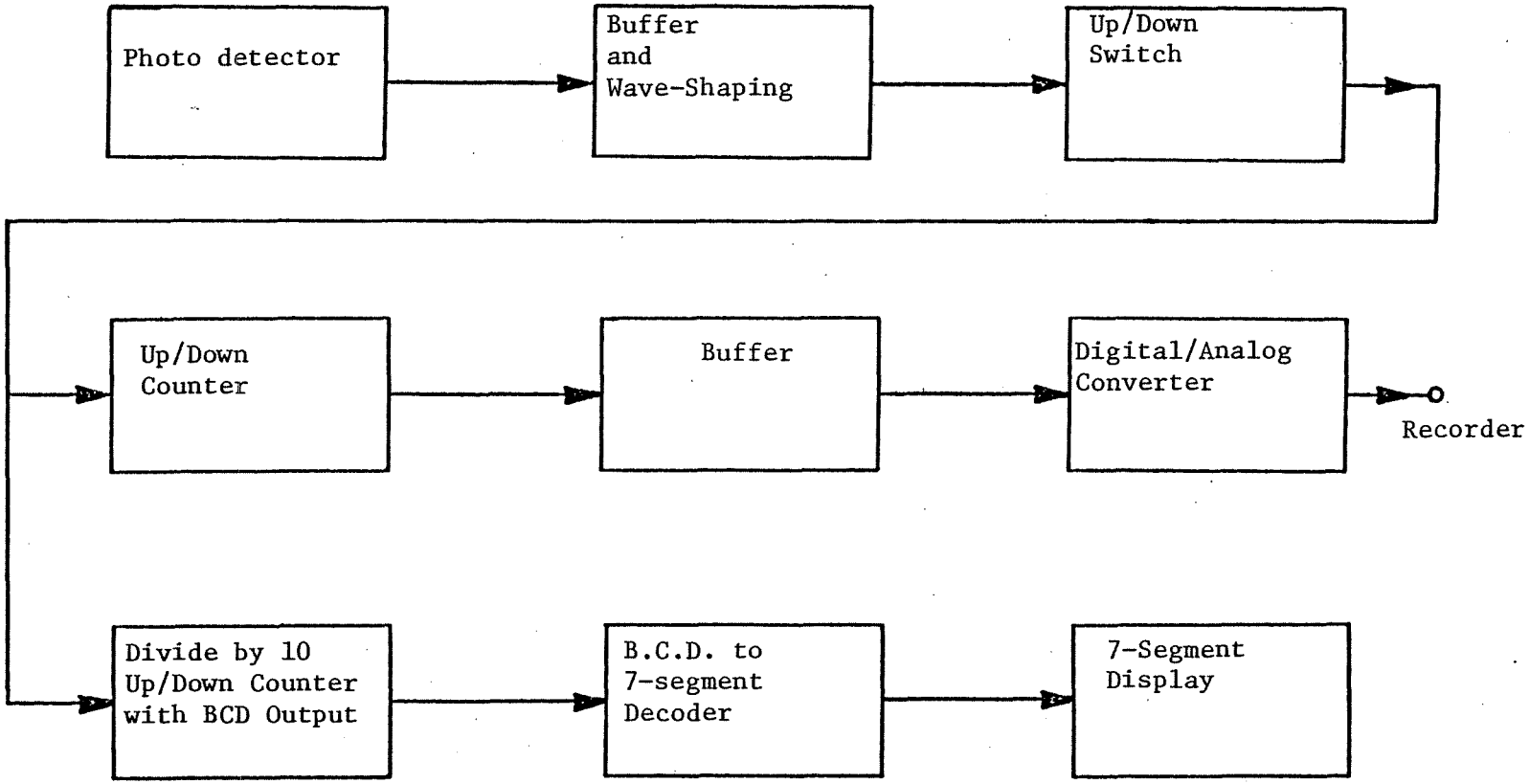


Fig. 5.23. Block Diagram of Distance Measuring Unit.

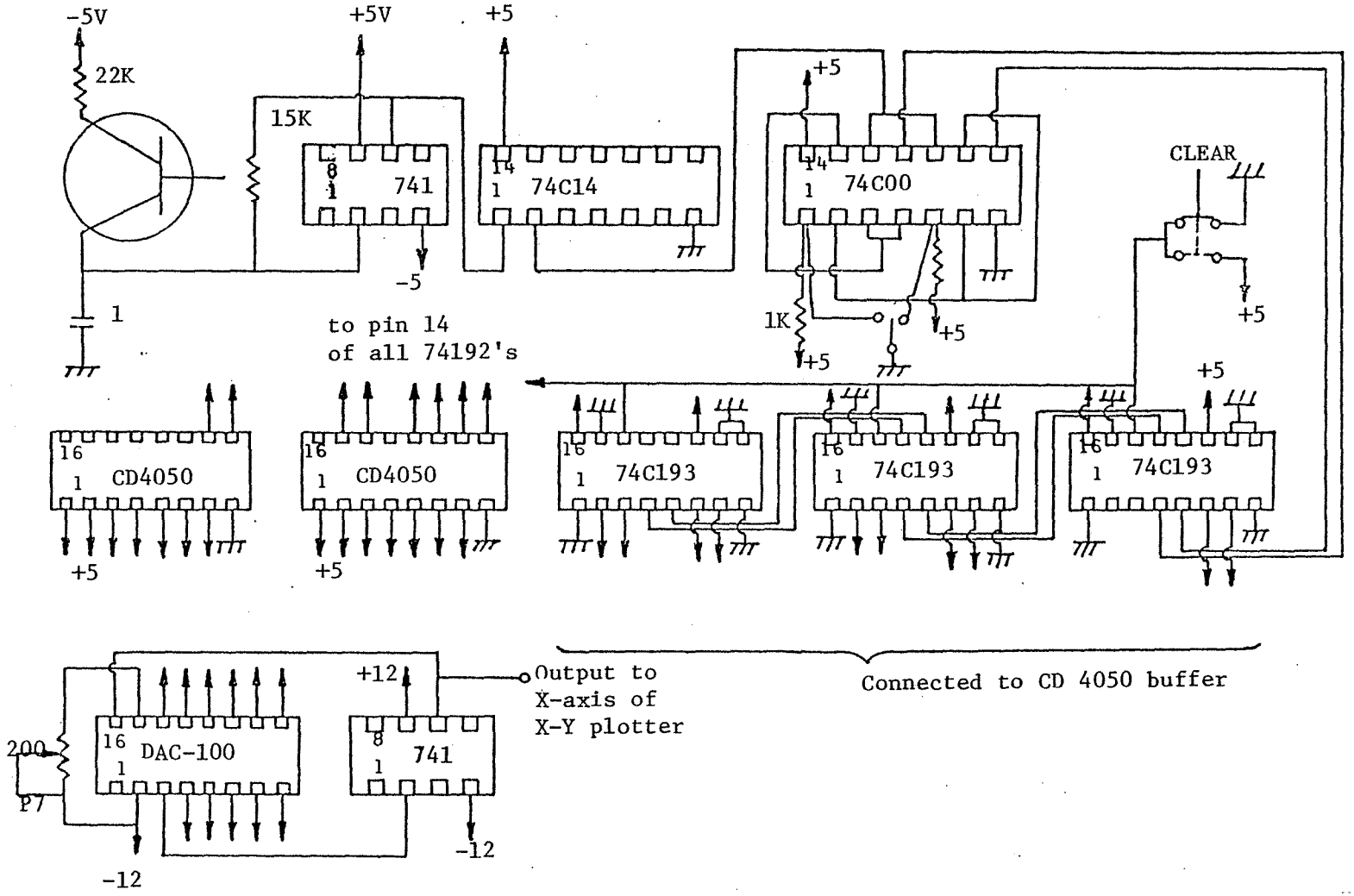


Fig. 5.24. I.C. Connection Schematic for Distance Measuring Unit

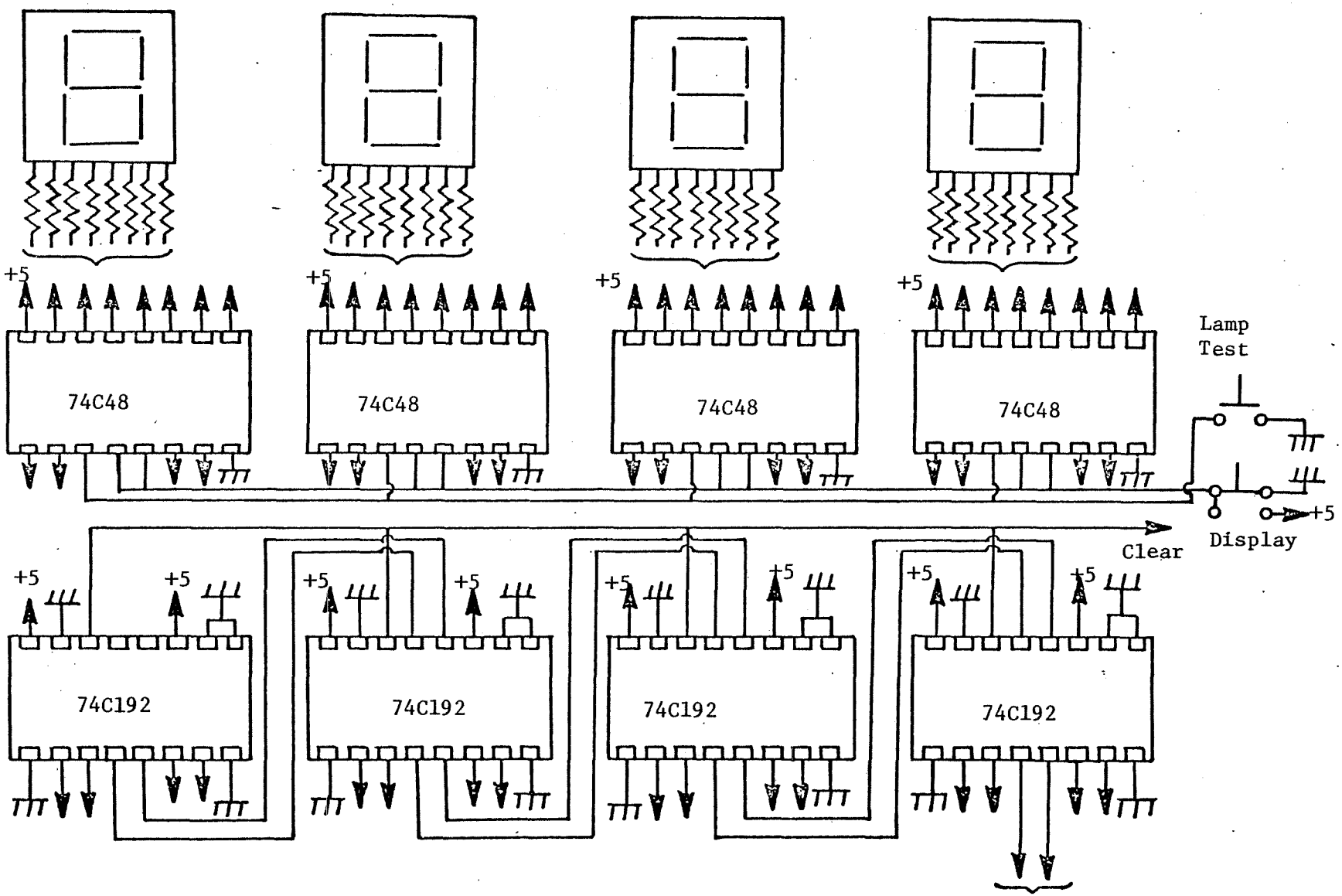


Fig. 5.25. Display Unit I.C. Connections.

circuit. Depressing the "TEST" button will light up the seven-segment displays to check if they are functioning properly. Depressing the display button will display the count representing the actual distance traveled.

The UP-DOWN switch facilitates counting either in the "UP" direction while moving away from the reference electrode, or the "DOWN" direction while moving towards the electrode.

5.3.8 Calibration

The whole system is designed to minimize the number of field adjustments. The various adjustments are explained below:

1) Current source: Potentiometer P1 (see Fig. 5.17) should be adjusted to obtain the desired magnitude of current. This is indicated on the ammeter. If the reference and auxiliary electrodes are not connected to the current source leads, the ammeter output will read zero, which is an indication that electrode leads are disconnected.

2) Voltage detector: Field conditions are simulated in the laboratory to make two adjustments. The first adjustment is with Potentiometer P2 (see Fig. 5.20). The output of the phase shifter is compared with the detector signal and P2 is adjusted to bring the two signals in phase. This could be done using a dual channel oscilloscope to observe the waveforms, and adjusting P2 to bring the two signals in phase.

The sedond laboratory adjustment is that of the inverter/non-inverter outputs. This is done by adjusting Potentiometers P3 and P4 in the respective feedback loops, so that a filtered output of sufficient magnitude is obtained, for feeding to the X-Y Recorder.

The only field adjustment for the synchronous detector is the zero adjustment. The reference and auxiliary electrodes are connected to the current source. The supply is switched on and a 11 Hz signal driven into the earth. The aluminum wheel is shorted to the reference electrode. The output of the 741 amplifier is observed on the oscilloscope. The output should be zero since the differential input to the 741 amplifier is made zero by shorting the reference electrode to the wheel. If it is not zero, the oscilloscope output will be a square wave with a dc offset. Potentiometer P5 is adjusted until the square wave becomes smaller and smaller and ultimately a straight line. Potentiometer P6 is adjusted until the dc offset is made zero.

The voltage detector is now ready for use.

3) Distance Detector: The only adjustment for the distance detector is the adjustment of the full scale output of the D/A converter. This is done by adjusting the Potentiometer P7 in the laboratory until the desired output magnitude is obtained.

In the field the clear button is depressed to set all counters to zero at the reference electrode.

5.3.9 Laboratory Testing

The circuitry was subjected to intensive laboratory testing before being subjected to field tests.

The current source gave a constant current output for load resistances ranging from 0 to 1000 ohms. The ammeter circuit was calibrated and gave accurate (.01%) readings of the current.

The synchronous detector was tested for (a) output vs. input linearity and (b) ability to reject unwanted signals and filter out only 11 Hz signals.

Fig. 5.26 is a graph of the synchronous detector output vs. the peak-to-peak input voltage signal. As seen from the graph the output-input relationship is linear in almost the entire range except when the input voltage is very high and exceeds 15V peak-to-peak, when the synchronous detector begins to exhibit non-linearity. The above results were obtained using a signal generator to simulate the 11 Hz reference signal and 11 Hz voltage pick-up signal.

The synchronous detector was also tested for its ability to reject unwanted signals, and filter out only 11 Hz signals. This was done by injecting at the voltage pickup terminal a combination of 11 Hz signal and other signals of different magnitudes and frequencies. The output of the filter was not affected by the presence of extraneous signals. Only after the frequency of the extraneous signal was increased above 5 KHz there was a slight drop in the output (< .1%). Such high frequencies are however rarely encountered in mining operations and for all practical purposes the circuitry can be expected to function well.

The distance circuitry was tested and calibrated in the breadboard stage. It was tested for (a) digital input/analog output linearity and (b) synchronization between the display unit and analog output. The output of the digital/analog converter was found to vary linearly with the input (to within 0.5%). The display unit was also well synchronized with the D/A output.

5.3.10 Field Testing

The synchronous detector circuit and current source were subjected to a field test by measuring the gradient between an experimental ground bed near the West Virginia University Engineering Sciences Building and a remote electrode 200 feet from the ground bed. A constant speed recorder was used and the operator was also walking at a constant speed so that this corresponded to distance to a certain scale. Fig. 5.27 is the plot obtained. The general shape of the curve is what would be

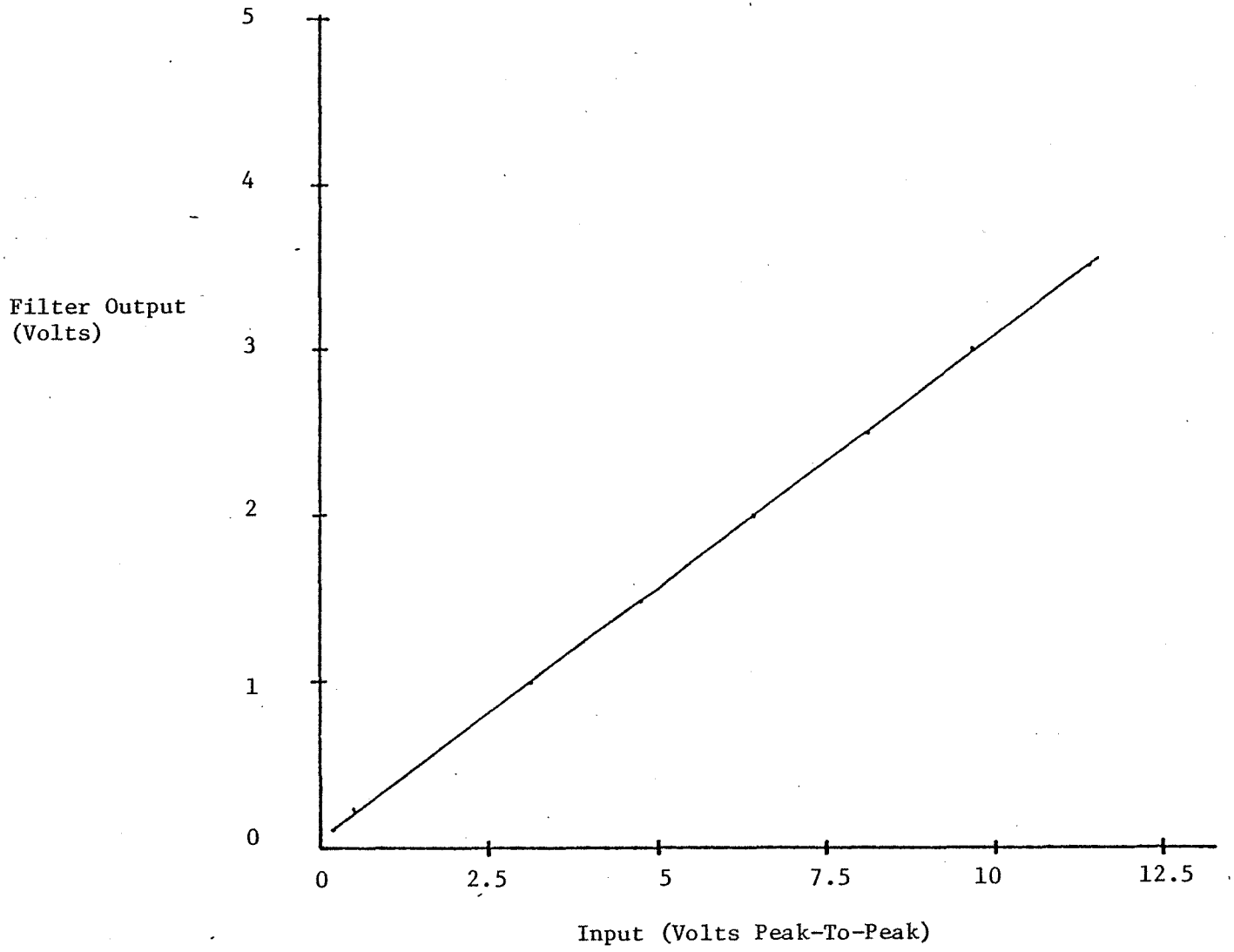


Fig. 5.2.6. Graph of Synchronous Detector Output.

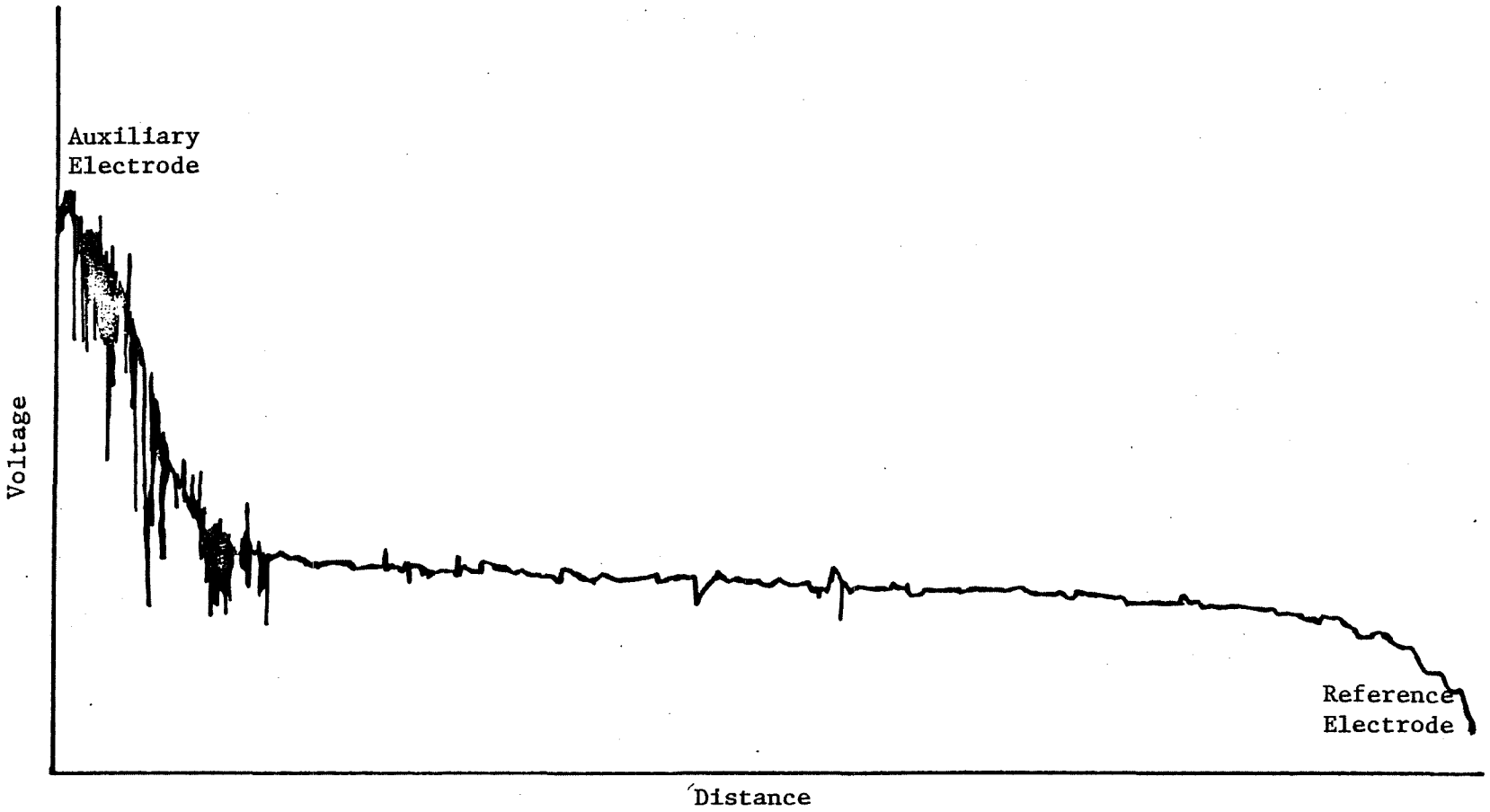


Fig. 5.27. Voltage Profile Between Reference Ground and Remote Electrode, Using Potential Gradient Plotter.

generally expected in a fall of potential measurement. The curve has a steep gradient at the auxiliary electrode and a comparatively smaller gradient at the reference electrode near the ground bed. The steep gradient near the auxiliary electrode can be expected because of the latter being just a single point electrode driven just a couple of feet into the earth. On the other hand the ground rods of the ground bed are driven deep into the earth and interconnected with each other to form a low resistance path. A low gradient can be therefore expected. From the graph it is seen that midway between the electrodes a current of 40 mA injected into the ground bed results in a 1.0 volt signal at the filter output. The actual value of the input pick-up signal can be obtained by dividing the filter signal by the gain of the input stage. Actual computations give the input stage gain to be 1.833. The actual pickup voltage is 1.0/1.833 = .545 volts. This value divided by the input current of 40 mA yields a resistance of 13.6 ohms. This result was compared with a fall-of-potential measurement made with the Bison meter, which yielded a bed resistance of 12 ohms. The slight difference in results obtained may possibly be due to slight adjustments to be made in calibration. The final prototype when tested will take into account these adjustments.

5.3.11 References

1. Electronic Measurement and Instrumentation, by Oliver and Cage, (pp. 257-259).

2. "Designing with Operational Amplifiers", Burr Brown Series.

3. "I.C. Op-Amp Cook Book" by Walter C. Jung.

4. Texas Instruments T.T.L. Data Book.

5. Texas Instruments Linear Data Book.

6. Integrated Electronics by Millman and Halkias.

7. "Measurement of the Resistance of the Ground Connections of a 220-110 KV Substation with Actual Short Circuit Currents," by V.E. Manilor and A.K. Torpov, #332,CIGRE, Paris 1937.

8. Voltage Gradients Through the Ground Under Fault Conditions" AIEE Committee Report, October 1958.

5.4 SURGE IMPEDANCE OF GROUND RODS

5.4.1 Discussion

Effort has been devoted to investigate the response of a borehole ground bed under lightning surges. The borehole ground bed, which is simply a bare wire running down a hole, can be suitably represented by a long ground rod.

A ground rod behaves quite differently from its dc characteristics upon encountering a rapid lightning impulse surge. In addition to its dc resistance, there exists a leakage capacitance as well as a leakage inductance. These happen when the impinged current as well as the induced voltage on the ground rod change rapidly with time, as governed by Ampere's and Gauss' Laws.

Hence the ground rod can be represented by an RLC circuit model as shown in Fig. 5.28.

The resistance R, inductance L and capacitance C can be calculated using the following equations:

$$R = \frac{\rho}{2\pi\ell} \ln \frac{2\ell}{a} \tag{5.76}$$

$$L = \frac{\mu\ell}{2\pi} \ln \frac{2\ell}{a} \tag{5.77}$$

$$C = 2\pi\varepsilon\ell \ln \frac{2\ell}{a} \tag{5.78}$$

where ℓ = length of the rod inside the earth, m
a = radius of the rod, m
ρ = resistivity of the surrounding earth, Ω-m
μ = permeability of the earth, H/m
ε = permittivity of its earth, F/m

Hence, the surge impedance of the ground rod can be approximated by

$$Z = j\omega L + \frac{1}{G+j\omega C} \tag{5.79}$$

which becomes

$$Z = \frac{\rho}{2\pi\ell} \ln\left(\frac{2\ell}{a}\right)\left[\frac{1}{1+(\omega\varepsilon\rho)^2} + j\left\{\frac{\omega\mu\ell^2}{\rho} - \frac{\omega\varepsilon\rho}{1+(\omega\varepsilon\rho)^2}\right\}\right] \tag{5.80}$$

This equation is valid for both the dc and high frequency response. However, based on equations 5.76, 5.77 and 5.78 the time constants of the model are so very small that the inductance and capacitance become insignificant for low- and medium-frequencies. So the ground rod can just be represented by a lumped resistance given by equation 5.76.

A series of calculations have been performed on the surge impedance using equation 5.80 with different values of frequency and length. The impedance stays fairly constant over a broad range of frequency. At higher frequencies (> 10 KHz), the values go up quite fast, mainly due to the inductance of the model. A review of several papers which had presented experimental data on the response of ground rods under impulse tests revealed that the resistance of the rod dropped during the impulse tests. The resultant resistance ranged from 50 to 90% of its dc or low frequency value.

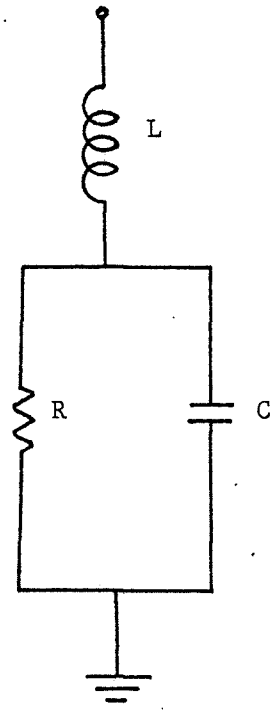


Fig. 5.28 Ground Rod Model for High Frequency

Another approach for finding the surge impedance of a ground rod is based on the transmission-line model of buried conductor, for which the derived equation is

$$Z = \frac{\rho}{2\pi\ell}\left[\ln\frac{\sqrt{2}\delta}{\gamma_o a} - j\frac{\pi}{4}\right] \quad \begin{matrix}(\sigma > \omega\varepsilon)\\(\ell << \delta)\\(\ell >> a)\end{matrix} \qquad (5.81)$$

where $\gamma_o = 1.781 \ldots$

$$\delta = \frac{1}{\sqrt{\pi f \mu_o \sigma}} \qquad (5.82)$$

The impedance calculated from equation 5.82 is rather insensitive to frequency. It indicates a steady drop in impedance with respect to increasing frequency. However, this equation cannot be used to calculate the dc response of the ground rod and is only valid under the conditions indicated to the right of equation 5.81.

Fig. 5.2.9 shows a comparison of results computed from equations 5.80 and 5.81.

5.4.2 References

1. "IEEE Guide for Safety in Alternating-Current Substation Grounding," IEEE No. 80, 1971.

2. Vance, E.F., "Electromagnetic Pulse Handbook for Electric Power Systems," Stanford Research Institute, 1974.

3. Impulse and 60 Cycle Characteristics of Driven Grounds, P.L. Bellaschi, AIEE Trans, Vol. 60, 1941, pp. 123-128.

4. Impulse and 60 Cycle Characteristics of Driven Grounds, P.L. Bellaschi, AIEE Trans, Vol. 61, 1942, pp. 349-363.

5. The Use of Concrete-Enclosed Reinforcing Rods as Grounding Electrodes," Eugene J. Fagan, Ralph H. Lee, IEEE Trans Ind & Gen. Appl., Vol. IGA-61, No. 4, July/August 1970.

6. A Comparison of Concrete Enclosed Grounding Electrodes to Driven Ground Rods, Paul Wiener, IEEE Trans. Ind. & Gen. Appl., Vol. IGA-6, No. 3, May/June 1970.

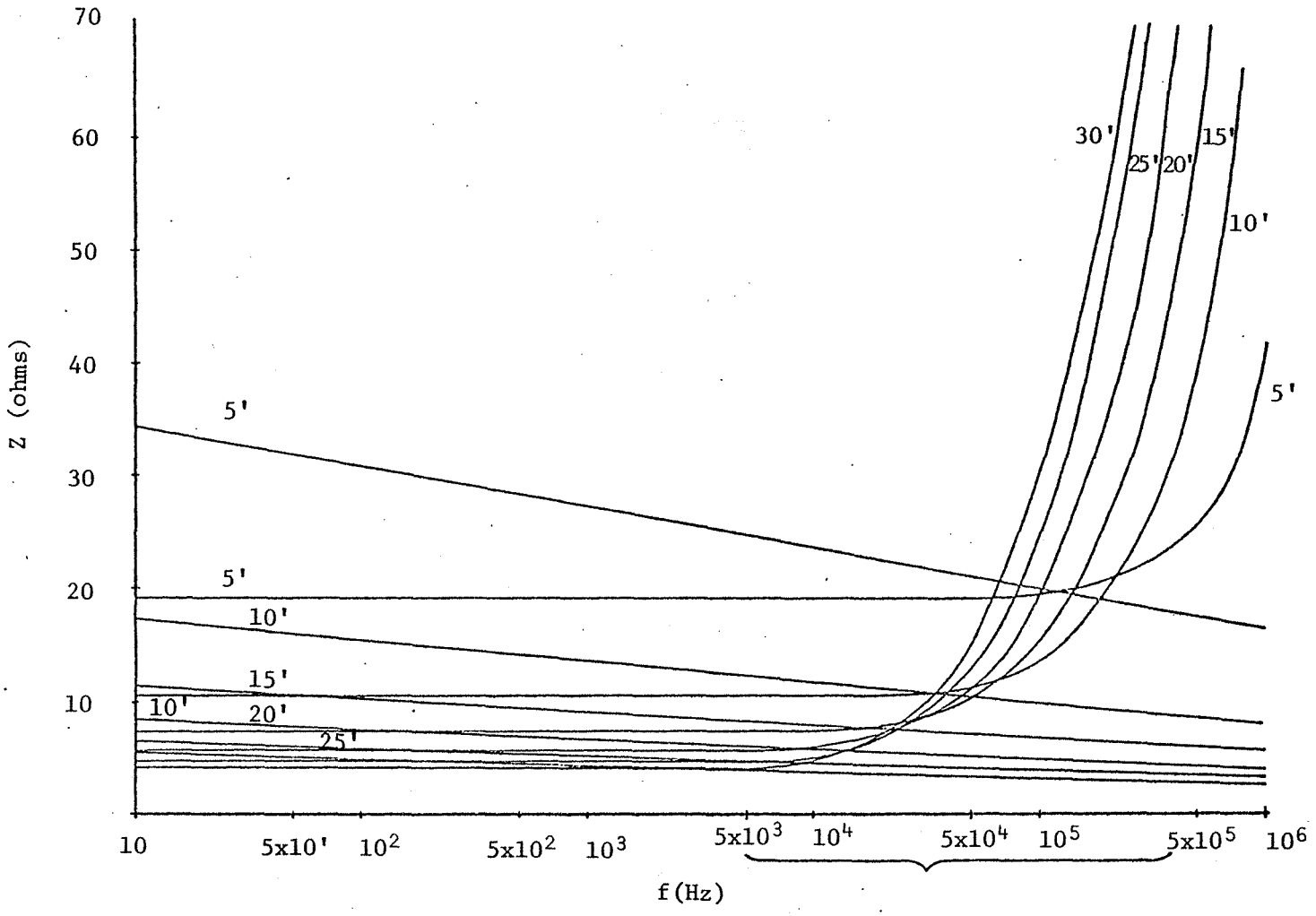


Fig. 5.29 Impedance of Ground Rod vs Frequency for Various Rod Lengths

CHAPTER VI: GROUND CHECK MONITORS

The ground check monitor effort for the reporting period falls into three categories. The modular monitor is taking on new directions. Monitor evaluation is moving into the area of high voltage monitors. Assistance was given to MESA for technical seminar on ground check monitors.

6.1 MODULAR MONITOR

Work on the modular monitor falls into two categories: MESA acceptance and multiple circuit monitoring.

6.1.1 MESA Acceptance

Two monitor types have been redesigned to be fail-safe in order to meet MESA acceptance standards. The redesign effort involved both fail-safe design and improving the monitoring function to overcome limitations observed in field testing and theoretical studies on monitoring techniques.

The two monitors designed for MESA acceptance are dc-potential-impedance-pilot wire and ac potential-impedance-pilot wire types. Circuit diagrams are given in Figs. 6.1 and 6.2. Both circuits use a bridge for resistance measurement and two comparators for a window detector to measure high and low impedance levels. The low impedance levels are not adjustable and are used only to detect pilot-to-ground wire shorts. The fail-safe techniques used in both are similar. The comparators are switched off and on with the outputs driving a charge pump which drives a relay as long as the outputs are switching. In the dc monitor case, the switching signal is provided by an external 60 Hz signal. In the ac monitor case, the switching signal is inherent in the ac source applied to the bridge.

The dc monitor has received laboratory approval but has not been field tested so that full acceptance has not been given. The ac monitor was returned by the MESA engineers as it failed to work in their laboratory. The biggest problem was that the adjustment range was made too small in an attempt to eliminate the possibility of incorrect adjustment during installation. Circuit tolerances proved to be too great to allow the small range. The necessary changes were made and the monitor has been returned to MESA.

6.1.2 Multiple Circuit Monitor

Now that there are several monitors accepted by MESA for low voltage face equipment, attention is being turned toward high voltage monitoring and monitoring stationary equipment. In these cases,

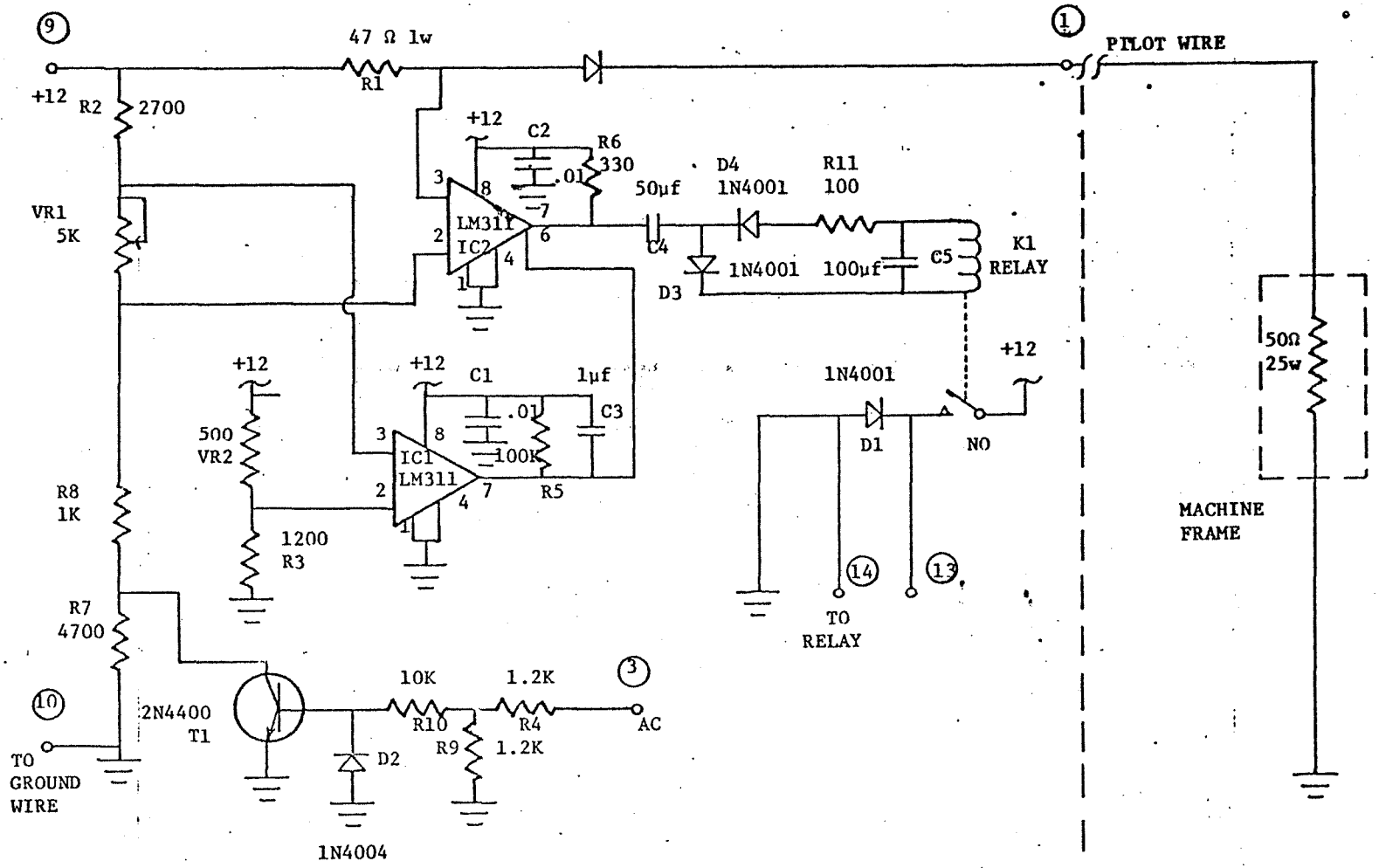


Fig. 6.1. Circuit Diagram-DC Comparator.

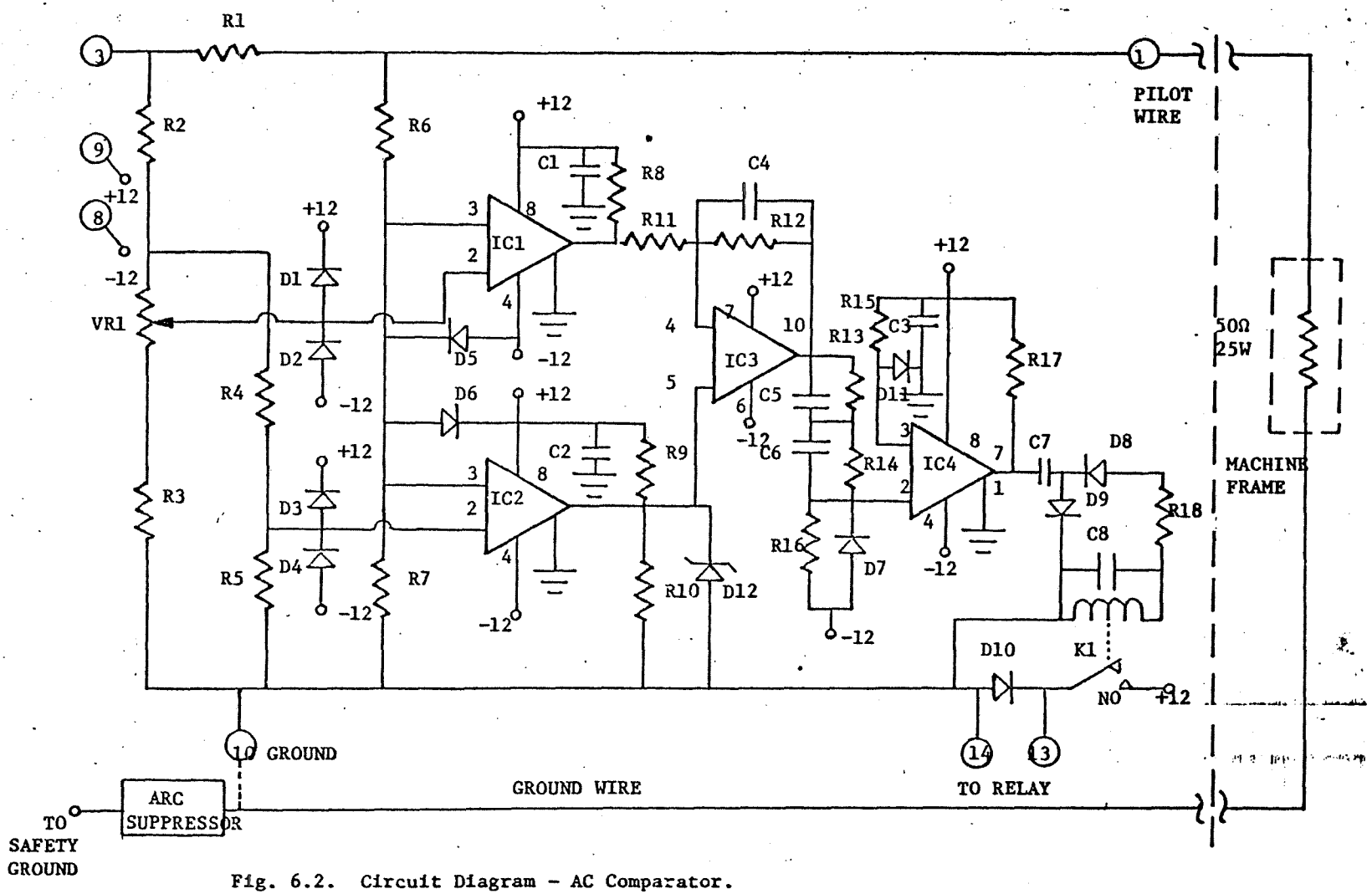


Fig. 6.2. Circuit Diagram - AC Comparator.

there are some extra problems. The biggest problems are larger transients and multiple branches with multiple machine frames tied to the ground wire. A typical example of a multiple machine frame system is shown in Fig. 6.3a. Another type of multiple branch circuit is shown in Fig. 6.3b.

In the case shown in Fig. 6.3a, a monitor in the power center can check the continuity of the pilot-ground connection. Unfortunately, the electrical connection between the motor starter box and the ground wire cannot be checked. This can lead to serious shock hazards. Similarly, the parallel frame to ground wire connections in Fig. 6.3b cannot be checked with a serial type monitor.

A method is outlined in Fig. 6.4 to monitor the multiple connections. A monitor is placed in the power center that can distinguish between each of the selective isolators between pilot and ground connections. Thus the monitor can determine the connection between pilot and ground at each load frame.

A number of approaches can be used with this basic configuration. The selective isolators could be passive devices or could be made active. Active isolators could be interrogated periodically or continuously at different frequencies or codes.

A block diagram of the proposed design is shown in Fig. 6.5. The initial design effort for the multiple circuit monitor will use passive filters at each frame. The voltage controlled oscillator will send out audio frequency signals at the resonant frequency of each filter. As long as each filter has a good connection, it will pass its resonant frequency. A frequency f_o is generated to check for pilot-to-ground shorts and is also used as a fail-safe check in the detection circuitry. The coincidence detectors are used to verify that all the frequencies except f_o are passed by the filters. Many fail-safe features are inherent in this design. The combination logic is the most difficult to make fail-safe. Extra checking circuitry is necessary to verify correct operation. Feedback to the stepping oscillator circuit causes the ring counter to stop if a failure is detected either in the monitor or ground system. Indicator lights driven by the ring counter would show which ground circuit or detector circuit failed.

Initial circuits have been designed for the ring counter, D/A converter, and VCO. Also completed are preliminary designs for the combination logic, relay driver and the checking circuitry. Some difficulty has been encountered in the power driver and filter circuits, but recent experiments indicate that the problems can be solved. If these problems cannot be resolved, a more sophisticated and difficult active selective isolator must be used on each frame. Completion of the initial designs and a breadboard model are expected soon.

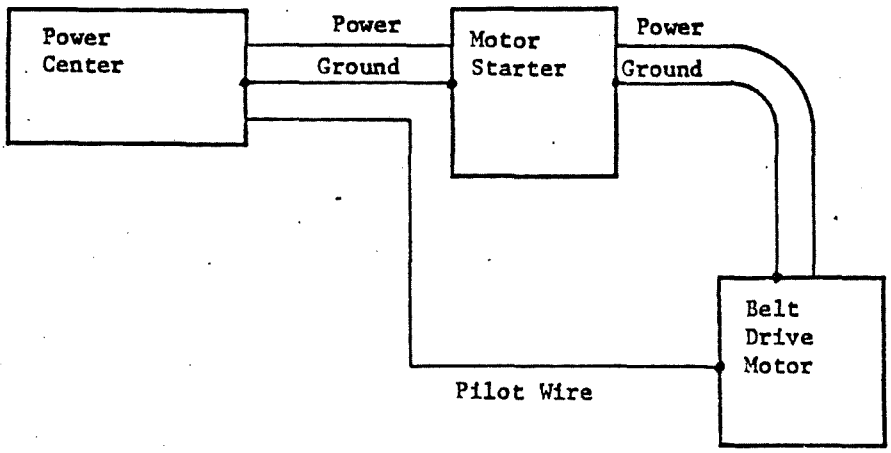


Fig. 6.3a. A Typical Multiple Machine Frame System. The Pilot Wire is Run Separately to the Second Frame for Monitoring Purposes.

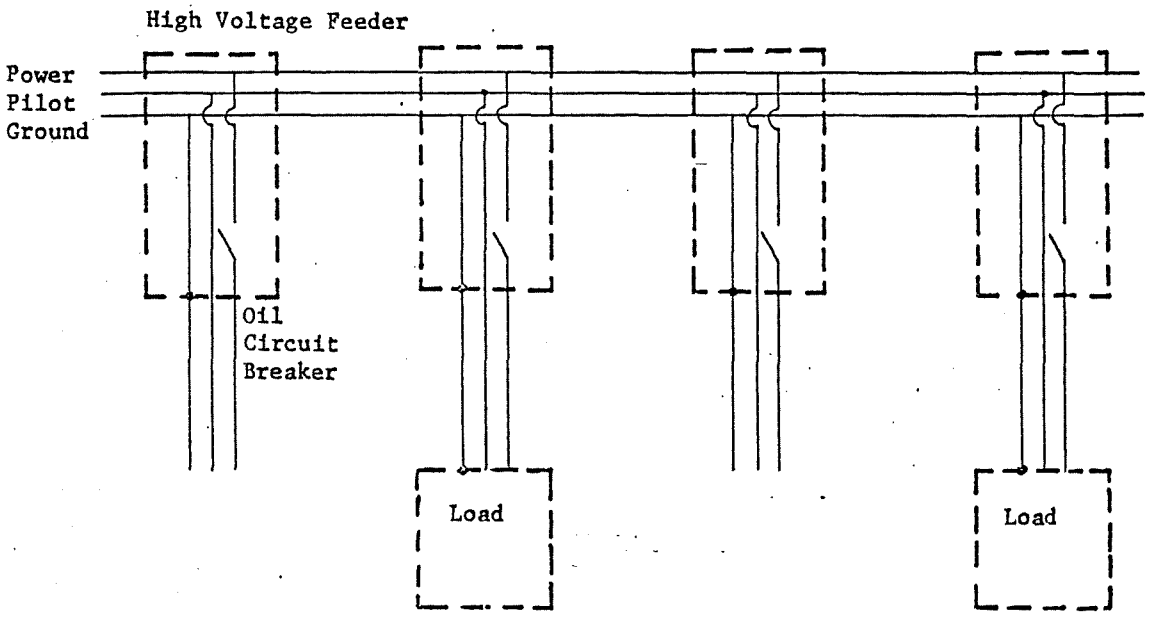


Fig. 6.3b. A Typical Multiple Branch System Used in High Voltage Distribution.

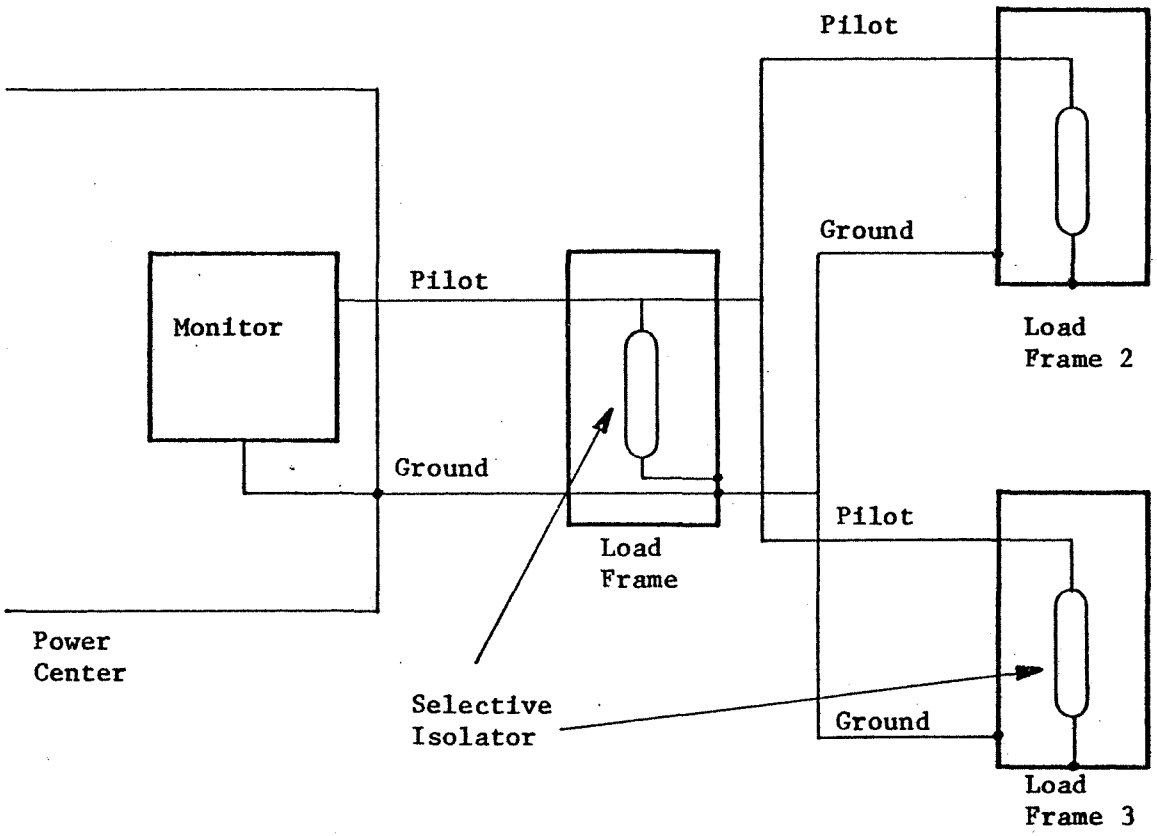


Fig. 6.4. Proposed Method for Monitoring Multiple Frame Ground Connections.

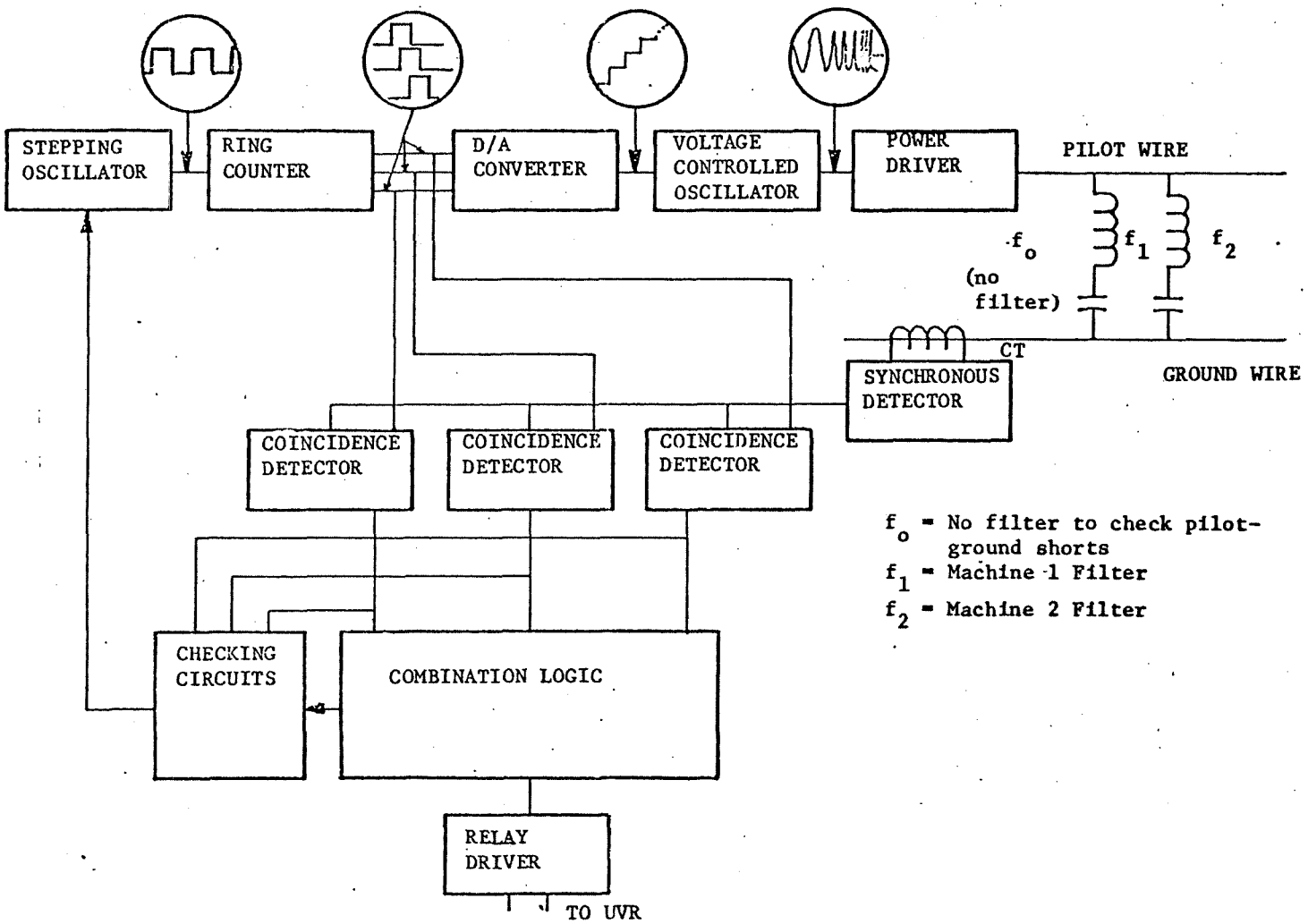


Fig. 6.5. Proposed Design for a Multiple Circuit Ground Check Monitor.

6.2 HIGH VOLTAGE MONITOR TESTING

6.2.1 Introduction

The purpose of the testing program is to evaluate the performance of various commercially available high voltage ground wire monitors under abnormal system conditions, simulated in the laboratory. However, since the tests are being conducted in strictly a laboratory type of environment, the actual performance in the field might differ considerably.

Ground wire monitors are designed to continuously monitor the pilot-ground wire loop under various conditions covered by the MESA criteria and to trip the main power circuit breaker when there is a break in the ground wire, in the pilot wire, or a short between the ground and pilot wires. The various criteria were discussed by the research team at WVU.

As a result of the discussion, tests will be conducted in the laboratory in compliance to the MESA criteria plus the criteria which are felt necessary by the research team. The evaluation consists of the electrical tests and environmental tests and a theoretical study of the circuitry of individual monitors.

Attempts are made to compare the various monitors from the standpoint of sensitivity, reliability, safety, ease of installation and maintenance, etc. Work in this area has started recently and this report is based on the preliminary tests conducted on two of the available monitors. A comparison in performance is made and some modifications are suggested to improve the circuit performance.

The two available monitors on which initial tests have been conducted are:

1. Atkinson Armature Works Co. Type AAW7700 Omser (hereafter referred to as Atkinson)

2. Central Electric Company Type RJL-300 (hereafter referred to as CEMSCO)

Attempts are also being made to procure monitors from the following known manufacturers:

1. General Electric Co.

2. Consolidation Coal Co.

3. AMF Potter - Brumfield Co.

6.2.2 Evaluation Procedure

The MESA criteria for continuous ground check circuits for high voltage applications are briefly listed below.

1. The ground check circuit shall trip the circuit breaker if:
   a. break in ground check wire
   b. break in ground wire or the impedance of the grounding circuit increases beyond the amount necessary to cause a 100 volt drop in the grounding circuit external to the grounding resistor under fault conditions.
2. All electromechanical relays shall be normally energized.
3. Maximum 250 msec time delay for tripping on power interruption.
4. Maximum 250 msec time delay for tripping after ground circuit opened up.
5. Maximum 96 volts used on ground check circuit.
6. No interference leading to incorrect tripping when operating monitors in series or parallel.
7. Minimum cable length for monitoring is 5000 feet of 250 MCM -5kV cables.
8. Continuous phase-to-pilot faults shall not destroy any device in series with the pilot wire.
9. Operate properly with any combination of the following
   a. Temperature variation of -20°C to +60°C
   b. Control voltage variation of -25% to +10% of nominal.
   c. 10 A dc in ground wire
   d. 10 times nominal input voltage to input terminal and 20 times nominal input between input and ground wire terminals and input and case at a frequency of 30 kHz in 2 msec pulses at 3-5 minutes intervals with less than 20 ohms source impedance.
   e. Phase-to-ground faults

f. 9kV pulse with 3 msec duration and less than 10 ohms source impedance between ground terminal and case and pilot terminal and case

g. Induced 60 Hz voltage between pilot and ground terminals is

50 V for class A
25 V for class B
10 V for class C

h. Maximum 9kV transients across pilot and ground terminals.

10. Test switch provided for proper adjustment

11. Reliability extensions up to MESA.

Among the various criteria it is felt that temperature in some mid-west coal regions can easily go below -20°F and above +160°F. In addition, humidity plays an important role during a large variation of temperature within a day. Hence, these will be included in the testing program if equipment can be made available at a later stage.

A preliminary test has been conducted and is described in detail in the following test along with the test results.

The monitor test box which was built to evaluate the low voltage monitors is used for testing without much modification. The circuit diagram of the test-box is given in Fig. 6.6. The various types of system abnormalities simulated for which the monitors have been tested are given below along with the corresponding connections in the monitor test box.

System Condition	Test Box Connection
1. Open ground wire	Open switch S_1
2. Pilot-to-ground short-circuit at the machine	Close switch S_2
3. Change in impedance of the pilot and ground wires	Change the settings of potentiometers R_1 & R_2
4. Parallel paths	Connect E_3-G and vary the resistance of the parallel path by R_3.
5. Induced voltages in pilot-ground circuit	Connect the secondary of a variac between G_2 & G_3.

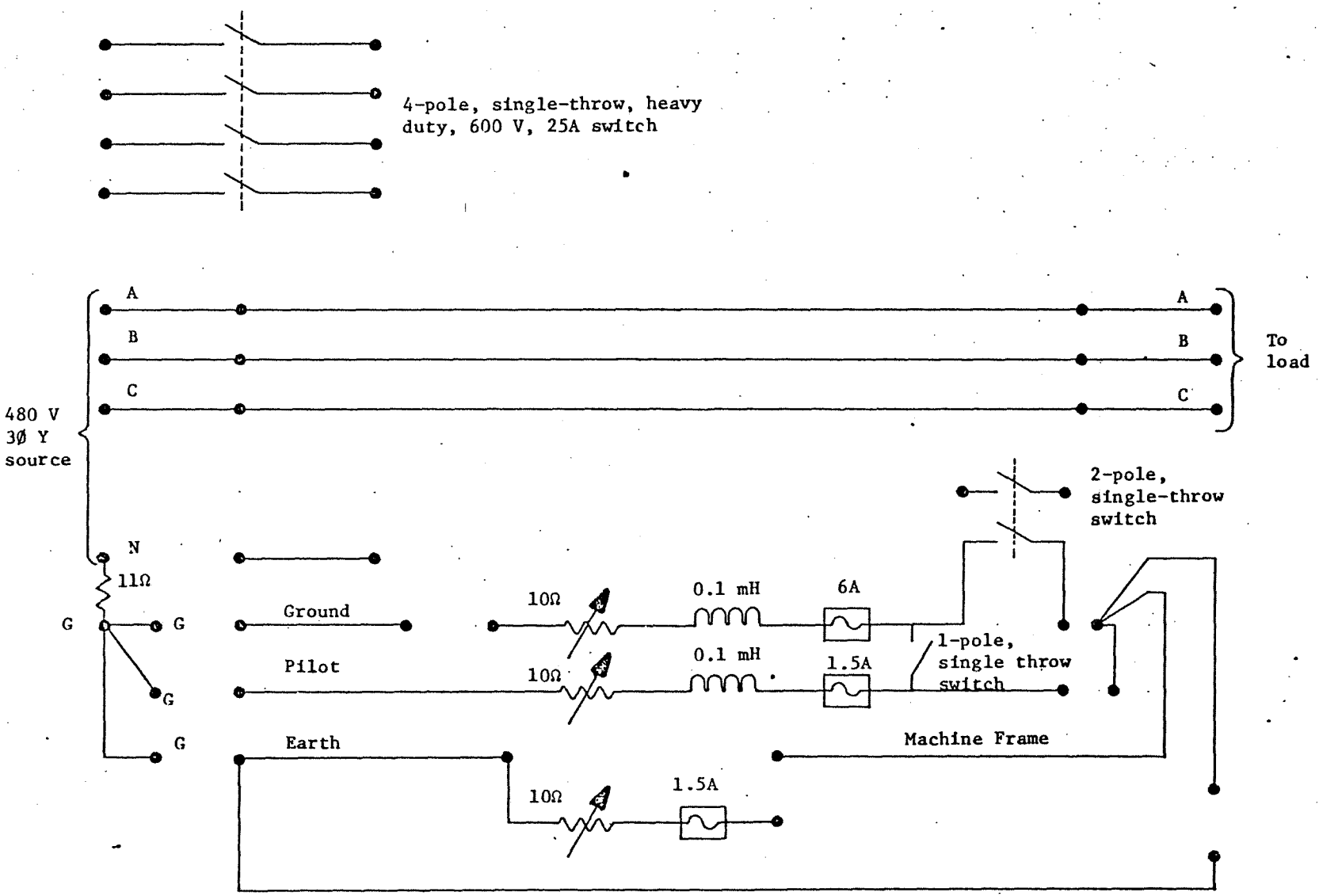


Fig. 6.6. Test Panel for Ground Wire Monitors.

System Condition	Test Box Connection
6. Variations in supply voltage	
7. A combination of above.	

It is proposed to carry out further testing of the monitors in the following areas.

1. Transient over-voltages on the pilot-to-ground circuit supply transformer and between case and ground.

2. Variations of temperature and humidity.

3. Dc stray currents.

6.2.3 Connection Diagrams

a. Atkinson

The connection diagram for the Atkinson monitor is given in Fig. 6.7. It is a bridge-type circuit in which the pilot-to-ground loop forms one arm of the bridge. Any increase or decrease in the resistance of the pilot-to-ground loop creates an unbalance and if the change in resistance is greater than the set-point the monitor trips. The monitor is also equipped with pilot lights to indicate whether the tripping was due to the pilot-to-ground resistance being too high or too low. It also uses a 4Ω resistor connected between the pilot and the ground on the machine frame to detect pilot-to-ground short-circuit.

b. CEMSCO

The connection diagram for the CEMSCO unit is given in Fig. 6.8. In this monitoring technique a dc current ($\simeq$ 0.9A) is circulated in the pilot-to-ground circuit. A small dc voltage ($\simeq$ 2mV) which is developed across a ground-wire shunt is fed to a meter relay. The meter relay senses any decrease in the pick-up voltage and trips in case the voltage is less than the set point. This will happen for any substantial increase in resistance of the pilot-ground circuit. There is a small circuit breaker in series with the pilot wire. This breaker is equipped with a thermal trip which is set for a time delay of approximately 10-15 secs for a current of around 2A. In case there is a pilot-to-ground short-circuit, the current will increase, thereby tripping the circuit-breaker and opening the pilot-ground circuit. This in turn will operate the monitor. The monitor also uses a 25Ω adjustable resistor connected between the pilot and ground at the machine frame. The dc voltage in the monitoring loop is around 24V.

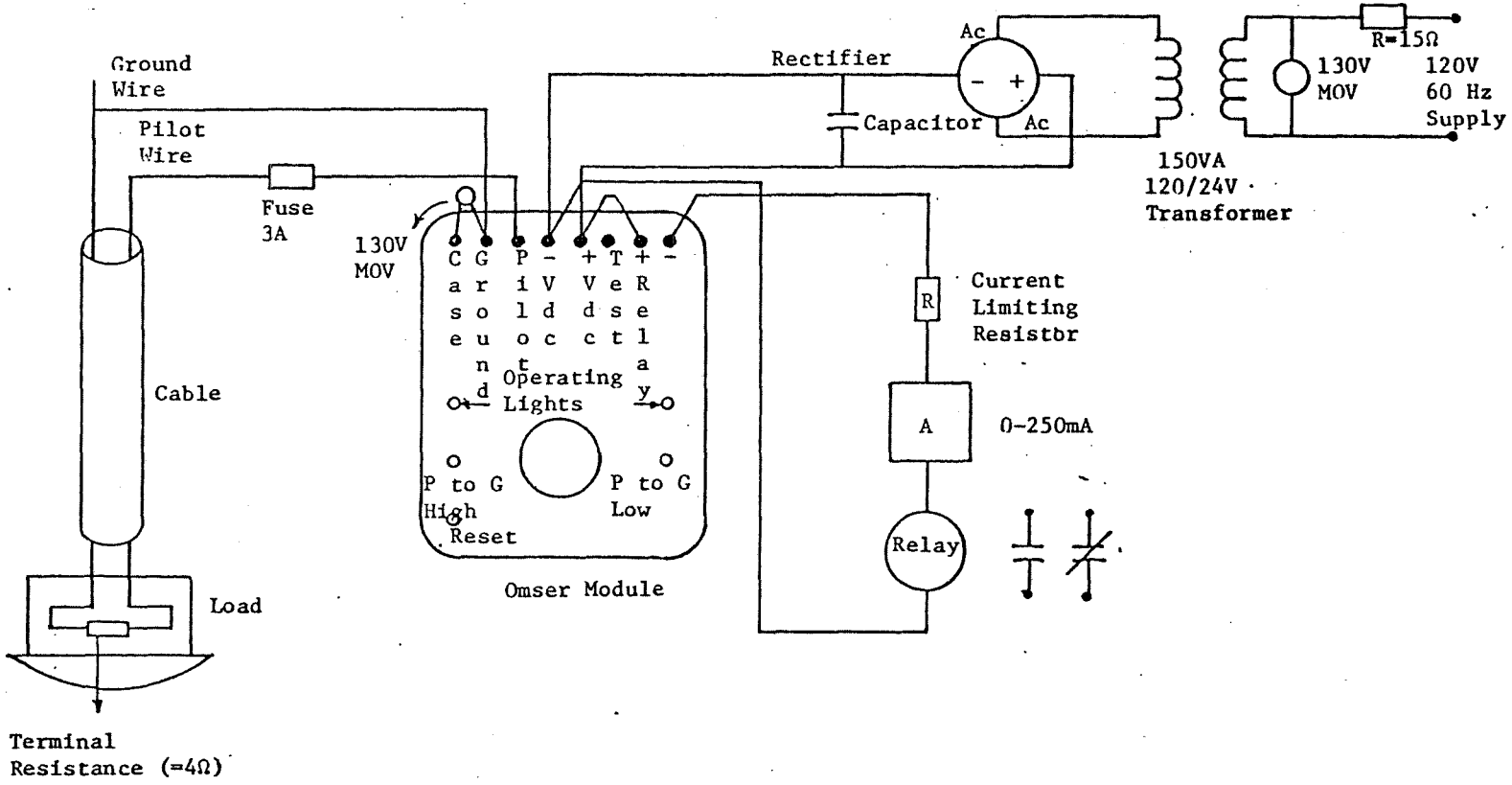


Fig. 6.7. Connection Diagram for Atkinson Ground Wire Monitor.

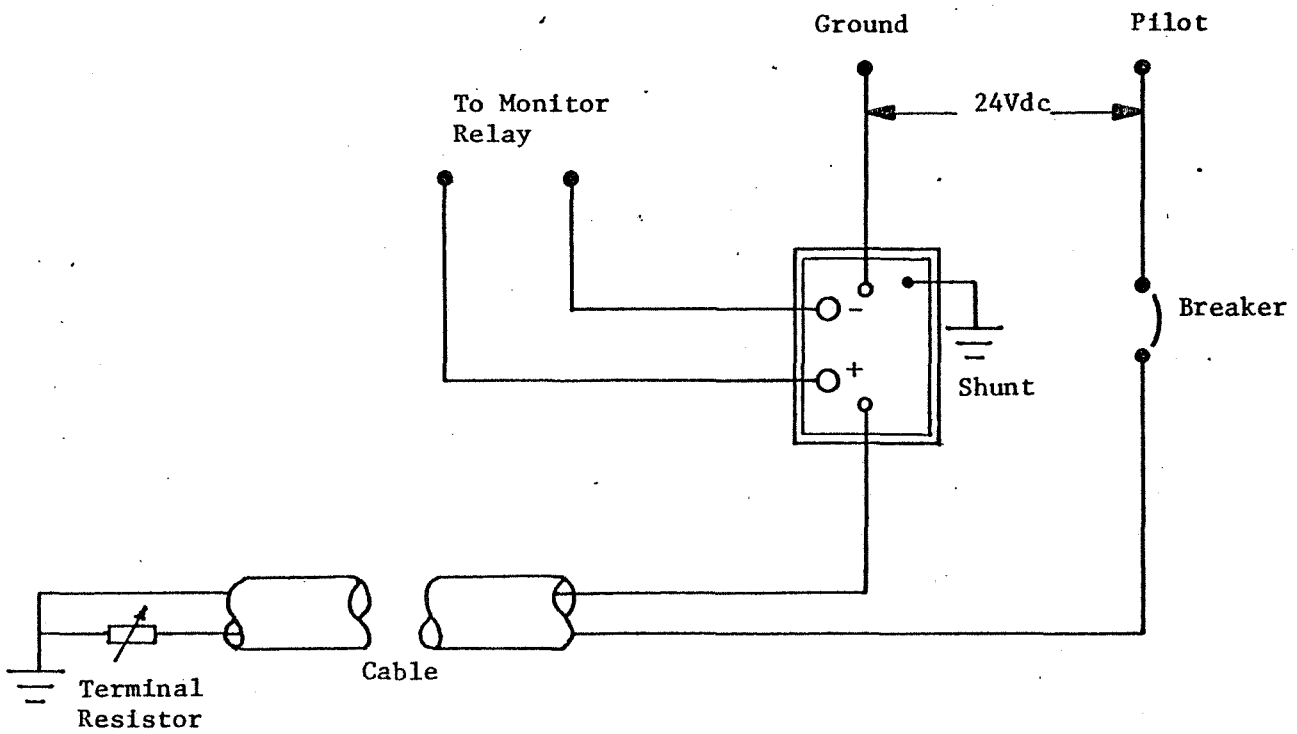


Fig. 6.8. Connection Diagram for the Central Electric Ground Wire Monitor.

6.2,4 Test Results

Both the monitors were set for approximately 6000 ft. of 4/0 cable. This is equivalent to about 0.5Ω of ground wire resistance and 4.0Ω pilot wire resistance. The following are the test results:

Test Description	Atkinson	CEMSCO
A. Both the monitors were set for a parallel path of 1Ω and following tests performed:		
1. opened the ground wire	Did not trip	Tripped in about 1 sec.
2. Pilot to ground short-circuit (at the machine terminals)	Tripped in about 1 sec.	Tripped in about 15 sec.
3. Decreased the pilot wire resistance	Tripped at pilot wire resistance ≃ 2.5Ω	Did not trip even when pilot was decreased all the way to zero
4. Increased the pilot wire resistance	Tripped at pilot wire resistance ≃ 6Ω	Did not trip
5. Increase the ground wire resistance	Did not trip	Tripped
6. Disconnected the parallel path	Did not trip	Did not trip
The following tests were performed with an open parellel path. The monitor settings were not changed		
1. Opened the ground wire	Tripped	Tripped
2. Pilot to ground short-circuit at the machine	Tripped in about 2 secs.	Tripped in about 15 secs.

Test Description	Atkinson	CEMSCO
3. Increased the pilot wire resistance	Tripped at pilot wire resistance ≃ 6.5Ω	Did not trip
4. Decreased the pilot wire resistance	Tripped at pilot wire resistance ≃ 2.5Ω	Did not trip
5. Increased the ground wire resistance	Tripped	Did not trip even when the ground wire resistance was increased to 10Ω. It is a potentially dangerous situation.
B. Both the monitors were set for an open parallel path. The following tests were performed		
1. Opened the ground wire	Tripped	Tripped
2. Pilot-to-ground short-circuit at the machine terminals	Tripped in about 1 sec	Tripped in about about 18 secs
3. Decreased pilot wire resistance	Tripped at pilot wire resistance	Did not trip
4. Increased pilot wire resistance	Tripped at pilot wire resistance ≃ 6Ω	Did not trip
5. Increased the ground wire resistance	Tripped	Did not trip even when the ground wire resistance was increased to 10Ω. Again a potentially dangerous situation.

Test Description	Atkinson	CEMSCO
6. Connected and decreased the parallel path resistance	Did not trip	Tripped when parallel path resistance 20.4Ω. It indicates nuisance tripping.
Now the parallel path was shorted in case of the Atkinson monitor and set at 1Ω for the CEMSCO unit. The monitor settings were not changed and the following tests were performed.		
1. Opened the ground wire	Did not trip	Tripped
2. Pilot-to-ground short circuit at the machine terminals	Tripped in about 1 sec.	Tripped in about 16 secs.
3. Decreased the pilot wire resistance	Tripped at pilot wire resistance ≃ 2.5Ω	Did not trip
4. Increased the pilot wire resistance	Tripped at pilot wire resistance ≃ 6Ω	Did not trip
5. Increased ground wire resistance	Did not trip	Tripped at ground wire resistance ≃ 2Ω
C. The following tests were performed to evaluate the effect of variations in supply voltages.		
1. The supply voltage has adjusted at +10% of nominal, ie. 132V	The monitor performed well and tripped under all abnormal conditions	The monitor tripped under all abnormal conditions except increase and decrease in the pilot-wire resistance.

Test Description	Atkinson	Cemsco
2. Supply voltage was adjusted to -20% of nominal, ie 96 V	The operating relay failed to hold and thus the monitor was inoperable. The dc voltage measured in the circuit was ≃ 26 Vdc	The monitor failed to trip under pilot-to-ground short circuit. It also gave a false trip when the parallel path was shorted. Also failed to trip for increase or decrease in pilot-wire resistance.
3. Supply voltage was adjusted to -10% of nominal, i.e. 108 V	The monitor operated normally. The threshold voltage seems to be around 105 V a dip of around 12% from nominal	Same performance as above.
D. The following tests were performed to evaluate the effect of induced ac voltages in pilot-to-ground circuit.		
1. An ac voltage of 10 V was impressed across the pilot-to-ground circuit. Both the monitors were set for an open parallel path.	The monitor performed well and tripped under all abnormal conditions.	The monitor did not trip when the ground wire resistance was increased to 10Ω. It also failed to operate when the pilot wire resistance was increased or decreased. Also failed to operate under a pilot-to-ground short-circuit in case a parallel path of 10Ω has present.
2. Increased the induced voltage to 20 V	The monitor performed well and tripped under all abnormal conditions.	Same performance as above.

6.2.5 Preliminary Test Conclusions

After the preliminary testing of the Atkinson and CEMSCO monitors and comparing their relative performance, it seems that the Atkinson unit performed better than the CEMSCO unit. It is more sensitive to changes in resistance and seems immune to parallel path and induced voltage effects. It has the additional advantage of having pilot lights to indicate the cause of monitor tripping, i.e. increase or decrease in pilot-ground resistance. This will facilitate the troubleshooting. The best performance of the unit was obtained when it was set in the center of the window as recommended by the manufacturers. One of the major problems with the unit was that the operating relay failed to hold unless the external connections provided in the unit were jumped.

The CEMSCO unit has much simpler circuitry, but is a little difficult to install in the field because of its accessories. It seems to work well for induced voltages of a short duration (<10 secs). For sustained induced voltages the performance was poor. From the circuit point of view it also does not seem immune to stray dc currents, although this test has not been tried so far. Both units seem to be sensitive to dips in supply voltage and show uncertain performances for a voltage dip in excess of 10%.

However, since the Atkinson unit uses electronic circuitry it may be more susceptible to voltage surges generated due to lightning and system faults. This important performance criterion will be evaluated in the near future.

6.2.6 Comments on Atkinson Circuit Design from Patent

The Atkinson monitor uses a similar circuit to the dc monitor WVU has had laboratory approval from the MESA Electrical Testing Group in Beckley. Basically it is a dc monitor which uses a bridge circuit with a voltage comparator to measure resistance (see Fig. 6.9). A second comparator is used to detect a "too low" resistance representing a pilot-to-ground fault. In other words, the two comparators form a window detector. The two reference voltages are derived from two taps on the reference side of the bridge. For the low resistance model (732-10), the resistance window is about 2 ohms. This seems much smaller than necessary; particularly when a pilot-to-ground short would reduce the resistance by at least 4Ω, the resistance connected between pilot and ground at the machine. The way the sensitivity adjustment is made does, however, prevent a high resistance setting too far above the present resistance.

The narrow limits could have a detrimental effect during transients or stray currents. Filtering is provided at the bridge connection to overcome this problem. The filtering scheme looks like a good idea. The long time constants on the filters, however, may restrict the

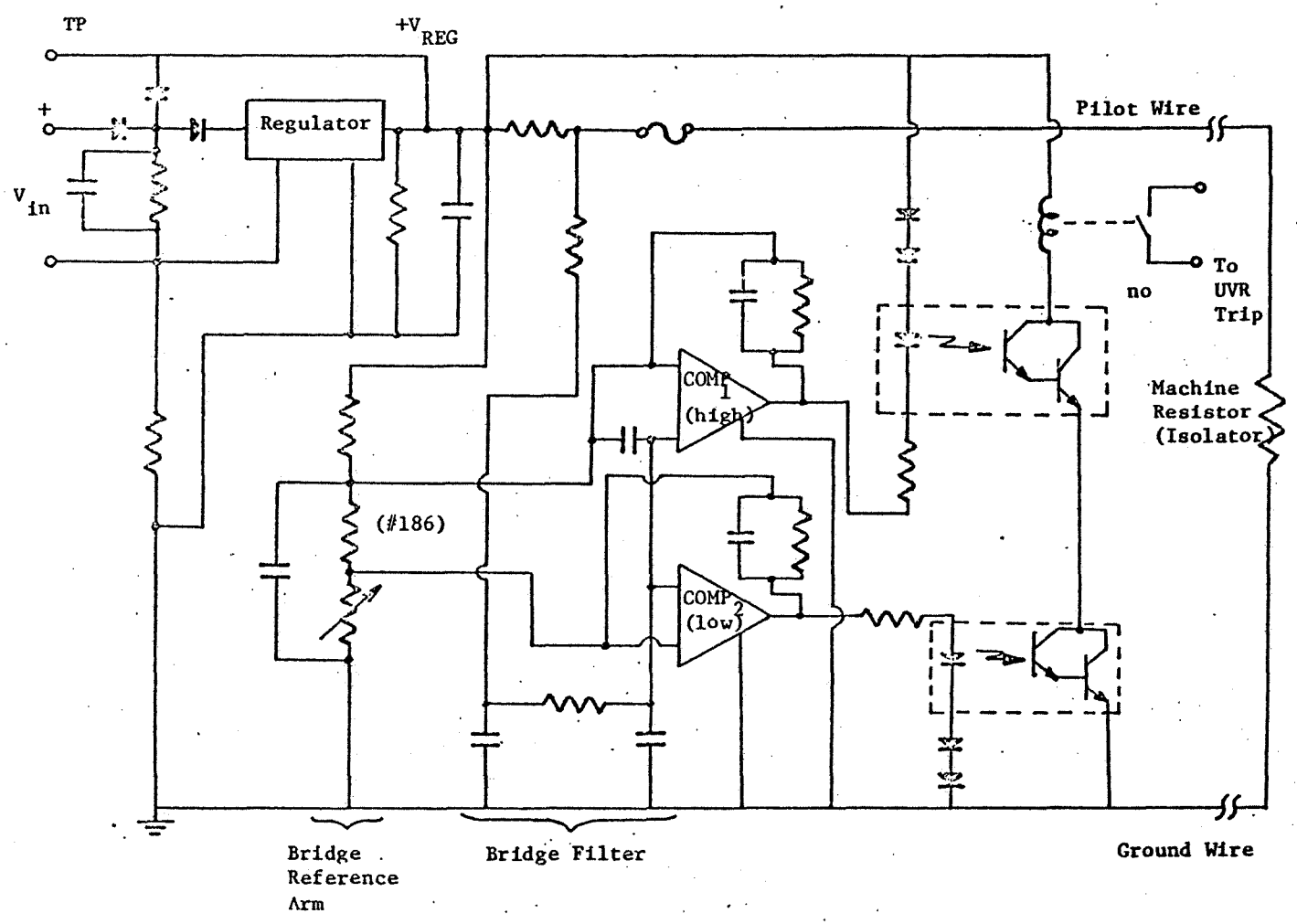


Fig. 6.9. Circuit Diagram of Atkinson Monitor.

operating speed of the monitor.

As presently designed, the Atkinson monitor is not fail-safe; even by MESA's relaxed criteria. Some fairly simple modifications could be made to provide a fail-safe design. The three critical areas of possible failure sensitivity are 1) the comparators 2) the relay driver transistors (in the opto-isolators) and 3) open circuiting a bridge resistor (#186 on patent).

The necessity of the isolation function provided by the opto-isolators is not readily apparent. Perhaps the designers were attempting to provide redundancy or fail-safe operation. If so, they failed. A short circuit failure at either transistor output would negate the operation by its respective comparator. The design would probably be more reliable using discrete transistor drivers. Additionally, no inductive kick-back protection is provided for these transistors. A free-wheeling diode should be added for the protection of these transistors. Unless protection has been added to the circuitry, the monitor would be destroyed by a phase-to-pilot wire short.

6.2.7 CEMSCO Monitor Circuit Analysis

The basic monitoring circuit diagram for the CEMSCO monitor is shown in Figure 6.10. The monitor is basically of the shunt type. It uses a dc source with a resistance isolator on the machine frame. Although the source is a full-wave rectified sine wave, the meter relay is an averaging device so that the effect is dc. The impedance sensitivity can only be determined by experiment because of lack of information on the meter relay.

This monitor has all of the problems that any dc-shunt monitor would have. It can be defeated by stray dc currents as can any dc monitor. However, very little stray dc will be found in open pit mines. Another possible problem could be a stray dc current flowing through the shunt would be mistaken for monitor current. This could cause a false reading if the pilot wire is broken or if the ground wire were broken in such a way that the stray dc could still be picked up.

Parallel paths could also cause a problem. The monitor current might by-pass the shunt. The meter relay would then sense a low current and trip at the monitor. This problem can readily be eliminated by using a diode-type arc suppressor between connection A on Figure 6.10 and the power center frame ground.

The remainder of the circuit is shown in Figure 6.11. In this section a number of relay contacts and switches are interlocked to provide a sequencing of operation. A time delay contact is used to prevent tripping the circuit breaker during start-up and short power interruptions. Both shunt and series contacts are provided on the

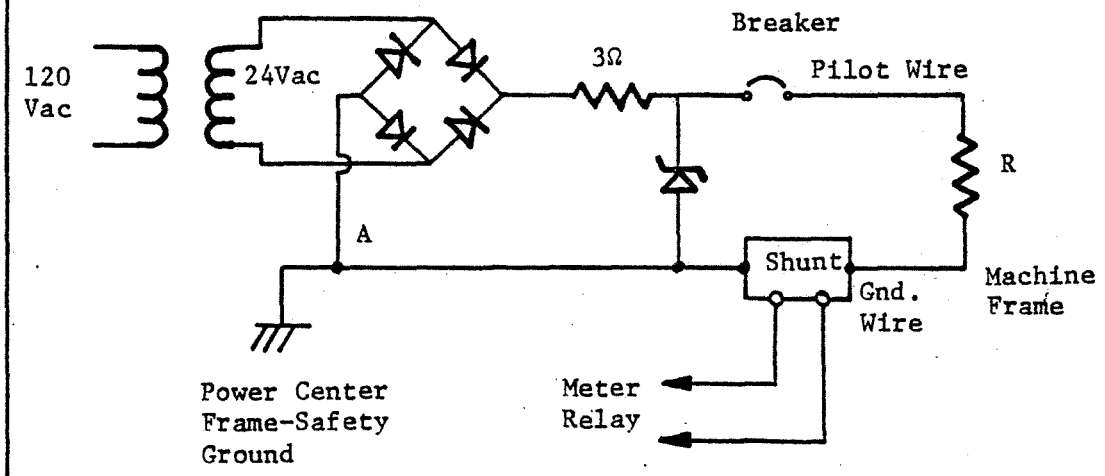
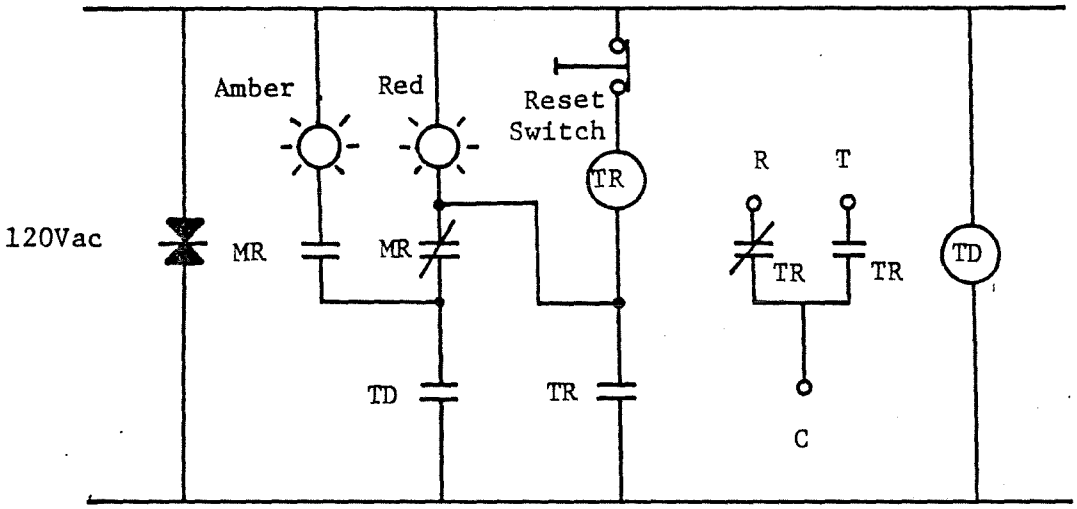


Figure 6.10. Basic Circuit Diagram CEMSCO Monitor.



TD - Time delay contact closes several seconds after power turned on.

TR - Trip relay - picks up to trip.

MR - Meter relay - detector MR pulled in with "Good" ground.

Figure 6.11. Relay Contact Connectors For the CEMSCO Monitor.

trip relay for flexibility. The trip relay and light are latched on by a contact on the trip relay.

The biggest problem with this monitor is the trip relay configuration. The trip relay must be energized to trip. Thus, the circuit is not fail-safe. It seems that a reorganization of this part of the circuit could easily make the circuit fail-safe. Of course, this assumes that the meter relay itself is a fail-safe device.

A second problem that is inherent in this monitor is the time delay provided by the meter relay. It seems that other detection methods would work just as well without the time delay unless substantial problems are encountered with transients.

6.3 MESA SEMINAR

Dr. Wils L. Cooley participated as a speaker in a MESA-sponsored seminar on ground-check monitors for low- and medium-voltage trailing cables. The seminar was designed to acquaint coal operators with the details behind the MESA decision to enforce the 1969 Coal Mine Health and Safety Act as it pertains to these monitors. Speakers included a representative from the Bureau of Mines, Dr. Cooley, a representative of the Bituminous Coal Operators Association, several speakers from MESA Technical Support, other MESA officials, and eight manufacturers' representatives. The seminar was held in Beckley, West Virginia on March 8, 1977; in Birmingham, Alabama on March 11, 1977; in Pittsburgh, Pennsylvania on March 15, 1977; in Denver, Colorado on March 22, 1977; and in St. Louis, Missouri on March 24, 1977. Total attendance was in excess of 500 persons. The text of Dr. Cooley's presentation is included as Appendix E of this report.

CHAPTER VII - LIGHTNING DAMAGE TO MONITORS

It was discovered within the last year that a significant error was made in estimating the probability of a severe ground-to-case transient at the monitor due to lightning surges traveling along the incoming high-voltage transmission lines. The following analysis represents a corrected estimate. There are two modes by which the surge enters via the phase conductor, namely shielding failure and backflash.

7.1 SURGES COUPLED BY SHIELDING FAILURES

This is due to the failure of the overhead static wire to protect the phase conductor from lightning strokes. Lightning strikes directly onto the phase conductor producing a very high surge voltage magnitude that travels in both directions. When this voltage passes under the insulators at a pole line and its magnitude is greater than the insulating level, flashover occurs and the surge will be directed to earth along the pole line footing resistance. However, flashover won't occur until the surge wave reaches a value greater than the crest value of the installed insulators. Consequently, the wave front with a magnitude of about that of the rated value of the insulator will bypass the insulators and travel toward the substation and be directed to the station ground bed eventually by its surge arrestors.

7.2 SURGES COUPLED BY BACKFLASH

This is another case in which the phase conductors are being affected by lightning strokes. Lightning current strikes the static wire and induces a very high voltage on the static wire. At the first pole line the surge encounters reflection takes place because of the pole footing resistance. The remaining surge voltage raises the potential of the pole and if this potential is greater than the crest value of the insulators, which insulate the phase conductors from the pole, flashover occurs and the surge voltage is directed to the phase conductors, then travels along them and reaches the substation ground bed via the surge arrestor.

7.3 REVISED ESTIMATED SURGE PROBABILITY

In order to estimate the frequency of occurrence of monitor failure via this path, several factors have to be taken into consideration. The length of transmission lines that supply power to the primary side of the substation; the attenuation coefficient on the phase conductors; the geometry of the transmission system; the destructive voltage level of the monitor, etc.

The empirical formula[1] for the attenuation of lightning surge is as follows:

$$V = \frac{V_o}{KSV_o + 1} \qquad (7.1)$$

where V = resultant voltage, kV
V_o = initial voltage, kV
K = empirical constant, 0.0007
S = distance of travel, miles

The whole process starts with first estimating the occurrence through shielding failure. This begins with computing the voltage level for individual lightning discharge current that causes shielding failure on the phase conductor. Then determine if this voltage is high enough to cause flashover. By assuming a reasonable flashover voltage, then the distance, from the substation, over which the surge voltage is being attenuated to the level which will cause monitor failure at the station ground bed. Then the frequency of occurrence can be calculated accordingly using the modified version of the HP-65 program listed in the previous annual report.

The same procedure can be applied to estimating the occurrence via backflash mode. The only difference is that the frequency of lightning hitting the static wire that will cause flashover is calculated instead of the frequency of occurrence of shielding failure.

The above two computations are based on the assumption that the flashover voltage is the magnitude of the wave front that will travel toward the substation. Another assumption is that the wave front is a sharp chopped wave and hence the empirical constant for attenuation used is 0.0007.

With the same geometry of configuration of the transmission system it was calculated that only the discharge current of magnitude equal or less than 10kA will cause shielding failure and current magnitude equal or greater than 50kA will cause backflash, using 1000 volts as the destructive voltage level and 20 ohms as the contact resistance of the lightning arrestor to ground. Since no information is obtained on the length of transmission lines and it varies from substation to substation, a series of calculations were made based on the above conditions. It was found out that the frequency of occurrence of monitor failure by this path is directly (linearly) proportional to the distance. That is, if the distance is twice as long, the frequency of occurrence is doubled. The combined result of the two modes is computed to be 3.41 per year for a 10 miles transmission line. For any distance of line, the frequency of occurrence is computed by simply multiplying the distance in miles by the factor 0.341.

From the above results, this pathway could be very significant. A simple way to reduce the frequency of occurrence of this pathway is to install some kind of lightning arresters or protective devices on the pole location one or two spans from the substation.

7.4 REFERENCE

1. Wagner, C. F. and G. D. McCann. "Chapter 15 - Wave Propagation on Transmission Lines" in Electrical Transmission and Distribution Reference Book. Westinghouse Electric Corporation, 1950.

APPENDIX A

Fortran Program for solution of α, for Perpendicular Boundaries with Equal Spacings

```
V G LEVEL  21                    MAIN                    DATE = 77221      12/02/55

C  ***************************************************************************************
C  *                                                                                     *
C  *   THIS PROGRAM DETERMINES THE EFFECT OF A PAIR OF NONCONDUCTING                     *
C  *   PERPENDICULAR BOUNDARIES WITH EQUAL SPACING ON THE RESISTANCE                     *
C  *   MEASUREMENTS IN A FINITE VOLUME.  THE PROGRAM CALCULATES 'ALPHA' FOR              *
C  *   DIFFERENT VALUES OF PERPENDICULAR BOUNDARY DISTANCES, WHERE ALPHA IS THE          *
C  *   RATIO OF POTENTIAL ELECTRODE DISTANCE AT WHICH THE TRUE RESISTANCE IS             *
C  *   MEASURED TO THE DISTANCE OF CURRENT ELECTRODE FROM THE GROUND ROD                 *
C  *   UNDER CONSIDERATION.                                                              *
C  *                                                                                     *
C  *   INPUT:-      C=CURRENT ELECTRODE DISTANCE                                         *
C  *                                                                                     *
C  *   OUTPUT:-     ALPHA=P/C                                                            *
C  ***************************************************************************************

      LOGICAL PRNT
      DIMENSION ROOTS(4)
      COMMON NT,C,X
      EXTERNAL SUM
      NT=65
      PRNT=.TRUE.
      NS=4
      READ(5,1) C
    1 FORMAT(F5.2)
      PRINT 2,C
    2 FORMAT(5X,F5.2)
      DO 11 K=1,70,5
      X=K/C
      PRINT 22,X
   22 FORMAT(5X,F5.2)
      CALL ZEROES(SUM,ROOTS,NF,NS,.000001,.999999,.25,.1,25,PRNT)
      PRINT 300,(ROOT(I),I=1,NF)
  300 FORMAT(5X,E13.7)
   11 CONTINUE
      END
```

```
C     ************************************************************************
C     *  SUMMATION OF INFINITE SERIES USING EULER'S TRANSFORMATION           *
C     ************************************************************************
      FUNCTION SUM(AL)
      COMMON NT,C,X
      DIMENSION W(65,65)
      I=1
      DC 20 N=1,NT
      I=-I
   20  W(N,1)=I*(1./C)*(2./(N+2.*N*X)+1./(N+2.*X*(N-1))
     *-1./((N-1)+2.*N*X)-1./((N-AL)+2.*X*(N-1))
     *-1./((N-AL)+2.*N*X)+1./((N+AL-1.)+2.*X*(N-1))
     *+1./((N+AL-1.)+2.*N*X))
      DO 30 J=2,NT
      IUP=NT-J+1
      DO 30 I=1,IUP
   30 W(I,J)=W(I,J-)+W(I+1,J-1)
      S=.5
      SUM=.5*W(1,1)
      DO 40 J=2,NT
      S=.5*S
   40 SUM=SUM+S*W(1,J)
      RETURN
      END
```

```
G LEVEL  21                    MAIN              DATE = 77213         15/36/01

C   ********************************************************************************
C   *   CALCULATION OF ALPHA TO YIELD POTENTIAL ELECTRODE DISTANCE AT WHICH    *
C   *   TRUE RESISTANCE IS MEASURED                                           *
C   ********************************************************************************
      SUBROUTINE ZEROES(FUN,ROOTS,NF,NS,XL,XR,HSTAR,HMIN,HMAX,PRNT)
      LOGICAL PRNT
      DIMENSION ROOTS(NS)
      NF=0
      H=HSTAR
      ZL=XL
      FL=FUN(ZL)
      IF(PRNT)PRINT 800,ZL,FL
  800 FORMAT(5X,E13.7)
      IF(FL.NE.0.)GO TO 10
      NF=NF+1
      PRINT 400
  400 FORMAT*5X,'ROOT FOUND')
      ROOTS(NF)=ZL
      IF(NF.EQ.NS)RETURN
   10 ZR=ZL+H
   20 FR=FUN(ZR)
      IF(PRNT)PRINT 800, ZR,FR
      IF(FR.NE.0.)GO TO 30
      NF=NF+1
      PRINT 400
      ROOTS(NF)=ZR
      GO TO 65
   30 IF(FL*FR.GE.0.)GO TO 90
      TUP=AMAX1(ABS(FR),ABS(FL))*10.
      IF(ABS(FR).GT.ABS(FL)GO TO 40
      XI=ZR
      FI=FR
      XM=ZL
      FM=FL
      GO TO 50
   40 XI=ZL
      FI=FL
      XM=ZR
      FM=FR
```

```
 50  XP=XI-FI*(XI-XM)/(FI-FM)
     FP=FUN(XP)
     IF(PRNT)PRINT 800, XP,FP
     IF(ABS(FP).LT.TUP)GO TO 55
     PRINT 500
500  FORMAT(5X,'SINGULARITY')
     GO TO 90
 55  IF(FP.EQ.0.)GO TO 60
     IF(ABS(XI-XM).GT.9.E-7*(ABS(XP)+1.))GO TO 70
 60  NF=NF+1
     PRINT 400
     ROOTS(NF)=XP
 65  IF(NF.EQ.NS)RETURN
     H=HMIN/3.
     PRINT 600
600  FORMAT(5X,'RESTART')
     GO TO 90
 70  IF(FP*FI.GT.0.)GO TO 80
     XM=XI
     FM=FI
     GO TO 85
 80  FM=FM*FI/(FI+FP)
     PRINT 700
700  FORMAT(5X,'RERULA FALCI FAILED')
 85  XI=XP
     FI=FP
     GO TO 50
 90  IF(ZR.EQ.XR)RETURN
     P=FR*(FR-FL)/((ABS(FR)+ABS(FL))*ABS(FR))
     IF(P.EQ.0.)GO TO 100
     IF(P.GT.0..AND.H.GE.HMAX)GO TO 100
     IF(P.LT.0..AND.H.LE.HMIN)GO TO 100
     H=H*(2.+P)/(2.-P)
100  ZL=ZR
     FL=FR
     ZR=ZR+H
     IF(ZR.GT.XR)ZR=XR
     GO TO 20
     END
```

APPENDIX B

Fortran Program for solution of α, for Perpendicular Boundaries with Unequal Spacings

```
C   ********************************************************************************
C   *                                                                              *
C   *  THIS PROGRAM DETERMINES THE EFFECT OF A PAIR OF NONCONDUCTING               *
C   *  PERPENDICULAR BOUNDARIES WITH UNEQUAL SPACINGS ON THE RESISTANCE            *
C   *  MEASUREMENTS IN A FINITE VOLUME.  THE PROGRAM SIMULATES SITUATION, WHERE    *
C   *  FALL-OF-POTENTIAL ELECTRODES (INCLUDING THE GROUND ELECTRODE) ARE           *
C   *  MOVED FROM ONE PERPENDICULAR BOUNDARY TO ANOTHER AND CALCULATES 'ALPHA'     *
C   *  IN EACH CASE WHERE ALPHA IS THE RATIO OF POTENTIAL ELECTRODE DISTANCE       *
C   *  AT WHICH THE TRUE RESISTANCE IS MEASURED TO THE DISTANCE OF CURRENT         *
C   *  ELECTRODE FROM THE GROUND ROD UNDER CONSDIERATION.                          *
C   *                                                                              *
C   *  INPUT:-     A=LENGTH OF THREE DIMENSIONAL MODEL                             *
C   *              C=CURRENT ELECTRODE DISTANCE                                    *
C   *  OUTPUT:-    ALPHA=P/C                                                       *
C   *                                                                              *
C   *                                                                              *
C   ********************************************************************************
      LOGICAL PRNT
      DIMENSION ROOTS(8)
      COMMON NT,C,X,Y
      EXTERNAL SUM
      NT=65
      PRNT=.TRUE.
      NS=8
      READ(5,1) A,C
    1 FORMAT(F6.2,F4.1)
      PRINT 200,A,C
  200 FORMAT(5X,F6.2,F4.1)
      K=A
      DO 11 L=1,K,10
      X=L/C
      Y=K/C-1.-X
      PRINT 22,X,Y
   22 FORMAT(5X,F4.1,F4.1)
      IF(X.LT.0.)STOP
      IF(Y.LT.0.)STOP
      CALL ZEROES(SUM,ROOTS,NF,NS,.000001,.999999,.25,.1,.25,PRNT)
      PRINT 300,(ROOTS(I),I=1,NF)
  300 FORMAT(5X,E15.9)
   11 CONTINUE
      END
```

```
C    ***************************************************************************
C    *   SUMMATION OF INFINITE SERIES USING EULER'S TRANSFORMATION              *
C    ***************************************************************************
      FUNCTION SUM(AL)
      COMMON NT,C,X,Y
      DIMENSION W(65,65)
      I=1
      DO 20 N=1,NT
      FN=2.*N*(1.+X+Y)
   20 W(N,1)=(1./C)*(2./(FN)-1./(FN-2.*(X+Y)-1.)-1./(FN-2.*Y-1.)
     *+1./(FN-2.*Y)+1./(FN-2.*(1.+X))-1./(FN-2.*X-1.)
     *-1./(FN-2.*Y-AL)-1./(FN-AL)-1./(FN-(FN/N)+AL)
     *-1./(FN-2.*(X+1.)+AL)+1./(FN-2.*X+AL-1.)+1./(FN+AL-1.))
      DO 30 J=2,NT
      IUP=NT-J+1
      DO 30 I=1,IUP
   30 W(I,J)=W(I,j-1)+W(I+1,J-1)
      S=.5
      SUM=.5*W(1,1)
      DO 40 J=2,NT
      S=.5*S
   40 SUM=SUM+S*W(1,J)
      RETURN
      END
```

```
G LEVEL   21                MAIN              DATE = 77213         15/36/01

C  ***************************************************************************
C  *  CALCULATION OF ALPHA TC YIELD POTENTIAL ELECTRODE DISTANCE AT WHICH     *
C  *  TRUE RESISTANCE IS MEASURED                                            *
C  ***************************************************************************
      SUBROUTINE ZEROES(FUN,ROOTS,NF,NS,XL,XR,HSTAR,HMIN,HMAX,PRNT)
      LOGICAL PRNT
      DIMENSION ROOTS(NS)
      NF=0
      H=HSTAR
      ZL=XL
      FL=FUN(ZL)
      IF(PRNT)PRINT 800,ZL,FL
  800 FORMAT (5X,E13.7)
      IF(FL.NE.0.)GO TO 10
      NF=NF+1
      PRINT 400
  400 FORMAT(5X,'ROOT FOUND')
      ROOTS(NF)=ZL
      IF(NF.EQ.NS)RETURN
   10 ZR=ZL+H
   20 FR=FUN(ZR)
      IF(PRNT)PRINT 80C,ZR,FR
      IF(FR.NE.0.)GO TO 30
      NF=NF+1
      PRINT 400
      ROOTS(NF)=ZR
      GO TO 65
   30 IF(FL*FR.GE.0.)GO TO 90
      TUP=AMAX1(ABS(FR),ABS(FL)*10.
      IF(ABS(FR).GT.ABS(FL))GO TO 40
      XI=ZR
      FI=FR
      XM=ZL
      FM=FL
      GO TO 50
   40 XI=ZL
      FI=FL
      XM=ZR
      FM=FR
```

```
 50  XP=XI-FI*(XI-XM)/(FI-FM)
     FP=FUN(XP)
     IF(PRNT)PRINT 800,XP,FP
     IF(ABS(FO).LT.TUP)GO TO 55
     PRINT 500
500  FORMAT(5X,'SINULARITY')
     GO TO 90
 55  IF(FP.EQ.0.)GO TO 60
     IF(ABS(XI-XM).GT.9.E-7*(ABS(XP)+1.))GO TO 70
 60  NF=NF+1
     PRINT 400
     ROOTS(NF)=XP
 65  IF(NF.EQ.NS)RETURN
     H=HMIN/3.
     PRINT 600
600  FORMAT(5X,'RESTART')
     GO TO 90
 70  IF(FP*FI.GT.0.)GO TO 80
     XM=XI
     FM=FI
     GO TO 85
 80  FM=FM*FI/(FI+FP)
     PRINT 700
700  FORMAT(5X,'RERULA FALCI FAILED')
 85  XI=XP
     FI=FP
     GO TO 50
 90  IF(ZR.EQ.XR)RETURN
     P=FR*(FR-FL)/((ABS(FR)+ABS(FL))*ABS(FR))
     IF(P.EQ.0.)GO TO 100
     IF(P.GT.0..AND.H.GE.HMAX)GO TO 100
     IF(P.LT.0..AND.H.LE.HMIN)GO TO 100
     H=H*(2.+P)/(2.-P)
100  ZL=ZR
     FL=FR
     ZR=ZR+H
     IF(ZR.GT.XR)ZR=XR
     GO TO 20
```

APPENDIX C

Fortran Program for solution of α, for Parallel Boundaries with Equal Spacings

```
G LEVEL  21                    MAIN                DATE = 77221        12/06/45
C  ********************************************************************************
C  *                                                                              *
C  *  THIS PROGRAM DETERMINES THE EFFECT OF A PAIR OF NONCONDUCTING,PARALLEL      *
C  *  BOUNDARIES WITH EQUAL SPACINGS ON THE RESISTANCE MEASUREMENTS IN A          *
C  *  FINITE VOLUME. THE PROGRAM CALCULATES 'ALPHA' FOR DIFFERENT VALUES OF       *
C  *  PARALLEL BOUNDARY DISTANCES,WHERE ALPHA IS THE RATIO OF POTENTIAL           *
C  *  ELECTRODE DISTANCE AT WHICH THE TRUE RESISTANCE IS MEASURED TO THE          *
C  *  DISTANCE OF CURRENT ELECTRODE FROM THE GROUND ROD UNDER CONSIDERATION.      *
C  *                                                                              *
C  *  INPUT:-      C=CURRENT ELECTRODE DISTANCE                                   *
C  *                                                                              *
C  *  OUTPUT:-     ALPHA=P/C                                                      *
C  *                                                                              *
C  ********************************************************************************
      LOGICAL PRNT
      DIMENSION ROOTS(4)
      COMMON NT,C,X
      EXTERNAL SUM
      NT=65
      PRNT=.TRUE.
      NS=4
      READ(5,1) C
    1 FORMAT(F5.2)
      PRINT 2,0
    2 FORMAT(5X,F5.2)
      DO 11 K=1,70,5
      X=K/C
      PRINT 22,X
   22 FORMAT(5X,F5.2)
      CALL ZEROES(SUM,ROOTS,NF,NS,.000001,.999999,.25,.1,.25,PRNT)
      PRINT 300,(ROOTS(I),I=1,NF)
  300 FORMAT(5X,E13.7)
   11 CONTINUE
      END
```

```
C  ***********************************************************************
C  *  SUMMATION OF INFINITE SERIES USING EULER'S TRANSFORMATION          *
C  ***********************************************************************
      FUNCTION SUM(AL)
      COMMON NT,C,X
      DIMENSION W(65,65)
      I=1
      DC 20 N=1,NT
      FN=(2.*(N-1.)*X)**2
   20 W(N,1)=(1./C)*(1./(N=X)-2./SQRT(1.+FN)-2./SQRT(AL**2+FN)
     *+2./SQRT((1.-AL)**2+FN)
      DO 30 J=2,NT
      IUP=NT-J+1
      DO 30 I=1,IUP
   30 W(I,J)=W(I,J-1)+W(I+1,J-1)
      S=.5
      SUM=.5*W(1,1)
      DO 40 J=2,NT
      S=.5*S
   40 SUM=SUM+S*W(1,J)
      FM=(1./C)*(1.+1./AL-1./(1.-AL))
      SUM=SUM+FM
      RETURN
      END
```

```
G LEVEL  21                          MAIN                DATE = 77213      15/36/01

  C  ********************************************************************************
  C  *  CALCULATION OF ALPHA TO YIELD POTENTIAL ELECTRODE DISTANCE AT WHICH
  C  *  TRUE RESISTANCE IS MEASURED
  C  ********************************************************************************
        SUBROUTINE ZEROES(FUN,ROOTS,NF,NS,XL,XR,HSTAR,HMIN,HMAX,PRNT)
        LOGICAL PRNT
        DIMENSION ROOTS(NS)
        NF=0
        H=STAR
        ZL=XL
        FL=FUN(ZL)
        IF(PRNT)PRINT 800,ZL,FL
    800 FORMAT(5X,E13.7)
        IF(FL.NE.0.)GO TO 10
        NF=NF+1
        PRINT 400
    400 FORMAT(5X,'ROOT FOUND')
        ROOTS(NF)=ZL
        IF(NF.EQ.NS)RETURN
     10 ZR=ZL+H
     20 FR=FUN(ZR)
        IF(PRNT)PRINT 800,ZR,FR
        IF(FR.NE.0.)GO TO 30
        NF=NF+1
        PRINT 400
        ROOTS(NF)=ZR
        GO TO 65
     30 IF(FL*FR.GE.0.)GO TO 90
        TUP=AMAX1(ABS(FR),ABS(FL))*10.
        IF(ABS(FR).GT.ABS(FL))GO TO 40
        XI=ZR
        FI=FR
        XM=ZL
        FM=FL
        GO TO 50
     40 XI=FL
        FI=
        XM=ZR
```

```
 50 XP=XI-FI*(XI-XM)/(FI-FM)
    FP=FUN(XP)
    IF(PRNT)PRINT 800,XP,FP
    IF(ABS(FP).LT.TUP)GO TO 55
    PRINT 500
500 FORMAT(5X,'SINGULARITY')
    GO TO 90
 55 IF(FP.EQ.0.)GO TO 60
    IF(ABS(XI-XM).GT.9.E-7*(ABS(XP)+1.))GO TO 70
 60 NF=NF+1
    PRINT 400
    ROOTS(NF)=XP
 65 IF(NF.EQ.NS)RETURN
    H=HMIN/3.
    PRINT 600
600 FORMAT(5X,'RESTART')
    GO TO 90
 70 IF(FP*FI.GT.0.)GO TO 80
    XM=XI
    FM=FI
    GO TO 85
 80 FM=FM*FI/(FI+FP)
    PRINT 700
700 FORMAT(5X,'RERULA FALCI FAILED')
 85 XI=XP
    FI=FP
    GO TO 50
 90 IF(ZR.EQ.XR)RETURN
    P=FR*(FR-FL)/((ABS(FR)+ABS(FL))*ABS(FR))
    IF(P.EQ.0.)GO TO 100
    IF(P.GT.0..AND.H.GE.HMAX)GO TO 100
    IF(P.LT.0..AND.H.LE.HMIN)GO TO 100
    H=H*(2.+P)/(2.-P)
100 ZL=ZR
    FL=FR
    ZR=ZR+H
    IF(ZR.GT.XR)ZR=XR
    GO TO 20
    END
```

APPENDIX D

Fortran Program for solution of α, for Parallel Boundaries with Unequal Spacings

```
C  ********************************************************************************
C  *                                                                              *
C  *  THIS PROGRAM DETERMINES THE EFFECT OF A PAIR OF NONCONDUCTING,PARALLEL      *
C  *  BOUNDARIES WITH UNEQUAL SPACINGS ON THE RESISTANCE MEASUREMENTS IN A        *
C  *  FINITE VOLUME. THE PROGRAM SIMULATES SITUATION WHERE FALL-OF-POTENTIAL      *
C  *  ELECTRODES(INCLUDING THE GROUND ELECTRODE)ARE MOVED FROM ONE PARALLEL       *
C  *  BOUNDARY TO ANOTHER AND CALCULATES 'ALPHA' IN EACH CASE WHERE ALPHA IS      *
C  *  THE RATIO OF POTENTIAL ELECTRODE DISTANCE AT WHICH THE TRUE RESISTANCE      *
C  *  IS MEASURED TO THE DISTANCE OF CURRENT ELECTRODE FROM THE GROUND ROD        *
C  *  UNDER CONSIDERATION.                                                        *
C  *                                                                              *
C  *  INPUT:-     B=WIDTH OF THE THREE DIMENSIONAL MODEL                          *
C  *              C=CURRENT ELECTRODE DISTANCE                                    *
C  *                                                                              *
C  *  OUTPUT:-    ALPHA=P/C                                                       *
C  *                                                                              *
C  ********************************************************************************
      LOGICAL PRNT
      DIMENSION ROOTS(8)
      COMMON NT,C,X,Y
      EXTERNAL SUM
      NT=65
      PRNT=.TRUE.
      NS=8
      READ(5,1) B,C
    1 FORMAT(F6.2,F4.1)
      PRINT 200,B,C
  200 FORMAT(5X,F6.2,F4.1)
      K=B
      DO 11 L=1,K,10
      X=L/C
      Y=K/C-X
      PRINT 22,X,Y
   22 FORMAT(5X,F4.1,F4.1)
      CALL ZEROES(SUM,ROOTS,NF,NS,.000001,.999999,.25,.1,.25,PRNT)
      PRINT 300,(ROOTS(I),I=1,NF)
  300 FORMAT(5X,E13.7)
   11 CONTINUE
      END
```

```
C   ********************************************************************************
C   *  SUMMATION OF INFINITE SERIES USING EULER'S TRANSFORMATION                    *
C   ********************************************************************************
      FUNCTION SUM(AL)
      COMMON NT,C,X,Y
      DIMENSION W(65,65)
      I=1
      DO 20 N=1,NT
      FA=2.*N*(X+Y)
      FB=FA-2.*Y
      FC=FA-2.*X
      FD=FB**2
      FE=FC**2
   20 W(N,1)=(1./C)*(1./FB+1./FC+2./FA-1./SQRT(1.+FD)-1./SQRT(1.+FE)
     *-2./SQRT(1.+FA**2)-1./SQRT(AL**2+FD)-1./SQRT(AL**2+FE)
     *-2./SQRT(AL**2+FA**2)+1./SQRT((1.-AL)**2+FD)
     *+1./SQRT((1.-AL)**2+FE)+2./SQRT((1.-AL)**2+FA**2))
      DO 30 J=2,NT
      IUP=NT-J+1
      DO 30 I=1,IUP
   30 W(I,J)=W(I,J-1)+W(I+1,J-1)
      S=.5
      SUM=.5*W(1,1)
      DO 40 J=2,NT
      S=.5*S
   40 SUM=SUM+S*W(1,J)
      FM=(1./C)*(-1.-1./AL+1./(1.-AL))
      SUM=SUM+FM
      RETURN
      END
```

```
G LEVEL  21
C  ***************************************************************************
C  *  CALCULATION OF ALPHA TO YIELD POTENTIAL ELECTRODE DISTANCE AT WHICH     *
C  *  TRUE RESISTANCE IS MEASURED                                            *
C  ***************************************************************************
      SUBROUTINE ZEROES(FUN,ROOTS,NF,NS,XL,DR,HSTAR,HMIN,HMAX,PRNT)
      LOGICAL PRNT
      DIMENSION ROOTS(NS)
      NF=0
      H=STAR
      ZL=XL
      FL=FUN(ZL)
      IF(PRNT)PRINT 800,ZL,FL
  800 FORMAT(5X,E13.7)
      IF(FL.NE.0.)GO TO 10
      NF=NF+1
      PRINT 400
  400 FORMAT(5X,'ROOT FOUND')
      ROOTS(NF)=ZL
      IF(NF.EQ.NS)RETURN
   10 ZR=ZL+H
   20 FR=FUN(ZR)
      IF(PRNT)PRINT 800,ZR,FR
      IF(FR.NE.0.)GO TO 30
      NF=NF+1
      PRINT 400
      ROOTS(NF)=ZR
      GO TO 65
   30 IF(FL*FR.GE.0.)GO TO 90
      TUP=AMAX1(ABS(FR),ABS(FL))*10
      IF(ABS(FR).GT.ABS(FL))GO TO 40
      XI=ZR
      FI=FR
      XM=ZL
      FM=FL
      GO TO 50
   40 XI=ZL
      FI=FL
      XM=ZR
      FM=FR
```

```
 50 XP=XI-FI*(XI-XM)/(FI-FM)
    FP=FUN(XP)
    IF(PRNT)PRINT 800,XP,FP
    IF(ABS(FP).LT.TUP)GO TO 55
    PRINT 500
500 FORMAT(5X,'SINGULARITY')
    GO TO 90
 55 IF(FP.EQ.0.)GO TO 60
    IF(ABS(XI-XM).GT.9.E-7*(ABS(XP)+1.))GO TO 70
 60 NF=NF+1
    PRINT 400
    ROOTS(NF)=XP
 65 IF(NF.EQ.NS)RETURN
    H=HMIN/3.
    PRINT 600
600 FORMAT(5X,'RESTART')
    GO TO 90
 70 IF(FP*FI.GT.0.)GO TO 80
    XM=XI
    FM=FI
    GO TO 85
 80 FM=FM*FI/(FI+FP)
    PRINT 700
700 FORMAT(5X,'RERULA FALCI FAILED')
 85 XI=XP
    FI=FP
    GO TO 50
 90 IF(ZR.EQ.XR)RETURN
    P=FR*(FR-FL)/((ABS(FR)+ABS(FL))*ABS(FR))
    IF(P.EQ.0.)GO TO 100
    IF(P.GT.0..AND.H.GE.HMAX)GO TO 100
    IF(P.LT.0..AND.H.LE.HMIN)GO TO 100
    H=H*(2.+P)/(2.-P)
100 ZL=ZR
    FL=FR
    ZR=ZR+H
    IF(ZR.GT.XR)ZR=XR
    GO TO 20
     ND
```

APPENDIX E

WVU Contribution to Ground-Check Monitor Research

WVU CONTRIBUTION TO GROUND-CHECK MONITOR RESEARCH

by

Wils L. Cooley[1]

INTRODUCTION

West Virginia University has worked with ground-check monitors since June 1973, when a grant was received from the U. S. Bureau of Mines to evaluate commercially available ground-check monitors. A modest effort has continued on various aspects of the monitoring problem up to the present time. This paper is intended to cover in approximate chronological order the work that was undertaken and the results reported to USBM and MESA.

EVALUATION OF GROUND-CHECK MONITORS

The first task undertaken was to evaluate several of the ground-check monitors which were commercially available in 1973. Monitors studied in the first year included devices manufactured by Ensign Electric, Ohio Brass, FEMCO, Westinghouse, Joy, General Electric, Eltron, and Control Products Corp. The designs varied considerably from manufacturer to manufacturer. Consequently, the monitors often had very different electrical characteristics, making it difficult to compare them. They all monitored the ground wire under ideal conditions, but their differences became apparent when they were put into the hostile mine electrical environment. The WVU task therefore became three sub-tasks: a) assist USBM and MESA in conducting monitor field tests under actual mine conditions, b) conduct laboratory evaluations of monitors, and c) develop meaningful standards or performance criteria to apply to ground-check monitors.

That first year of USBM-MESA field testing was enlightening, in that about a dozen monitors were installed without achieving a single satisfactory performance. Monitors were difficult or impossible to install, false-tripped hundreds of times per shift, or just plain refused to work.

The WVU laboratory testing was somewhat less frustrating. Besides making some basic electrical tests, the monitor designs were studied closely for the basic soundness of the approach. Estimates were made of the effects of various mine conditions on monitor performance.

---

[1]Associate Professor of Electrical Engineering, West Virginia University, Morgantown, WV 26506.

Suggestions were made for the redesign of several of the units, and a complete analysis of four monitors (Ensign, FEMCO, Westinghouse and General Electric) was transmitted to USBM in July 1974. The overall conclusion was that each monitor had at least one serious shortcoming.

The work done by WVU to develop meaningful performance criteria was perhaps the most important. At this time MESA had only those criteria which appeared in the Code of Federal Regulations, 75.902. While these criteria were certainly valid, they did not provide the kind of detailed design goals that were needed by manufacturers. We felt that a more detailed set of requirements should be considered. The initial list contained fourteen items, as follows:

1. The ground-wire monitor should function properly in the presence of stray ac and dc currents normally found on coal-mine power system grounds. If very high stray currents occur, these should cause the monitor to indicate an unsafe condition.

2. Severe current and voltage transients are common on mine power systems. If the monitor derives its power from the mine power system, such transients should not damage the monitor or cause false indications of unacceptable ground circuits.

3. The ground wire monitor should be unaffected in its ability to monitor the ground circuit by variations of at least +10% to -30% of the nominal line voltage from which it draws its power.

4. The monitor should be designed as much as possible so that a failure of components within the monitor itself (including its power supply) will trip the circuit breaker.

5. The ground-wire monitor should be capable of operating with the various sizes, types, and lengths of portable power cables normally found in the mine. No special training or extensive procedures should be required to calibrate the monitor when it is installed. The ideal monitor should work with any cable anywhere without an adjustment of its characteristics.

6. The ground-wire monitor should not itself be capable of producing currents or voltages on the ground wire which are considered hazardous to mine personnel.

7. The ground-wire monitor should not affect other electrical components placed in the system, such as inter-machine arc suppressors, ground-fault locators, or other monitors in other branches of the system.

8. The ground-wire monitor must continue to function properly in the presence of diode packs or other devices which have been inserted in the ground conductor, provided these devices do not violate safety requirements.

9. The ground-wire monitor should not be damaged by line-to-ground faults which are not cleared because of stuck circuit breakers.

10. If a ground-check or pilot wire is used, the monitor should check the ground circuit all the way to and including the contact with the machine frame. It should signal an unacceptable condition if a pilot-to-ground fault develops within the system.

11. If the monitor is used on a reel-type machine, the ground wire is carried to the machine frame through a sliding contact (brush). During movement of the reel, the impedance of the contact can easily exceed 1.6 ohms for short periods (tenths of seconds). Such a situation should not cause nuisance tripping of the monitor.

12. Since the ground circuits are frequently bypassed by many unexpected ground paths, the monitor should operate properly in spite of these additional paths to ground.

13. Since investment in low-voltage cable is substantial, the ground-monitoring system should not require replacement of present cable with a new cable of special design.

14. Any device connected in series with the ground wire as part of the monitor must be capable of withstanding fault currents without burning open or increasing the impedance of the safety ground circuit. It should be capable of carrying as much current as the ground conductor itself.

These items were transmitted to USBM in July 1974.

MONITOR TEST EQUIPMENT & PROCEDURES

The early work that was done by WVU, USBM and MESA clearly indicated a need for a reliable method of predicting monitor performance based on laboratory tests. WVU therefore attempted to develop equipment and procedures for carrying out such testing. This was begun with the construction of a monitor test panel, shown in Figure 1. The panel was designed to simulate conditions under which a monitor might operate when monitoring an underground low-voltage trailing cable. It provided for the testing of immunity to parallel paths, stray currents, pilot-to-ground shorts, power-supply voltage fluctuations, and many other aspects of monitor operation. The inductance and resistance of the pilot wire and

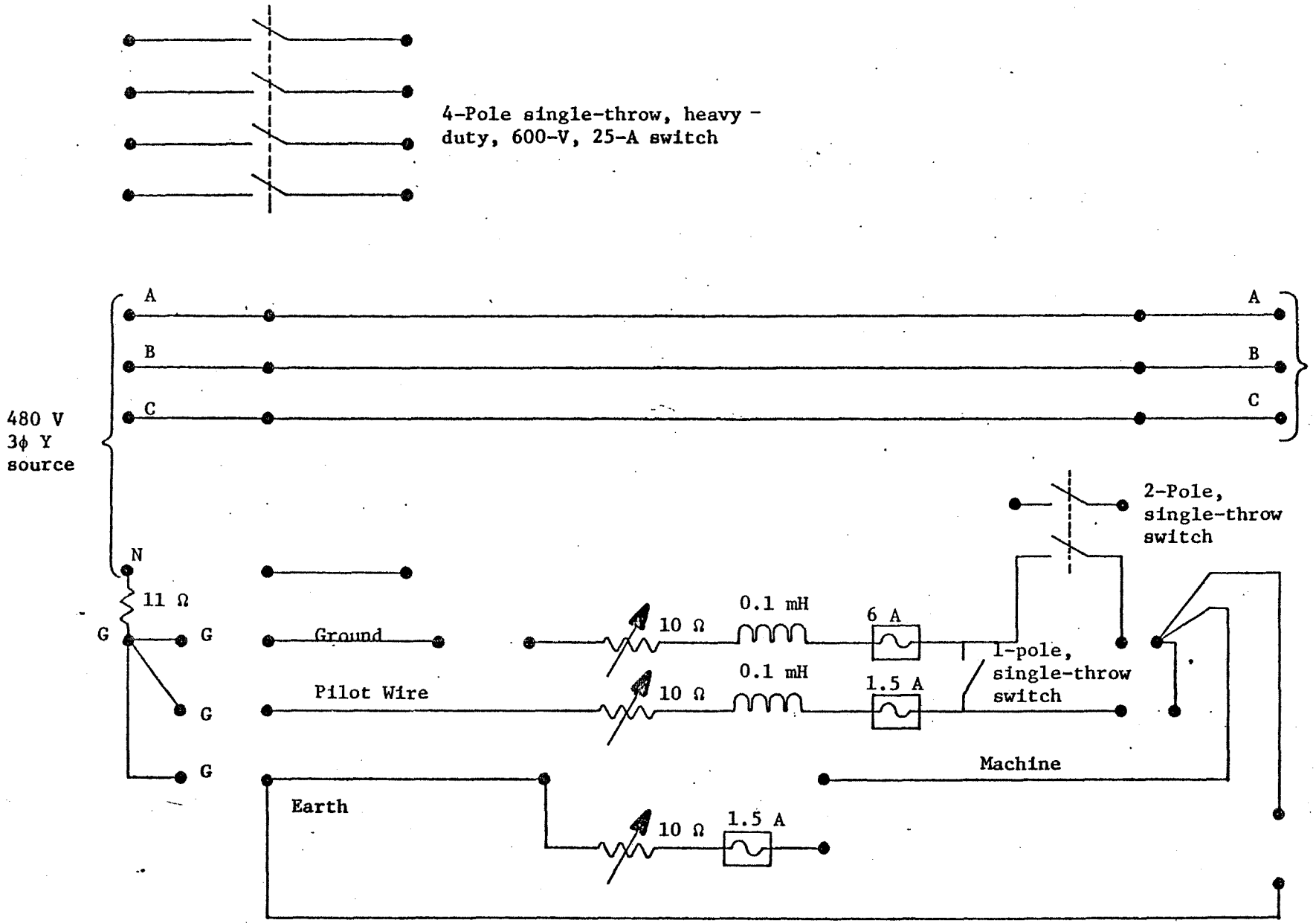


FIGURE 1. Test Panel for Ground Wire Monitors.

ground wires were simulated, and a stray-current generator was built capable of circulating up to several amperes ac and dc through the ground wire in any combination.

A basic test program was developed to determine whether the monitor under study could meet the most fundamental requirements of operation in the presence of:

a) a low-impedance parallel path,
b) a pilot-to-ground fault,
c) loss of input power,
d) power-line transients, and
e) stray currents.

At the time these tests were developed there was no consensus as to the maximum permissible resistance of a "safe" ground wire. Since the law allows 25 A of ground-fault current to flow and restricts the maximum frame voltage to 40 volts, the implied maximum ground wire resistance is 1.6Ω. Rather than using this number, however, we chose to perform two tests:

1. Drop-out test. The resistance of the simulated ground wire connected to the monitor is increased until the monitor indicates an open ground wire. (Monitor initially indicates intact ground).

2. Pull-in test. The resistance of the simulated ground wire connected to the monitor is decreased until the monitor indicates an intact ground wire. (Monitor initially indicates open ground).

These two tests were repeated each time an electrical or environmental factor was changed, such as the amount of stray ground current present.

Six monitors were analyzed in detail in our July 1975 annual report[1] circuits by Eltron, FEMCO, USBM, Continential Conveyor, Joy, and Ohio Brass. The Eltron and FEMCO were judged to work well, and extensive suggestions were made to the manufacturers for improving monitor performance. The EEEI monitor was gone over in detail shortly afterwards, and suggestions made for its improvement.

We have had the opportunity to evaluate redesigned monitors by both FEMCO and EEEI. Both manufacturers have incorporated many of our suggestions or used other design changes to answer our criticisms. We find that these monitors work essentially perfectly in our laboratory simulations. We understand that several other monitors which we have not seen recently also work very well in the laboratory and in the field. Eight have currently been approved by MESA.

GENERIC DESIGN CHARACTERISTICS

WVU has worked for several years on a classification scheme for monitors. So many different types of monitors exist that it has become difficult for the mine operator or engineer to identify the most effective monitor for a particular mine application. We have found it possible to categorize monitoring schemes in a way that identifies their basic characteristics. This has proved very useful to our understanding. The classification scheme has been presented at two USBM Technology Transfer Seminars and elsewhere.

Figure 2 shows the monitor classification scheme. First, all monitors require some flow of current in the ground wire in order to determine its resistance or continuity. This current may be classified as dc, ac, or audio. Dc monitors use power supplies, batteries, or rectified ac power to provide a one-way flow of current through the ground wire. Ac monitors are defined as those which use a 60 Hz current derived from the power system to assess continuity or impedance of the ground wire. Audio monitors are defined as those which generate their own independent test current with an oscillator. Monitors which use 2500 Hz, 4000 Hz, 900 Hz, 11 Hz, 8 Hz and several different waveforms are all put into this category. A monitor may be classified as one of these three kinds according to the type of signal it uses.

Monitors can be classified also according to the ways in which they verify continuity, as shunt-detector or potential-detector models (see Figure 3). Shunt-detector models actually sense the flow of monitoring current through the ground conductor. This can be accomplished with a current transformer or with a shunt or diode package in series with the ground wire. Potential detectors measure a signal voltage which exists between the ground wire and phase wire or pilot wire as the result of the flow of signal current.

Monitors can be sorted further into pilot-type or pilotless, depending on whether they require the presence of a special conductor within the cable which is neither a phase conductor nor ground wire. This special conductor is the insulated pilot wire.

Finally, monitors can be classified according to their type of connection to the power system and equipment (see Figure 4). Some monitors are connected in a loop configuration. Here, the monitor applies a signal to the source (outby) end of the cable, either to the pilot wire or the phase conductors. The signal travels to the machine and then returns along the ground wire to the outby end of the cable, completing a loop by which the ground wire can be monitored. Alternately, a monitor can consist of two separate active units, a sender and a receiver. A sender located at the machine or load end of the cable sends a signal out on the ground conductor. This signal is picked up at the other end of the cable to determine continuity

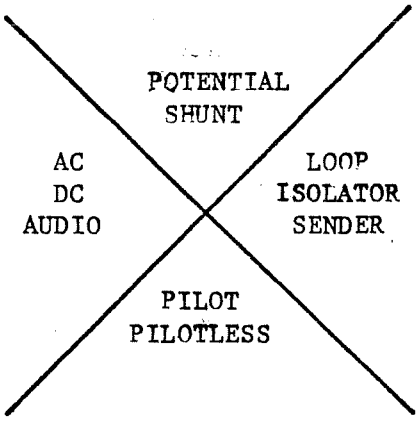


FIGURE 2. WVU Monitor Classification Scheme.

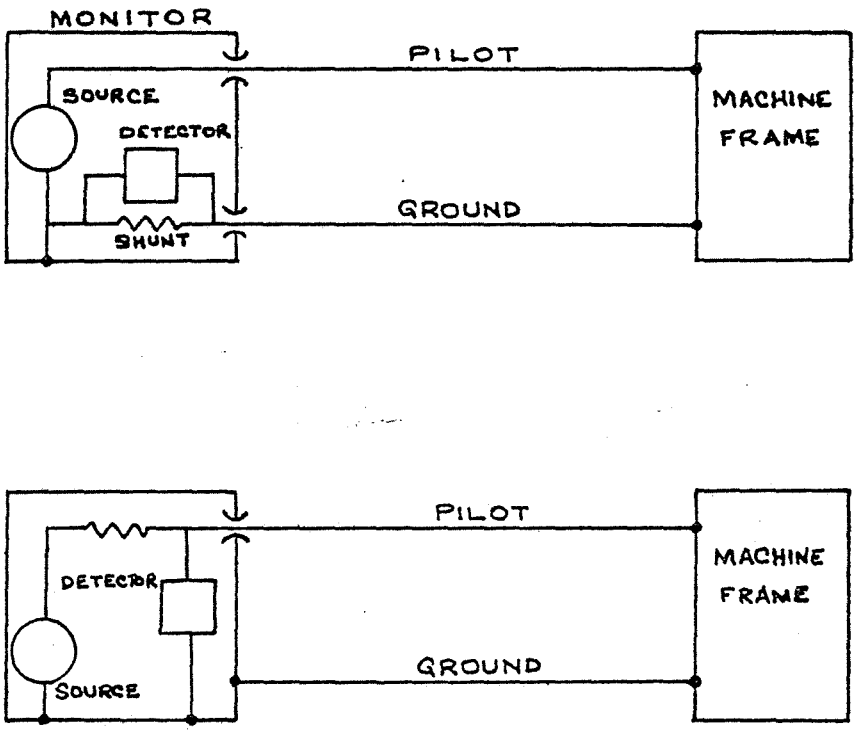


FIGURE 3. Shunt-Detector (Top) and Potential-Detector (Bottom) Monitor Configurations.

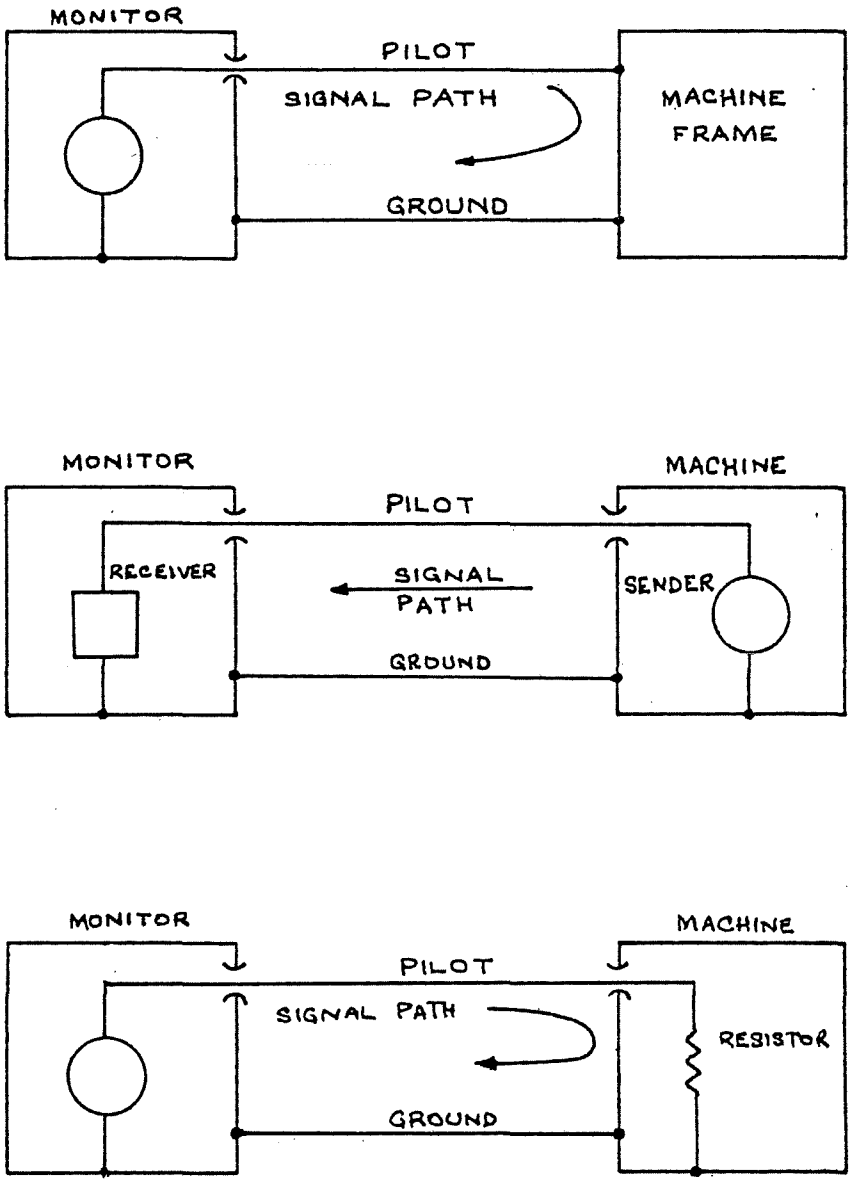


FIGURE 4. Loop (Top), Sender (Center) and Isolator (Bottom) Ground-Check Monitor Arrangements.

of the ground wire. A third type of connection falls between loop and sender. The basic configuration is that of a loop, but some passive device (resistor, diode, filter) is placed on the machine frame to operate on the signal as it passes. It has been called an isolator here.

Each of these classification schemes possess certain inherent characteristics. The audio monitors, for instance, are the only types which can be completely free from the effects of stray ground currents. The potential-type monitors are particularly susceptable to parallel paths, and must be used in conjunction with arc suppressors for most installations. Simple loop monitors cannot detect pilot-to-ground shorts, and therefore may be unacceptable to some operators.

Two tables are included to assist in evaluating monitors. Table 1 lists the basic characteristics of each generic monitor type. The other, Table 2, shows the WVU classification of each of the monitors which has received a letter of acceptance from MESA. These tables can be used in two ways. If one knows he has a particular requirement, such as the need to be immune to stray dc current, then he can look up characteristics in Table 1. Once it has been ascertained which monitor classes have the desired characteristic, Table 2 can be used to identify the manufacturers of such monitors. Alternately, one can look up the classification of a particular monitor in Table 2, and then use Table 1 to ascertain its basic characteristics.

It should be remembered that the entries are quite general. One should check with the manufacturer about exact monitor characteristics.

TABLE 1. GENERAL GROUND-CHECK
MONITOR CHARACTERISTICS*

MONITOR TYPE	CHARACTERISTICS
Ac	Immunity to dc
Dc	Immunity to ac
Audio	Immunity to ac and dc
Shunt	Always trips on broken ground - may false trip with parallel path
Potential	Failure to trip with low parallel path unless arc suppressor is used
Loop	Failure to detect pilot-to-ground fault
Sender	Must be bypassed to power-up, bulky machine-mounted components
Isolator	Detects pilot-to-ground fault, small machine-mounted component, reduced sensitivity
Pilot	Requires pilot wire
Pilotless	Requires filters one machine-mounted

*for MESA Technical Seminar
by Wils L. Cooley
West Virginia University

TABLE 2. CLASSIFICATION OF MESA
ACCEPTED MONITORS*

	MONITOR MANUFACTURER	DESCRIPTION
1.	American Mine Research	Audio, Isolator, Pilotless, Shunt
2.	Eltron Corporation	Audio, Loop, Pilot, Shunt Audio, Isolator, Pilotless, Modified Shunt[1]
3.	Ensign Electric	AC, Loop, Pilot, Potential
4.	FEMCO	Audio, Isolator, Pilot, Potential[2] Audio, Isolator, Pilotless, Potential[2]
5.	Kaiser Engineers (EEEI)	Audio, Isolator, Pilot, Potential[3] Audio, Isolator, Pilotless, Potential
6.	Line Power Corp.	AC, Loop, Pilot, Potential
7.	Ohio Brass Co.	Audio, Loop, Pilot, Shunt[4]
8.	Pemco	AC, Loop, Pilot, Potential

*For MESA Technical Seminar
by Wils L. Cooley
West Virginia University

NOTES:

1 2 CT's on ground wire eliminate false trip due to parallel paths.
2 Recommend use of Arc suppressor to make immune to parallel paths.
3 Use ground-line inductor to make immune to parallel paths.
4 Use of special diode shunt eliminates false trip due to parallel paths.